THE UNIVERSITY *of* EDINBURGH

This thesis has been submitted in fulfilment of the requirements for a postgraduate degree (e. g. PhD, MPhil, DClinPsychol) at the University of Edinburgh. Please note the following terms and conditions of use:

- This work is protected by copyright and other intellectual property rights, which are retained by the thesis author, unless otherwise stated.
- A copy can be downloaded for personal non-commercial research or study, without prior permission or charge.
- This thesis cannot be reproduced or quoted extensively from without first obtaining permission in writing from the author.
- The content must not be changed in any way or sold commercially in any format or medium without the formal permission of the author.
- When referring to this work, full bibliographic details including the author, title, awarding institution and date of the thesis must be given.

Models and Mechanisms of Sexual Dimorphism in Cardiovascular Calcification

Holly Joanne Woodward BSc (Hons) MScR

Thesis presented for the degree of

Doctor of Philosophy

College of Medicine and Veterinary Medicine
University of Edinburgh
2022

DECLARATION

I hereby declare that all the work included in this thesis submitted for the degree of Doctor of Philosophy at the University of Edinburgh is my own original work. Chapter 1 contains figures based on a published review that I am first author of and wrote. I have done all the work unless acknowledged otherwise. No part of this has been, or will be, submitted for any other degree or qualification.

Holly Joanne Woodward

November 2022

AKNOWLEDGEMENTS

A thesis does not take two people to raise, but a village.

First and foremost, I would like to thank my supervisors, Prof. Patrick Hadoke and Dr. Vicky MacRae. The mentorship I received from both of my supervisors during my project was outstanding. The environment you have both created in your lab is one that nurtures students as well as produces good data and is something you should both be very proud of. I would also like to mention Dr Kanchan Phadwal whose guidance I would have been lost without. Thank you for everything you have done for me these last four years and it is to you whom I dedicate this thesis. Your brilliance does not go unnoticed.

Secondly, to my family who has supported me throughout the last 9 years of higher education- we finally got here. I would be nowhere without you, especially my brother Tom, my dad, my grandparents, aunts, uncles, cousins, and my best friend Liz.

A special thank you to all the incredible friends I have made in Edinburgh. I have been blessed with my fellow doctoral students in the CVS, my year in EASTBIO and Holly and Hris. I would have never made it to this endpoint without all of you. Mainly to complain to and drink with, but also for the emotional support. A special mention to Maggie, Pop and Kiani because Powerpuff girls are forever.

I would also like to thank all the members of the core facilities that have helped me over the years. Adrian Thomson from ultrasound, whose friendship and advice I have greatly cherished. Thank you also to Adriana Tavares for all the help with my PET/CT needs and Dominic Kurian and Judit Aguilar in the proteomics facility. I would also like to thank Alex Loftus for all the help with the proteomics analysis.

Finally, to my boyfriend, Joe, thank you for keeping me sane in the last stretch of this thesis, which is undoubtedly the hardest job.

ABSTRACT

Cardiovascular calcification is the active process of calcification of the cardiovascular soft tissue. It is currently predicted to be present in over 70 % of the population aged 65 years and over. One of the most common types of cardiovascular calcification occurs in the aortic valve and is named calcific aortic valve disease (CAVD). In later stages, CAVD can cause stenosis, blood regurgitation and significant cardiac dysfunction and morbidity. Males are at greater risk of developing aortic calcification and androgens are a risk factor in this condition. There is no effective pharmaceutical treatment for CAVD. The mechanisms underlying male predisposition to aortic valve calcification have yet to be elucidated and this is hampered by the lack of appropriate animal models; particularly valve-injury models which develop stenosis and calcification.

This project aimed to examine the sexual dimorphism in cardiovascular calcification by deducing what molecular mechanisms sex hormones influence both in valve interstitial cells and vascular smooth muscle cells and by examining sex differences in *in vivo* murine models of calcification.

Culturing valve interstitial cells in either a 'pro-activated' or 'pro-quiescent' state did not change the deposition of *in vitro* calcium. In both valve interstitial cells (VICs) ($p<0.01$), and vascular smooth muscle cells (VSMCs) ($p<0.01$), calcification was enhanced (4.8-fold in VSMC, 15.7-fold in VICs) with testosterone treatment (concentration and length of exposure) whereas estrogen (concentration and length of exposure) had no effect. Proteomics analysis of calcified male rat VICs treated with testosterone found 398 differentially expressed proteins compared to control cells. This included differential expression of proteins associated with metabolism and cellular transport.

Next, the sex differences in the ApolipoproteinE null ($ApoE^{-/-}$) western diet murine model of cardiovascular calcification were analysed. During the 12 weeks of western diet treatment, neither male nor female mice developed aortic stenosis or regurgitation. Increased microcalcification ($p<0.05$) in the hearts of female mice was seen with PET/CT imaging. Additionally, there were larger atherosclerotic plaques ($p<0.01$) in the aortae of female compared to male mice. There was a higher prevalence of macrocalcification in the aortic root plaques of females, but no valve calcification was observed. However, circulating cholesterol

and LDL were significantly lower in females ($p<0.05$) compared to males. Female mice also displayed reduced tibial trabecular bone volume ($p<0.001$) and trabecular number ($p<0.001$).

Due to the sexual dimorphism in the ApoE$^{-/-}$ murine model not reflecting the sexual dimorphism in humans, a new, surgical model of valvular calcification was developed, the wire injury model. A pilot study was first undertaken which revealed that the surgery and imaging could be performed with a low mortality rate. The subsequent 'mild injury' study was modified so both male and female mice were included, and the post-operative time was lengthened to 8 weeks. Males had a higher mortality rate and females gained significantly more body weight post-operativity than males ($p<0.05$). After the wire injury, females had significantly higher blood velocity across the aortic valve than males ($p<0.05$), although this did not change after the surgery. There was also no evidence of sexually dimorphic responses to the wire injury in other cardiovascular parameters (measured by echocardiography) or evidence of regurgitation. Valve cusps displayed thickening (from 30 μM to 1402.8 μM), fibrosis and stained positive for Mac2. The protocol was then developed to include further injury and extend the post-operative period again. Finally, this 'moderate' injury study displayed no aortic regurgitation and no change to aortic velocity post-surgery.

To conclude, sex hormones may drive the sexual dimorphism seen in cardiovascular calcification, but further development of translational *in vivo* models is required to fully elucidate the underpinning mechanisms.

LAY ABSTRACT

Calcification is a disease where organs start turning into bone. This can happen in your heart and blood vessels. There are many reasons why this can happen. It may be due to 'wear-and-tear', age or being male. Men are more likely to get this disease and we don't know why. When your cardiovascular system starts turning into bone it increases your likelihood of getting heart disease, heart failure and the need for patients to undergo risky heart surgery. We do not currently have any drugs to treat calcification. Part of the reason for this stems from the lack of suitable models of the disease to investigate in a lab. Also, because we do not understand the biological pathways that could explain why men are more likely to get calcification.

In this project, I hypothesised that testosterone, the main male hormone, would increase calcification. The most commonly used mouse model of calcification is a genetically modified mouse fed a high-fat diet, therefore I also hypothesized that male mice would get more calcification compared to female mice.

I added testosterone to cells isolated from blood vessels and heart valves and saw an increase in calcium. I also added oestrogen, the main female hormone, and found no changes in calcification. I then calcified male rat valve cells and compared them to cells which had testosterone added to them. I found 400 differences in the proteome.

When looking at mice that had been fed a high-fat diet there was more calcification in the blood vessels of female mice. Females also had bigger fatty lesions around their hearts. In contrast, males had higher levels of fat and cholesterol in their blood. The higher rates of fatty plaques and calcification in females are opposite to what we see in humans.

A new model was next established where direct damage to the heart valve was made. This has previously been shown to cause calcium deposition. I conducted a pilot study where I found the surgery was safe to perform. A mild injury surgery was next performed a mild injury to the valve which did cause some valve thickening but no calcification. I then caused further damage but again saw no calcification in either male or female mice.

To conclude, male and female hormones can affect calcification, but we currently do not have good enough animal models to be able to establish the biological pathways through which this is happening.

Table of Contents

CHAPTER 1: INTRODUCTION 2

1.1 OVERVIEW OF CARDIOVASCULAR CALCIFICATION 2
1.2. THE AORTIC VALVE 2
1.2.1 The healthy aortic valve structure 2
..... 3
1.2.2 The healthy function of the aortic valve 4
1.2.3 Predominant cells and function in the aortic valve 5
1.2.3.1 Valve interstitial cells (VICs) 5
1.3 AORTIC VALVE CALCIFICATION 6
1.3.1 Initial stage of CAVD 6
1.3.2 Propagation Stage 8
1.4 MOLECULAR PATHWAYS OF CALCIFICATION. 9
1.4.1 Osteogenic calcification in the aortic valve 9
1.4.2 Lipoproteins and valve calcification 10
1.5.3 Matrix vesicles and calcification 11
1.5. REGULATION OF CALCIFICATION 13
1.5.1 Apoptosis and autophagy 13
1.5.2 Stretch can induce calcification in VICs 14
1.5.3 The role of MicroRNAs in calcification 14
1.6 MICRO- AND MACRO-CALCIFICATION 15
1.7 VASCULAR CALCIFICATION 15
1.7.1 Vascular smooth muscle cells (VSMCs) 15
1.7.2 Vascular Medial Calcification 16
1.7.3 Vascular intimal calcification 16
1.7.3 Mechanisms of vascular calcification 17
1.8 SEX HORMONES IN CALCIFICATION 19
1.8.1 Sex hormones in calcific aortic valve disease 19
1.8.2 Androgens 21
1.8.3 Oestrogens 22
1.8.4 Sex hormone-mediated pathways in CAVD 23
1.9 ANIMAL MODELS OF VALVE CALCIFICATION 24
1.9.1 Large animal models 24
1.9.2 Small animal models 25
1.10 CURRENT INTERVENTIONS 29
1.10.1 Surgical intervention 29
1.10.2 Drug interventions 30
1.11 STUDY HYPOTHESIS AND AIMS 32

2.0 CHAPTER 2: MATERIALS AND METHODS 34

2.1 MATERIALS 34
2.1.1 Chemicals and reagents 34
2.1.2 Buffers 34
2.1.3 Sex hormones 34
2.1.4 Software 35
2.1.5 Plastics 36
2.2 ANIMALS 36
2.3 IN VIVO ECHOCARDIOGRAPHY IMAGING 36
2.4 WIRE INJURY AORTIC STENOSIS MURINE MODEL DEVELOPMENT 37

2.4.1 Mice *37*
2.4.2 Surgery *37*
2.4.3 Tissue collection after wire injury *38*
2.5 ApoE$^{-/-}$ SEX DIFFERENCE STUDY 39
2.5.1 Mice *39*
2.5.2 Tissue collections for ApoE$^{-/-}$ study *39*
2.6 Ex Vivo IMAGING 39
2.6.1 Positron Transmission Tomography (PET)/ Computed Tomography (CT) imaging *39*
2.6.2 Micro-computed tomography (μ-CT) imaging *40*
2.7 HISTOLOGY 41
2.7.1 Processing *41*
2.7.2 Processing for staining *42*
2.7.3 Staining *42*
2.7.4 Immunohistochemistry Mac2/CD31/aSMA *46*
2.7.5 Analysis of Histology *46*
2.8 CELL CULTURE 47
2.8.1 Source of cells *47*
2.8.2 Cell culture media *48*
2.8.3 Cell maintenance *48*
2.8.4 In vitro induction of calcification *49*
2.9 BIOCHEMICAL ASSAYS 49
2.9.1 Quantification of calcification *49*
2.9.2 Quantification of total cellular protein *50*
2.10 FLUORESCENT IMMUNOCYTOCHEMICAL STAINING 50
2.11 QUANTITATIVE PCR 50
2.11.1 RNA extraction *51*
2.11.2 Complementary DNA (cDNA) generation *51*
2.11.3 Quantitative PCR *52*
2.12 WESTERN BLOTS 54
2.12.1 Lysis and protein quantification *54*
2.12.2 Western blot *54*
2.13 PROTEOMICS 55
2.13.1 Protein extraction *55*
2.14 STATISTICS 55

CHAPTER 3: TESTOSTERONE AUGMENTS *IN-VITRO* AORTIC VALVULAR CALCIFICATION 57

3.1 INTRODUCTION 57
3.1.1 Testosterone in vascular calcification *57*
3.1.2 Oestrogens in vascular calcification *58*
3.1.3 Sex hormones and calcific valve interstitial cells *59*
3.2. HYPOTHESIS AND AIMS 61
3.3: MATERIALS AND METHODS 62
3.3.2 Source of cells *62*
3.3.3 Cell characterisation using Immunofluorescence (IF) *62*
3.3.4 Optimisation of cell culture conditions to induce calcification *62*
3.3.6 Detection of changes in osteogenesis-related genes using qRT-PCR *62*
3.3.6 Detection of changes in osteogenesis-related proteins using western blot *63*
3.3.7 Optimisation of assays to measure sex hormone effects on valvular calcification *63*

3.3.8 Characterisation of sex hormone machinery expression in male and female rat tissues using qRT-PCR *63*
3.3.9 Proteomics *63*
..... 65
3.4: RESULTS 66
3.4.1 Cell line characterisation *66*
3.4.2 Optimisation of calcification media *66*
3.4.3 Determination of whether VIC phenotype affects in vitro calcification *68*
3.4.4 Determining the effect of sex hormones on in vitro calcification *72*
3.4.5 Characterising the distribution of the sex hormone receptors *75*
3.4.6 Investigating the mechanisms underpinning of testosterone driving calcification using proteomics *79*
3.4.7 Testosterone treatment significantly changed the expression of 356 proteins in calcified VICs from male rats *83*
3.5 DISCUSSION 88
3.5.1 RVICs can be used as an in vitro model of valve calcification *88*
3.5.2 RVICs can be used to investigate the effect of sex hormones on in vitro calcification *89*
3.5.3 Testosterone augments in vitro calcification of RVICs, potentially through the androgen receptor *90*
3.5.4 Testosterone alters respiration and energy metabolism in calcified male-derived RVICs. *91*
3.5.6 Limitations and future investigations *93*
3.5.7 Conclusion *94*

CHAPTER 4: APOE$^{-/-}$ MICE DISPLAY MORE VASCULAR CALCIFICATION AND LARGER ATHEROSCLEROTIC LESIONS IN FEMALES COMPARED WITH MALES 96

4.1 INTRODUCTION 96
4.1.1 Apolipoprotein E (ApoE) *96*
4.1.2 ApoE$^{-/-}$ mice as a model of aortic valve calcification *96*
4.1.3 Detection of calcification in murine models *97*
4.1.3 Sex differences in models of CAVD *97*
4.2 HYPOTHESIS AND AIMS 99
4.3: MATERIALS AND METHODS 100
4.3.1: Mice *100*
4.3.2: Western Diet Protocol *100*
4.3.4 Tissue Collection *100*
4.3.5 Echocardiography of ApoE$^{-/-}$ Mice *101*
4.3.6 Ex-vivo PET/CT of ApoE$^{-/-}$ Mice *101*
4.3.7 Autoradiography *101*
4.3.8 Histology *101*
4.3.9 Blood Lipid Analysis *101*
4.3.11 Micro-computed tomography (μ-CT) imaging *101*
4.4 RESULTS 103
4.4.1 Weight and Necropsies of Western Diet Fed ApoE$^{-/-}$ Mice *103*
4.4.2 The Western Diet Had no Significant Effect on Cardiac Function of ApoE$^{-/-}$ Mice. *107*
4.4.3 PET/CT of Western Diet Fed ApoE$^{-/-}$ *111*
4.4.4 Histological analysis of the Aortic root of Western Diet Fed ApoE-/- *117*

4.4.5 Micro-CT analysis of the Tibia *120*
4.4.6 Plasma Lipid levels. *125*
4.5 DISCUSSION 126
4.5.1 ApoE$^{-/-}$ mice fed a western diet for 12 weeks do not develop aortic stenosis or aortic valve calcification *126*
4.5.2 ApoE$^{-/-}$ mice fed a western diet for 12 weeks develop, vascular but not valvular, calcification with a sexual dimorphism. *127*
4.5.3 Western diet -fed ApoE$^{-/-}$ female mice have less bone mass than males *128*
4.4.5 Differences in Dyslipidaemia did not correlate with sexual dimorphism in atheroma. *129*
4.4.6 Future Investigations *130*
4.4.7 Conclusions *131*

5.0 DEVELOPMENT OF THE WIRE INJURY MODEL OF CAVD 133

5.1 INTRODUCTION 133
5.1.1 Limitations with models of CAVD *133*
5.1.2 The currently used murine models of CAVD *133*
5.1.3. The wire injury model of calcification *134*
5.2 AIMS AND HYPOTHESIS 135
5.3 MATERIALS AND METHODS 136
5.3.1 Mice *136*
5.3.2 Wire injury surgery *136*
5.3.2.1 Development of the wire injury protocol *136*
5.3.3 Echocardiography of wire injury mice to determine haemodynamic changes *138*
5.3.4 Aortic valve pathology *138*
5.4 RESULTS 139
5.4.1 Pilot Study *139*
5.4.1.1 LOW MORTALITY AND WEIGHT LOSS FOLLOWING WIRE INJURY SURGERY. 139
5.4.1.2 INVESTIGATING MORBIDITY OF THE CULLED MICE FROM THE PILOT STUDY 139
5.4.1.3 AORTIC VELOCITY AND CARDIAC FUNCTION WERE UNALTERED DURING THE PILOT STUDY. 142
5.4.1.4 VALVE CUSPS DISPLAY EVIDENCE OF REMODELLING AFTER WIRE INJURY 144
5.4.2 Mild Injury Study *145*
5.4.2.2 STUDY TO INVESTIGATE SEX-DIFFERENCES IN CARDIAC FUNCTION AFTER THE MILD WIRE INJURY SURGERY 147
5.4.3 Moderate Injury Study *152*
5.4.3.2 STUDY TO DETERMINE SEX-DIFFERENCES IN CARDIAC FUNCTION AFTER THE MODERATE WIRE INJURY SURGERY 154
..... 156
5.4.4 Identifying the cause of unexpectedly high mortality post-operative morbidity/ mortality in response to wire injury surgeries *160*
5.5 DISCUSSION 167
5.5.1 The wire injury surgery method is safe to perform *167*
5.5.2 The mild-moderate injury was not sufficient to produce CAVD *168*
5.5.3 Identifying the cause of morbidity/ mortality in later studies *170*
5.5.4 Wire injury to the aortic valve cannot be performed on 25-week-old ApoE$^{-/-}$ mice. *170*
5.5.5 Limitations of these studies *171*
5.5.6 Further studies *173*
5.5.7 Conclusion *173*

6.0 GENERAL DISCUSSION 176
6.1 RECAPITULATION 176
6.2 KEY FINDINGS 176
6.2.1 Testosterone augments the calcification of valve interstitial cells 176
6.1.2. ApoE$^{-/-}$ mice on a western-fed diet do not develop valve calcification and have more vascular calcification in females compared with mice 178
6.1.3. The wire injury model of CAVD is safe to perform on male and female mice and produces valvular remodelling. 179
6.3 FUTURE DIRECTIONS AND LIMITATIONS 180
6.4 CONCLUSION 184
7.0 REFERENCES.....185
APPENDIX I 201
APPENDIX II.....202
APPENDIX III…….204

LIST OF FIGURES

Figure 1.1: Structure of the aortic valve……3
Figure 1.2: Stress exerted on the aortic valve during opening and closing……..4
Figure 1.3: Basic pathology of CAVD……..9
Figure 1.4: Molecular pathways involves in valvular calcification……..11
Figure 1.5: Matrix vesicles (MV) generate microcalcification……12
Figure 1.6.: Common types of cardiovascular calcification……18
Figure 1.7: Molecular structure and synthesis of sex hormones……..20
Figure 2.1: Schematic diagram of wire injury surgery……..38
Figure 2.2: Figure demonstrating analysis point of the tibia bone……41
Figure 2.3: Examples of aortic root histology……42
Figure 2.4: Examples of histology positive staining……45
Figure 2.5: Validation of qPCR primers……*53*
Figure 3.3.2: Flow chart of proteomics data processing……65
Figure 3.4.1: Characterisation of the RVSV40T cell line……66
Figure 3.4.2: Optimisation of in vitro calcification conditions……67
Figure 3.4.3: MRNA expression of osteogenic genes in RIVCs calcified in pro-actived or pro-quiescent media……69
Figure 3.4.4. Proteins expression of known modulators of calcification in RVICs when calcified in pro-activated and pro-quiescent media ……70
Figure 3.4.5: Optimisation of in vitro calcification conditions in pro-quiescent media……..71
Figure 3.4.6: Effect of testosterone administration on calcification in VSMCs……72
Figure 3.4.7: Effect of exposure to sex hormones on in vitro calcification of immortalised RVICs on immortalised RVICs……73
Figure 3.4.8: Effect of sex hormone administration on calcification of primary RVICs from male rats……..74
Figure 3.4.9: Effect of sex hormone administration on calcification of primary VICs from female rats……..74
Figure 3.4.10. Expression of sex hormone receptor and the CYP191α mRNA in male rats…76
*Figure 3.4.11. Expression of sex hormone receptor and the CYP191α mRNA in female rats.*77
Figure 3.4.12: Effect of DHT administration on calcification of primary VSMCs from male rats and RVICs from male and female rats……78
Fig 3.4.13. Total protein abundance in each sample by LC-MS……79
Fig 3.4.14. Proteomics sample correlation……..80
Fig 3.4.15. Proteomics sample correlation after sample exclusion……81
Fig 3.4.16. Proteomics sample correlation after sample exclusion……82
Fig 3.4.17. Heat map of significantly differentially expressed proteins between control and testosterone treated male RIVCs……..84
Fig 3.4.18 Gene ontology of hits from proteomics between control and testosterone treated RIVCs……86
Fig 3.4.19 Protein interactions network of protein hits associated with tricarboxylic acid metabolism……86
Figure 3.5.1: Potential Mechanism of Testosterone fuelling calcification……92
Figure 4.3.1: Timeline of ApoE$^{-/-}$ western diet study……100
Figure 4.4.1: Body mass and bone length of western diet-fed ApoE$^{-/-}$ mice……..104
Figure 4.4.2 Colour Doppler images of blood flow in the ascending aorta of western diet-fed ApoE$^{-/-}$ mice……108
Figure 4.4.3: Aortic blood flow during exposure of male and female ApoE$^{-/-}$ mice to western diet……109

Figure 4.4.4: Cardiac function in mice exposed to western diet……110
Figure 4.4.5: M-Mode measurements of cardiac function in mice fed western diet……111
Figure 4.4.6: CT densities of aortas and hearts from western diet-fed ApoE$^{-/-}$ mice. ……113
Figure 4.4.7:^{18}F uptake in aortas of western diet-fed ApoE$^{-/-}$ mice……114
Figure 4.4.8 :^{18}F uptake in hearts of western diet-fed ApoE$^{-/-}$ mice. ……115
Figure 4.4.9 :^{18}F uptake in aortic root sections of western diet-fed ApoE$^{-/-}$ mice……116
Figure 4.4.10: Calcium staining of the aortic root in western diet-fed ApoE$^{-/-}$ mice……118
Figure 4.4.11: Histological staining of the aortic root in western diet-fed ApoE$^{-/-}$ mice……119
Figure 4.4.12: Trabecular architecture analysis of Western diet-fed male and female ApoE$^{-/-}$ mice……121
*Figure 4.4.13 Analysis of cortical region of tibiae 37% of bone length below growth plate*122
Figure 4.4.13 Analysis of the cortical region of tibiae 50% of bone length below growth plate. ……123
*Figure 4.4.15 Analysis of cortical region of tibiae 75% of bone length below growth plate*124
*Figure 4.4.16 Analysis of plasma levels in western diet-fed male and female ApoE$^{-/-}$ mice.*125
Figure 5.3.1: Timeline of pilot study……136
Figure 5.3.2: Timeline of mild injury study. ……137
Figure 5.3.3: Timeline of moderate injury study. ……137
Figure 5.4.1: Pilot study survival and body weight……140
Figure 5.4.2: Case study of mouse morbidity……141
Figure 5.4.3: Cardiovascular consequences of wire injury surgery……142
Figure 5.4.4: Histological staining of the aortic root after the pilot study……144
Figure 5.4.5: Calcium staining of mouse aortic root in sections obtained from the pilot study……145
Figure 5.4.6: Investigating the sex differences in survival after mild wire injury. ……146
Figure 5.4.7: Investigating the sex differences after mild wire injury……148
Figure 5.4.8: Investigating the sex differences in cardiac function after mild wire injury, measured using M-mode echocardiography ……149
Figure 5.4.9: Histological staining of the aortic root after mild injury……150
Figure 5.4.10: Calcium staining of aortic root after the mild injury study……151
Figure 5.4.11: Investigating the sex differences in weight and survival after moderate wire injury. ……153
Figure 5.4.12: Investigating the sex differences in echocardiography measurements after moderate wire injury. ……155
Figure 5.4.13: Investigating the sex differences in cardiac function after moderate wire injury……157
Figure 5.4.14: Investigating the sex differences in thickness and fibrosis after moderate wire injury……158
Figure 5.4.15: Calcium staining of aortic root after moderate injury ……159
Figure 5.4.16: Mac2 immunohistochemistry staining in the aortic valve of mice subject to the moderate injury surgery. ……160
Figure 5.4.17: Trouble shooting the unexpected reactions of the C57Bl/6 mouse strain to the wire injury protocol……162
Figure 5.4.18: Mortality in the wire injury surgeries which led to discontinuation of the protocol……163
Figure 5.4.19: Photograph of the incomplete Circle of Willis observed in the mice used in this study ……164
Figure 5.4.20: Mortality in the wire injury surgeries on ApoE mice$^{-/-}$……165
Figure 5.4.21: Sex differences in echocardiography measurements after wire injury on ApoE$^{-/-}$ mice……166

Figure 5.4.22: Histology of the aortic root after WI surgery.....166
Figure 6.1. Heat map of significantly differentially expressed proteins calcified RVICs from male and female mice.....181

LIST OF TABLES

Table 1.1: Sex differences in rodent studies of cardiovascular calcification…...……..28

Table 2.1: Table of software and manufacturers……..35

Table 3.4.1 The most significantly upregulated proteins after testosterone treatment to male calcified RIVCs…….……..85

Table 3.4.2 The most significantly downregulated proteins after testosterone treatment to male calcified RIVCs…….……..85

Table 4.1 Necropsy masses (normalised to body mass) of organs from ApoE-/- mice fed a western diet……105

Table 4.2 Necropsy masses (normalised to tibia length) of organs from ApoE-/- mice fed a western diet……..……..106

Table 5.4.1: Cardiovascular functional measurements of wire injury pilot study…….……..143

LIST OF ABBREVIATIONS

17OH-preg	17-OH-pregnenolone
17OH-prog	17-OH progesterone.
18F	18F-Sodium fluoride
AA	ascending aorta
Ab	absorbance
ACE	angiotensin-converting enzyme
adVICS	adipogenic valvular interstitial cells
ALP	alkaline phosphatase
ApoE	apolipoprotein E
AR	androgen receptor
ARBS	angiotensin II-receptor blockers
aSMA	alpha smooth muscle actin
ATP	adenosine 5′-triphosphate
AV	aortic valve
aVICs	activated valvular interstitial cells
BMP2	bone morphogenetic protein 2
BV/TV	bone volume
CA	calcium
CAC	coronary artery calcium
CAVD	calcific aortic valve disease
cDNA	complementary DNA
cGMP	cyclic guanosine monophosphate
chVICs	chondrogenic valvular interstitial cells
CKD	chronic kidney disease
Col1A1	collagen type I alpha1
CT	computerised tomography
CV	cardiovascular
CVD	cardiovascular disease
CYP	cholesterol side-chain cleavage enzyme
dH20	deionised water
DHEA	dehydroepiandrosteron
DHT	dihydrotestosterone
DIA	data-independent analysis
DMEM	dulbecco's Modified Eagle Medium
DMSO	dimethyl sulfoxide
ECG	electrocardiogram
ECL	electrochemiluminescence
ECM	extracellular matrix
EDTA	ethylenediaminetetraacetic acid
EKV	echo kilohertz visualisation
endoMT	endothelial to mesenchymal transition
ENPP1	ecto-nucleotide pyrophosphatase/phosphodiesterase 1
ER	estrogen receptor
ERN	extended-release niacin
FAVD	fibrotic aortic valve disease
FBP	filtered back projection
FBS	foetal bovine serum
FS	fractional shortening
FSH	follicle-stimulating hormone
GACI	generalized arterial calcification of infancy

GnRH	gonadotropin-releasing hormone
H&E	haematoxylin and eosin
HA	hydroxyapatite
HBSS	hank's balanced salt solution
HDL	high-density lipoproteins
HMG-CoA	3-Hydroxy-3-methylglutaryl-coenzyme A
HRT	hormone replacement therapy
HSD	hydroxysteroid dehydrogenase
HTGL	hepatic triglyceride lipase
ICAM-1	intercellular adhesion molecule 1
IL	interleukin
IL-6	interleukin 6
IMS	industrial methylated spirit
LC-MS	liquid chromatography-mass spectrometry
LDL	low-density lipoprotein
LDLR	low-density lipoprotein receptor
LDS	lithium dodecyl sulphate
LH	luteinizing hormone
Lpa	lipoprotein a
LPS	lipopolysaccharides
LV	left ventricle
LV mass	left ventricle mass
LV thickness	left ventricle thickness
LVEDD	left ventricular end-diastolic diameter
LVESD	left ventricular end-systolic diameter
MAP K	mitogen-activated protein kinases
MC	mast cells
MDV	mitochondrial-derived vesicles
MEM	minimum Essential Media
MGP	matrix Gla Protein
miRNA	micro-RNAs
MMP	metalloproteinases
MS	mass spectrometer
MT	masson's trichrome
MVs	matrix vesciles
NADH	nicotinamide adenine dinucleotide phosphate
NADPH	nicotinamide adenine dinucleotide phosphate (reduced)
NaF	sodium fluoride
NBF	neutral buffered formalin
NFKB	nuclear factor kappa-light-chain-enhancer of activated B cells
NICD	notch intracellular domain
NIH	national institute for health
NO	nitric oxide
NODAT	new-onset diabetes after transplant
NOTCH1	neurogenic locus notch homolog protein 1
obVICs	osteogenic valvular interstitial cells
OPG	osteoprotegerin
OPN	osteopontin
ox-LDL	oxidised low-density lipoproteins
PAMPs	pathogen-associated molecular patterns
PBS	phosphate buffered saline
PBS-T	PBS supplemented with 0.1 % (v/v) Tween 20
PCOS	polycystic ovary syndrome

PECAM1	platelet endothelial cell adhesion molecule 1
PET	positron emission tomography
PFA	paraformaldehyde
PGN	peptidoglycan
Pi	phosphate
PPAR-y	peroxisome proliferator-activated receptor gamma
Ppi	pyrophosphate
PSLA	parasternal long axis view
PVICs	porcine valve interstitial cells
PWT	posterior wall thickness
QPCR	quantitative PCR
qVICS	quiescent valvular interstitial cells
RANK	receptor activator of nuclear factor κ B
RANKL	RANK ligand
RB	retinoblastoma protein
RIPA	radioimmunoprecipitation assay buffer
ROS	reactive oxygen species
RUNX2	runt-related transcription factor 2
SDS	sodium dodecyl sulphate
SM22a	smooth muscle 22 alpha
SMI	structural model index
SNP	single nucleotide polymorphism
SurF	shared university research facilities
SVICs	sheep aortic valve interstitial cells
TAVR	transcatheter aortic valve replacement
TB.N	trabecular number
TB.Sp	trabecular separation
Tb.th	trabecular thickness
TGFb	transforming growth factor beta
TIMPs	tissue inhibitors of metalloproteinases
TLR	toll-like receptors
TNAP	tissue non-specific alkaline phosphatase
TNF-A	tumour necrosis factor-alpha
u-CT	micro-computed tomography
UK	united kingdom
UPR	unfolded protein response
UTP	uridine triphosphate
VCAM-1	vascular cell adhesion molecule 1
VECS	valve endothelial cells
VEGFA	vascular endothelial growth factor aplha
VICs	valvular interstitial cells
vLDL	very low-density lipoprotein
VOIs	volume of interest
VSMCs	vascular smooth muscle cells
VTI	velocity time integral
W/O	weeks of age
WHHL	watanabe heritable hyperlipidaemic
WHI	women's Health Initiative
WI	wire injury
WT	wild type

ACHIEVEMENTS

Publications

Woodward HJ, Thomson AJW, Hurr H, Alcaide-Corral CJ, Tavares AAS, MacRae VE, Hadoke PWF. The development of calcification in the ApoE$^{-/-}$ murine model is sexual dimorphic towards females, related to atherosclerosis. *In preparation*

Woodward HJ, Zhu D, Hadoke PWF, MacRae VE. Regulatory Role of Sex Hormones in Cardiovascular Calcification. Int J Mol Sci. 2021 Apr 28;22(9):4620

Suchacki KJ, Thomas BJ, Fyfe C, Tavares AAS, Sulston RJ, Lovdel A, Woodward HJ, Han, X, Mattiucci D, Brain EJ, Alcaide-Corral CJ, Gray, GA, Whitfield, PD, Stimson RH, Morton NM, Johnstone AM, Cawthorn, WP. The effects of caloric restriction on adipose tissue and metabolic health are sex- and age-dependent. *In submission*

Scientific Grants

2021-2022 Roslin Institute Early Career Grants scheme £2165.88 Title: Using proteomics to discover how testosterone enhances cardiovascular calcification.

2020 Deanery of Clinical Sciences Funding Challenge. £2450.48 Title: Using 18F to detect microcalcification in the wire injury model of calcific valve disease.

Prizes

Oral Presentation
Shortlist: Roger Wadsworth Prize, Scottish Cardiovascular Forum.
Winner: Oral Communication Runner-up Prize, RDSVS Student Research Day.

Public Engagement Prize
2020 CVS Public Engagement Award, for ASCUS; Art in Science workshops.

Internship

During my PhD I undertook a 3-month internship outside of academia with the company European Citizen Science Association. I interned for the communications and community officer. My main role was supporting the organization of the annual conference, including chairing events, preparing media advertisements, and reporting for the event. I developed my skills in online learning, teaching, and delivering symposiums. The reflection of my internship are located in appendix I.

Presentations

Oral

Models and mechanisms of sexual dimorphism in cardiovascular calcification. Woodward HJ, Thomson AJW, Alcaide-Corral CJ., Tavares ADA, MacRae VE and Hadoke PWF Scottish Cardiovascular Forum 06/05/22

Poster

Deducing mechanisms of sexual dimorphism in valvular calcification. Woodward HJ, Thomson AJW, Alcaide-Corral CJ, Kurian D, Tavares ADA, MacRae VE and Hadoke, PWF. PET is Wonderful 16/09/22

Sex differences in western diet-fed ApoE-/- mice as a model of calcific aortic valve disease (CAVD). Woodward HJ, Thomson AJW, Alcaide-Corral CJ, Tavares ADA, MacRae VE and Hadoke PWF. Scottish Cardiovascular Forum 05/02/21

PET-CT imaging detects microcalcification in western diet-fed ApoE-/- mice: a model of calcific aortic valve disease (CAVD). Woodward HJ, Thomson AJW, Tavares ADA, Alcaide-Corral CJ, MacRae VE. and Hadoke PWF. PET is Wonderful 27/10/2020

Developing a Wire injury Model of Aortic Stenosis. Woodward, H. J., Thomson, A. J. W., MacRae, V. E., Hadoke, P. W. F. Scottish Cardiovascular Forum. 01/02/2020

Chapter 1: Introduction

Chapter 1: Introduction

1.1 Overview of cardiovascular calcification

Ectopic calcification refers to the process of calcium deposition outside of the bone, usually in soft tissue. Evidence of vascular calcification in mummies from 1000BCE indicates that it is not a modern disease (Clarke *et al.*, 2014). Currently, it is estimated that up to 90 % of men and 67 % of women over the age of 70 have calcification in their coronary arteries and heart valves (Mohan *et al.*, 2021). Despite previous assumptions that calcification was a passive deposition of calcium in soft tissue, it is now known that this disease is physiologically regulated in a process similar to bone formation (Bucay *et al.*, 1998).

Cardiovascular calcification refers to calcification in the cardiovascular system, usually occurring in the arteries and heart valves and is extremely common in the ageing population. Calcification is more common in patients with other prevalent diseases such as diabetes mellitus, chronic kidney disease, atherosclerosis and hypertension (Chen, Zhao and Wu, 2020). No single cause of ectopic calcification has been identified but there are known risk factors such as smoking, high low-density lipoprotein (LDL) levels, male sex, and older age (Chen, Engert and Thanassoulis, 2019). Despite cardiovascular calcification being prevalent in the older population, there are currently no pharmaceutical interventions which can cure, or slow down the progression, of this disease (Vossen *et al.*, 2020). Currently, only surgical interventions can remove affected soft tissue. Under 50 years of age males tend to develop aortic valve calcification at a much higher rate than females, this sexual dimorphism changes after menopause (Kuller *et al.*, 2008). There is little understanding of this sex difference. This thesis will investigate whether sex hormones contribute to the sexual dimorphism seen in valve calcification and characterise the sex differences in murine models of calcific aortic valve disease (CAVD).

1.2. The aortic valve

1.2.1 The healthy aortic valve structure

The human aortic valve is located between the left ventricle and the opening of the aorta where its role is to prevent the backflow of blood after a heartbeat. The valve is comprised of three separate leaflets, each leaflet has the same three-layered structure (Figure 1.1). These layers

are the fibrosa, spongiosa and ventricularis. Each valve leaflet is encased in a layer of endothelial cells.

Closest to the aortic side is the fibrosa which contains an abundance of circumferentially-oriented collagen I and III fibres (Lerman, Prasad and Alotti, 2015). This layer functions to provide tensile strength to the valve (Lerman, Prasad and Alotti, 2015). The next layer, the spongiosa, comprises of a loose layer of proteoglycan which acts as a cushion to protect against the hemodynamic forces the valve is subject to (Tseng and Grande-Allen, 2011). The layer closest to the ventricle, the ventricularis, primarily houses elastic fibres. This layer contributes to the flexibility of the valve as it rapidly changes shape from open to closed with every heartbeat (Lindman *et al.*, 2016). The predominant cell type found throughout the valves are the valvular interstitial cells (VICs).

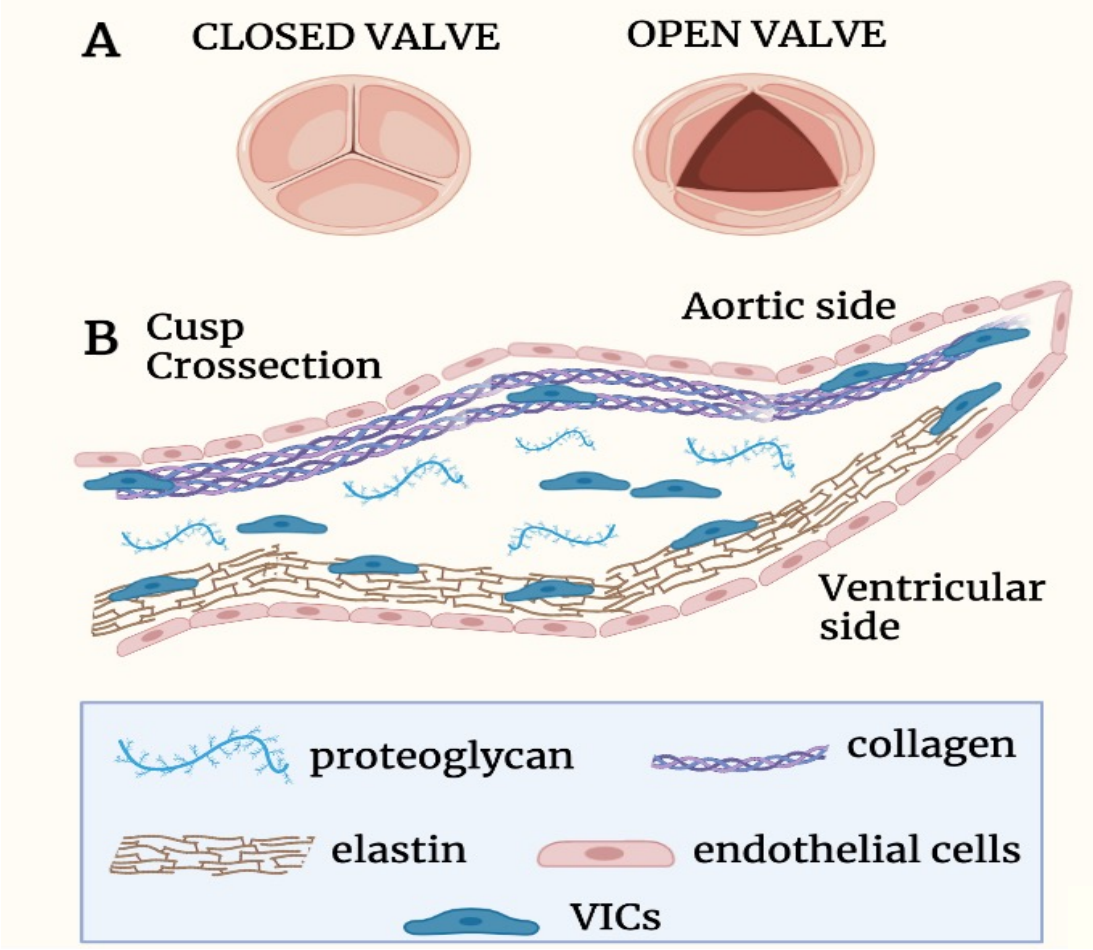

Figure 1.1: Structure of the aortic valve. A) Diagram of the aortic valve when the valve closes to prevent blood re-entering the heart during diastole and opens during systole to enable blood to be pumped into the aorta. (B) A cross section of a valve cusp demonstrates that it comprises three structurally distinct layers that contribute to its function. It contains two major cell types: endothelial cells, which line the surfaces of the valve and valvular interstitial cells (VICs). Figure adapted from Menon *et al.* (2018).

1.2.2 The healthy function of the aortic valve

The aortic valve is a mechanical structure which functions to prevent blood from flowing back into the heart, from the aorta, after a heartbeat (systole). During systole (the heart squeezing the blood out) the aortic valve opens and the velocity of blood flowing through the aortic valve reaches 1.2 m/s in most mammals (including humans) (Arjunon *et al.*, 2013). During diastole (the heart relaxing) the aortic valve closes, which acts as a barrier between the aorta and heart, so that blood cannot flow back into the ventricle. The aortic valve opens and closes over 100,000 times a day in humans (Menon and Lincoln, 2018).

The opening and closing of the valve (Figure 1.2) is governed by shear stress and pressure exerted on different parts of the valve during different points of the heartbeat. During systole, the flow of blood causes laminar shear stress on the ventricular side of the valve. A pressure gradient develops which affects the low-momentum blood nearest the aorta (Miller, 1980). This causes the blood flow to reverse in the sinus region of the valve, causing shear stress on the aortic side of the valve (Miller, 1980). These vortices behind the valve leaflets help close the valve. Once the valve is closed during diastole, pressure is exerted from the aortic side of the valve to keep the valve closed (Balachandran, Sucosky and Yoganathan, 2011).

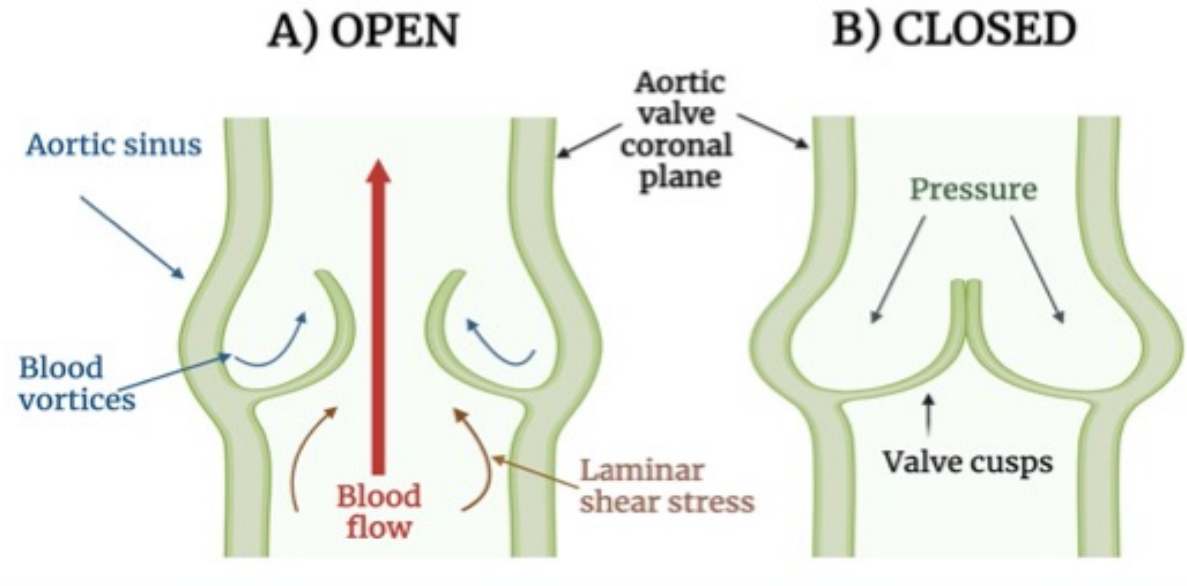

Figure 1.2: Stress exerted on the aortic valve during opening and closing. A) Blood is pushed out of the heart, opening the aortic valve. Blood will also start moving behind the valve cups exerting oscillatory shear stress behind the cusps. B) The oscillatory stress and pressure from aorta helps to close the aortic valve cusps, stopping backflow of blood to the heart. Figure adapted from Balachandran *et al*. (2011).

1.2.3 Predominant cells and function in the aortic valve

1.2.3.1 Valve interstitial cells (VICs)

The most predominant cells present in the aortic valve are VICs (section 1.2.1). The main role of VICs in the healthy valve is structural homeostasis. VICs can regulate physiological extracellular matrix (ECM) remodelling by regulating the deposition of structural proteins. Once structural proteins have been deposited in the valve VICs can produce and activate metalloproteinases (MMPs) (including MMP-1, MMP-2, MMP-3, MMP-9, and MMP-13) which degrade ECM proteins (Benton, Fairbanks and Anseth, 2009). VICs can also excrete tissue inhibitors of metalloproteinases (TIMPs) to stop ECM protein degradation (Moesgaard *et al.*, 2014).

VICs, which are considered to be fibroblastic cells, can exhibit plasticity and many (up to 7 other) sub-populations/phenotypes of VICs have been identified (Driscoll, Cruz and Butcher, 2021). In healthy valves, the predominant phenotype of VICs is 'healthy' quiescent VICs (qVICs). Both mesenchymal progenitor and osteoprogenitor cells can differentiate into VICs (Chen *et al.*, 2009). VICs can further differentiate into four different phenotypes- osteogenic (obVICs), adipogenic (adVICs), chondrogenic (chVICs) and activated (aVICs) (Chen *et al.*, 2009). It has also been demonstrated that endothelial cells can undergo a mesenchymal transition (EndMT), and become VICs (Dutta and Lincoln, 2018). VICs are therefore a highly plastic cell type that arises from a heterogenic origin.

1.2.3.2 Valve endothelial cells

Valve endothelial cells (VECS), like vascular endothelial cells, provide a barrier between the blood and the interstitial tissue. This barrier regulates the transport from the blood into the valve and out of the valve into the bloodstream (Driscoll, Cruz and Butcher, 2021). VECS have been shown to regulate the uptake of macromolecules, for example, lipoproteins, into the valve (Zeng *et al.*, 2007). One of VECs' most significant functions is the production of nitric oxide (NO) through nitric oxide synthase 3 (which is present in VECs). NO can diffuse out of VECS and into VICs, acting as a signalling molecule. Within healthy VICs, NO activates guanylate cyclase, thereby producing cyclic guanosine monophosphate (cGMP), cGMP interacts with neurogenic locus notch homolog protein 1 (NOTCH1) and notch intracellular domain (NICD). NOTCH1 and NICD have been linked to promoting a healthy VIC phenotype.

1.3 Aortic valve calcification

Aortic stenosis is the process of stiffening or thickening of the aortic valve, causing a narrowing of the valve opening. This results in increased blood velocity out of the aortic valve as the same volume of blood is pushed through a narrower opening (Chaudhry, Miao and Rehman, 2021). This can also cause the regurgitation of blood into the left ventricle. Aortic valve stenosis is diagnosed with an aortic blood velocity of over 2.0 m/s (measured using echocardiography). The most prevalent cause of aortic stenosis is calcific aortic valve disease (CAVD) (Nkomo *et al.*, 2006). CAVD is a complex disease which includes remodelling, inflammation, lipid infiltrations and calcification of the aortic valve. There are two types of calcifications which can be present in the valve, microcalcification and macrocalcification. Microcalcification is defined as calcium nodules which are less than 5 microns in thickness, macrocalcification is defined as nodules which are more than 5 microns in thickness (Joshi *et al.*, 2014). The progression of CAVD is outlined below.

1.3.1 Initial stage of CAVD

The exact cause of CAVD is unknown. One of the leading possibilities is that it develops as a result of mechanical injury to the endothelial cells caused by the valve cusps rubbing together when opening and closing. Damaged endothelial cells increase their expression of adhesion molecules, including vascular cell adhesion molecule 1 (VCAM-1), intercellular adhesion molecule 1 (ICAM-1) and E-selectin (Habas and Shang, 2018). This damage disrupts the endothelial cell barrier by altering the actin cytoskeleton and endothelial junctions (Clark *et al.*, 2007). As the barrier is damaged, the process of extravasation of leukocytes and recruitment of inflammatory cells begins (Muller *et al.*, 2000). Inflammatory cells, including monocytes, macrophages, T cells and dendritic cells migrate into the fibrosa of the valve, these cells will stay in the valve. The largest populations of these cells found in the valve in the early stages of CAVD are macrophages and dendritic cell-activated leukocytes (Zhou *et al.*, 2021). Activated leukocytes in the valve release interleukins (ILs) (including IL-21, IL-23 and IL-17), initiating and amplifying the chronic inflammatory process (Iwakura and Ishigame, 2006). The interleukins can promote VICs to produce interleukin 6 (IL-6) and tumour necrosis factor-alpha (TNF-α). Immune cells can also stimulate a phenotypic switch in the healthy 'quiescent' VICs (qVICs) to take on an activated or osteogenic phenotype (aVICs/obVICs) (Kaden *et al.*, 2003). The molecules which have been shown to stimulate this are TNF-α and tumour necrosis factor-

related apoptosis-inducing ligand TRAIL (from macrophages) and IL-1β, MMPs, TGF-β, (receptor-activated nuclear factor KB) receptor activator of nuclear factor κ B (RANK) and osteoprotegerin (OPG) (from T-lymphocytes) (Mathieu, Bouchareb and Boulanger, 2015).

The presence of chronic inflammation is one of the hallmarks of CAVD (García-Rodríguez *et al.*, 2018). Clinically the serum ratio of neutrophil/lymphocytes positively correlates with the severity of calcific stenosis (Avci *et al.*, 2014). In preclinical studies, culturing VICs (primary porcine cells) in a medium design for macrophages has been shown to promote trans-differentiation of VICs into an osteogenic state and to increase the expression of osteogenic markers such as runt-related transcription factor 2 (RUNX2) and osteopontin (OPN) (Grim *et al.*, 2020). VICs express toll-like receptors (TLRs), including TLR2 and TLR4, which respond to pathogen-associated molecular patterns (PAMPs) including lipoproteins and peptidoglycans (Meng *et al.*, 2008). During CAVD, activation of TLRs can induce intracellular transcription of IL-6 and ICAM-1 in VICs. Ligands of TLRs have been shown *in vitro* to induce the transition of VICs to an osteogenic phenotype (Kaden *et al.*, 2005). Therefore, inflammation can contribute to the induction of osteogenesis during CAVD.

In these initial stages, lipids and oxidised lipids also infiltrate into the valve through the damaged endothelial cell barrier (Yetkin and Waltenberger, 2009). The exact mechanism by which these lipids promote the development of CAVD is controversial. It is known that oxidised phospholipids (including Lp-PLA2) interact with VICs to upregulate IL-6, Lipoprotein (a) (Lpa) and bone morphogenetic protein 2 (BMP-2) (Boffa and Koschinsky, 2019). The addition of lipopolysaccharides (LPS) *in vitro* to human VICs activates osteogenic mediators such as RUNX2 and BMP-2 (Parra-Izquierdo *et al.*, 2019). Lpa has also been identified as a molecule of interest in the development of valve calcification; currently, two single nucleotide polymorphism (SNP) variants on the Lpa locus (rs10455872 and rs10455872), identified through genome-wide association (GWAS) studies, have been associated with enhanced risk of CAVD (Thanassoulis *et al.*, 2013; Arsenault *et al.*, 2014). CAVD has metabolic risk factors similar to those of atherosclerosis. Currently, recognised metabolic risk factors of CAVD are high levels of LDLs and triglycerides, and low high-density lipoproteins (HDL) levels (Chen, Engert and Thanassoulis, 2019).

1.3.2 Propagation stage

As previously stated (section 1.2.1), VICs are the main cell type in the aortic valve which exhibit a quiescent phenotype (qVICs) in a healthy valve (Wang, Leinwand and Anseth, 2014). However, VICs can also exist in other phenotypic states which have been linked to different disease pathologies. These are still being characterised with, recently, up to seven pathological phenotypes of VICs identified (Zhou *et al.*, 2021). In the initial stages of CAVD, VICs undergo a phenotypic transition as a result of signalling from inflammatory cells and lipids (Lee and Choi, 2018). VICs differentiate from qVICs into myofibroblastic/ activated VICs (aVICs). The new aVICs (identifiable by the presence of α-smooth muscle actin (α–SMA)) promote pathological matrix remodelling and are associated with fibrosis (Walker *et al.*, 2004). AVICs promote matrix remodelling through two mechanisms. One is the overexpression of proteolytic enzymes such as MMP-1, MMP-13, MMP-2, and MMP-9, and interleukin-1β (a cytokine that can induce secretion of proteolytic enzymes) which contributes to ECM degradation and collagen fragmentation (Rabkin *et al.*, 2001). AVICs also express procollagen-I mRNA, and consequently, retain the ability to synthesize collagen, alongside mediating fragmentation of existing collagen in the valve (Rabkin *et al.*, 2001). This creates the complicated fibrotic phenotype that is present in CAVD as well as in fibrotic aortic valve disease (FAVD). Overexpression of MMPs, secreted by aVICs and inflammatory cells, also contributes to ECM disorganisation (Cabral-Pacheco *et al.*, 2020).

In the later stages of CAVD, another phenotype of VICs (osteoblastic/osteogenic VICs (obVICs)) is observed. ObVICs produce matrix vesicles which deposit calcium in the valve in the form of hydroxyapatite (HA) crystals (Cui *et al.*, 2017). There is no specific cell marker for obVICs and usually, they are identified by the presence of pro-osteogenic proteins including alkaline phosphatase (ALP), bone morphogenetic protein (BMP)-2 and -4 and RUNX2 (Liu, Joag and Gotlieb, 2007). A more recent flow-cytometry study showed that all VICs which are responsive to calcification express Adenosine 5′-triphosphate (ATP)-binding cassette, sub-family G, member 2 (ABCG2) (Wang *et al.*, 2013). ObVICs secrete pro-osteogenic factors such as bone sialoprotein and osteocalcin into the valve (Zhu *et al.*, 2011). During the progression of calcification, a combination of events (including HA formation, inflammation, fibrosis and remodelling) creates calcium nodules, which can be seen on the aortic side of the valve in the late stages of the disease (Lindman *et al.*, 2016). The process of calcification is a highly regulated process similar to bone formation and, at the endstage of disease, lamellar

bone can be found in the valves (Dweck, Boon and Newby, 2012). The basic pathology of CAVD progression in shown in Figure 1.3.

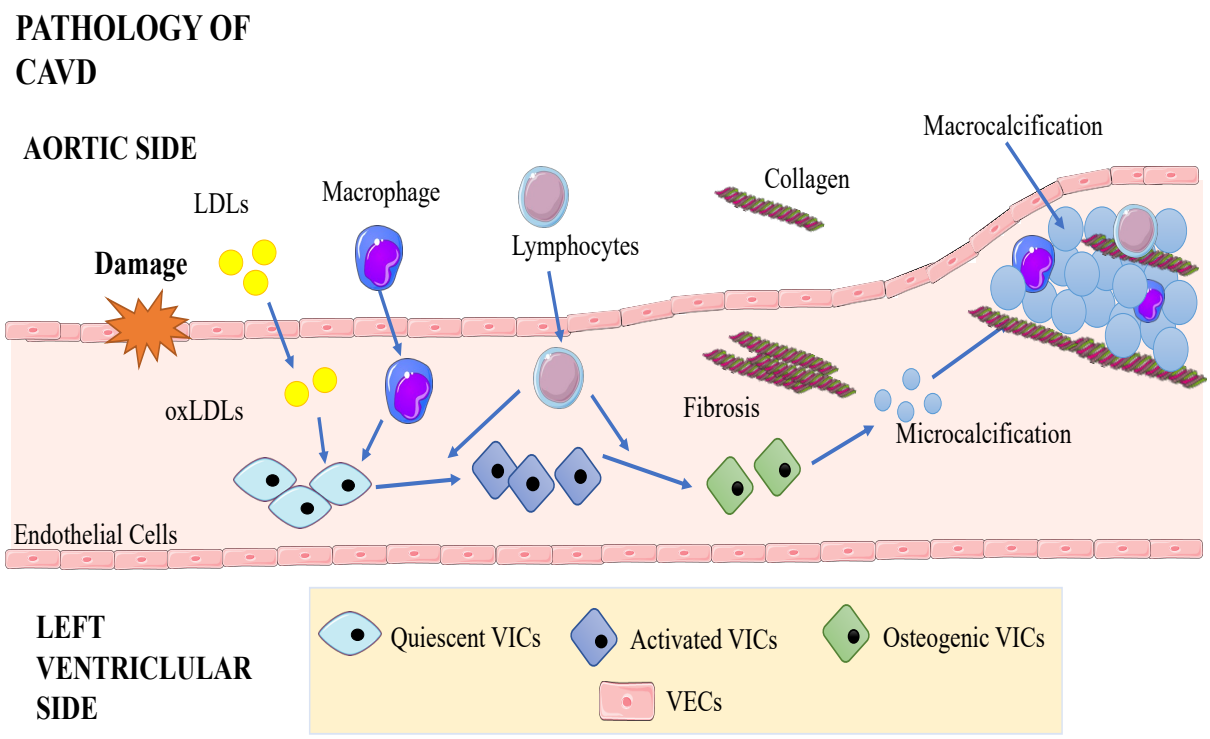

Figure 1.3: Basic pathology of CAVD. Valve interstitial cells (VICs) differentiate from quiescent (qVICs) in the healthy valve, to activated (aVICs) then osteogenic phenotypes (obVICs), under disease conditions. LDLs- Low density lipoproteins, oxLDLs- oxidized low-density lipoproteins, VECs, valve endothelial cells.

1.4 Molecular pathways of calcification

There are many molecular pathways involved in the induction of valvular calcification (Figure 1.4).

1.4.1 Osteogenic calcification in the aortic valve

Cytokines can be involved in the induction of calcification. RANK ligand (RANKL) and osteoprotegerin (OPG) are involved in bone turnover and are upregulated in calcification (Kearns, Khosla and Kostenuik, 2008). RANKL can promote osteogenic phenotypic trans-differentiation in VICs (Yetkin and Waltenberger, 2009). Osteopontin (OPN) has been demonstrated to have pro-inflammatory properties and is highly expressed in the aortic valves

and plasma of patients with CAVD (Passmore *et al.*, 2015). Another molecule that can drive osteogenic differentiation in VICs is BMP-2 (Woodward *et al.*, 2021). After treatment with BMP-2, osteogenic VICs have been observed to express further osteogenic factors including RUNX2, osteocalcin and alkaline phosphate (ALP) (Sun *et al.*, 2015).

1.4.2 Lipoproteins and valve calcification

The migration of lipoproteins into the aortic valve in the initial stages of CAVD can induce molecular changes in the pathology of valve interstitial cells (VICs) (Figure 1.4). It has been demonstrated previously that oxidised phospholipids (including Lp-PLA2) interact with qVICs not only to induce inflammation, through the upregulation of IL-6 but also to increase pro-osteogenic factors, including BMP-2 (Boffa and Koschinsky, 2019). An *in vitro* investigation demonstrated that LPS promotes VICs calcification and activates the production of pro-osteogenic factors including RUNX2 and BMP-2 (López *et al.*, 2012). Therefore, dyslipidaemia and lipid migration into the valve can also contribute to the development of calcification.

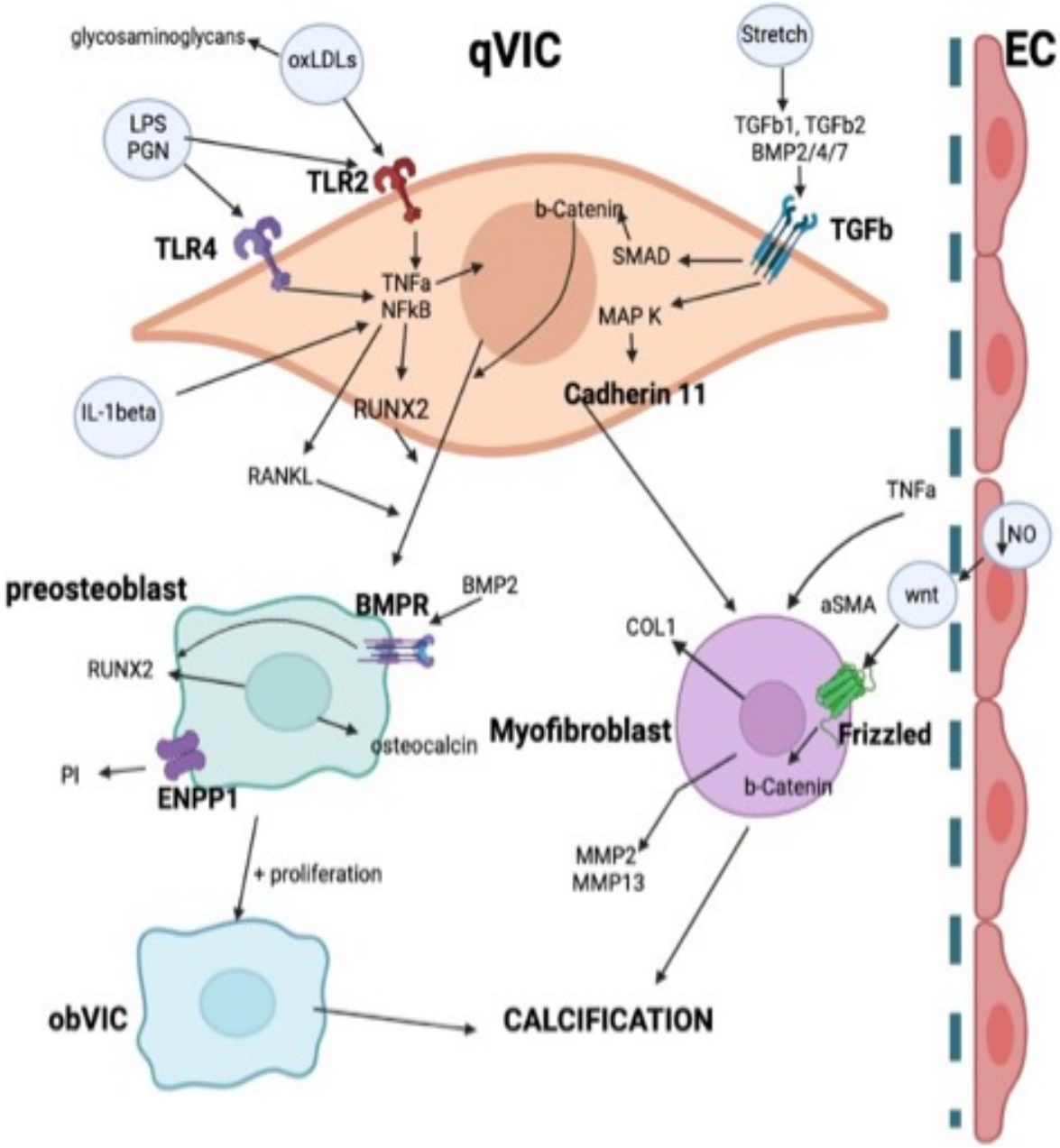

Figure 1.4: Molecular pathways involves in valvular calcification. This figure demonstrates proposed signalling pathways which are activated by lipoproteins, stretch and wnt signalling which contribute to development of calcification. These external factors activate signalling cascades which contribute to VIC differentiation into an osteogenic (obVICS) or myofibroblast/ activate (aVIC) phenotype. OxLDLs- oxidized low-density lipoproteins, LPS- lipopolysaccharide, TLR-toll like receptor, MAP K- mitogen-activated protein kinases, TGFB- transforming growth factor beta, BMP-bone morphogenic protein, RUNX2- Runt-related transcription factor 2, IL-1-interleukin 1, PI- phosphate, ENPP1- ecto-nucleotide pyrophosphatase/phosphodiesterase 1, COL1- Collagen 1, aSMA- alpha smooth muscle actin, MMP-matrix metalloproteinases. PGN- Peptidoglycan, NFkb- Nuclear factor kappa-light-chain-enhancer of activated B cells,

1.4.3 Matrix vesicles

Matrix vesicles (MVs) are nano-vesicles, derived from extracellular membranes, released by pro-osteogenic cells in conjugation with calcification. MVs can be secreted both by bone-derived cells (including chondrocytes and osteoblasts) and ectopically in tissue by vascular smooth muscle cells (VSMCs), macrophages, and VICs (Li *et al.*, 2022). MVs deposit calcium in the extracellular matrix (Anderson, 2003). The primary role of MVs in calcification is to nucleate HA. Matrix vesicle express phosphatases (including PHOSPHO1, tissue non-specific alkaline phosphatase (TNAP) and ectonucleotide pyrophosphatase/phosphodiesterase (ENPP1)) which generate phosphate (Anderson, 2003). Calcium and phosphate are attracted to the MVs due to the presence of annexins, including annexin A2, A5 and A6 (see Figure 1.5) (Cui *et al.*, 2016). Within the MVs, a first intermediate, octacalcium phosphate molecule (OCP; $Ca_8H_2(PO_4)6.5H_2O$), is created which is later converted into insoluble HA (Honda *et al.*, 2009). Matrix vesicles also contain a high number of micro-RNAs which are involved in osteogenic differentiation and, therefore, cardiovascular calcification (Goettsch, Hutcheson and Aikawa, 2013). An example of this is miR-30 which regulates the expression of osteogenic genes including SMAD1 and RUNX2 (Chaturvedi *et al.*, 2015).

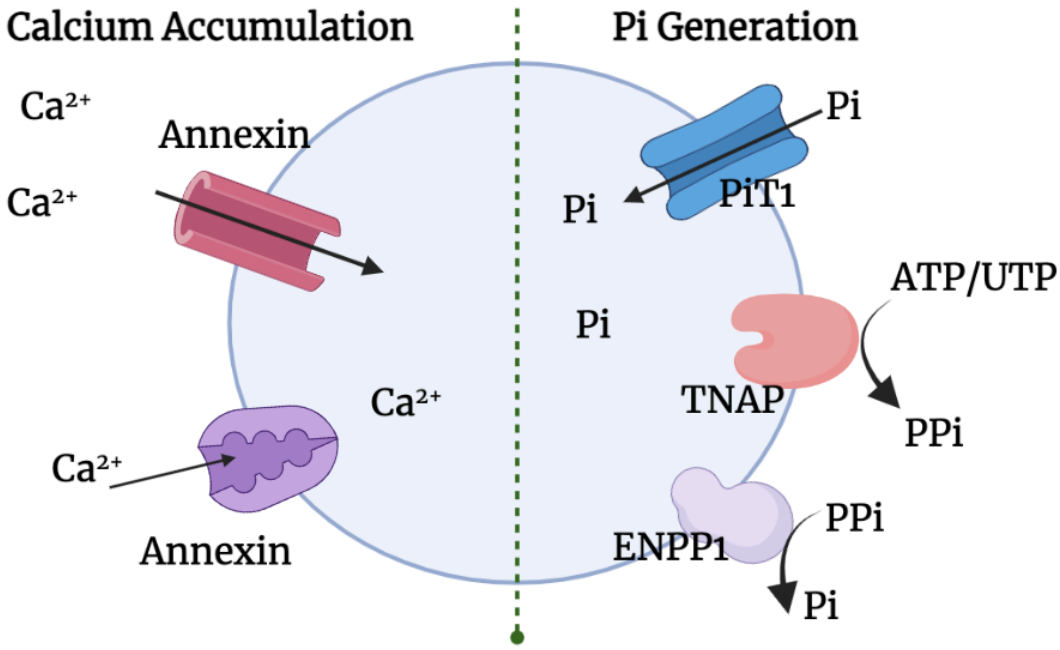

Figure 1.5: Matrix vesicles (MV) generate microcalcification. This diagram shows how matrix vesicles attract calcium and phosphate. MVs become rich in calcium and phosphate and become a nucleation site for hydroxyapatite. Pi-Phosphate, NNP1- Nucleotide pyrophosphatase/phosphodiesterase 1 ATP- Adenosine 5′-triphosphate UTP- Uridine triphosphate, TNAP- Tissue Nonspecific Alkaline Phosphatase PPi- Pyrophosphate, PiT/annexins- transport proteins. Figure based on Cui *et al.* (2016).

1.5. Regulation of calcification

1.5.1 Apoptosis and autophagy

Autophagy is a conserved mechanism in which dysfunctional proteins, damaged organelles and intracellular pathogens are removed from the cell (Parzych and Klionsky, 2014). New preclinical evidence suggests a role for autophagy in valve calcification. In high phosphate conditions (such as chronic kidney disease (CKD), which is a risk factor for valve calcification) mTOR signalling is inhibited, which leads to endothelial cells becoming dysfunctional through autophagy (Hsu *et al.*, 2015). *In vivo* models of CKD also display increased expression of LC3 (a marker of autophagosomes) in endothelial cells (Dai *et al.*, 2013).

Apoptosis refers to the process of programmed, regulated cell death and is enhanced in valvular calcification (Chen *et al.*, 2021; Proudfoot *et al.*, 2000). Apoptotic bodies are found in areas with HA deposition (Singh, Tandon and Tandon, 2021), and have been observed to act like MVs as sites of nucleation for crystal formation (Proudfoot *et al.*, 2000). A regulatory role for apoptosis has been highlighted by the demonstration that inhibiting apoptosis (with caspase inhibitor ZVAD-fmk) reduces vascular calcification, although this is yet to be examined in valve calcification (Proudfoot *et al.*, 2000). Apoptosis is triggered by mitochondria opening the permeability transition pores and therefore there is also a role for mitochondria during the calcification of the aortic valve (Orsucci *et al.*, 2019).

During calcification, mitochondria release mitochondrial-derived vesicles (MDV), containing Ca^{2+}, which can be transported to the ECM and deposit HA (Boonrungsiman *et al.*, 2012). BCL2-interacting protein depolarises mitochondria and induces mitophagy which also attenuates calcification (Zhu *et al.*, 2019). Preclinical investigations have also shown metformin, which induces autophagy and restores mitochondrial biogenesis and apoptosis, can block the osteogenic phenotypic transition of vascular smooth muscle cells *in vitro* (Ma *et al.*, 2019). Current research suggests mitophagy is defective in calcification (Phadwal *et al.*, 2021). Mitochondria also produce reactive oxygen species (ROS) which can accumulate in stenotic aortic valves and enhance the expression of osteogenic markers including TNAP, RUNX2, osteocalcin and collagen type I alpha1 (Col Iα1) (Phadwal *et al.*, 2021). There is a positive association between an increase in Mitochondrial (mt) DNA haplogroup H and aortic stenosis (Serrano-Teruel *et al.*, 2019).

1.5.2 Stretch can induce calcification in VICs

The aortic valve is a mechanical tissue which is subject to high pressures exerted from haemodynamic changes in the blood (section 1.2). In the vasculature, calcification is usually present in areas of lower shear stress (Schwartz and Mitchell, 1962). Force and stress on a tissue can cause soft tissue to stretch, often resulting in damage. Synthesis of collagen in VICs is regulated by the degree and duration of stretch (Ku *et al.*, 2006). VICs display increased calcium nodule formation *in vitro* in a strain-dependent manner (Fisher, Chen and Merryman, 2013). The strain-dependent activity of VICs is mediated by TGFβ, and calcium nodule formation displays a dose-dependent increase with TGF-β1 treatment *in vitro* (Fisher, Chen and Merryman, 2013). There is evidence that stretch induces TGFβ signalling in qVICs, inducing SMAD, B-catenin and MAP Kinase signalling, promoting osteogenic-phenotypic transdifferentiation (Rutkovskiy *et al.*, 2017). VICs have also been shown to exhibit a strain-dependent increase in the expression of bone morphogenic protein (BMP)-2, BMP-4 and transforming growth factor-β1 (Ferdous, Jo and Nerem, 2013). VICs also express stretch-activated calcium channels. Accumulation of intracellular Ca^{2+} has also been shown to be strain dependent (Hutcheson *et al.*, 2012). Intracellular Ca^{2+} mediates cell contraction and apoptosis (Hutcheson *et al.*, 2012). The amounts of strain and stretch to which the aortic valve is subject can contribute to its vulnerability to calcification.

1.5.3 The role of MicroRNAs in calcification

Micro-RNAs (miRNAs) are small, evolutionarily conserved, non-coding RNAs that function as post-transcriptional modulators of gene expression (O'Brien *et al.*, 2018). This ability to modulate post-transcriptional genes is seen as molecular 'fine-tuning' (Small, Frost and Olson, 2010). MiRNAs were first thought of as biomarkers and some (miR-133a, miR-135a, and miR-218) are upregulated in plasma from patients with cardiovascular disease (Cipollone *et al.*, 2011). More recently, many miRNAs have been identified that contribute to calcification (Small, Frost and Olson, 2010). MiRNAs can contribute to osteogenic differentiation by regulating the expression of RUNX2 (Zhang *et al.*, 2011). In addition, miRNAs have been identified in preclinical studies which regulate calcification. For example, inhibition of miR-125b can induce calcification and upregulate markers of calcification including osterix and ALP (Goettsch *et al.*, 2011). Another example is miR-29b which has been shown to augment valvular calcification, increase the expression of Wnt3 β-catenin and inhibit the expression of

TGF-β3 (Fang *et al.*, 2020). There are many other micro-RNA which have been shown to augment valve calcification (reviewed in Goettsch *et al.*(2013)).

1.6 Micro- and macro-calcification

As briefly described, two types of calcification that can exist in the aortic valve. Microcalcification is defined as calcium nodules which are less than 5 microns in thickness and occurs at early disease stage (as described in section 1.2) (Joshi *et al.*, 2014). Microcalcification is associated both with active inflammation, injury and repair and with atherosclerotic plaque rupture (Shioi and Ikari, 2018). Microcalcification is released by matrix vesicles. Macrocalcification is defined as calcium nodules which are more than 5 microns in thickness (Joshi *et al.*, 2014). They are usually associated with established CAVD. These large calcium nodules significantly affect the hemodynamic function of the aortic valve. They impair the movement of valve leaflets which can result in valve stenosis (Aikawa and Blaser, 2021).

1.7 Vascular calcification

Calcification can also occur in blood vessels, usually within the arteries. Arteries function to deliver oxygenated blood to tissues (Goodwill *et al.*, 2017). The artery wall is comprised of three layers. The innermost layer is called the tunica intima which is made up of endothelial cells (Medina-Leyte *et al.*, 2021). The middle layer, the tunica media is predominantly made up of VSMCs. The outermost layer is the tunica adventitia and comprises of connective tissue and nerve endings (Medina-Leyte *et al.*, 2021). There are two main types of vascular calcification, medial and intimal (Figure 1.6). This terminology is based on the location of calcification within the artery, but it is now recognised that medial and intimal calcification have different pathologies and processes.

1.7.1 Vascular smooth muscle cells (VSMCs)

The main cell type which regulates vascular calcification is the VSMC which is the predominant cell type in the medial layer of the artery. As with VICs, VSMCs are a highly plastic cell type, where different phenotypes can exist which have different functions depending on the vessel environment. In a healthy artery, VSMCs main role is to control the luminal diameter of the blood vessel by contracting and relaxing (Jaminon *et al.*, 2019). The VSMCs in individual blood vessels have distinct origins in the embryo (Sorokin *et al.*, 2020).

For example, VSMCs in the descending aorta are derived from somatic precursors whereas VSMCs in the ascending aorta and arch are derived from the neural crest (Sorokin *et al.*, 2020). As with VICs, diverse precursors have been identified for VSMCs, including bone marrow-derived stem cells, stem cells in the adventitia, and endothelial cells which undergo EndoMT (Wang *et al.*, 2015).

1.7.2 Vascular medial calcification

Medial calcification presents as sparse calcification of the medial layer of the artery (Lanzer *et al.*, 2021). It usually occurs along the elastic fibres of the laminae without inflammatory cell or lipid infiltration into the vessel wall (Wu, Rementer and Giachelli, 2013). Clinically, medial calcification causes stiffening (sclerosis) in the vessels and loss of elasticity, which leads to decreased vessel compliance (Ho and Shanahan, 2016). This can contribute to an increase in blood pressure and local ischaemia at the site of calcification. If left untreated, medial calcification can cause increased vascular mortality (death caused by composite vascular disease) (Wu, Rementer and Giachelli, 2013). Medial calcification is linked to altered bone and mineral metabolism which is common as a secondary consequence of CKD and diabetes (Manzoor *et al.*, 2018). It can also occur in rare diseases such as Mönckeberg's Arteriosclerosis, Kawasaki disease and Generalized Arterial Calcification of Infancy (GACI) (Lanzer *et al.*, 2014; Brunet-Garcia *et al.*, 2022).

1.7.3 Vascular intimal calcification

Intimal calcification occurs in the innermost layer of the vessels and normally presents in atherosclerotic plaques (Amann, 2008). There is debate about whether intimal calcification in atherosclerotic plaques stabilises or destabilises the plaque (Shi *et al.*, 2020). This can be dependent on the pattern of deposition and plaque composition. Macrocalcification may stabilise the fibrous cap covering the atherosclerotic plaque (Libby and Pasterkamp, 2015). Conversely, microcalcification may destabilise the plaque as microcalcification can be deposited along collagen fibres, making the structure of the plaque cap less secure and therefore making it more likely to rupture. This can put a patient at risk of an ischemic event such as myocardial infarction or stroke (Bentzon *et al.*, 2014; Libby and Pasterkamp, 2015) . As intimal calcification is a result of atherosclerotic plaque development, it is also associated with classic cardiovascular (CV) risk factors such as hyperlipidaemia and metabolic syndrome (Durham *et al.*, 2018).

1.7.3 Mechanisms of vascular calcification

The main regulating cell in both types of vascular calcification is VSMCs (Durham *et al.*, 2018). VSMCs undergo a similar phenotypic transition to VICs during calcification (Tyson *et al.*, 2020), becoming osteogenic, and releasing HA-depositing MVs into the artery. Within the vasculature, endothelial cells, myofibroblasts in the adventitia, and pericytes in the microvessels can also become calcified (Woodward *et al.*, 2021). From a healthy contractile phenotype, VSMCs can differentiate into several forms of osteogenic phenotypes, including osteoblastic and chondrocytic phenotypes (Speer *et al.*, 2009). The loss of contractile phenotype can be marked by the loss of α-SMA and smooth muscle 22 alpha (SM22α) (Bardeesi *et al.*, 2017). In an osteogenic phenotype, cells express osteogenic-related transcription factors, including Sox9, Runx2, Msx2, and osterix which are responsible for osteoblast-like differentiation of VSMCs and therefore help to drive vascular calcification (Leopold, 2015).

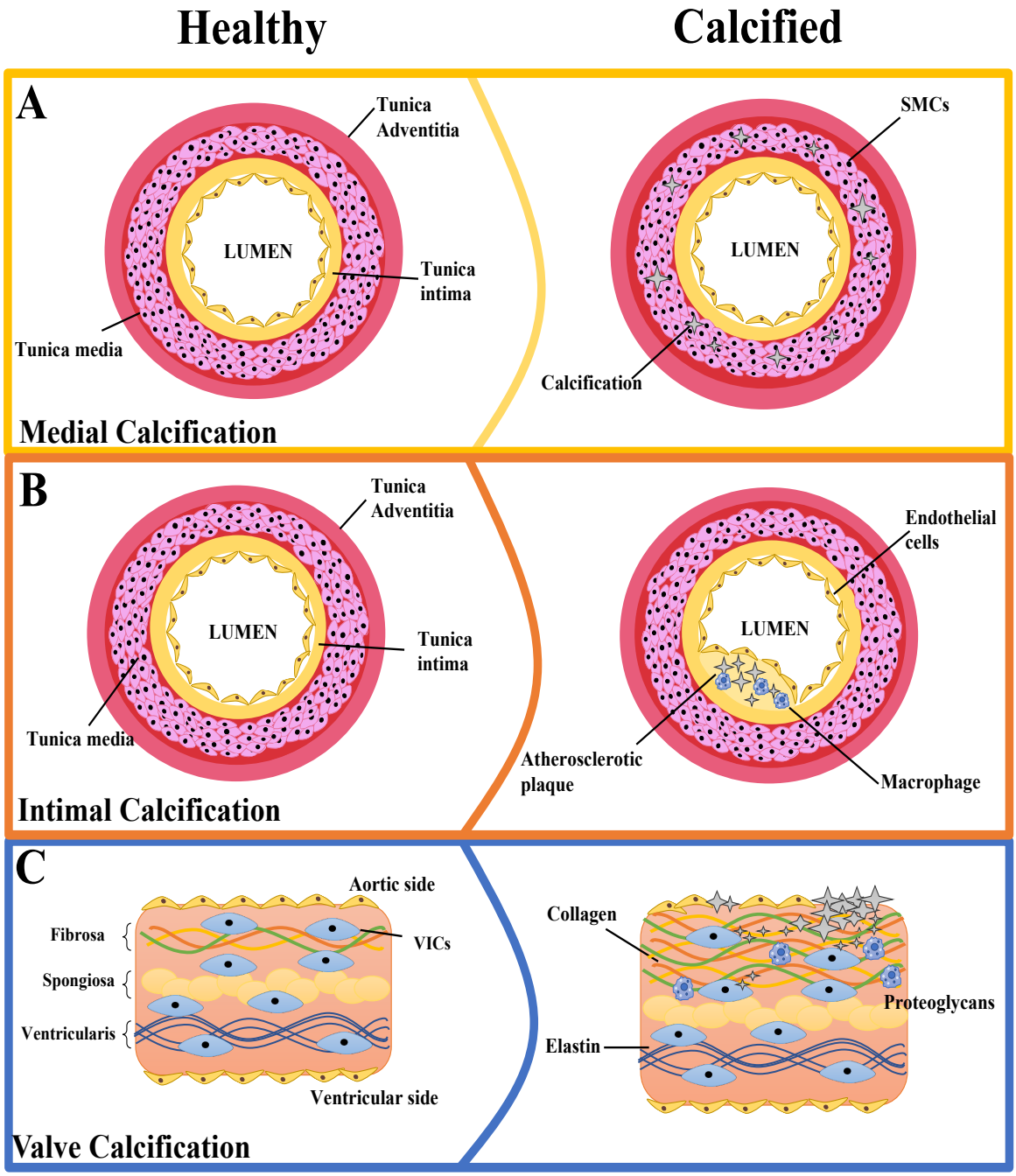

Figure 1.6.: Common types of cardiovascular calcification. The three most common types of ectopic calcification in the cardiovascular system are intimal vascular, medial vascular and aortic valvular. This figure displays both the normal and disease state for each of these diseases. A) Medial calcification occurs within the medial, smooth muscle layer of the vessel. B) Intimal calcification usually occurs as a result of calcification of atherosclerotic plaques in the intimal layer of the vessel. C) Aortic valve calcification usually occurs on the aortic side of the valve. Figure adapted from Woodward *et al.* (Woodward *et al.*, 2021)

1.8 Sex hormones in calcification

1.8.1 Sex hormones in calcific aortic valve disease

Calcific aortic valve disease displays a significant sexual dimorphism. For the same degree of stenosis, men will have more calcification and women will have more fibrosis (Simard *et al.*, 2017). In patients under 45 years of age, up to 70 % of those with CAVD are men. This sexual dimorphism changes after women go through menopause. Post-menopause, the rate of aortic valve calcification in women increases to such an extent that it overtakes men (Otsuka *et al.*, 2014). A recent clinical study by Simard *et al.*(2017) described the differences in the pathology of valve diseases between the sexes by analysing valves retrieved from patients after replacement surgery. Aortic valve cusps from males were significantly heavier and had a higher degree of calcification, whereas valve cusps from females had a greater proportion of moderate-severe fibrosis (following the Warren-Young score) (Simard *et al.*, 2017; Summerhill *et al.*, 2020). Another clinical study showed that, for the same stenotic severity, female patients had a smaller aortic valve area, lower left ventricle (LV) mass indexes, were older, and had a higher incidence of hypertension than men. This study also demonstrated that the prevalence of moderate-to-severe valve calcification was higher in men, even when adjusting for the severity of stenosis (Thomassen *et al.*, 2017). Another biomarker study from patients with aortic valve disease showed that women had a higher likelihood of expressing biomarkers associated with fibrosis (including suppression of tumorigenicity 2 protein and galanin protein) (Peeters *et al.*, 2020). Men also had a higher likelihood of expressing biomarkers associated with inflammation and calcification, including interleukin 1 receptor antagonist (Peeters *et al.*, 2020).

The mechanism behind this sexual dimorphism is unknown. One possibility is that CAVD and FAVD have two separate pathophysiologies and should be treated accordingly. Alternatively, some hypothesize that FAVD is an early stage of CAVD (Sathyamurthy and Alex, 2015). Certainly, there is some evidence that qVICs exist in a pro-fibrotic phenotype (aVICs) before they differentiate into an osteogenic state (obVICs). One potential mechanism behind the differentiation of valve phenotypes is TGFB-β signalling which can promote the expression of genes associated with fibrosis (Tang *et al.*, 2022). Conversely, BMP signalling promotes osteogenic gene expression (Sritharen *et al.*, 2017). Sex comparison studies are rare in preclinical models of calcification. The majority of the studies which investigate sex display

no sex difference or show that females have increased levels of calcification compared to males (Table 1.1). One hypothesis is that this sexual dimorphism is driven by sex hormones.

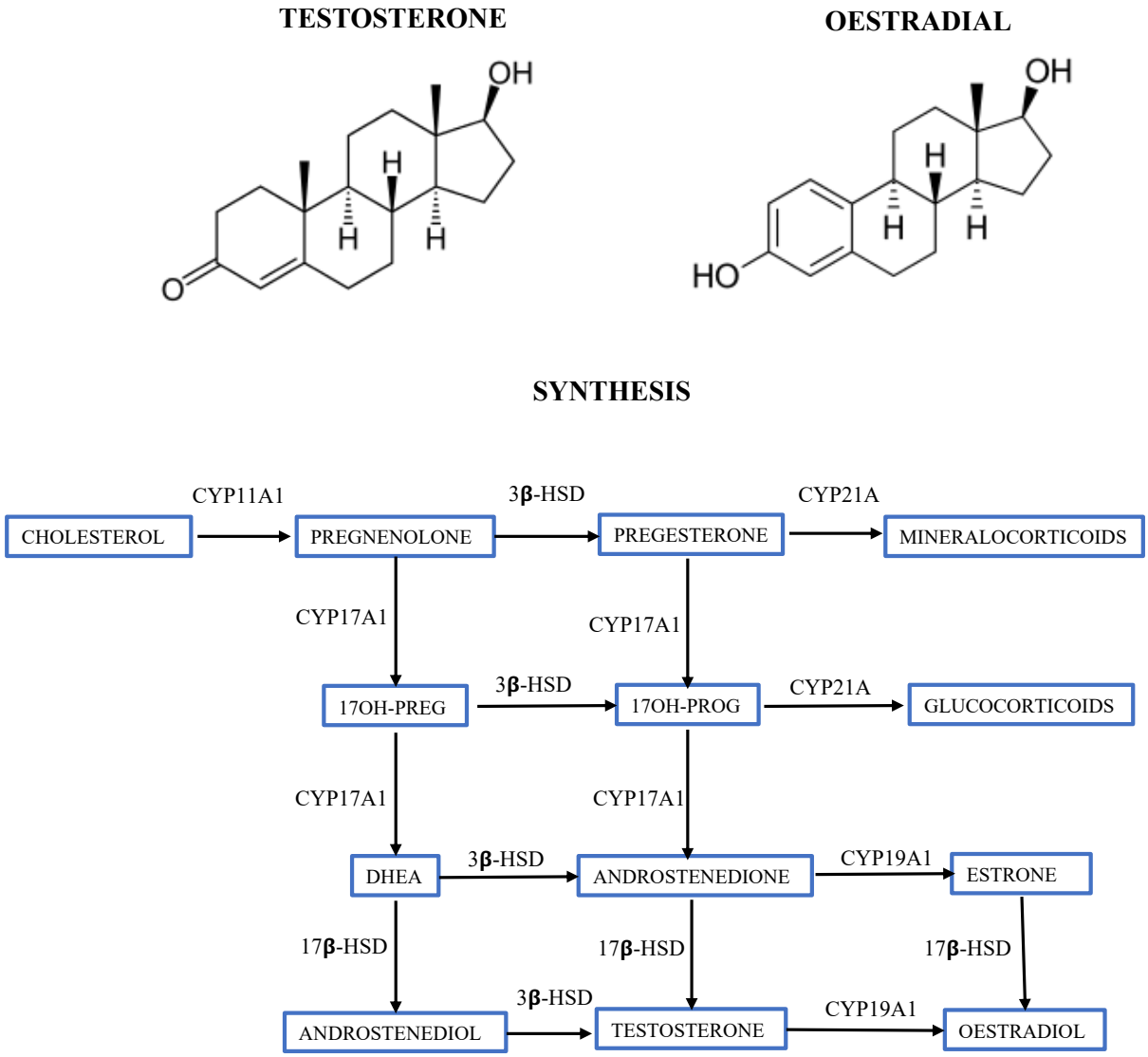

Figure 1.7: Molecular structure and synthesis of sex hormones. This figure displays the molecular structures of testosterone and oestradiol. The endogenous pathways for synthesizing sex hormones from cholesterol and the enzymes needed are also demonstrated. HSD= Hydroxysteroid dehydrogenase, CYP= Cholesterol side-chain cleavage enzyme, DHEA- Dehydroepiandrosterone, 17OH-PREG=17-OH-pregnenolone, 17OH-PROG=17-OH progesterone.

1.8.2 Androgens

Testosterone is the primary male sex hormone in mammals (structure and synthesis shown in Figure 1.7) (Handelsman, 2020). An androgen is a hormone capable of developing and maintaining masculine characteristics in reproductive tissues, and contributing to the anabolic status of non-reproductive body tissues (Handelsman, 2020). Testosterone is synthesized by Leydig cells in the testes and is then circulated in the blood. Testosterone secretion in the testes is regulated by luteinizing hormone (LH), through LH action on the rate-limiting conversion of cholesterol to pregnenolone (Eacker *et al.*, 2008). The main mechanism through which testosterone interacts with cells is through binding to the androgen receptor. The androgen receptor (AR) is a steroid nuclear receptor encoded by a single gene on the X chromosome (Davey and Grossmann, 2016). The AR is expressed in many tissues throughout the reproductive, cardiovascular, immune, and neural systems (Davey and Grossmann, 2016). Testosterone can also exert effects on tissues through a non-genomic pathway. Hormone-bound nuclear receptors can interact with other transcription factors by binding to the gene promotors and altering the transcription of other genes (Santos, Fairall and Schwabe, 2011).

Elevated androgen levels are a risk factor for many CVDs, including CAVD. This relationship is also reflected in women who suffer from polycystic ovary syndrome (PCOS). Women with PCOS have an elevated level of testosterone and an increased risk of CVD (Calderon-Margalit *et al.*, 2014). In postmenopausal women, higher free testosterone is associated with calcium progression (Subramanya *et al.*, 2019). My group has previously shown that deletion of the androgen receptor in VSMCs prevents testosterone-induced VSMC calcification (Zhu *et al.*, 2016). Although this relationship is yet to be established in VICs.

The relationship between cardiovascular disease and testosterone is complicated though. Both high and low serum testosterone levels are positively associated with cardiovascular disease in clinical trials. There have not been many clinical trials investigating how testosterone influences CAVD. A few studies exist that have been conducted on vascular calcification, which maybe provide some insight into how testosterone is influencing general cardiovascular calcification. A clinical study in men demonstrated a negative association between testosterone and vascular calcification (Park *et al.*, 2012). Contrary to this, the Framingham Heart Study reported no significant association between testosterone and vascular calcification (Travison *et al.*, 2016). Preclinical studies also demonstrate conflicting messages. In both male and female apolipoprotein E knockout ($ApoE^{-/-}$) mice, testosterone administration increases

atherosclerotic intimal calcification (Son *et al.*, 2010). It is more likely that testosterone has a U-shaped relationship with disease. As with many hormones both high and low levels can have negative impacts on health.

1.8.3 Oestrogens

Oestrogens are a class of sex hormones that are predominant in women. Oestrogens are mainly synthesized and secreted by the ovaries during a woman's reproductive years. The most abundant form of circulating oestrogen is oestradiol, also termed 17β-oestradiol. Oestradiol synthesis is stimulated by follicle-stimulating hormone (FSH) (Dorrington, Moon and Armstrong, 1975). Oestradiol mainly exerts its effects on tissues through the estrogen receptor (ER) family, consisting of ERα and ERβ. The ER family are ligand-dependent transcription factors. ERα and ERβ are distinct proteins encoded by two genes; the ERα protein is encoded by ESD1 and the ERβ protein is encoded by ESR2 (Paterni *et al.*, 2014). ERα is predominantly expressed in the kidneys, the pituitary glands and the reproductive system of both men and women (including in the testis, epididymis, ovaries and uterus). ERβ is mainly expressed in the reproductive system and brain (Lee, Kim and Choi, 2012).

Oestrogens and ER activation are believed to have cardioprotective properties. In preclinical trials, oestrogen application lowered coronary vascular resistance and enhanced coronary blood flow (Node *et al.*, 1997). It has long been established that oestrogens can inhibit the development of atherosclerosis (Mendelsohn, 2000). It has also been shown clinically that oestrogen therapy decreases serum levels of LDLs while raising HDLs. It is thought this mechanism is through oestrogens augmenting hepatic apoprotein gene expression (Mendelsohn and Karas, 1999). One of the most prominent effects of oestrogen on the cardiovascular system is the ability of oestrogen to induce vasodilation. This is a rapid effect after hormone administration so is believed to be mediated through oestrogen’s non-genomic effects, possibly through local production of NO (Mendelsohn, 2000). Women are at significantly less risk of developing cardiovascular disease during their pre-menopausal years. Studies have found that oestrogens can inhibit lipid accumulation and inflammation, as well as stimulate NO production (Miller and Duckles, 2008). The stimulation of NO production can protect against arterial stiffening (Miller and Duckles, 2008). There is a long history of clinical studies which have demonstrated that when oestrogen levels drop after menopause women become more prone to developing cardiovascular disease (Sullivan and Fowlkes, 1996).

In more recent years the relationship between oestrogens and cardiovascular risk has been questioned due to the inconclusive application of hormone replacement therapy (HRT) in women. HRT is a therapy which replaces the oestrogens lost during menopause and would theoretically give women protection from cardiovascular disease. The results of clinical trials have suggested that the outcome is more complex than this hypothesis suggests. In the 1998 HERS II study, there was no difference in cardiovascular outcomes between the oestrogen and progesterone treatment group and the placebo group (Hulley *et al.*, 2002). Another clinical trial performed by the Women's Health Initiative (WHI) found the risk of venous thromboembolism, stroke, and myocardial infarction was increased in women assigned to HRT (Petitti, 2002). Moreover, some trials were stopped due to the rising incidence of invasive breast cancer during the trial (Rossouw *et al.*, 2002).

1.8.4 Sex hormone-mediated pathways in CAVD

The androgen receptor activates downstream signalling pathways which have been associated with augmented calcification. These include WnT signalling and pathways containing NADPH (Nicotinamide adenine dinucleotide phosphate) and PPAR-γ (peroxisome proliferator-activated receptor gamma). Conversely, there is also evidence that the pathways being activated downstream of the AR are cardioprotective, including upregulation of NO, and downregulation of NFkB and caspases (primarily caspase 3) (Sritharen *et al.*, 2017b).

A study conducted on bone showed oestrogen being protective of inflammation by blocking infiltration of IL-1, IL-6 and TNF-α into osteoclasts. There is evidence in bone that oestradiol inhibits transcription of TLR2 and TLR4; therefore, blocking TNF-α, IL-6 and iNOS downstream of TLRs, which would reduce inflammation (Marie and Bonnelye, 2022). A clinical study demonstrated that female patients with aortic stenosis showed enhanced expression of inflammatory markers (including those downstream of NFκβ), despite normalising to aortic valve damage (Xiao *et al.*, 2017). Female patients also display increased collagen expression in the fibrosa and ventricularis of aortic valves. Increased platelet endothelial cell adhesion molecule 1 (PECAM1) expression has also been observed in the aortic valve of female patients, which may indicate higher rates of neovascularisation in the aortic valve (Xiao *et al.*, 2017). In response to LPS and IFN-α, cultured VICs derived from female patients had higher protein expression of VEGF-A and MMP1 without a pro-calcific response compared to VICs from male patients. In VICs derived from male patients, LPS and

IFN-α caused a pro-calcific and pro-angiogenic response (Parra-Izquierdo *et al.*, 2018). The sexual dimorphism in the development of CAVD is well-charactered in clinical yet the mechanism remains elusive. Despite the clinical presentation very few studies are conducted on sex differences and using female subjects in preclinical investigations of CAVD.

1.9 Animal models of valve calcification

1.9.1 Large animal models

The human cardiovascular system is complex, and when calcification develops, the diseased valve interacts with many biological systems including the immune and metabolic systems. Consequently, the disease is hard to model *in vitro*. Large animal models are more translatable to human pathology than murine models (Ziegler, Gonzalez and Blikslager, 2016). One of the most commonly used large models of calcification is pigs (porcine). The standard method of inducing vascular calcification in pigs is a high-cholesterol diet (van Ditzhuijzen *et al.*, 2016) (Sider *et al.*, 2014). Valve calcification induced in pigs has been shown to mimic human disease with calcification developing more readily on the aortic side of the valve (Simmons *et al.*, 2005). Studies including sex differences in porcine models are limited, although a few have been conducted on cultured VICs from pigs. One demonstrated that cells derived from male pigs had more calcification than those from females, combined with over-expression of calcification-related pathways including apoptosis and proliferation (Masjedi *et al.*, 2017). Genomic data have also been analysed which demonstrated a significant increase of osteogenic markers in cultured calcified porcine valve interstitial cells (PVICs). Porcine valves are so similar to their human equivalents that they can be used as replacement valves for humans. The benefit of porcine models is that they have comparable lipid profiles, and hemodynamic and valve anatomy to humans (Woodward *et al.*, 2021). As with humans, they also show age-dependent insulin resistance (Badin *et al.*, 2019). Lesions in the porcine aortic valve have also been observed to have similar pathological features to CAVD in humans, including a fibrosa with regions rich in proteoglycans, collagens and elastins (Sider *et al.*, 2014).

Another large animal model that can be used is the sheep (ovine) model. Ovine models have been used previously to model the outcomes of prosthetic valve implantation (Robb *et al.*, 2012). One ‘omics’ study has been conducted demonstrating a balance between genes that promote and suppress mineralization during development and across cardiovascular tissues (Tsang *et al.*, 2020). Cell culture models using sheep aortic valve interstitial cells (SVICs) and

vascular smooth muscle cells have shown that the cells mineralise when a pro-osteogenic medium is applied (Tsang *et al.*, 2018). Cultured SVICs also show expression of markers which are associated with calcification, including RUNX2 and PiT1(Tsang *et al.*, 2018).

The main advantage of large animal models is the size of the models, which means human equipment can be tested on them, and the aortic valve is sometimes even used to replace diseased human valves: for example, prosthetic valve implantations (Tsang *et al.*, 2016). Another advantage is these animal models have valve structures that are a close anatomical equivalent to valve structures in humans. The main issues with large model studies are the cost and the lack of available laboratory tools which are species-specific, including antibodies and assays (Tsang *et al.*, 2016). Some more problems of large animal models include the large amount of time these studies need to be conducted over compared to small animal studies. It is also more difficult to get licences and the provisions to carry out these experiments, especially in the UK.

1.9.2 Small animal models

A common example of a small animal model of CAVD is the rabbit (Sider, Blaser and Simmons, 2011). There are published methods to induce CAVD in rabbits including ageing rabbits on a Watanabe heritable hyperlipidaemic (WHHL) background to 30 months (Hara *et al.*, 2018). Although the more common method of inducing CAVD in rabbits is feeding them a combination of cholesterol and vitamin D (Drolet, Arsenault and Couet, 2003; Anousakis-Vlachochristou *et al.*, 2020). Calcification in rabbits has successfully displayed calcification through computerised tomography (CT) (Rajamannan *et al.*, 2005), von Kossa and alizarin red staining, micro positron emission tomography (PET) imaging (Choi, B. et al. (2017)) and increased expression of osteopontin (a marker of calcification) in the aortic root (Rajamannan *et al.*, 2005). Unfortunately, these studies were only conducted on male rabbits. The benefit of rabbit models is that, unlike mice, they have a tri-layered valve leaflet which is similar to that in humans. Rabbit models also provide a larger volume of tissue for analysis. The disadvantage is that rabbits are expensive, and fewer available laboratory reagents have been validated for use in rabbits.

Most *in vivo* studies performed on small animals are predominantly in mice and rats. To investigate cardiovascular calcification in rodent models, this pathological process must be artificially induced. The most common genetically mutated rodent model of cardiovascular

calcification is the apolipoprotein E knock-out ($ApoE^{-/-}$) mouse (Sider, Blaser and Simmons, 2011). This model induces dyslipidaemia which leads to atherosclerosis and intimal calcification of the atherosclerotic plaques; the low-density lipoprotein receptor (LDLR) knock-out ($LDLR^{-/-}$) model induces calcification in a similar way (Ishibashi *et al.*, 1993). Many variations of the $ApoE^{-/-}$ mice and $LDLR^{-/-}$ mouse exist and often are combined to produce calcification, for incidence the double $ApoE^{-/-}LDLR^{-/-}$ mouse (Lo Sasso *et al.*, 2016) and the triple $Lr^{-/-}ApoB^{100/100}IGF\text{-}II^{+/-}$ mouse (Fleury *et al.*, 2022). To note, these models are often combined with another insult to produce calcification, for incidence an $ApoE^{-/-}$ mouse on a high cholesterol diet (Lo Sasso *et al.*, 2016). The $ApoE^{-/-}$ model of calcification is the most commonly used because it develops both vascular and valvular calcification as well as aortic stenosis. Calcification has been observed in these mice with the addition of a cholesterol-rich diet, and aortic stenosis has been reported on a normal chow diet at 110-120 weeks of age in the $ApoE^{-/-}$ mouse (Tanaka *et al.*, 2005).

Many other murine models exists of vascular calcification although the valvular calcification in these models is not well-established. These include the ABCC6 model of medial calcification which has significantly reduced inorganic pyrophosphate (PPi) levels and exhibits ectopic mineralization in the blood vessels, aorta, eyes, kidneys and skin (Li *et al.*, 2017). Other genes which are targeted to induce calcification include Matrix Gla Protein (MGP) conditional knock-out, which alters vitamin K metabolism, and has been shown to produce vascular calcification, both intimal and medial (Jaminon *et al.*, 2020).

Another method of inducing calcification in mice is through the recently introduced surgical model: the wire injury model (Honda *et al.*, 2014). This model induces valve calcification through direct mechanical damage to the aortic valve, which can be graduated for different severities of disease (Niepmann *et al.*, 2019). Other ways to model calcification *in vivo* in mice are to use models of diseases where calcification is a consequence. An example of this is vascular calcification as a result of CKD; therefore, models of CKD can also be used to model calcification. These include the 5-6 nephrectomy model and dietary supplementation of vitamin D or adenine (Sider, Blaser and Simmons, 2011). Another example is klotho knock-out mice, which induces vascular calcification as a result of CKD (Hu *et al.*, 2011). Another common diet model of both vascular and valvular calcification is a high dose of warfarin, usually in rats (Sider, Blaser and Simmons, 2011).

There are many limitations to using mice to model human diseases and this is no different for calcification. The two main problems with modelling calcification are that firstly, mice do not naturally develop calcification and this disease must be artificially induced. Secondly, there are significant differences between the anatomy and physiology of the human and rodent cardiovascular systems. The human aortic valve has three layers in each valve leaflet whereas in mice it has two. Other differences between mice and humans include the composition of their blood and circulating blood lipid concentrations. The benefits of murine models are that they are relatively cost-effective and easy to maintain compared to large animal models. There are also many more techniques and reagents developed for use in murine models. Compared to *in vitro* assessment, small animal models allow for investigation into target effects of drugs which models the whole-body physiological system. There is also new state of the art imaging options for small animal models of CAVD including PET micro-CT and electron microscopy (Bogdanova *et al.*, 2022).

Table 1.1: Sex differences in rodent studies of cardiovascular calcification. In rats, increased calcification was observed in males. Studies in mice have demonstrated either no sex difference or increase incidence of calcification in females. ApoE- Apolipoprotein E, DHT- Dihydrotestosterone. Adapted from Woodward et al. (2021)

Model	Secondary Insult	Type of calcification	Sex differences in calcification	Ref
Mouse				
ApoE$^{-/-}$	Aged to 36 weeks	Vascular and valvular	↑ calcification in females (aortic sinus)	(McRobb *et al.*, 2017)
ApoE$^{-/-}$	Crossed with *Itga8$^{-/-}$*	Vascular	↑ calcification in females	(McRobb *et al.*, 2017)
Klotho$^{-/-}$		Vascular	None	(Tang *et al.*, 2020)
Klotho$^{-/-}$		Vascular	None	(Shah *et al.*, 2019)
ApoE$^{-/-}$		Vascular, aortic sinus	↑ calcification in females	(McRobb, Handelsman and Heather, 2009)
ApoE$^{-/-}$	18 months	Vascular	More vascular calcification in males	(Hartley *et al.*, 2000)
ApoE$^{-/-}$	Uraemia	Vascular	↑ calcification in females	(Qiao *et al.*, 1994)
C57Bl/6J		Vascular	None	(Qiao *et al.*, 1994)
ApoA-II		Vascular	None	(Qiao *et al.*, 1994)
ApoE$^{-/-}$		Vascular	↑ calcification in females	(Qiao *et al.*, 1994)
ApoE$^{-/-}$	Hyperlipidaemic diet	Vascular	↑ calcification in females (medial arteries)	(Wang *et al.*, 2009)
Rat				
Fisher	1α-Hydroxyvitamin D3	Vascular	↑ calcification in males	(Ng *et al.*, 2011)
Wistar		Vascular	↑ calcification in males	(Kohn, Price and Pelz, 2008)
Lewis Polycystic Kidney		Vascular	None	(Ng *et al.*, 2011)

1.10 Current interventions

1.10.1 Surgical intervention

The most common treatment for aortic stenosis is transcatheter aortic valve replacement (TAVR). This surgery replaces the stenotic aortic valve with a prosthetic valve. The process involves insertion, via a catheter, of a stainless-steel stent with an attached equine or bovine pericardial trileaflet valve. Once in place, this prosthesis is expanded using a balloon (Horvath *et al.*, 2011). The first type of prosthetic valve was the Starr–Edwards caged-ball mechanical valve, first developed in 1960 (Amrane *et al.*, 2017). Many other mechanical valves have been developed since this initial design, including the disk valves (low profile (flat lying) mechanical prosthesis with a small size, which would not intrude on the left ventricular cavity) and omniscience valve (polyester knit sewing ring) (Rajashekar, 2015). The Medtronic Hall valve has titanium housing, a Teflon sewing ring, and a carbon-coated disc (Svennevig, Abdelnoor and Nitter-Hauge, 2007).

For aortic valve replacement, there are also two types of biological valves: bioprosthetic valves (derived from bovine/ porcine/ equine tissues), and true biological valves (including tissue grafts) (Ali and Chowdhury, 2022). The main type of bioprosthetic valve is porcine, where a valve taken from a porcine donor is sewn onto a stent to allow for successful implantation (Aslam *et al.*, 2007). Other than porcine, the next most common bioprosthetic valves are bovine. These are usually made out of the bovine pericardium which is mounted on a frame (Dellgren *et al.*, 2002). Grafts are obtained from human heart donors, where the heart valve and the peri-annular tissue are taken from the donor (Ali and Chowdhury, 2022). These are though less frequently available.

Despite having well-developed surgical interventions for CAVD, there is a clear need for pharmaceutical interventions. This is because there are many complications associated with surgery. Firstly, patients with mechanical valves are prone to thrombus developing in the valve (Roudaut, Serri and Lafitte, 2007). Furthermore, patients with valve replacements usually have to be maintained on anticoagulants and, depending on the type of valve replacement, immunosuppressants for the rest of their life (Panduranga *et al.*, 2012). Anticoagulants can lead to complications with bleeding, which may be a small risk at first but can accumulate substantially over the patient's lifetime (Panduranga *et al.*, 2012). Immunosuppressants cause significant side effects, including gastrointestinal (GI) upset, neurotoxicity, nephrotoxicity and

development of new-onset diabetes after transplant (NODAT) (Mecadon, 2021). Furthermore, there are many high risks of being immunosuppressed. These include an increased likelihood of contracting and dying from pathogens including viruses and bacteria. The foremost issue with surgery is the risk of post-surgical death. Despite reports that this is low (for example 4 % in bovine replacement), this risk can increase as patients with CAVD also can have significant other co-morbidities, including diabetes, CKD and aged patients may be unsuitable candidates for surgery (Dellgren *et al.*, 2002). These problems are why there is a strive to develop new drugs for CAVD.

1.10.2 Drug interventions

There are currently no successful drugs which reverse valve calcification. One of the previous candidates was statins (3-Hydroxy-3-methylglutaryl-coenzyme A (HMG-CoA) reductase inhibitors). Statins have been used since the 1980s and significantly reduce cardiovascular mortality and morbidity (Gould *et al.*, 1998). Statins were proposed to treat CAVD since they lower cholesterol and lipid levels (which are risk factors for CAVD) and potentially reduce inflammation (involved in the propagation of CAVD) (Libby and Aikawa, 2003). There have been many clinical trials for use of statins in CAVD, with mixed results. For those studies which displayed positive results, a 2001 retrospective study found patients who were using statins had a slight improvement in aortic valve remodelling and a decrease in peak aortic velocity (Aronow *et al.*, 2001). The 2007 RAAVE trial saw that statins slowed the progression of the haemodynamic changes that develop with CAVD (Moura *et al.*, 2007). On the other hand, many clinical studies have found no effect of statins. Examples of this include the SALTIRE and SALTIRE II trials which found no change in valve calcification or disease pathology and the more recent 2010 SEAS and ASTRONOMER trials which also found no difference (Gerdts *et al.*, 2010; Chan *et al.*, 2010). Another drug which was designed to target lipid levels includes Niacin or nicotinic acid. This drug was proposed to lower LDL and increase HDL. A trial conducted on extended-release niacin (ERN) did not show a significant change in the risk of cardiovascular outcomes compared to a placebo (Nakamura *et al.*, 2003; Kalil *et al.*, 2015).

Another potential drug target that was investigated for use in CAVD is angiotensin II. Stenotic aortic valves have significantly higher expression levels of enzymes associated with angiotensin II production such as mast cell (MC)-derived chymase and angiotensin-converting enzyme (ACE), as well as high expression of the angiotensin II type 1 receptor (O'Brien *et*

al., 2002; Helske *et al.*, 2004). Angiotensin II-receptor blockers (ARBs) can also depress TGF-β1 signalling, which has been associated with the development of valve disease (Fang *et al.*, 2018). Again, the results of angiotensin II-targeting trials have had mixed conclusions. A retrospective study performed to model the effectiveness of targeting angiotensin in CAVD found the positive effects were inconclusive (Olsen *et al.*, 2004). A contrasting study found patients treated with ARBs had significantly slower progression of CAVD and reduced mortality than those with any other treatment (Nadir *et al.*, 2011).

There are many further proposed drug targets for CAVD, including cadherin-11. Cadherin-11 is associated with fibrotic remodelling and is upregulated in osteoblasts (Okazaki *et al.*, 1994) and calcific regions of leaflets from patients (Hutcheson *et al.*, 2013). Another proposed drug target for CAVD is purinergic signalling, specifically, the P2Y receptor family. Many P2Y receptors have been identified as potential drug targets (Orriss and Arnett, 2012), and specifically P2Y 2R has been shown to promote the expression of carbonic anhydrase CAXII and can regress calcification in mice (Bouchareb *et al.*, 2015). Other groups of drugs that were investigated for use in CAVD were calcimimetics such as cinacalcet (Kim and Hwang, 2021). Unfortunately, no successful therapies have been yet developed from these proposed targets.

The reason for the current lack of success of drug interventions for calcification is unknown. The failure may be because the current molecular mechanisms behind the development of CAVD are also unknown. The translatability of murine models of CAVD has also been put into question (Sider, Blaser and Simmons, 2011). A further obstacle to understanding the pathophysiology of calcification is the lack of understanding of the sexual dimorphism of this disease. Females are severely underrepresented in preclinical testing, even for CAVD, which shows a unique pathology in women. One study reported that in biological and medical science, 80 % of studies that specified sex used only male subjects (Holdcroft, 2007). Elucidating the mechanisms behind the sexual dimorphism in CAVD could provide crucial insight into further disease mechanisms and drug targets of this extremely prevalent illness.

1.11 Study hypothesis and aims

Hypothesis: Male sex hormones drive calcification, leading to calcific aortic valve disease, and murine models of calcification will reflect the sexual dimorphism seen in humans.

Aims:

1. To determine whether male sex hormones promote calcification in valve interstitial cells.

2. To determine whether atherosclerotic male mice develop more extensive valve calcification than females.

3. To establish the wire injury surgical model of calcific aortic valve disease, first developed by Honda and colleagues (Honda *et al.*, 2014), and determine any sexual dimorphism in response to the wire injury of the aortic valve.

Chapter 2: Material and Methods

2.0 Chapter 2: Materials and Methods

2.1 Materials

2.1.1 Chemicals and reagents

Unless otherwise stated all chemicals and reagents were purchased from Sigma-Aldrich (Gillingham, UK).

2.1.2 Buffers

Phosphate Buffered Saline (PBS): 10 x PBS tablets (Thermo-Fisher Scientific, Renfrew, UK) were dissolved in 1000 mL distilled H_2O. PBS was stored at room temperature.

Sodium citrate buffer: The buffer was first made in a 10 x concentration. This contained tri-sodium citrate (dehydrate) 29.4 g dissolved in 1000 mL of distilled H_2O. This was diluted 1:10 in distilled H_2O with 0.1 % Tween-20, and pH adjusted to 6.0.

Western running buffer: NuPAGE™ MOPS SDS Running Buffer (20X) (Thermo-Fisher Scientific, Renfrew, UK) was dissolved in a 1:20 ratio in distilled H_2O.

Western transfer buffer: 480 mM Tris Base, 390mM Glycine, 20 % ethanol and were diluted in 100 mL distilled H_2O.

Hank's Balanced Salt Solution (HBSS): Purchased from Thermo-Fisher Scientific (Renfrew, UK).

2.1.3 Sex hormones

For *in vitro* investigations, all hormones purchased (Sigma-Aldrich, Gillingham, UK) were diluted in dimethyl sulfoxide (DMSO) to 1 M stock and kept at -20 ^{o}C. Stocks were diluted incrementally to an appropriate final concentration in DMSO. Hormones were added directly to cell culture media and the final concentration of DMSO was kept constant throughout experimental groups.

2.1.4 Software

See table for software details:

Table 1.1: Table of software and manufacturers

Software	**Use**	**Manufacturer**
Zen Blue edition	LSM 710 confocal microscope/ Zeiss Imager Z1/Image capture	Carl Zeiss Microscopy (Cambridge, UK)
ImageJ	Image analysis	See PMID 22743772
Vevo LAB	Ultrasound image quantification	FUJIFILM VisualSonics, (Geesinkweg, Amsterdam)
PMOD	PET/CT image quantification	PMOD Technologies LLC (Zürich, Switzerland)
CTan	Analysis of μ-CT	Skyscan, Bruker (Kontich, Belgium)
NRecon	Reconstruction of μ-CT	Skyscan, Bruker (Kontich, Belgium)
MXPro	RT-qPCR	Aligent (Santa Clara, USA)
Nanodrop 100 software v3.8.1	Nanodrop, analysis of RNA quality	Thermo-Fisher Scientific, (Renfrew, UK)
GeneTools	Western chemiluminescence image capture	Syngene (Cambridge, UK)
Gen5	Plate reader	BioTek Instruments (Winooski, USA)
Prism 8	Statistical analysis	GraphPad (San Diego, USA)
Perseus	Analysis of proteomics data	Max-Planck-Institute of Biochemistry (Planegg, Germany)
Cytoscape	Visualisation of protein networks	Institute for Systems Biology (Seattle, USA).

2.1.5 Plastics

All sterile tissue culture plastics were purchased from Corning® (Ewloe, UK).

2.2 Animals

C57Bl6/J and Apolipoprotein E (ApoE)$^{-/-}$J mice were purchased from Envigo (Blackthorn, UK) or Charles River (Elphinstone, UK). All mice were group housed on a 12-hour light/dark cycle at 22-24 ºC and 55 % humidity. Mice were provided *ad libitum* access to water, chow, and environmental enrichment. Experimental groups were aged-matched. All procedures were performed in accordance with the UK Home Office, under Home Office Licences (Project licence: PFF7D0506, Personal licence: I8A164EDC) and the University of Edinburgh Ethics guidelines.

2.3 In vivo echocardiography imaging

Mice were anaesthetised using isoflurane inhalation (Zoetis Ltd., Leatherhead, UK) mixed with oxygen, with induction of anaesthesia induced at 4-5 % isoflurane and maintained at 1-3 %. The depth of anaesthesia was confirmed using the plantar reflex test. Mice were placed supine on a heated monitoring imaging table. Parker Spectra 360 Electrode Gel (Parker Laboratories Inc., Fairfield, USA) was applied to paws, then paws were taped to table electrocardiogram (ECG) electrodes to monitor ECG, respiration, and heart rate (450-550 bpm). Body temperature was measured using a rectal probe and maintained at 37 ºC ± 0.5 ºC. Thoracic hair was removed using depilation cream (Nair™ hair removal cream, Church & Dwight, Folkestone, UK). Parkers' Aquasonic 100 ultrasound gel was applied before imaging. Echocardiography measurements were acquired using a VisualSonics Vevo 3100 high-frequency ultrasound imaging system (FUJIFILM VisualSonics, Inc. Yonge Street, Toronto, Canada) with an MX550D transducer (centre transmit frequency: 40 MHz Axial and Resolution: 40 μm) (Castellan *et al.*, 2020).

Echo kilohertz visualisation (EKV) imaging of the LV was acquired in the parasternal long axis view (PSLA). M mode images in the parasternal short axis were taken at the LV midpoint with the papillary muscles visible at 2 and 4 o'clock positions to enable LV cardiac functional measurements. Measurements taken or calculated from measurements taken, from images acquired in the PSLA, include left ventricular mass (mg), left ventricular wall thickness (mm),

cardiac output (mL/min) and ejection fraction (%) and M mode measurements were taken including fractional shortening (FS) (%), posterior wall thickness (mm, PWT), left ventricular end-diastolic diameter (LVEDD) (mm) and left ventricular end-systolic diameter (LVESD) (mm).

For aortic valve function, images of the aortic valve (AV) and ascending aorta (AA) were initially acquired in B mode of either a modified right-side PSLA or a Suprasternal view. Colour Doppler was utilised for the optimal placement of the Pulse-wave Doppler sample window in the ascending aorta (above the aortic valve). This facilitated the correct Doppler angle between the incident ultrasound beam and the direction of blood flow, for accurate velocity measurements and aortic function. Aortic function measurements that were taken include velocity time integral (VTI, mm), peak velocity (mm/s), mean gradient (mmHg), and peak gradient (mmHg)). Echocardiography scans were performed by myself and Adrian Thomson (Edinburgh Pre-clinical Imaging Facility). Diagrams of how the echocardiography measurements were taken and the calculations behind the parameter are described in Appendix III.

2.4 Wire injury aortic stenosis murine model development

2.4.1 Mice

C57Bl/6 mice were kept on a standard chow diet with standard environmental conditions stated in Section 2.2. Males and females were age-matched. All surgeries took place between 12-16 weeks of age, depending on individual study requirements.

2.4.2 Surgery

The surgical procedure followed that described by Honda *et al.* (2014). Mice were anaesthetised (as described in Section 2.3) and the depth of anaesthesia was confirmed using the plantar reflex test. Mice were given a subcutaneous injection of Vetergesic (Cera, Redditch, UK, Buprenorphine, 0.05mg/kg body weight). Blunt dissection was used to expose the right carotid artery. The artery was ligated immediately proximal to the carotid bifurcation. A temporary ligature was placed proximally to control blood flow and an arteriotomy was performed. A straight-sprung angioplasty guidewire (0.014” diameter, Cook Medical, Limerick, Ireland) was inserted into the carotid artery. Under ultrasound guidance, the wire

was advanced through the artery, across the aortic valve and into the left ventricle (Figure 2.1). The wire was then advanced back and forth across the aortic valve. Finally, the wire was removed, the artery ligated, and the wound sutured. Vetbond Tissue Adhesive was used to secure the wound (3M, Bracknell, UK) (Honda *et al.*, 2014).

2.4.3 Tissue collection after wire injury

At the end of the experiment, mice were culled by exposure to increasing concentrations of CO_2, with death confirmed by cervical dislocation. Hearts were harvested and fixed in 10 % neutral buffered formalin (NBF) for 24 hours before being transferred to 70 % ethanol.

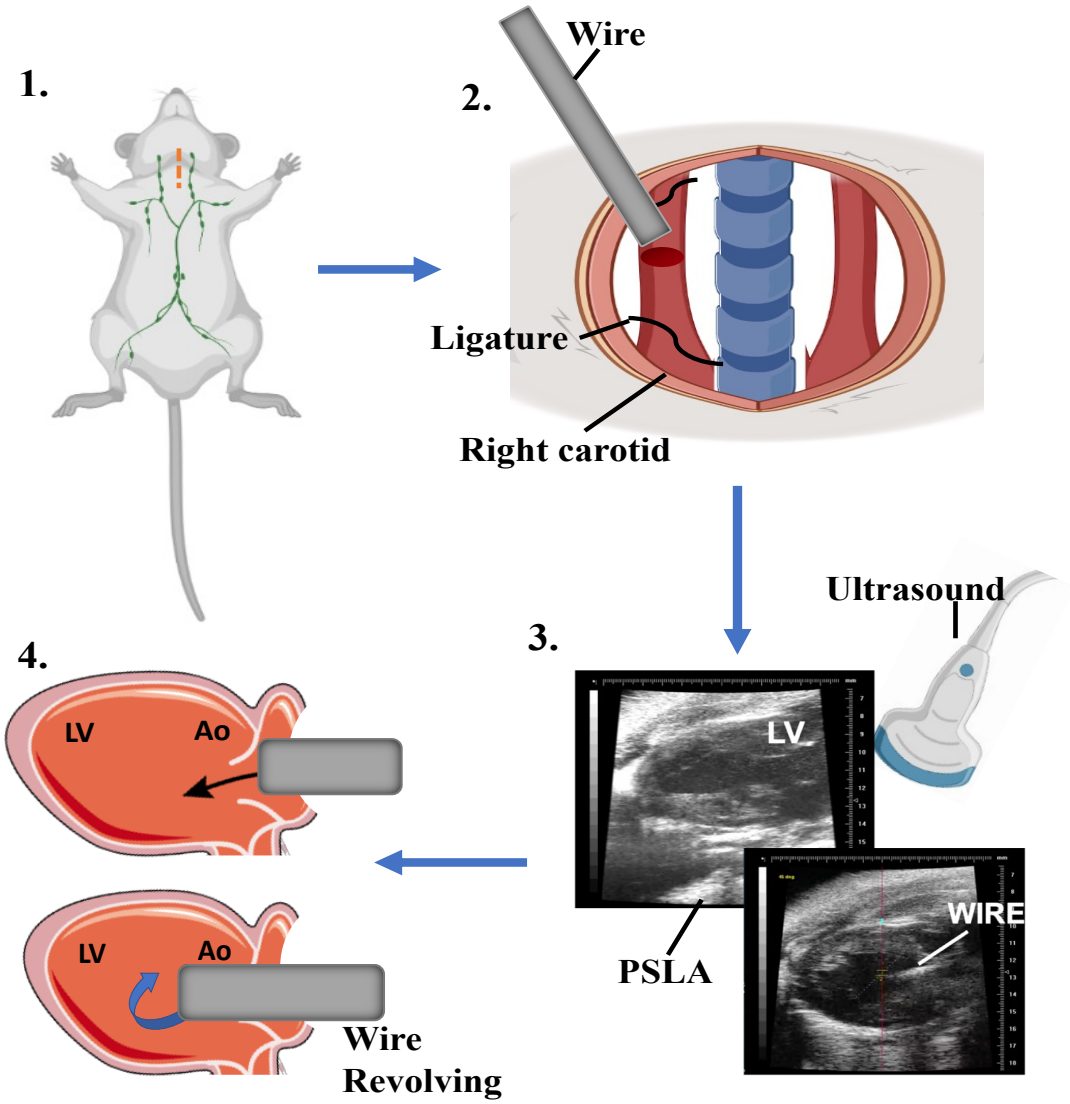

Figure 2.1: Schematic diagram of wire injury surgery. The wire injury surgery follows four main steps. 1) Mouse is anaesthetised, and a transverse incision made across the neck. 2) Blunt dissection exposes the right carotid artery where it is ligated distally, and a wire is inserted into the artery. 3) Ultrasound imaging of the heart (in PSLA- parasternal long axis view) guides the wire into the left ventricle. 4) The wire is advanced back and forth across the aortic valve and rotated to ensure damage. LV- left ventricle. Ao- Aortic valve. Figure made using BioRender and Microsoft PowerPoint. Protocol based on previously published method by Honda *et al.* (2014).

2.5 ApoE$^{-/-}$ sex difference study

2.5.1 Mice

In vivo studies used ApoE$^{-/-}$ mice on a C57Bl6/J background (Charles River, Tranent, UK). Male and female mice were aged to 20-26 weeks and the diet was altered for the following 12 weeks to a western diet (Research Diets, USA). Mice were weighed weekly after diet alteration.

2.5.2 Tissue collections for ApoE$^{-/-}$ study

At the end of the experiment, mice were culled by exposure to increasing concentrations of CO_2 and death was confirmed by cervical dislocation. Blood was collected rapidly from the cervical cavity, using a syringe without a needle, and stored in anticoagulant ethylenediaminetetraacetic acid (EDTA)-treated tubes (Sarstedt, Leicester, UK). Plasma was separated from whole blood by centrifugation (2000 g x 10 min at 4 °C) for storage at -20 °C. Hearts and aortas were isolated, weighed, and fixed in NBF for 24 hours before transfer to 70 % ethanol and kept at room temperature. Livers, fat pads, kidneys and leg bones were removed, weighed, and halved (half snap frozen in liquid nitrogen and stored at -80 °C and half fixed in NBF for 24 hours before transfer to 70 % ethanol and kept at room temperature).

2.6 Ex Vivo imaging

2.6.1 Positron emission tomography (PET)/ Computed tomography (CT) imaging

18F-NaF micro-PET/computed tomography (micro-PET/CT) was used for the detection of hydroxyapatite (as a marker of calcification) (Creager *et al.*, 2019). Hearts and aortas were placed in 10 % NBF (Sigma-Aldrich, Gillingham, UK) for 24 hours and then transferred to 0.1M PBS. Tissues were incubated in an 18F-Sodium fluoride (100 ± 2.35 kBq/mL) PBS solution for 1 hour and then washed twice in 0.1 M PBS (1 minute per wash). Tissues were then mounted on a Petri dish for imaging (nanoPET/CT, Mediso, Budapest, Hungary).

Specimens were scanned using high-resolution microPET (1:5 coincidence mode, acquisition time 30 minutes) and microCT (semi-circular full trajectory, maximum field of view 360 projections and maximum zoom 720 projection, 300 ms, 50 kVp 1:4 binning; Mediso nanoScan PET/CT, Mediso Medical Imaging Systems, Hungary). PET data were reconstructed using Mediso iterative Tera-Tomo 3D reconstruction algorithm. This algorithm used 4 iterations, 6 subsets, full detector model, spike filter on, normal regularization a 400 to 600 keV energy

window and voxel size of 0.4 mm. CT data were reconstructed using filtered back projection (FBP). Scans were performed by Carlos Alcaide Corral of the Preclinical Imaging Facility at the University of Edinburgh. Analysis of PET/CT data was performed on PMOD 3.7 software (PMOD Technologies, Zurich, Switzerland). When analysing scans, a volume of interest (VOI) was drawn around each tissue in every section. VOIs were drawn on overlayed CT scans to eliminate the inclusion of unspecific PET signal. Both the measurement for averages and hot averages were calculated by PMOD software (MacAskill *et al.*, 2020).

2.6.2 Micro-computed tomography (μ-CT) imaging

Tibiae were fixed in NBF (10 %) and stored in 70 % ethanol prior to scanning. Bones were scanned using a micro-computed tomography (μ-CT) system (Skycan 1173, Bruker, Kontich, Belgium) to determine the trabecular architecture and cortical geometry. High-resolution scans were acquired with a 5 μM pixel size, 0.5 mm AI filter, 0.6 rotations steps and X-Ray set to 60 volts and 167 amps (Staines *et al.*, 2020). Tibiae were scanned in pairs with a lag time of approximately 2 hours per scan. CT scans were reconstructed using NRecon software.

For trabecular analysis, the growth plate was used as a reference point. Bone sections were taken from 5 % of the total bone length below the growth plate. Growth plate was identified in the μ-CT scans by a consistent observer. Trabecular analysis was performed between this point and the 250 sections below. Cortical analysis was conducted at three points, 37 %, 50 %, and 70 % of the bone length from the top of the bone (Lim *et al.*, 2015). For each of these points, 100 sections were analysed. For cortical analysis bone was detected with a consistent threshold of 100 to 255 (previously optimised) on the image histogram, demonstrated in Figure 2.2**.**

The following parameters were analysed using CTan software. In trabecular bone, trabecular number (TB.N;/mm), trabecular thickness (Tb.Th; mm), trabecular separation (Tb.Sp), bone volume (BV/TV) and structural model index (SMI) were evaluated. For cortical bone, % BV/TV, BMD (g/cm^3), cortical thickness, cross-sectional area (mm^2) and percentage porosity (Po.op %) were measured.

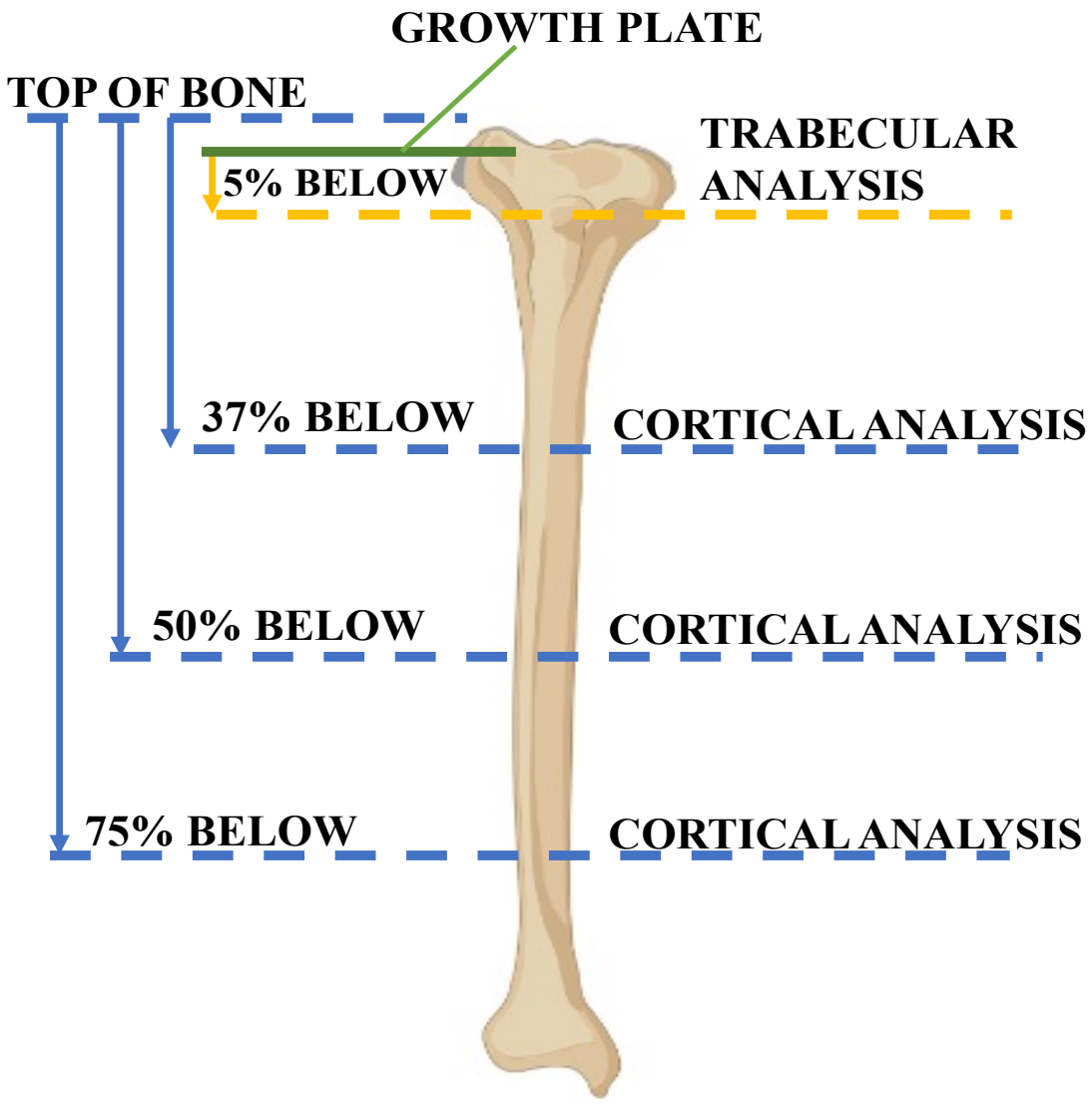

Figure 2.2: Figure demonstrating analysis point of the tibia bone. This figure demonstrates the points that were chosen to conduct bone analysis. The green line represents the growth plate. Trabecular analysis is in yellow. Cortical analysis is in blue.

2.7 Histology

2.7.1 Processing

Mice were culled by asphyxiation in CO_2 and death was confirmed with cervical dislocation. After CO_2 inhalation, tissues were isolated, immersed in 10 % NBF, and stored for 24 hours at 4 °C then transferred to 70 % ethanol at room temperature. A labelled histology image of the aortic valve is seen in Figure 2.3.

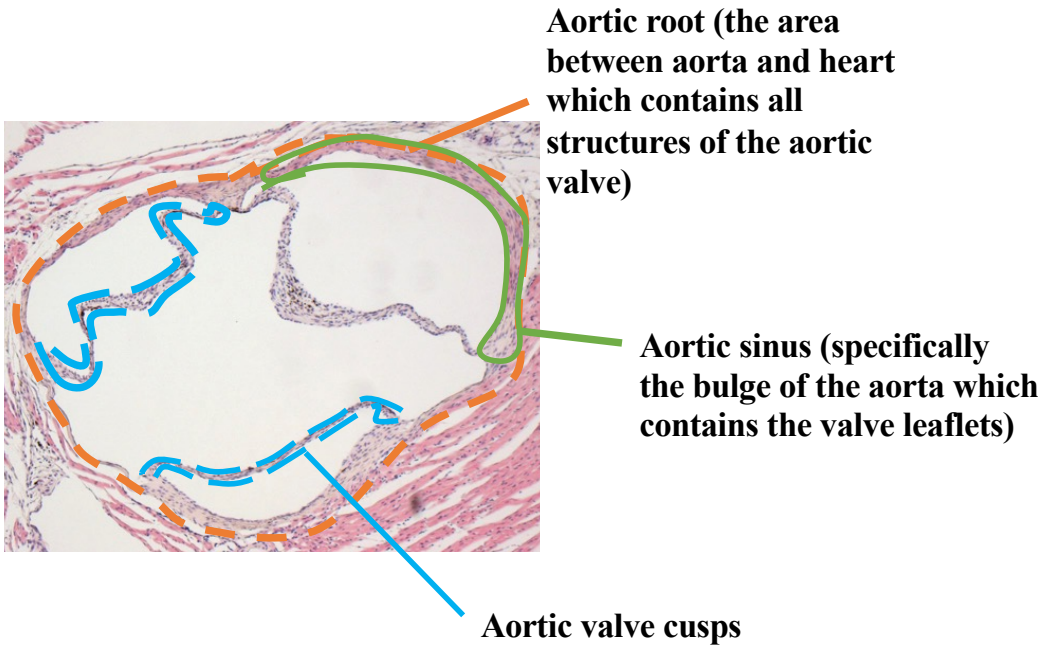

Figure 2.3: Examples of aortic root histology. The figure demonstrates Haematoxylin and Eosin (H&E) staining of the aortic root. The aortic root is labelled in orange, the valve cusps are labelled in blue and the aortic sinus is labeled in green.

2.7.2 Processing for staining

For aortic valve histology, fixed hearts were cut transversely below the atria. The top half (containing the aortic root and atria) was embedded. Embedding was carried out at the histology core at The University of Edinburgh's Shared University Research Facilities (SuRF). Tissues were processed and embedded in Sakura Tissue-Tek III paraffin wax (melting point 54 – 57 °C). Tissue sections were cut using a Peloris Tissue Processor (Leica, microsystems, Germany) into 6 µm sections. Sections were floated on the surface of a 45 ºC water bath (Sakura Finetek Europe, The Netherlands), to remove wrinkles and then mounted onto Superfrost Plus glass slides (Thermo-Fisher Scientific, Renfrew, UK). Slides were dried overnight at 37 °C to ensure adhesion. For both aortic valve and brachiocephalic arterial processing, sections were observed using light microscopy to confirm whole tissue sectioning.

2.7.3 Staining

2.7.3.1 Haematoxylin and eosin (H&E):

Slides were submerged in two rounds of xylene (Sigma-Aldrich, Gillingham, UK) for 5 mins each, to remove paraffin wax. Slides were then rehydrated in decreasing concentrations of ethanol (100 %, 90 %, 80 %, 70 %) for 20 seconds each. Next, they were submerged in

haematoxylin (DakoCytomation, Ely, UK) for 5 mins and acid ethanol (1 % HCl, 70 % ethanol) for 20 seconds. Slides were then transferred to eosin (Sigma, Gillingham, UK) for 10 seconds and then were then dehydrated using increasing concentrations of ethanol (70 %, 80 %, 90 %, 100 %) for 20 seconds each. They were then mounted using xylene and imaged using an AxioImager Z1 microscope (Zeiss, Cambridge, UK).

2.7.3.2 Masson's trichrome:

Masson's Trichrome: Masson's Trichrome staining (MT) was carried out at the histology core at The University of Edinburgh's SuRF using established protocols as described below.

Steps for Masson's Trichrome:

1. Slides were submerged in two rounds of xylene for 5 minutes each.
2. Slides were then rehydrated in decreasing concentrations of ethanol (100 %, 90 %, 80 %, 70 %) for 20 s each.
3. Slides were incubated in Bouin solution overnight at room temperature and were then washed in tap water.
4. Slides were transferred to Wiegert's iron haematoxylin solution and were then washed in deionised water (dH_2O).
5. They were next stained with trichrome stain (Sigma-Aldrich, Gillingham, UK) and rinsed again in dH_2O.
6. Slides were then transferred to phosphotungstic/ phosphomolybdic acid solution.
7. They were then counterstained in Aniline Blue and immersed in 0.2 % acetic acid solution.
8. Slides were washed in dH_2O and dehydrated in increasing concentrations of industrial methylated spirit (IMS) (95 % then 100 %).
9. Slides were then cleared in xylene and mounted.

2.7.3.3 Alizarin red

Paraffin-embedded slides were de-waxed by submersion in xylene (7-10 minutes). Slides were then rehydrated in decreasing concentrations of ethanol (100 %, 90 %, 80 %, 70 %). Slides were submerged in a 2 % alizarin red solution (pH 4.1-4.2) from 30 seconds to 5 minutes and the reaction was observed microscopically. They were then dehydrated in acetone and acetone-xylene (1:1) solution, 20 dips each and finally cleared in 100 % xylene. Slides were mounted in a synthetic mounting medium.

2.7.3.4 Von kossa

Von Kossa staining was carried out in the histology core at The University of Edinburgh's SuRF. Briefly, slides were submerged in two rounds of xylene (Sigma-Aldrich, Gillingham, UK) for 5 mins each. Slides were then rehydrated in decreasing concentrations of ethanol (100 %, 90 %, 80 %, 70 %) for 20 s each. Samples were placed in 2 % silver nitrate solution and exposed to strong light. Positive control samples became dark brown to black in colour which was observed microscopically. Samples were washed in dH_2O and then transferred to sodium thiosulphate solution. Finally, samples were counterstained with green solution and had a final wash in dH_20. Samples were then dehydrated in increasing concentrations of ethanol and mounted (as in section 2.7.3.1).

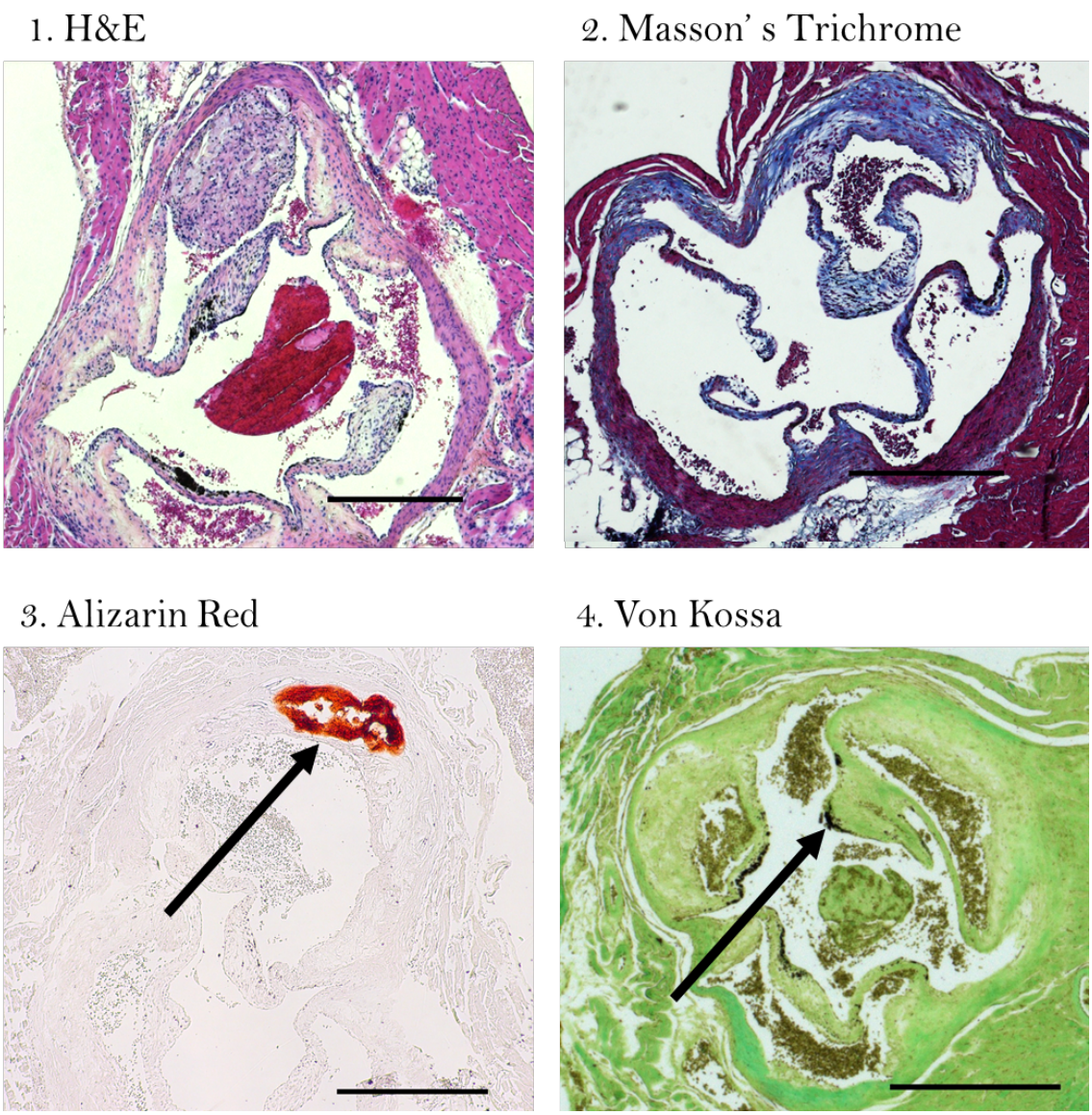

Figure 2.4: Examples of histology positive staining. This figure displays examples of positive staining that has been used for each histological stain 1. Haematoxylin and Eosin (H&E) 2. Masson's Trichrome 3. Alizarin Red 4. Von Kossa. The arrows indicate positive calcium staining. Black lines on the graphs represents 400 µM.

2.7.4 Immunohistochemistry Mac2/CD31/aSMA

Slides were deparaffinised in xylene (two incubations of 5 minutes) and then rehydrated in decreasing concentrations of ethanol for 20 seconds each (100 %, 90 %, 80 %, 70 %). Antigen retrieval was performed in sodium citrate buffer (pH6, 10 mM) for 5 minutes and heated to boiling point. Slides were blocked for 1 hour with 10 % goat serum. All primary antibodies were incubated overnight at 4^{o}C at the following dilutions: α-SMA-cy3 (Sigma-Aldrich, Gillingham, UK, C6198P) 1:1250, Mac2 (Cedarlane, Burlington, Canada) 1:800, and CD31 (Ab28364) 1:50. Secondary antibodies were incubated at room temperature for 1 hour and used at 1:500 (Goat anti-Rat 488, Abcam, A-31570 and Goat anti-Rabbit 647, Life Technologies, A21244). Slides were stained with DAPI (Sigma-Aldrich, D9542) and then mounted using Permafluor Mountant (Thermo-Fisher Scientific, Renfrew, UK, TA-030-FM).

2.7.5 Analysis of histology

2.7.5.1 Quantification of tissue area

After capture on ZEN blue software images were converted to TIFF files. Analysis was performed on ImageJ software. Scaling was directly imported into ImageJ and checked manually. The area was calculated by using ImageJ freehand drawing tool and measuring tool. For aortic valves, each cusp was measured, and an average cusp area was calculated. For atherosclerotic plaque measurements, plaques and lumens were measured and then percentage occlusion was calculated.

2.7.5.2 Quantification of staining

After capture on ZEN blue software images were converted to Big TIFF files. Analysis was performed on ImageJ software. Scaling was directly imported into ImageJ and checked manually. For all stains, images were converted into RGB-type images. Colours were then separated using the ‘colour devolution’ tool. Within this, automated plugins are available to analyse histological stains. Once positive stains were separated, the positive area was selected using the ‘colour threshold’ and measured. Finally, the positive area was normalised to the tissue area. Tissue area is drawn manually around the whole tissue and calculated using ImageJ software.

2.8 Cell culture

2.8.1 Source of cells

2.8.1.1 Valve cell line: The rat valve interstitial cell line, RVIC Sv40T, was generated by transducing rat valve interstitial cells (VICs) with recombinant lentivirus expressing Simian virus (SV) 40 large T antigen. Immortalisation of these cells was achieved by silencing the expression of tumour suppressors including p53 and retinoblastoma protein (Rb) through a siRNA expressed by the lentivirus. Production of this cell line was carried out by Capital Biosciences, Gaithersburg, USA (Cui *et al.*, 2017a). Cells were used between passages 12-20 for experiments.

2.8.1.2 Rat valve interstitial cells (VICs): All primary cell extractions took place in a ventilated hood and tools were sterilised by autoclaving prior to dissection. VICs were obtained from 5-week-old, Sprague Dawley rats. Rats were culled by cervical dislocation. The abdomen was dissected laterally. The ribcage, lungs and fatty tissues were gross dissected to expose the heart and the aorta. The heart and aorta were extracted and placed in cold HBSS. These tissues were separated just above the aortic root. To extract heart valves, the cardiac muscle was trimmed to expose the aorta and aortic root. Under a microscope, the aortic root was opened, and valve leaflets dissected out. The leaflets were stored in cold wash buffer (2.1.2) until all dissections were complete. Once all leaflets were dissected, they were centrifuged at 100 g, for 1 minute to pellet and separate the HBSS. The leaflets were then digested in 100 µL (425 U/mL) of Collagenase II (Worthington, New Jersey, USA) for 5 minutes at 37°C. Next, they were centrifuged again for 30 seconds at 100 g. The supernatant was removed, the pellet was washed in 500 µL of HBSS and centrifugation was repeated. The supernatant was discarded, and the pellet was digested with 100 µL (425 U/mL) of Collagenase II (Worthington) for 2 hours, at 37 °C. The VICs were spun at 670 g for 5 minutes and transferred to a flask (Corning, Surrey, UK.

2.8.1.3 Primary mouse aortic vascular smooth muscle cells: Aortas were isolated (as above) using the same techniques in both mouse and rat samples. Once the aortas were isolated all connective tissue and adventitia from the aortas were removed using gross dissection. The aortas were cut longitudinally, and the endothelial layer was removed using sterile cotton swabs soaked in Minimum Essential Media (MEM) (see 2.8.2). Aortas were digested in Collagenase

II (175 U/mL) for 20 minutes at 37 °C. Tissues were then centrifuged for 1 minute at 28 g, the supernatant removed, and the pellet washed in MEM. Samples were then digested in Collagenase II (175 U/mL) and Elastase type III (0.25 mg/ml) for 45-60 minutes at 37 °C. The tube was disturbed every 10 minutes. An equal volume of media was added, and cells were centrifuged at 112 g for 5 minutes. The supernatant was removed. Cells were then re-suspended in media and placed in a sterile incubator (37 °C, 5 % CO_2).

2.8.2 Cell culture media

Primary RVICs and RVIC Sv40T: Cells were cultured in Phenol Red-free F-12 Dulbecco's Modified Eagle Medium (DMEM F-12) (Thermo-Fisher Scientific, Renfrew, UK) supplemented with 1 % gentamicin (Thermo-Fisher Scientific, Renfrew, UK) and 10 % heat-inactivated foetal bovine serum (FBS) (Thermo-Fisher Scientific, Renfrew, UK). FBS was sterilised by passaging through a 0.22 μm filter.

Primary aortic smooth muscle cells- Smooth muscle cells were cultured in minimum essential media (MEM) α **(**Thermo-Fisher Scientific, Renfrew, UK) supplemented with 1 % gentamicin (Thermo-Fisher Scientific, Renfrew, UK) and 10 % heat-inactivated foetal bovine serum (FBS) (Thermo-Fisher Scientific, Renfrew, UK). FBS was sterilised by passaging through a 0.22 μm filter (Lin *et al.*, 2017a).

Media for freezing cells- The freezing mixture was made by combining 60 % DMEM F-12 (Thermo-Fisher Scientific, Renfrew, UK) with 20 % heat-inactivated FBS and 20 % DMSO (Thermo-Fisher Scientific, Renfrew, UK).

2.8.3 Cell maintenance

Serial passaging: All cells were kept in a sterile incubator at 37 °C with 5 % CO_2. All cells were serially passaged after they grew to 70-80 % confluence. Cell media was removed, and cells were washed with HBSS. For detachment, cells were incubated at 37 °C for 3-5 minutes in TypLE and the reaction was neutralised by adding at least an equal amount of cell culture medium. Cells were then centrifuged at 1200 g for 5 minutes, the supernatant discarded, and the pellet re-suspended in cell culture medium. To count the number of viable cells, a haemocytometer was used and the cells were moved to a larger flask.

Cell storage freezing and thawing: Cells intended for freezing were grown to 90-100 % confluence in a T175 flask and counted using a haemocytometer. Cells were centrifuged at 670 g for 5 minutes and re-suspended in a 1:1 mix of culture media and freezing media at a density of 2.7 x 106 cells/ mL. Cells were transferred to cryovials (Corning, UK) and transferred to a polystyrene box. For short-term storage (initial 48-72 hours) cells were kept at -80 °C. For long-term storage, cells were kept at -1500 °C. To thaw cells, cryovials were warmed in a 37 °C water bath and 20mL of pre-warmed cell culture media was added dropwise. The cells were then centrifuged at 670 g for 5 minutes, the supernatant discarded, and the cell pellet was re-suspended in culture media and transferred to a T175 flask.

2.8.4 *In vitro* induction of calcification

Cells were grown to confluence. Calcification media was made by supplementing standard cell culture media with 4.5mM of calcium (Ca) and 5.0mM of phosphate (Pi). VICs were incubated in calcification media for 48 hours and VSMCs were incubated in calcification media for 9 days (with the media replenished halfway through the incubation period).

2.9 Biochemical assays

2.9.1 Quantification of calcification

Cells were washed twice with HBSS and then decalcified with an appropriate volume of 0.6 M HCl at room temperature for 1.5 hours. A colourimetric assay was used to determine free calcium, utilising the calcium interaction with phenolsulphonethalein. The work described in this thesis used a commercially available kit and followed the manufacturer's instructions (Randox Laboratories Ltd., County Antrim, UK). Per well, 250 µL of 1:1 ratio of 2-amino-2-methyl-propan-l-ol (R1) and O-Cresolphthalein complexone, 8-Hydoxyquinoline, HCl (R2) was added. A negative control of the leaching solution, 0.6 M HCl was included. Assays were performed in duplicate on a 96-well plate and were incubated for 15 minutes at room temperature before readings. Absorbance (Ab) was measured at 670 nm using a Synergy HT Multi-Mode Microplate reader (BioTek, Bedfordshire, UK). Calcium measurements were obtained using a calcium standard (2 mg/mL; Bio-Rad) which was prepared in 0.6 M HCl solution. Calcium concentration was calculated using the following equation where Ab is absorption (Zhu *et al.*, 2011a):

$$Concentration\left(\frac{mmol}{L}\right) = \left(\frac{sample\ Ab}{standard\ Ab}\right) * standard\ concentration\left(\frac{mmol}{L}\right)$$

2.9.2 Quantification of total cellular protein

Biochemical calcium quantification was normalised to total cellular protein. The cellular monolayer was washed with PBS to remove any excess solution. A consistent volume (200 μL in a 12-well plate and 500 μL in a 6-well plate) of 0.1 M NaOH with 0.1 % sodium dodecyl sulphate (SDS) lysis buffer was added to the monolayer to denature cellular proteins. Plates were incubated at room temperature on a shaker for 30 minutes. Cells were scraped and the supernatant centrifuged at 1120 rpm for 10 seconds at room temperature. Protein was quantified using a Bio-Rad DC Protein Assay (Bio-Rad Hertfordshire, UK) kit according to the manufacturer's instructions. Assays were performed in duplicate on a 96-well plate and were incubated for 15 minutes at room temperature before readings were taken. Absorbance (Ab) was measured at 690 nm using a Synergy HT Multi-Mode Microplate reader (BioTek, Bedfordshire, UK). Protein measurements were obtained using a protein standard curve of bovine γ-globulin protein (0.125 – 2 mg/mL; Bio-Rad) which was prepared in 0.1 M NaOH 0.1 % SDS solution.

2.10 Fluorescent immunocytochemical staining

Cell monolayers were grown on glass coverslips, fixed with 4 % paraformaldehyde (PFA) and washed with PBS. Once fixed, cells were permeabilised with 0.3 % Triton X-100 (Sigma, Gillingham, UK). Cells were then incubated overnight at 4 ^{o}C with various antibodies including anti-α-smooth muscle actin (α-SMA; 1:100; Sigma), anti-vimentin (1:900) or anti-CD31 (1:900) (Abcam, Cambridge, UK). Cells were then washed in sterile PBS and then incubated with Alexa Fluor® 594 goat-anti-mouse antibody or Alexa Fluor® 488 donkey-anti-rabbit antibody (1:250; Thermo-Fisher Scientific, Renfrew, UK) for 1 hr in the dark. Coverslips were mounted with ProLong Gold Antifade Mountant (Invitrogen, Renfrew, UK). Fluorescence was detected using a Leica DMRB fluorescent microscope (Leica Biosystems, Milton Keyes, UK).

2.11 Quantitative PCR

Nuclease-free Eppendorf™ tubes and nuclease-free distilled H_2O (Thermo-Fisher Scientific, Renfrew, UK) were used throughout.

2.11.1 RNA extraction

For cell monolayers: Total RNA was extracted using an RNAeasy Kit (Qiagen, UK) following manufacturer's guidelines. RLT cell lysis buffer (a guanidine-thiocyanate–containing lysis buffer; Qiagen) supplemented with 1 % β-mercaptoethanol was directly added to the cell monolayer. Cells were scraped and everything was transferred into an Eppendorf. An equal volume of 100 % ethanol was added and the solution was mixed. The solution was then transferred to an RNAeasy spin column. Columns were centrifuged at 8000 g and flow-through discarded. The column was washed in three steps. Firstly, by adding RW1 buffer, centrifuging at 8000 g and discarding flow-through. Then by adding RPE buffer, centrifuging at 8000 g and discarding flow-through. This step was repeated twice. The RNA was eluted from the column with 40 µL of dH_2O. Total RNA was measured by absorbance at 260 nm using a using Nanodrop spectrophotometer (Labtech, Tampa, USA). The samples were stored at -80 ºC.

For tissue: Small portions (~2 g) of frozen tissue were dissected and transferred to Eppendorfs containing RLT cell lysis buffer supplemented with 1 % β-mercaptoethanol (Qiagen). Tissues were homogenised using a Tissue homogeniser (T 10 basic Ultra-Turrax, IKA). Solutions were transferred to an Eppendorf with an equal amount of 100 % ethanol. Samples were then transferred to RNAeasy columns where protocol followed the same used for cell monolayers).

2.11.2 Complementary DNA (cDNA) generation

RNA samples were diluted to 20 µL. Random primers (50 ng/µL, 4uL per sample, Life Technologies) were added to each sample. Samples were heated to 70 ºC for 10 minutes in a Hybaid PCR Express Thermal cycler (Thermo-Fisher Scientific, Renfrew, UK). Samples were cooled on ice. A master mix for each sample was made of 4 µL dithiothreitol (DTT; 0.1 M; Thermo-Fisher Scientific, Renfrew, UK), 2 µL deoxyribose nucleoside triphosphate (dNTP; 10 mM; Life Technologies), 8 µL 5x First-Strand buffer (Life Technologies) and 2 µL SuperScript II Reverse Transcriptase (Invitrogen; Renfrewshire, UK), and then added to each sample. Samples were heated at 25 ºC for 10 minutes, 42 ºC for 50 minutes and 70 ºC for 15 minutes and held at 4 ºC using a Hybaid PCR Express Thermal cycler (Thermo-Fisher Scientific, Renfrew, UK). Samples were stored at -80 ºC.

2.11.3 Quantitative PCR

Quantitative PCR (qPCR) preparation took place in a ventilated hood and reactions were conducted in a 96-well PCR plate (Thermo-Fisher Scientific, Renfrew, UK). cDNA was loaded at a concentration of 5 ng/µL and volume of 5 µL. Each reaction contained 5 µL of cDNA, 0.5 µL of forward and 0.5 µL of reverse primer (10 µM), 4 µL of nuclease-free dH_2O and 10 µL of 2x PrecisionPLUS SYBR Green Mastermix (Primer Design; Southampton, UK). The qPCR was performed in a Stratagene Mx3000P PCR cycler (Agilent Technologies, Santa Clara, USA) using the following programme: 1 cycle of 10 minutes at 95 ºC, 40 cycles of 15 seconds at 95 ºC, and 1 minute at 60 ºC. The last cycle comprised 1 minute at 95 ºC, 30 seconds at 55 ºC and 30 seconds at 95 ºC. Each reaction was run in duplicate. Negative controls were generated by replacing samples with dH_2O during the cDNA generation process. The specificity of the primers was confirmed with the production of a clean single peak in the dissociation curve (Figure 2.5). Analysis of the reactions used the amplification plots. A baseline for the amplification plots was defined by a reference dye (Rox). For data analysis the comparative CT method (Livak and Schmittgen, 2001) was used, comparing the fold change of the expression relative to the housekeeping gene, *Gapdh*. This housekeeping gene was chosen based on a literature review of housekeeping genes commonly used in murine cardiovascular tissue, which was then optimised in the lab (He *et al.*, 2020). All primers, Runx2, Alpl, Phospho1, Mgp, Enpp1 and Gapdh were sourced from Qiagen, and sequences are unavailable (Zhu *et al.*, 2015).

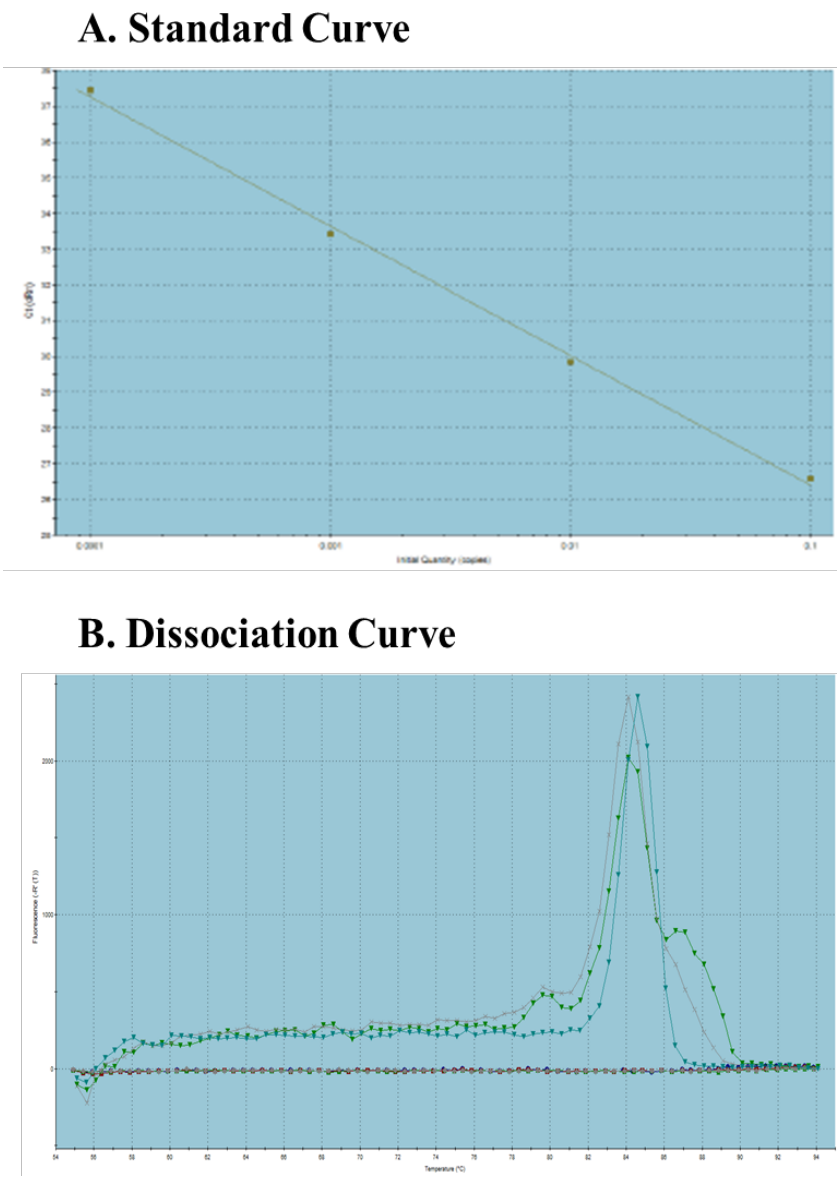

Figure 2.5: Validation of qPCR primers. The primer efficiency and specificity was detected using both the standard curve and the dissociation plot.

2.12 Western blots

2.12.1 Lysis and protein quantification

The cell lysing process was carried out on ice. Cells were lysed with an appropriate volume of Radioimmunoprecipitation assay buffer (RIPA; Thermo-Fisher Scientific, Renfrew, UK). Cells were scraped and transferred to Eppendorfs, then vortexed and left on ice for 10 minutes. This was repeated three times. Samples were then centrifuged at 112 rpm for 5 minutes and the supernatant was taken. Protein was quantified using a BCA assay kit (Thermo-Fisher Scientific, Renfrew, UK) in accordance with manufacturer's instructions. Assays were performed in duplicate in a 96-well plate, and absorbance was measured at 690 nm using a Synergy HT Multi-Mode Microplate reader (BioTek, Bedfordshire, UK). Protein measurements were obtained using a protein standard curve of bovine γ-globulin protein (0.125 – 2 mg/mL; Bio-Rad) which was prepared in RIPA buffer.

2.12.2 Western blot

All incubation and washing steps following protein transfer were carried out on a shaker. Samples were prepared for western blotting by dilution to 20 µg of protein in PBS. Solutions of 4x lithium dodecyl sulphate (LDS) loading buffer and 10x sample reducing agent (Thermo-Fisher Scientific, Renfrew, UK) were added to samples. Samples were heated at 95 ºC for 6 minutes to denature proteins. Samples were separated by SDS-page in precast Novex gels (Thermo-Fisher Scientific, Renfrew, UK). The western blot tank was filled with cold (4 ºC) NuPAGE™ MOPS (3-(N-morpholino)propanesulfonic acid) SDS Running Buffer (Thermo-Fisher Scientific, Renfrew, UK). The samples were run in an XCell surelock western blot module, at 170 V for 5 minutes and 150 V for approximately 45 minutes at room temperature. The resolved proteins were transferred using a standard semi-dry transfer protocol in transfer buffer. The transfer was conducted at 18 V for 45 minutes onto a Hybond electrochemiluminescence (ECL) nitrocellulose membrane (GE Healthcare, Lanarkshire, UK). Membranes were blocked for 1 hour with 5 % milk at room temperature (Zhu *et al.*, 2011b).

All blocking, washing and antibody equilibrations were performed in PBS supplemented with 0.1 % (v/v) Tween 20 (PBS-T) at room temperature. After blocking, all primary antibodies were incubated overnight at 4 ºC with PBS-T with 5 % milk. Membranes were then washed three times in PBS-T for 15 minutes each. Secondary antibodies were diluted in PBS-T with 5 % milk. Membranes were incubated in this solution for 1 hour at room temperature (30 minutes

for β-actin antibody*)*. Membranes were again washed three times in PBS-T for 15 minutes each. Bound antibodies were detected by chemiluminescence with Amersham Enhanced Chemiluminescence (ECL) Western blotting detection kit (GE Healthcare, Lanarkshire, UK). Chemiluminescence was visualised in a GeneGnome Chemiluminescence imaging system (Syngene, Cambridge, UK). All protein chemiluminescence was normalised to β-actin chemiluminescence. Details of antibodies used are located in Appendix II (Zhu *et al.*, 2011b).

2.13 Proteomics

2.13.1 Protein extraction

2.13.2 Liquid chromatography-mass spectrometry (LC-MS)

Samples were analysed in the Proteomics and Metabolomics Facility at the Roslin Institute, University of Edinburgh. Samples underwent proteolytic digestions employing S-TRAP. Peptide samples were then analysed by diaPASEF (a data-independent analysis (DIA) method) for proteome wide label-free quantifications across treatments. LC-MS was performed on a nanoLC (Dionex Ultimate) interfaced to a timsTOFfleX MS (Bruker, Kontich, Belgium)(Karagianni *et al.*, 2021). Raw spectral data will be processed using Perseus software and networks visualised using Cytoscape.

2.14 Statistics

Statistical significance was determined using GraphPad Prism software (Version 8), using either Student's t-test, One-Way (with post-hoc Dunnett's test) or Two-Way ANOVA, as described in the figure legends. The normality of data was tested with a Shapiro-Wilks test and equivalent non-parametric tests were used if appropriate. All data graphs were generated with GraphPad Prism and figures were made in Microsoft PowerPoint unless otherwise stated. Data are presented as mean ± SEM unless otherwise stated. The significance threshold was $P < 0.05$, the analyses were performed blind to treatment.

Chapter 3: Testosterone augments *in-vitro* aortic valvular calcification

Chapter 3: Testosterone augments *in-vitro* aortic valvular calcification

3.1 Introduction

3.1.1 Testosterone in vascular calcification

Men are more likely to develop cardiovascular disease (CVD) then pre-menopausal women and exhibit symptoms approximately ten years earlier (Wingard, Suarez and Barrett-Connor, 1983; Maas and Appelman, 2010). It has been proposed the reason for males developing CVD earlier is due to testosterone, however no clear mechanistic link has been established. There is clinical evidence that high levels of circulating testosterone is associated with CVD. This includes studies of men who abuse anabolic steroids that demonstrate a positive correlation between increased circulating levels of androgens, including testosterone, with an increased (over two-fold) risk of cardiovascular disease (Dickerman *et al.*, 1996; Sullivan *et al.*, 1998). Sullivan *et al.* (1998) proposed that the mechanism underpinning the effect of anabolic steroids on CVD includes increased serum levels of LDL, increased hepatic triglyceride lipase (HTGL) activity, and endothelial cell dysfunction. As CAVD has a distinct sexual dimorphism (Simard *et al.*, 2017), it has also been proposed that testosterone may drive the development of this disease, but as with CVD, no clear link has been established.

Preclinical investigations have demonstrated that testosterone augments cardiovascular calcification. A recent *in vitro* study demonstrated that testosterone can promote calcification of isolated vascular smooth muscle cells, by acting as a ligand at the androgen receptor (Zhu, *et al.*, 2016). Deletion of the androgen receptor led to decreased expression of pro-calcific genes including *OSTERIX* and *ALP*, indicating that androgen signalling contributes to development of calcification in the vascular wall (Zhu *et al*., 2016). Testosterone treatment also increased condyle size and ossification *in vitro* in murine bones, suggesting a contribution to bone formation and, therefore, potentially to soft tissue calcification (Maor, Segev and Phillip, 1999). Testosterone administration to $ApoE^{-/-}$ mice increases atherosclerotic plaque calcification and serum cholesterol levels both in females and in males (McRobb, Handelsman and Heather, 2009). In contrast, contradictory data showed that dihydrotestosterone (DHT, a more potent form of testosterone) treatment had no effect on plaque calcification or lipid metabolism in $ApoE^{-/-}$ mice (McRobb, Handelsman and Heather, 2009). In summary, whilst there is both clinical and preclinical evidence suggesting that testosterone contributes to

vascular calcification, this is has not been established unequivocally and no clear mechanism of action has been identified.

Conversely low circulating testosterone levels have also been linked with cardiovascular disease. Low serum testosterone has been shown to be a risk factor for CVD and, specifically, to be associated with a rise in circulating LDL (Morris and Channer, 2012). This relationship has also been shown in vascular calcification. A 2012 clinical study highlighted an inverse relationship between bioavailable testosterone and coronary artery calcium (CAC) score (Park *et al.*, 2012), supported by a subsequent study that replicated these findings (Lai *et al.*, 2015). The more recent Framingham Heart clinical study showed an association between decreased serum testosterone levels and increased CAC score (Travison *et al.*, 2016). These clinical associations are supported by preclinical studies showing that androgen inhibits VSMC calcification *in vitro,* potentially by activation of growth arrest-specific gene 6 (Gas6), a vitamin K dependant protein (Son *et al.*, 2010). Furthermore, in ovariectomized rats, high testosterone treatment reduced the incidence of microcalcification in mammary tissue (Oliveira *et al.*, 2019).

Thus, there is extensive clinical and preclinical evidence that testosterone can both diminish and augment cardiovascular calcification. This relationship is likely more complex than a simple linear effect. Many hormones display a U-shaped relationship with physiological outcomes, in this context, potentially both too much and too little testosterone increases the incidence of cardiovascular calcification (Mateo, 2008).

3.1.2 Oestrogens in vascular calcification

An alternative theory to CAVD in men being driven by abnormal circulating testosterone levels is the possibility that the greater incidence of valve calcification in men is attributable to reduced protection from oestrogens. Oestrogens have historically been considered cardioprotective and may be protective against cardiovascular calcification (Iorga *et al.*, 2017). This is related to the observation that women tend to not develop cardiovascular calcification during their reproductive years, when oestrogen levels are high (Shemesh *et al.*, 2010). During menopause, when serum oestrogen levels fall, there is an increased incidence of cardiovascular disease and vascular calcification (Pardhe *et al.*, 2017). Preclinical *in vitro* studies have shown that oestrogen treatment can reduce calcification in VSMCs, and in murine models of atherosclerosis ovariectomy increases aortic vascular calcification (Wu *et al.*, 2020).

Phytoestrogens (estrogen-like compounds derived from plants) have also shown promise in reducing vascular calcification and osteogenic markers in the aorta, including *RUNX2* and *ALP*, in preclinical studies (Hammad *et al.*, 2021). Clinical trials have used oestrogen and progesterone replacement therapy (hormonal replacement therapy (HRT)) in post-menopausal women but with mixed results. HRT has been shown to both increase and decrease cardiovascular disease outcomes (Manson *et al.*, 2007). HRT is also associated with a reduced of incidence of CAC in patients, although no clinical trial has investigated the effect of HRT on valvular calcification (Gudmundsson *et al.*, 2017)

After the mixed results in clinical trials, the assumption that oestrogens are cardioprotective was questioned (see section 1.8.3). In a preclinical study using human VSMCs, over-expression of ERα caused an increase in calcification and expression of RUNX2 and ALP (Nanao-Hamai *et al.*, 2016). Another preclinical study demonstrated that oestrogen acts to decrease osteoclast formation (osteoclasts are cells that degrade bone and reducing osteoclasts therefore reduces the breakdown of bone minerals). In ovariectomized rats, oestradiol treatment increased the incidence of microcalcification in mammary tissue (Oliveira *et al.*, 2019). Overall, there is not a simple direct correlation between oestrogens and risk for cardiovascular disease, including cardiovascular calcification.

3.1.3 Sex hormones and calcific valve interstitial cells

CAVD displays a significant sexual dimorphism (described in 1.8.1). Males tend to have more pro-calcific valve disease, whereas females have more pro-fibrotic valve disease during their reproductive years (Simard *et al.*, 2017). After menopause females much more rapidly develop calcification. Despite the identification of this sexual dimorphism in valve calcification, and the previous demonstration in preclinical studies that sex hormones influence calcification in VSMCs, little research has been conducted on the effect of sex hormones on calcific valve disease. In particular there has been little investigation into the effect of sex hormones on calcification of VICs. Previous research has highlighted a significant sexual dimorphism in VICs, whereby VICs isolated from male and female pigs displayed different gene ontologies for proteins associated with ossification and bone development (McCoy, Nicholas and Masters, 2012). VICs isolated from male rats have shown a higher propensity for calcification and increased expression of *ALP* (Masjedi *et al.*, 2017). However, there is currently a lack of

research comparing how sex hormones affect the calcification of VICs isolated from male versus female animals.

3.2. Hypothesis and aims

The work described in this chapter addresses the hypothesis that testosterone drives, whereas oestrogen is protective against, valvular calcification. A combination of *in vitro* assays and proteomics analysis was used to detect sex differences in the calcification of VICs and the molecular effects of exposure to testosterone.

This hypothesis was addressed by pursuing the following aims:

1. To optimise the *in vitro* conditions under which VICs calcify

2. To investigate whether sex hormones modulate the calcification of VICs *in vitro*

3. To use proteomics to identify pathways through which testosterone influences calcification of isolated VICs

3.3: Materials and Methods

3.3.2 Source of cells

Cells were sourced as described in section 2.8. Optimisation of calcification media conditions was performed on the RVIC Sv40T cell line (a rat cell line of aortic valve cells). All other cell work was performed on primary murine cells (isolations performed as in section 2.8).

3.3.3 Cell characterisation using Immunofluorescence (IF)

Immunofluorescent staining of cells was performed as described (section 2.10). VICs were characterised using Vimentin and α-SMA as VIC markers (Cui *et al.*, 2017). Given the structure of the valve (section 1.2) endothelial cells can become isolated with VICs when performing the cell extractions. Therefore our population of cells was stained with CD31 (an endothelial cell marker (Cui *et al.*, 2017)) to exclude the presence of VECs.

3.3.4 Optimisation of cell culture conditions to induce calcification

Standard media conditions are stated in section 2.2.8. Calcification medium was optimised using an increasing concentrations of calcium (2.7-5.4 mM) and phosphate (2-5nM) and combining calcium and phosphate to deduce the optimum conditions for calcification in VICs. Previous publications have assessed the media conditions in which VICs are cultured showing that standard medium containing 10 % FBS induces a 'activated' state in VICs whereas medium containing 2 % FBS induced a 'quiescent/healthy' state of VICs (Tan *et al.*, 2019) (details of cell culture media supplementation in section 2.8.2). Therefore, calcification media optimisation was performed in both 'activated' and 'quiescent' media conditions to investigate whether cell phenotype would affect calcification. Once optimised, calcification conditions were adapted as described (section 2.8.4).

3.3.6 Detection of changes in osteogenesis-related genes using qRT-PCR

To investigate whether culturing VICs in 'activating' or 'quiescent' media would produce significantly different amounts of calcification, RNA was extracted after calcification of VICs cultured in either media condition, and subject to RT-QPCR analysis (carried out as described in section 2.11). Quantification was carried out for genes known to regulate cardiovascular calcification, including *Enpp1 Bglap Alp Phospho1 Mgp and Runx2* mRNA. These genes were chosen as they have been cited in many previous publication to regulate calcification and are used in the literature as hallmarks of calcification (Romanelli *et al.*, 2017; Tsang *et al.*, 2020).

3.3.6 Detection of changes in osteogenesis-related proteins using western blot

To investigate whether culturing VICs in activated or quiescent media would produce differentiating calcification, protein was extracted after calcification of VICs in either media condition and subject to western blot (as described in Chapter 2 section 2.12). Quantification of two proteins associated with augmentation of cardiovascular calcification BMP2 (Li, Yang and Giachelli, 2008) and RUNX2 (Lin *et al.*, 2015) as well as quantification of a protein shown to inhibit cardiovascular calcification, ENPP1(Lorenz-Depiereux *et al.*, 2010) was made.

3.3.7 Optimisation of assays to measure sex hormone effects on valvular calcification

Optimisation of assays to assess whether treatment of sex hormones would either augment or dimmish calcium deposition in VICs was carried out next. The assay was first optimised in VSMCs, this was to validate the assays and investigate whether the testosterone induced calcification in VSMCs from Zhu *et al.*, (2016) could be replicated. Ones the assay was validated it was then repeated in isolated VICs. Hormones were tested over the following concentration ranges; testosterone (10-200 nM), DHT (10-200 nM), oestrogen (4-40 nM).

3.3.8 Characterisation of sex hormone machinery expression in male and female rat tissues using qRT-PCR

VICs, right and left ventricular tissue, ovaries, testes, liver, and kidneys were dissected from 6 rats of each sex aged 5 weeks old, species Sprague Dawley, and were subject to qPCR analysis. This included RNA extraction, reverse transcription and RT-QPCR analysis as described in Chapter 2 section 2.11. Each tissue was analysed for gene expression of *AR, ERα, ER β* and *CY191A,* mRNA expression was normalised relative to gonadal expression.

3.3.9 Proteomics

Calcified VICs from male rats and calcified VICs supplemented with 100 nM testosterone for 48 hours were submitted for MS proteomics analysis. The objective was to analysis changes in the proteome between and male calcified and testosterone-treated male calcified cells. Each group of treatment conditions were pooled into 4 technical repeats: calcified male cells (C1, C2, C3 and C4) and testosterone treated calcified cells (T1, T2 and T3, T4).

Before statistical analysis, samples were transformed using log2 of the data set using a standard protocol (Bosch *et al.*, 2008) which transforms the data set to a normal distribution (Figure

3.6.16 B). Workflow of data processing is shown in Figure 3.3.2. Proteomics was carried out by the Proteomics and Metabolomics Facility at the Roslin Institute as described in section 2.2.13. Data processing (Figure 3.3.2) was carried out using Perseus and Cytoscape software.

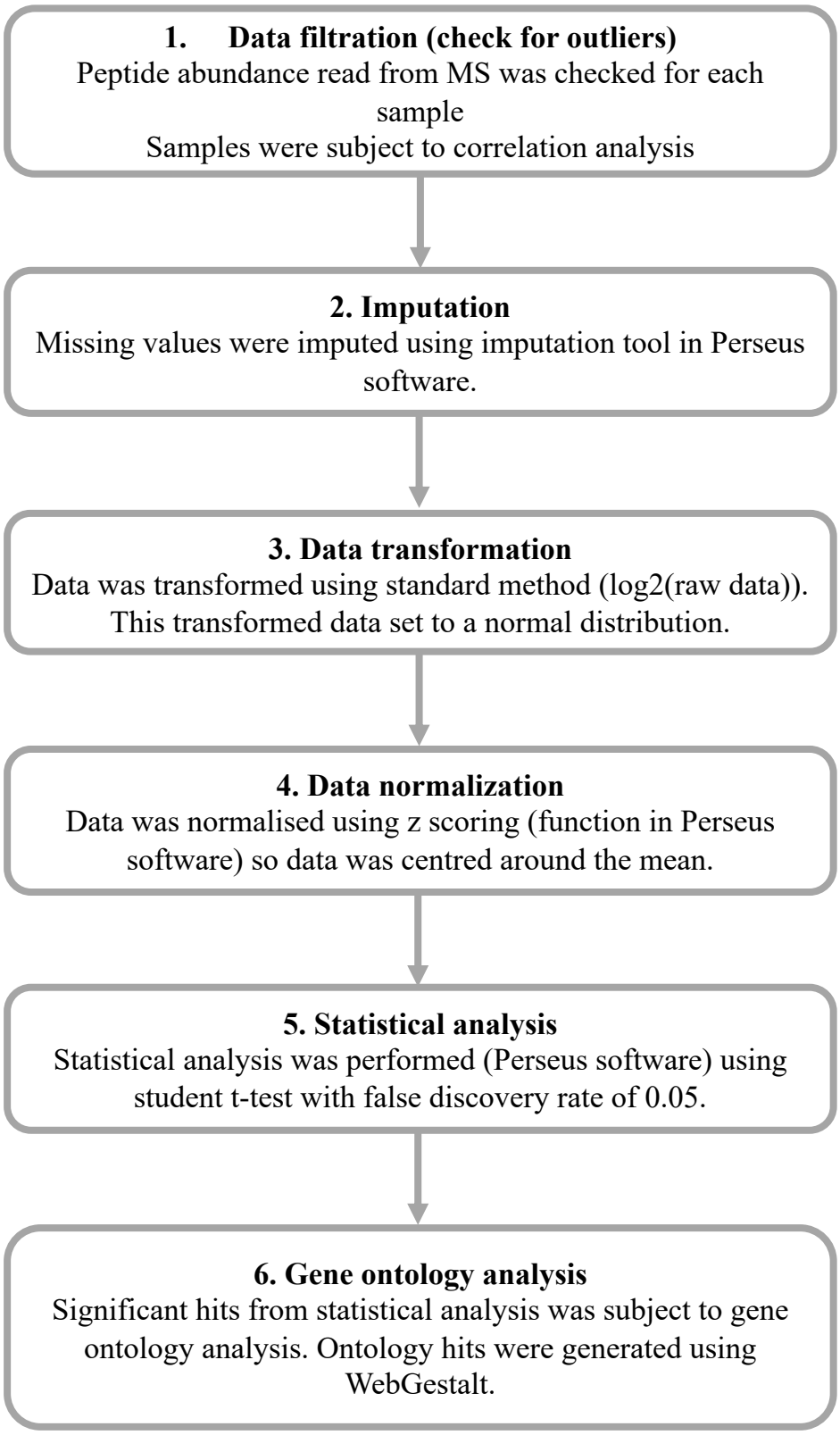

Figure 3.3.2: Flow chart of proteomics data processing. This flow chart outlines how the raw proteomics peptide readings were processed. MS- mass spectroscopy

3.4: Results

3.4.1 Cell line characterisation

The RVS40T cell line was characterised using immunofluorescent staining. The RVS40T cells showed positive immunofluorescence for α-SMA (Figure 3.4.1 A) and vimentin (Figure 3.4.1 B) with the overlaid image showing cells were double positive for these markers (Figure 3.4.1 C). In contrast there was no immunofluorescence for the endothelial cell marker CD31 (Figure 3.4.1 D) or in the IgG control (Figure 3.4.1 E).

3.4.2 Optimisation of calcification media

To determine calcium deposition, optimisation of the assay was carried. Increasing calcium concentrations caused no significant change in *in vitro* calcium deposition (Figure 3.4.2 A). Increasing phosphate concentration in the media caused a decrease in calcium deposition (Figure 3.4.2 B) at 2.0mM ($p=0.0035$, decrease of 0.66-fold), 3.0 mM ($p=0.0286$, decrease of 0.73-fold) and 5.0 mM ($p<0.0001$, decreased 0.56-fold) from control. Combining 2.4 mM Ca with 1.4 MM Pi significantly increased calcium deposition 6.4-fold ($p<0.0001$). Combining Ca 2.7mM and Pi 2.5 mM also significantly increased calcium deposition 4.28-fold ($p<0.0001$, Figure 3.4.2).

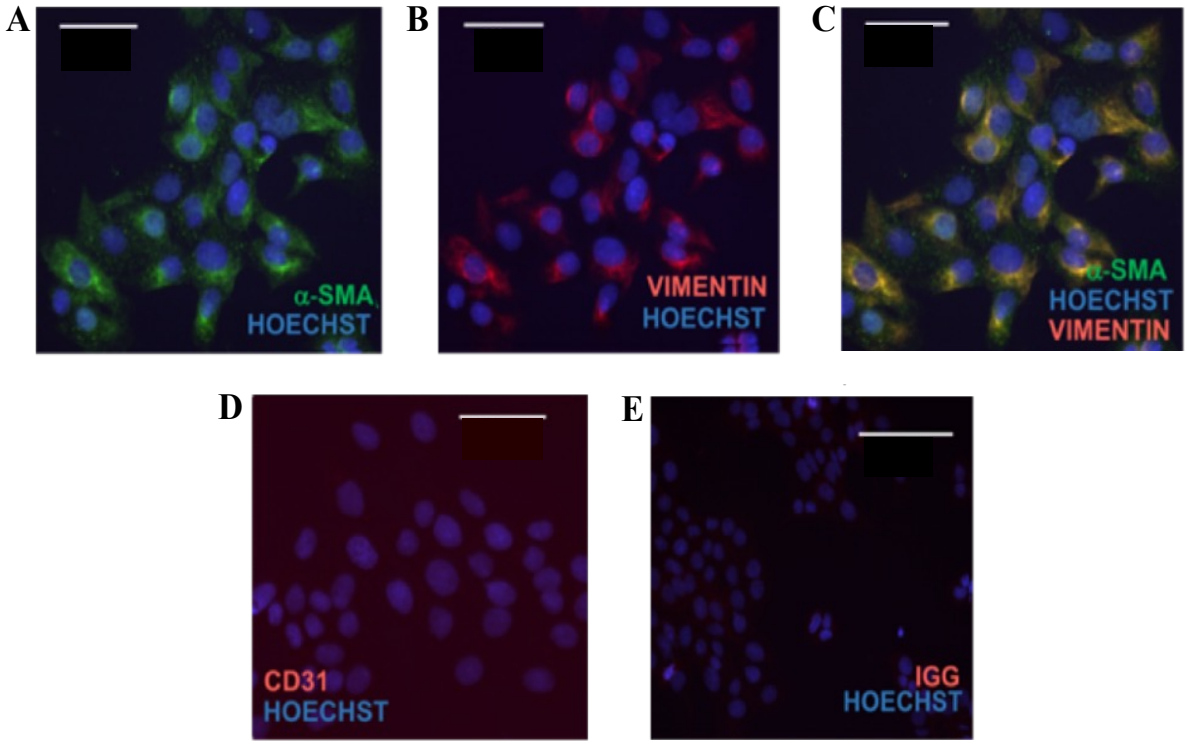

Figure 3.4.1: Characterisation of the RVSV40T cell line. Rat valve interstitial cells (RVICs) were grown to 70 % confluence on a coverslip and immunofluorescence staining was performed to confirm protein expression. A) Alpha-smooth muscle actin (α-SMA) staining B) Vimentin staining C) α-SMA and vimentin overlay D) Cluster of differentiation 31 (CD31) staining, E) IgG control. Scale bars represent 150 μM. Figure made using ImageJ software.

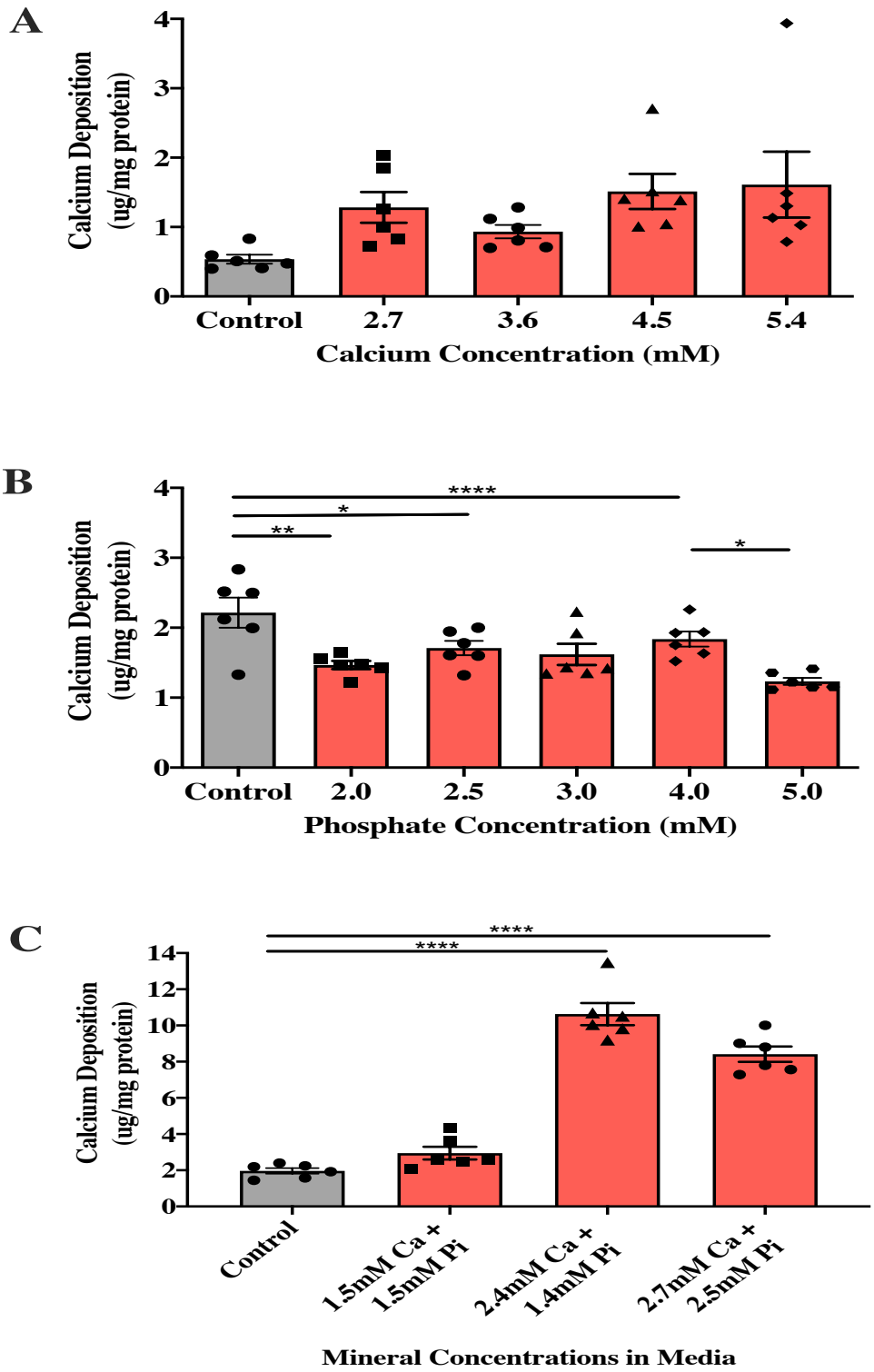

*Figure 3.4.2: Optimisation of in vitro calcification conditions in the RVS40T cell line***.** Rat valve interstitial cells (RVICs) were grown in standard media and were calcified for 48 hours using various concentrations of calcium and phosphate. Calcium deposition was measured with a colourimetric assay. A) Addition of increasing concentrations of calcium to the media caused no change in calcium deposition. B) Addition of increasing concentration of phosphate to the media caused a significant decrease in calcium deposition at 2.0 mM, 2.5 mM and 4.0 mM. C) Combining calcium and phosphate significantly increased calcium deposition at both 2.4mM Ca/1.4 mM Pi and 2.7mM Ca/2.5mM Pi. Columns represent mean±SEM, points are single data values. n=6 *=p<0.05, **=p<0.001, ***=p<0.0001,****=p<0.00001. Significance was determined using a One-Way ANOVA. Control- standard media with no mineral supplementation.

3.4.3 Determination of whether VIC phenotype affects *in vitro* calcification

To investigate whether the phenotype of VICs would affect *in vitro* calcification, VICs were calcified (with previously optimized conditions 2.7 mM Ca and 2.5 mM Pi, Figure 3.4.2) in both activation and quiescing media and then had the expression levels of genes for known modulators of calcification quantified

The expression of *Runx2* mRNA was significantly increased in cells cultured in quiescing media compared with those cultured in activating media (Figure 3.4.3 A, p=0.0355). Expression of of *Alp* and *Bglap* mRNA significantly increased between control and calcified media but there were no significant differences observed between actived and quiescent media (Figures 3.2.3 B and F). The expression of *Mgp* mRNA was significantly (p=0.0004) increased (15.00-fold) in quiescing media compared with activating media (Figure 3.2.3 C). The expression of *Enpp1* mRNA was not altered by incubation of RVICs in either activating or quiescing media (Figure 3.2.3 D). The expression of *phospho1* mRNA was significantly greater (4.68-fold; p=0.0021) when calcifying under quiescent media conditions compared to those grown in activating media conditions (Figure 3.2.3 E).

Protein expression of known modulators of calcification was confirmed using western blot analysis. Example western blots are shown in Figure 3.4.4 A. Culturing VICs in calcifying conditions reduced BMP2 protein. This decrease was not affected by whether the cells were incubated in activating or quiescing media (Figure 3.4.4 B). RUNX2 protein was significantly decreased in cells cultured in calcifying conditions but this change was not different between activating and quiescing media (Figure 3.4.4 C). ENPP1 expression was significantly (2.2-fold) increased in cells cultured in quiescing media compared with those cultured in activating media (Figure 3.2.4 D, p=0.0450)

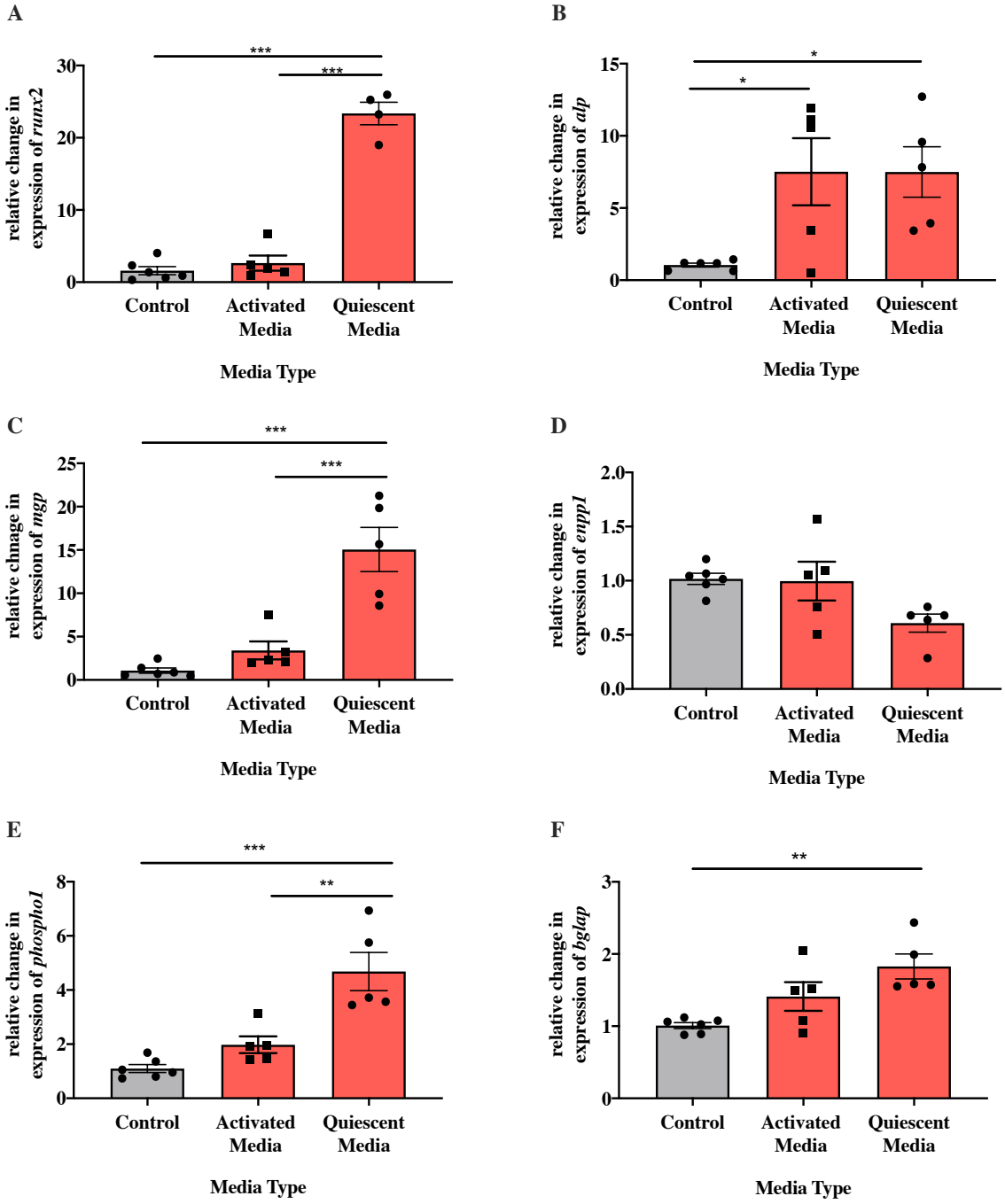

Figure 3.4.3: mRNA expression of osteogenic genes in RVS40T cells calcified in activing or quiescing media. Rat valve interstitial cells (RVICs) were calcified under different media conditions and mRNA expression was analysed using q-RT-PCR. Changing to a quiescing medium from anactivating medium, when calcifying, significantly increased the mRNA expression of A) *runx2* C) *mgp* and E) *phospho1*. There was no difference in mRNA expression of B) *alp* D) *enpp1* or F) *bglap* when calcifying RVICs in either a activatin or quiescing media. Columns represent mean±SEM, points are single data values. n=6. *=p<0.05, **=p<0.001 ***=p<0.0001****=p<0.00001. Significance was determined using a One-Way ANOVA.Control = standard media without supplementation.

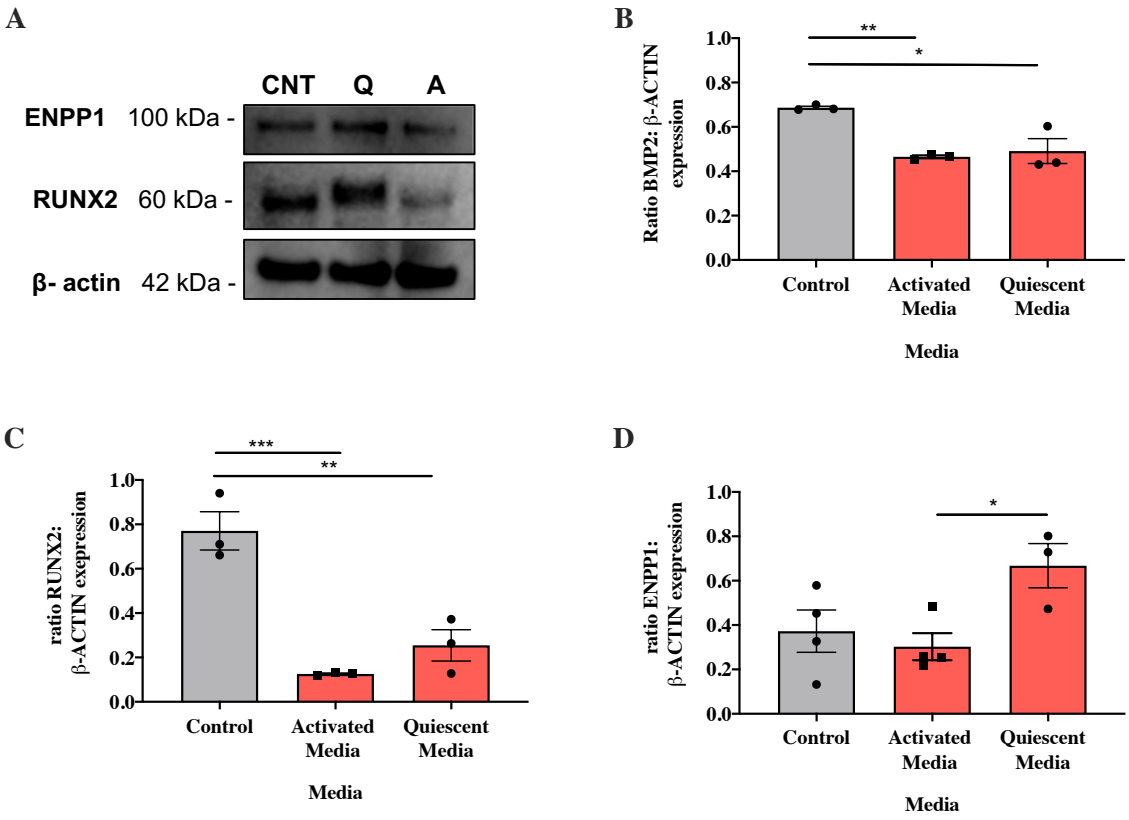

*Figure 3.4.4. The impact of calcification in activating and quiescing media on protein expression of known modulators of calcification in RVS40T cells***.** Rat valve interstitial cells (RVICs) were calcified under different media conditions and protein expression was analysed using western blot. A) Example western blots, including β-actin control B) There was no difference BMP2 expression when VICs were calcified in activating compared with quiescing media. C) There was no difference in RUNX2 expression when VICs were calcified in activating or quiescing media. D) ENPP1 expression was significantly greater in RVICs calcified in quiescing compared witho activaing media. Bars display mean±SEM, points are single data values. n=3. *=p<0.05 **=p<0.001 ***=p<0.0001. Significance was determined using a One-Way ANOVA. Control- standard media without supplementation.

To assess whether different culture conditions (which induce different VIC phenotypes) would affect *in vitro* calcification, optimisation of the calcification assays was repeated in the quiescing media. In quiescing media, increasing the concentration of calcium increased calcium deposition compared to control (0.50 ± 0.05 µg/mg) in a concentration-dependent manner, reaching significance at 5.4mM (5.53 ± 0.79 µg/mg) ($p<0.0001$, Figure 3.4.5 A). Increasing concentrations of phosphate had no significant effect on calcium deposition in the quiescing conditions (Figure 3.4.5 B)

Optimal *in vitro* supplementation concentrations were chosen as Ca 2.7mM and Pi 2.5 mM. Incubating RVICs in this medium did not produce significantly different calcium deposition when RVICs were cultured in either activating or quiescing conditions (Figure 3.4.5 C)

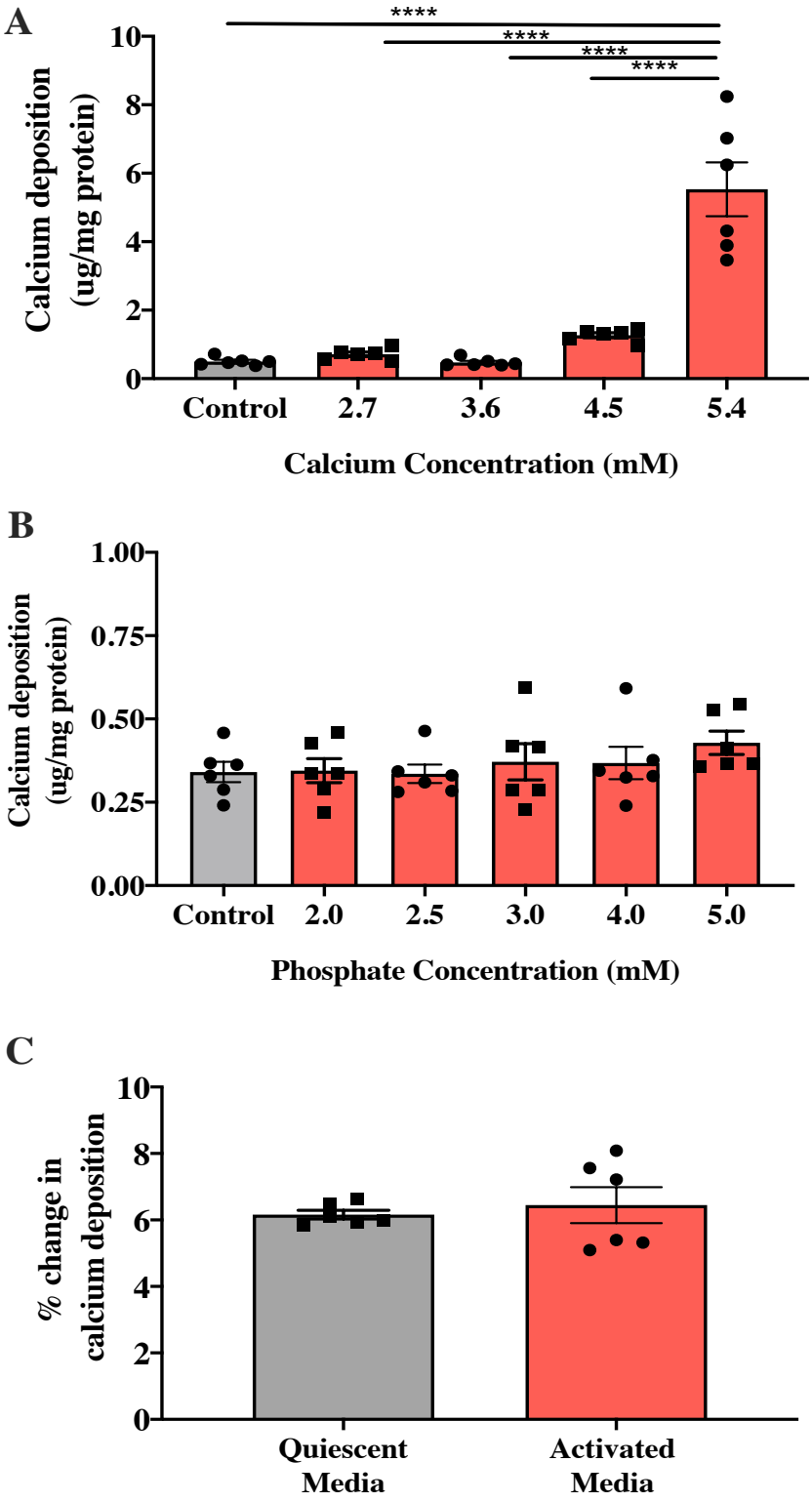

Figure 3.4.5: Optimisation of *in vitro calcification conditions in quiescent media in RVS40T cells.* Rat valve interstitial cells (RVICs) grown in standard media were calcified for 48 hours in various concentrations of calcium and phosphate. Calcium deposition was measured with a color imetric assay. A) Increasing the concentration of calcium increased calcium deposition in a concentration-dependent manner and reached significance at 5.4 mM. B) Increasing concentrations of phosphate had no significant effect on calcium deposition. C) Once the mineral concentrations were optimised, comparison of calcifying in quiescing or activating media demonstrated no difference in calcium deposition. Columns represent mean±SEM, points are single data values. n=6. *=p<0.05, **=p<0.001 ***=p<0.0001****=p<0.00001. A-B Significance was determined using a One-Way ANOVA, C- Significance was determined using un unpaired t-test. Control-standard media without supplementation

3.4.4 Determining the effect of sex hormones on *in vitro* calcification

Previously published data (Zhu *et al.*, 2016) demonstrated that testosterone enhances calcification in VSMCs *in vitro*. Initially, replication of these previous results was undertaken as a positive control for assessing the impact of testosterone on calcification in VICs. Under calcifying conditions, exposure to testosterone produced an increase in calcium deposition in primary VSMCs: from 425 ± 146 μg/mg (in control cells) to 2027 ± 116 μg/mg (1 nM, $p<0.001$), 1209 ± 88 μg/mg (10 nM $p=0.0013$), and 1771 ± 168 μg/mg (100 nM, $p<0.0001$).

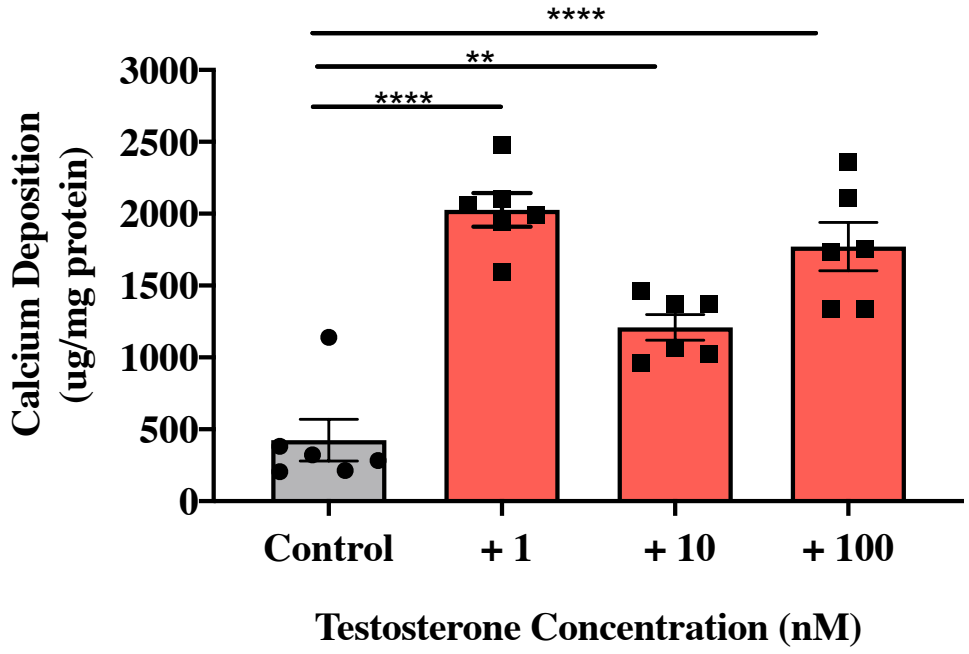

Figure 3.4.6: Effect of testosterone administration on VSMC calcification. Vascular smooth muscle cells (VSMCs) were grown to confluence and calcified for 9 days in the absence or presence of testosterone. Calcium deposition was measured with a colorimetric assay. Addition of testosterone produced a significantly increased calcium deposition at 1, 10 and 100 nM with maximal calcification achieved at 1 nM testosterone. Columns represent mean±SEM, points are single data values. **=p<0.001 ***=p<0.0001 ****=p<0.00001. Data were analysed using One-way ANOVA with post-hoc Dunnett's comparing all hormone treatments to control. Cells from 10 mice were grown together and 6 technical repeats were carried out.

Once the testosterone assay was validated using VSMCs it was used to test sex hormone-dependent calcification in VICs. Initially, studies were undertaken using the RVIC cell line (RVICs Sv40). It is important to note these cells are male derived which may affect how the hormones interact with the cells. RVICs Sv40 exhibited no significant change in calcium deposition with any concentration of testosterone (Figure 3.4.7 A) In contrast, there was a significant increase in calcium deposition (from 54.62 ± 5.08 μg/mg to 99.74 ± 9.194 μg/mg) after incubation with 4nM oestrogen (p=0.0173, Figure 3.4.7 B).

This experiment was next repeated in primary VICs from male rats. Incubation with testosterone significantly increased calcium deposition at all concentrations. Calcium deposition increased from 812.9 ± 183.9 μg/mg in controls to 12,763 ± 1283 μg/mg at 10nM, (p<0.0001, Figure 3.4.8 A), 10,946 ± 918.4 μg/mg at 100nM (p<0.0001, Figure 3.4.9 A) and to 7125 ± 614.6 μg/mg at 200nM (p=0.0002, Figure 3.4.9 A). There was no significant difference in calcium deposition after oestrogen administration at any of the concentrations used (Figure 3.4.8 B).

In RIVCs from female rats calcium deposition significantly increased from 254.4 ± 40.46 μg/mg in controls to 801.1 ± 125.3 μg/mg (100nM, p=0.0021, Figure 3.4.9 A) and to 1489 ± 140.9 μg/mg (200nM, p<0.0001, Figure 3.4.9 A). There was no significant difference in calcium deposition after oestrogen administration at any of the concentrations used (Figure 3.4.9 B).

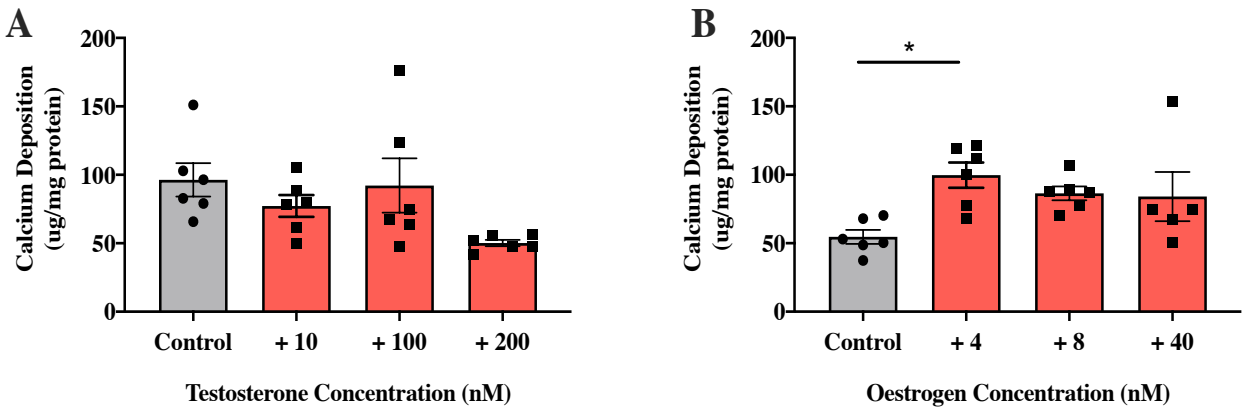

Figure 3.4.7: Effect of exposure to sex hormones on the in vitro calcification of immortalised RVICs. RVICs were grown to confluence and calcified for 48 hours in the presence/absence of sex hormones. Calcium deposition was measured with a colourimetric assay. A) Addition of testosterone produced no significant difference in calcium deposition. B) Addition of oestrogen significantly increased calcium deposition at 4nM. Columns represent mean±SEM, points are single data values. *=p<0.05. Controls were calcified cells only. Data were analysed using One-way ANOVA. n=6.

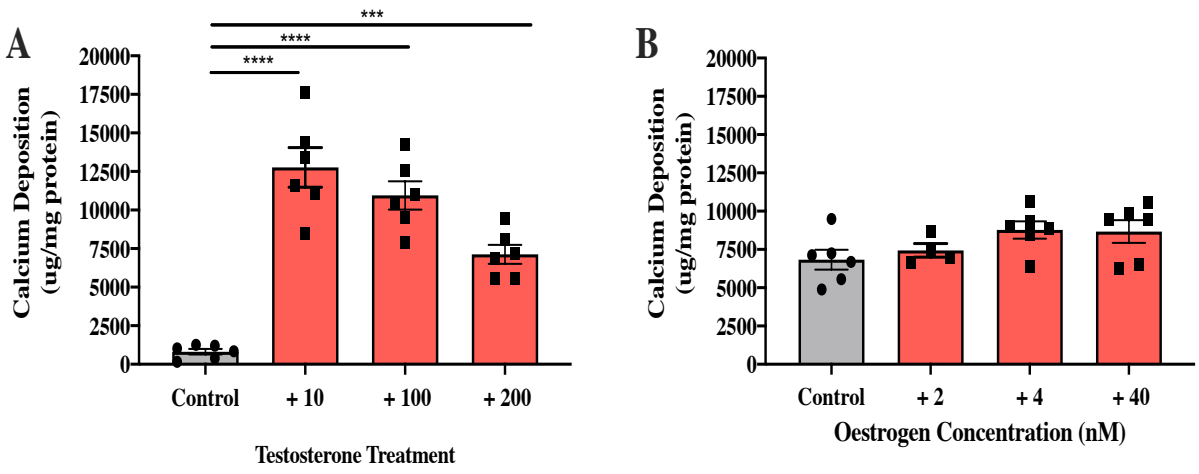

*Figure 3.4.8: Effect of sex hormone administration on calcification of primary RVICs from male rats***.** Rat valve interstitial cells (RVICs) were grown to confluence and calcified for 48 hours with or without addition of sex hormones. Calcium deposition was measured with a colorimetric assay. A) Addition of testosterone significantly increased calcium deposition at all concentrations (lowest at 10nM). B) Addition of oestrogen produced no significant difference in calcium deposition. Columns represent mean±SEM, points are single data values. Data were analysed using One-way ANOVA with post-hoc Dunnett's test comparing all hormone treatments to calcified cells only. Cells from 8 rats were grown together and 6 technical repeats were carried out. ***=p<0.0001, ****=p<0.00001. Control= osteogenic media only.

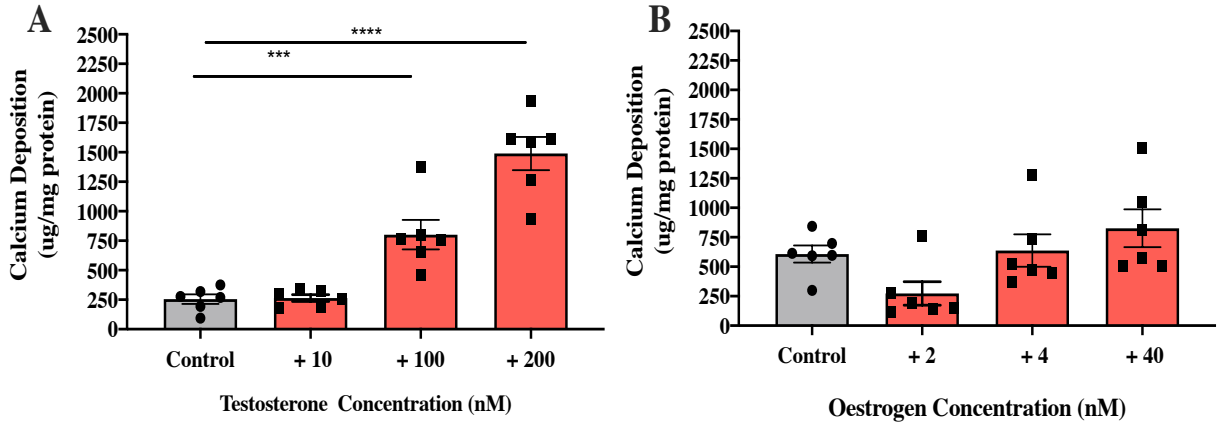

Figure 3.4.9: Effect of sex hormone administration on calcification of primary VICs from female rats. Rat valve interstitial cells (RVICs were grown to confluence and calcified for 48 hours with addition of sex hormones. Calcium deposition was measured with a colorimetric assay. A) Addition of testosterone significantly increased calcium deposition in a concentration-dependent manner, with the changes achieving significance at 100 and 200 nM. B) Addition of oestrogen produced no significant difference in calcium deposition. Columns represent mean±SEM, points are single data values. Data were analysed using One-way ANOVA with post-hoc Dunnett's test comparing all hormone treatments to control. Cells from 8 rats were grown together and 6 technical repeats were carried out. ***=p<0.0001, ****=p<0.00001, Control- calcification media only.

3.4.5 Characterising the distribution of the sex hormone receptors

Firstly, the distribution of mRNA expression of the *Ar, Erα, Erβ and CYP191a* was characterised in tissue from male and female rats. All mRNA expression was normalised to housekeeper genes and expressed as fold change of average gonadal expression. In male rats, mRNA expression of the *Ar* was significantly higher in the aorta (3.6-fold change, p= 0.0268) compared to testes (Figure 3.4.10 A). The mRNA expression of the *Ar* was also significantly (94-fold, p<0.0001) lower in the immortalised RVICs, compared to primary RVICs (Figure 3.4.10A). Expression of *Erβ* mRNA was significantly higher both in primary RVICs (56.4-fold, p<0.0001) and in immortalised RVICs compared to the testes (59.1-fold, p<0.0001, 3.4.10 B). The mRNA expression of *Erα* was significantly lower both in primary RVICs (9.7-fold, p=0.0083) and in immortalised RVICs, compared to the testes (13.2-fold, p=0.0062) (Figure 3.4.10 C). The mRNA expression of *Cyp191a* was significantly lower both in primary RVICs (7.2-fold, p=0.0013) and in immortalised RVICs compared to the testes (7.8-fold, p=0.0012) (Figure 3.4.10 D).

In tissues from female rats, mRNA expression of the *Ar* was significantly lower in the aortas (5.99-fold), ventricle (11.4-fold), liver (61.3-fold), and RVICs (3.3-fold), compared to the ovaries (p<0.0001, Figure 3.4.11 A). The mRNA expression of *Erα* was significantly lower in primary RVICs (2.9-fold, p=0.0010), liver (2.9-fold, p=0.0368) and ventricles (7.6-fold, p=0.0034, Figure 3.4.11 B) compared to the ovaries. The mRNA expression of *Erβ* was significantly lower in RVICs (p=0.0449), aorta (p=0.0437) and ventricles (p=0.0445, 3.4.11 C). The mRNA expression of *CYP191a* was significantly lower in both RVICs (7.2-fold, p=0.0376) and the ventricle, compared to the ovaries (7.8-fold, p=0.0474) (Figure 3.4.11 D).

DHT is produced endogenously from testosterone by the enzyme 5α-reductase and, unlike testosterone, does not have any non-genomic effects and only interacts with the AR (Li *et al.*, 2011). Incubation of rat VSMCs with 1nM DHT significantly increased (3.8-fold, p=0.002) calcium deposition (Figure 3.4.12 A). In male-derived primary RVICs, 10nM DHT significantly (1.5 fold, p=0.0286) increased calcium deposition (Figure 3.6.12 B). There was no change in calcification of female-derived RVICs after testosterone treatment (Figure 2.6.12 C).

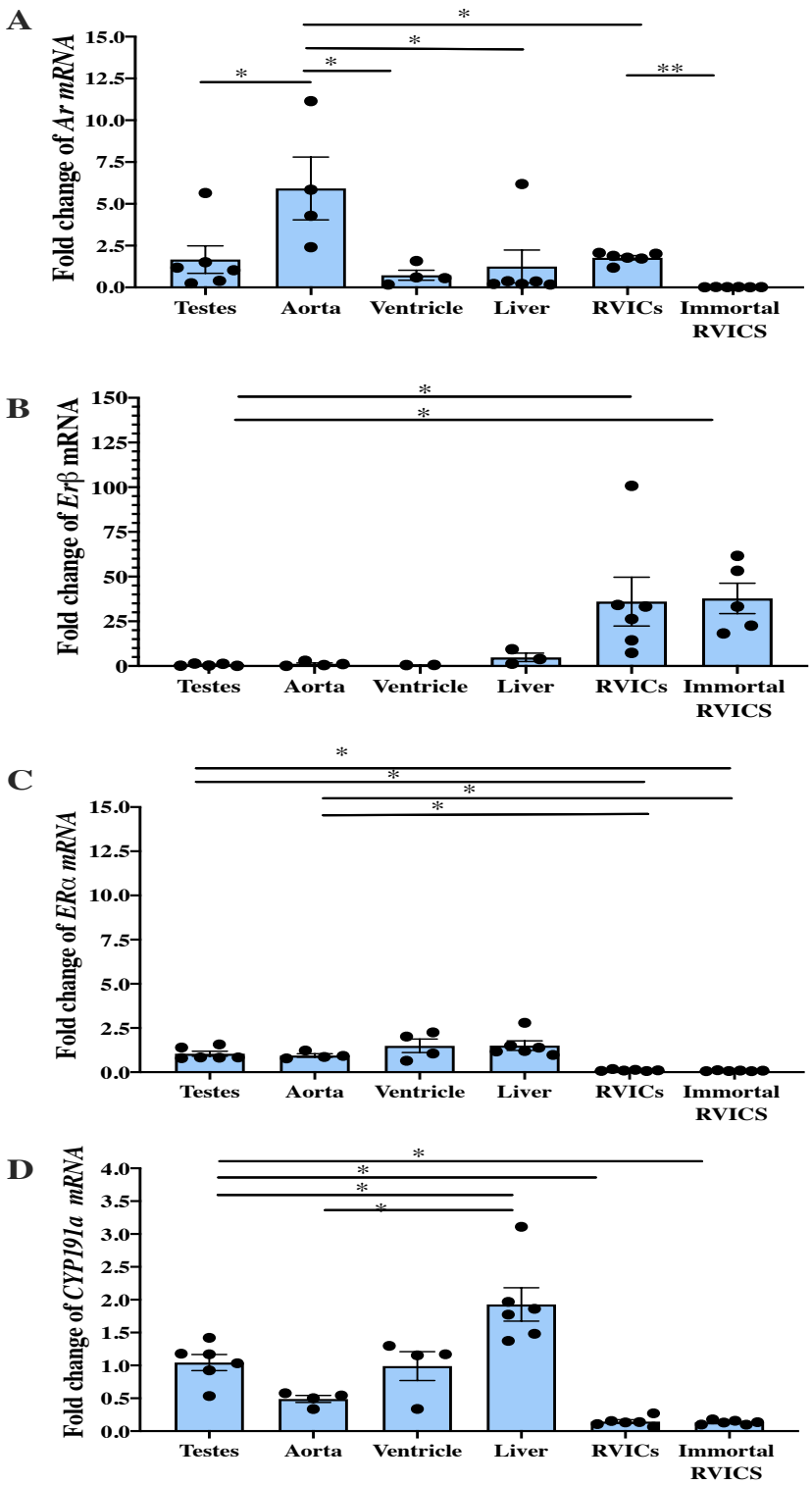

Figure 3.4.10. Expression of sex hormone receptors and the CYP191α mRNA in male rats. Male rats were culled at 8 weeks of age and tissues snap frozen. Rat valve interstitial cells (RVICs) were isolated from the aortic valve and grown to confluence. RNA was extracted, and gene expression was analysed using q-RTPCR. A) *Ar* mRNA expression was significantly higher in aortas compared to testes. B) *Erβ* mRNA expression was significantly higher in RVICs and immortalized RVIC compared with testes. C) *Erα* mRNA expression was significantly lower in RVICs and immortalized RVICs compared to testes D) *CYP191α* mRNA expression was significantly higher liver and reduced in RVICs and immortalized RVICs. Cells from 8 rats were grown together and 6 technical repeats were carried out. Data were analysed using One-way ANOVA with Tukey's post-hoc test*=$p<0.05$ **=$p<0.001$ ***=$p<0.0001$.

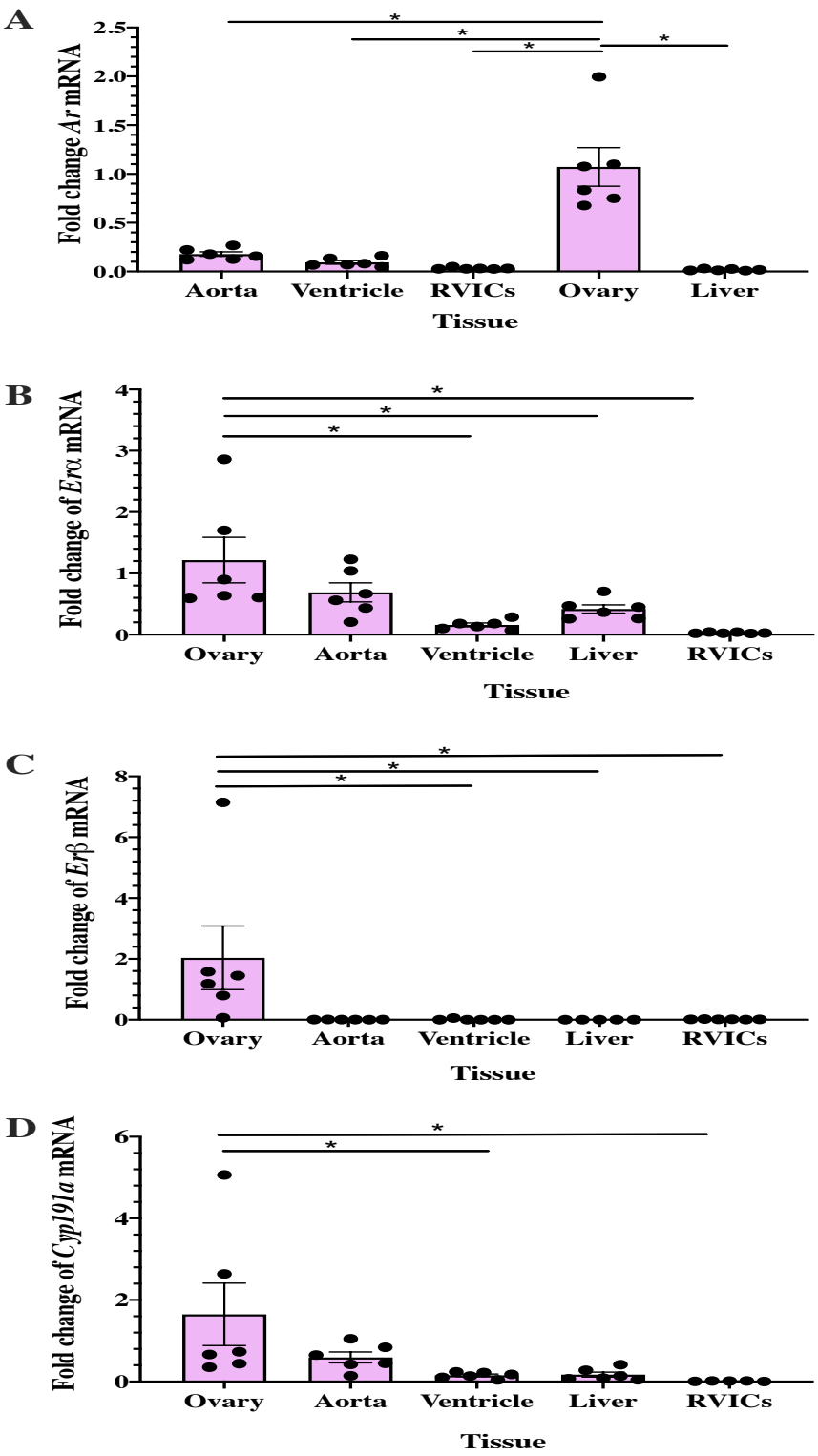

Figure 3.4.11. Expression of sex hormone receptors and the CYP191α mRNA in female rats. Female rats were culled at 8 weeks of age and tissues snap frozen. Rat valve interstitial cells (RVICs) were isolated from the aortic valve and grown to confluence. RNA was extracted, and gene expression was analysed using q-RTPCR. A) *Ar* mRNA expression was significantly lower in aortas, liver, RVICs and ventricles compared with ovaries. B) *Erα* mRNA expression was significantly lower in RVICs, livers and ventricles compared with ovaries C) *Erβ* mRNA expression was significantly lower in RVICs, livers and ventricles compared with ovaries D) *CYP191α* mRNA expression was significantly lower in ventricles and RVICs. compared with ovaries. Cells from 8 rats were grown together and 6 technical repeats were carried out. Data were analysed using One-way ANOVA with Tukey's post-hoc test*=$p<0.05$ **=$p<0.001$.

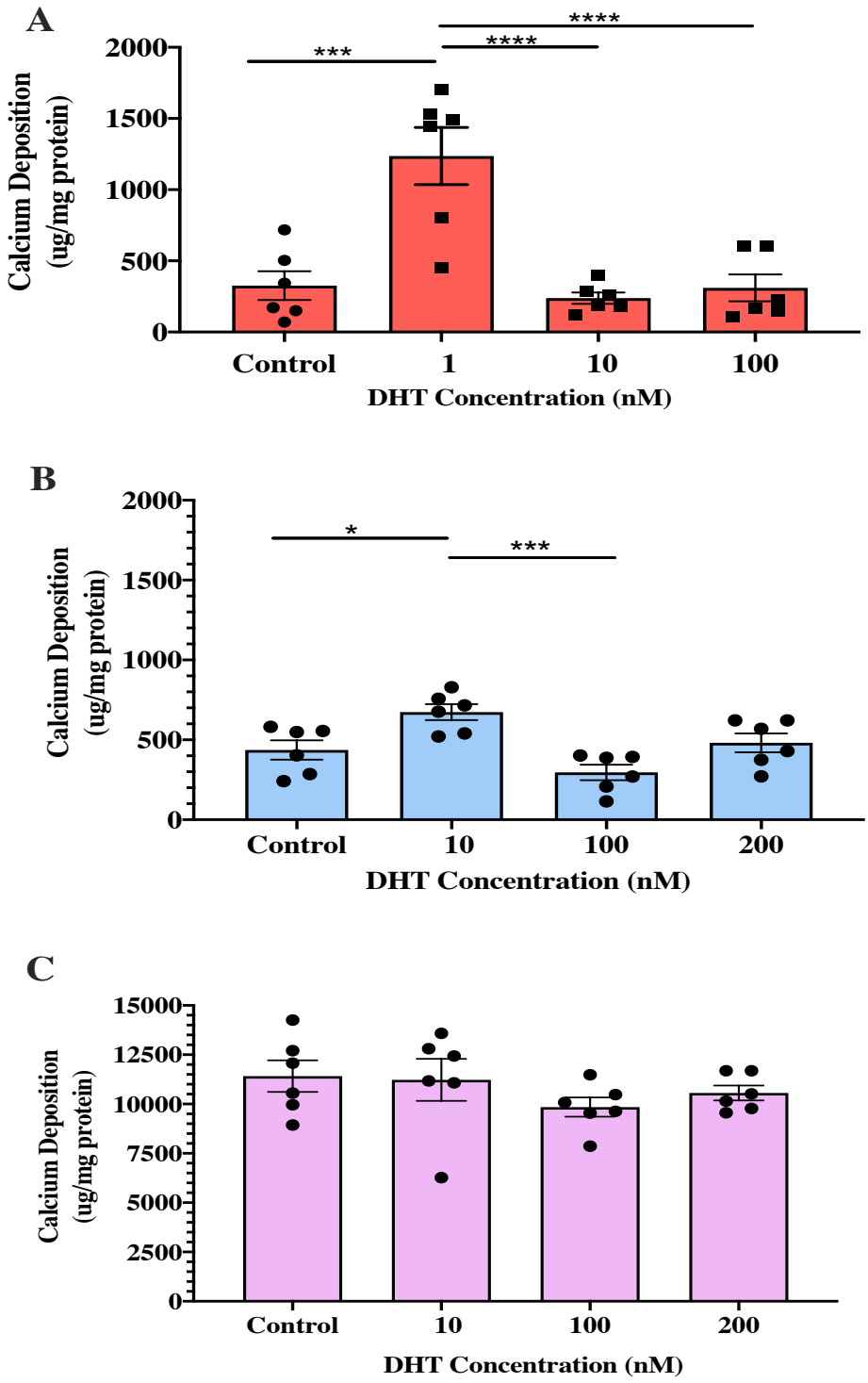

Figure 3.4.12: Effect of DHT administration on calcification of primary VSMCs from male rats and RVICs from male and female rats. Rat valve interstitial cells (RVICs) were grown to confluence and calcified for 48 hours. rat vascular smooth muscle cells (VSMCs) were grown to confluence and calcified for 9 days. Calcium deposition was measured with a colorimetric assay. A) Addition of DHT significantly increased calcium deposition at 1 nM in VSMCs from male rats. B) Addition of DHT significantly increased calcium deposition at 10 nM in VICs from male rats. C) Addition of DHT did not change calcium deposition in VICs from female rats. Columns represent mean±SEM, points are single data values. Data were analysed using One-way ANOVA with post-hoc Bonferroni's test. Cells from 8 rats were grown together and 6 technical repeats were carried out. *=$p<0.05$ ***=$p<0.0001$, ****=$p<0.00001$.

3.4.6 Investigating the mechanisms underpinning of testosterone driving calcification using proteomics

Samples were collected in two experimental groups: calcified male-derived rat VICs (control, C), and calcified male-derived rat VICs treated with testosterone (T, 100 nM, 48 hours). Samples were loaded in the same concentrations; the protein abundance was also calculated from the peaks that the mass spectrometer (MS) read. There was an outlier in sample C, repeat 1 (Figure 3.4.13) which had lower protein abundance than the other samples. The correlation between the peptide readouts between samples was also calculated. Repeat 1 (C1) of the male-derived calcified rat VICs did not correlate with any other sample (Figure 3.4.14). This sample was therefore excluded. The abundance of proteins in each remaining sample was subject to repeat correlation analysis, without the excluded sample. Repeated samples within each treatment group displayed a high correlation (Figure 3.4.15). The raw peptide data from the MS were negatively correlated in each sample (Figure 3.4.16 A) and were therefore transformed to become normally distributed (Figure 3.4.16 B).

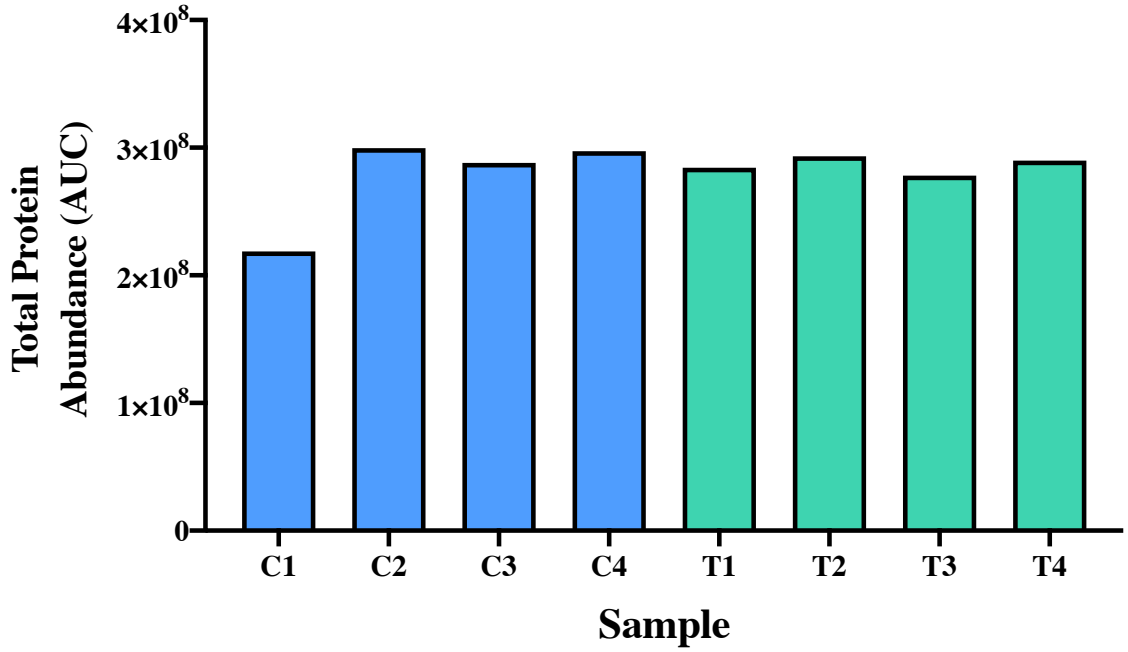

Fig 3.4.13. Total protein abundance in each sample by LC-MS. Rat valve interstitial cells (RVICs) from male rats were grown in the absence (M) or the presence (T) of testosterone (100nM; 48 hours), calcified for 48 hours and subject to LC-MS. This graph displays the total protein that was calculated by the mass spectrometer by calculating the total area under the curves of the MS peaks. Numbers are sample repeats.

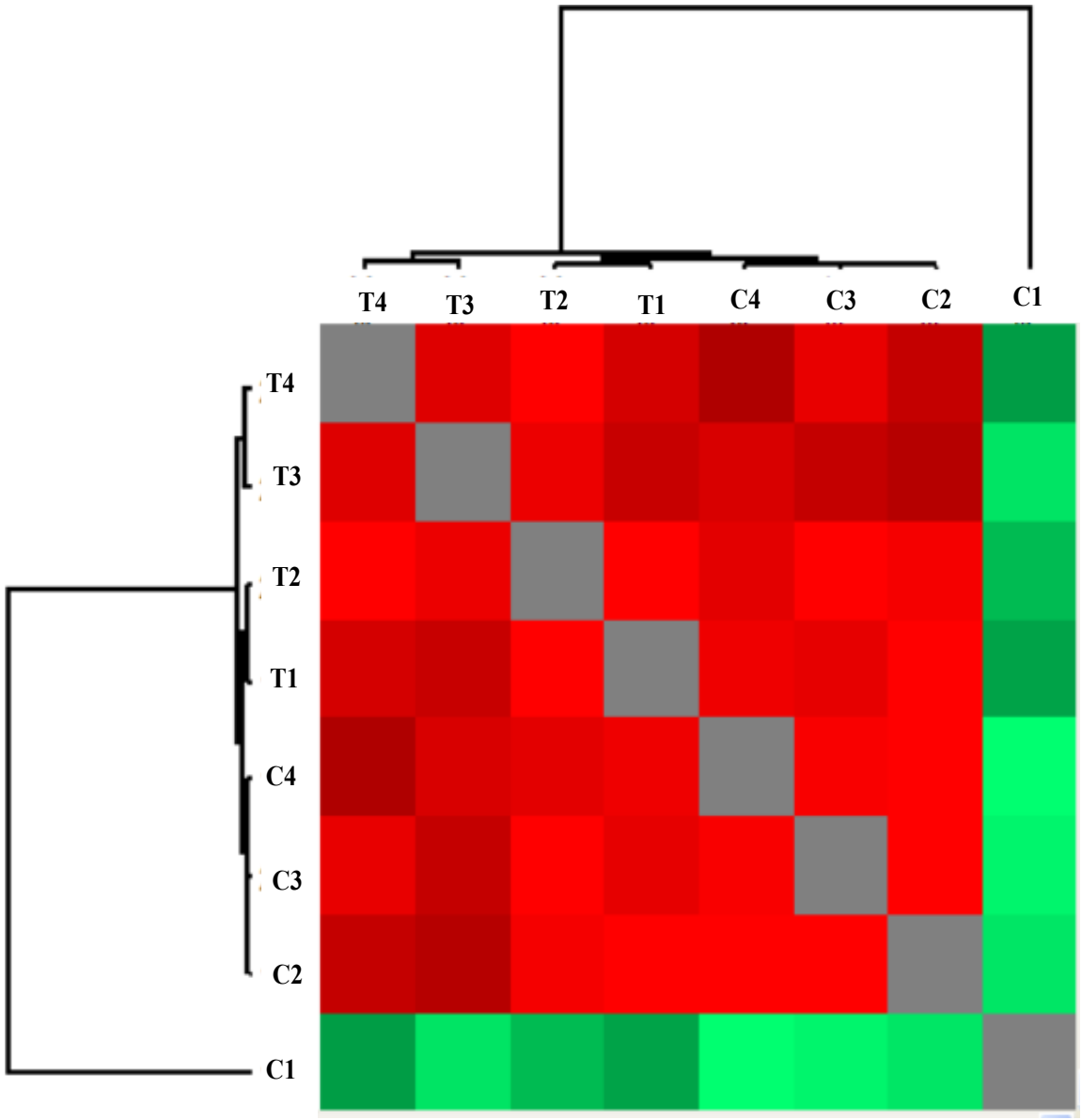

Fig 3.4.14. Proteomics sample correlation. Rat valve interstitial cells (RVICs) were grown to confluence , calcified for 48 hours and subject to LC-MS proteomics analysis. This heat map displays the correlation between each sample where red is high and green is low. M1 had very low correlation with other samples. M= Males, T= Male + Testosterone treatment (100 nM, 48 hours). There is an outlier here, M1, so this sample was excluded.

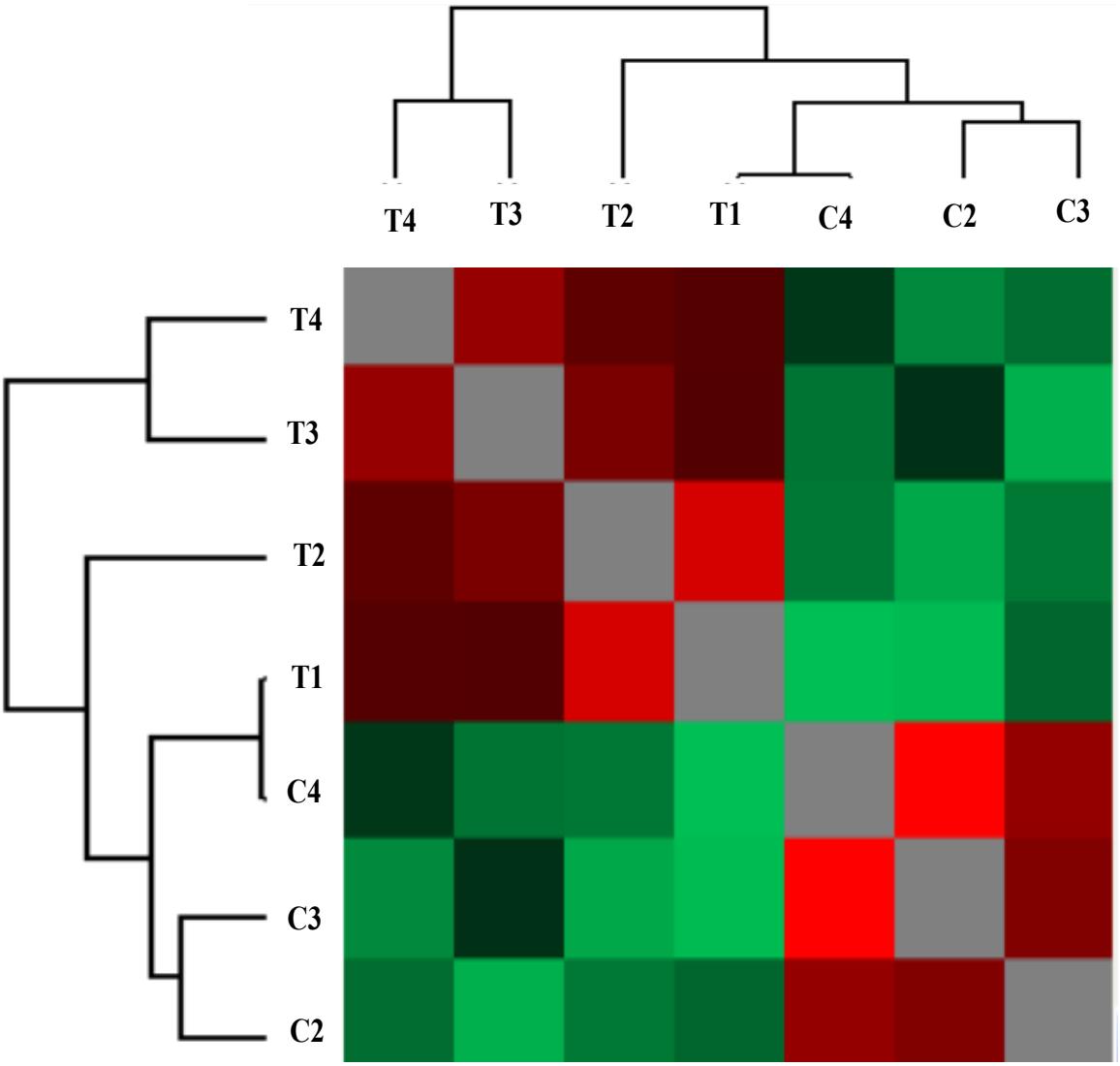

Fig 3.4.15. Proteomics sample correlation after sample exclusion. RVICs were grown to confluence, calcified for 48 hours and subject to LC-MS proteomics analysis. This heat map displays the correlation between each sample where red is high, and green is low. M= Males, T= Male + Testosterone treatment (100 nM, 48 hours) F=Females.

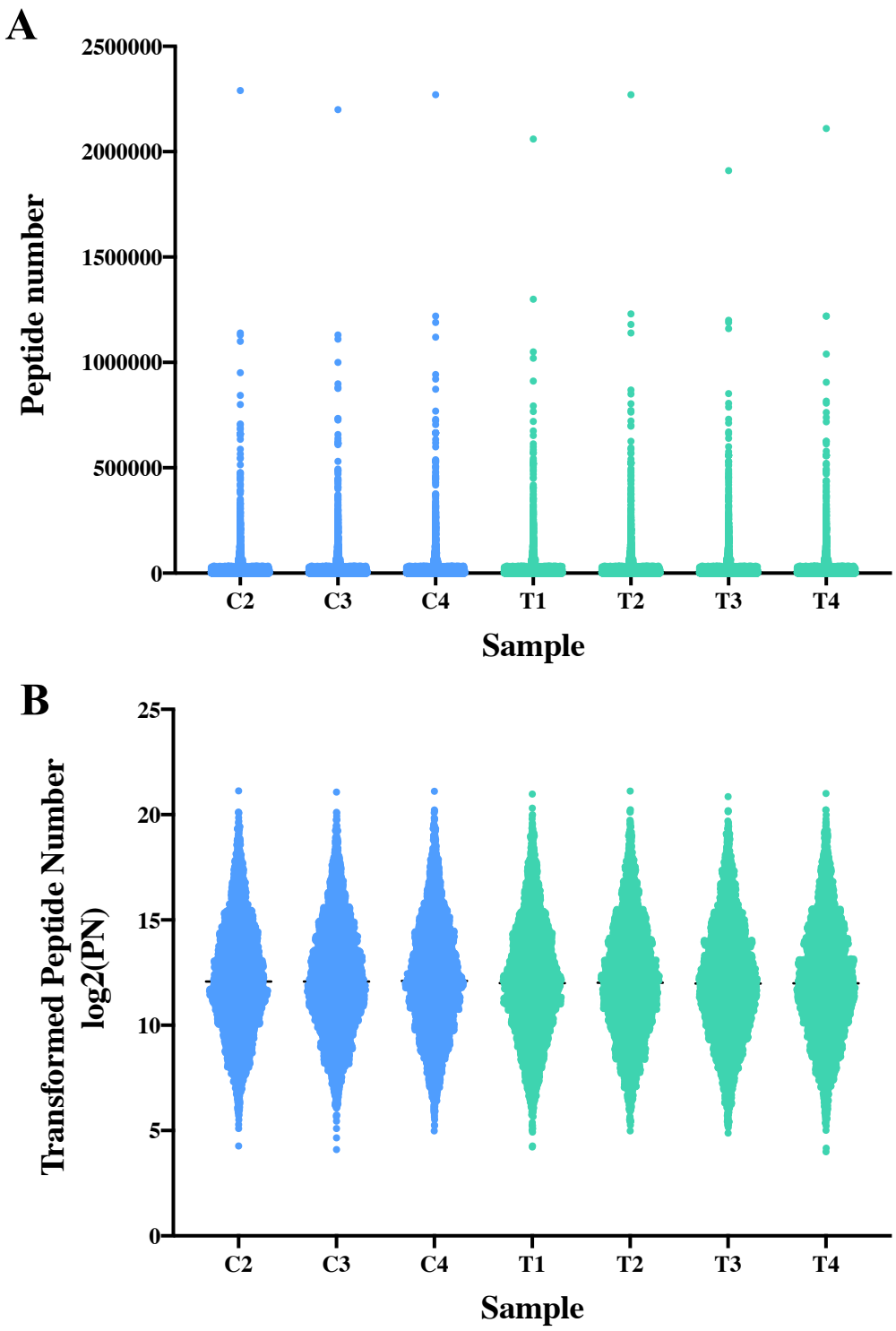

*Fig 3.4.16. Proteomics sample correlation after sample exclusion***.** Data normalisation to normal distribution. A) Direct readings of peptide numbers from LC-MS for each sample, peptides display a negatively skewed data set. B) Data were transformed by log2 to make the data normally distributed for analysis. M= Males, T= Testosterone treated (100 nM, 48 hours) F=Females.

3.4.7 Testosterone treatment significantly changed the expression of 356 proteins in calcified VICs from male rats.

The analysis found 356 significantly differentiated proteins after testosterone treatment in VICs isolated from male rats, majority of these being significantly downregulated (Figure 3.5.17). The top 10 upregulated proteins after testosterone treatment are shown in Table 3.5.1. The top 10 significantly downregulated proteins after testosterone treatment are shown in Table 3.5.2. The proteins that were differently expressed between the groups were then subject to gene ontology analysis (Figure 3.5.18). The most enriched ontological processes in this data set are show in Figure 3.5.18. Protein networks were made of the two most enriched ontologies, TCA metabolism (Figure 3.5.19) and NADH dehydrogenase assembly **(**Figure 3.5.20).

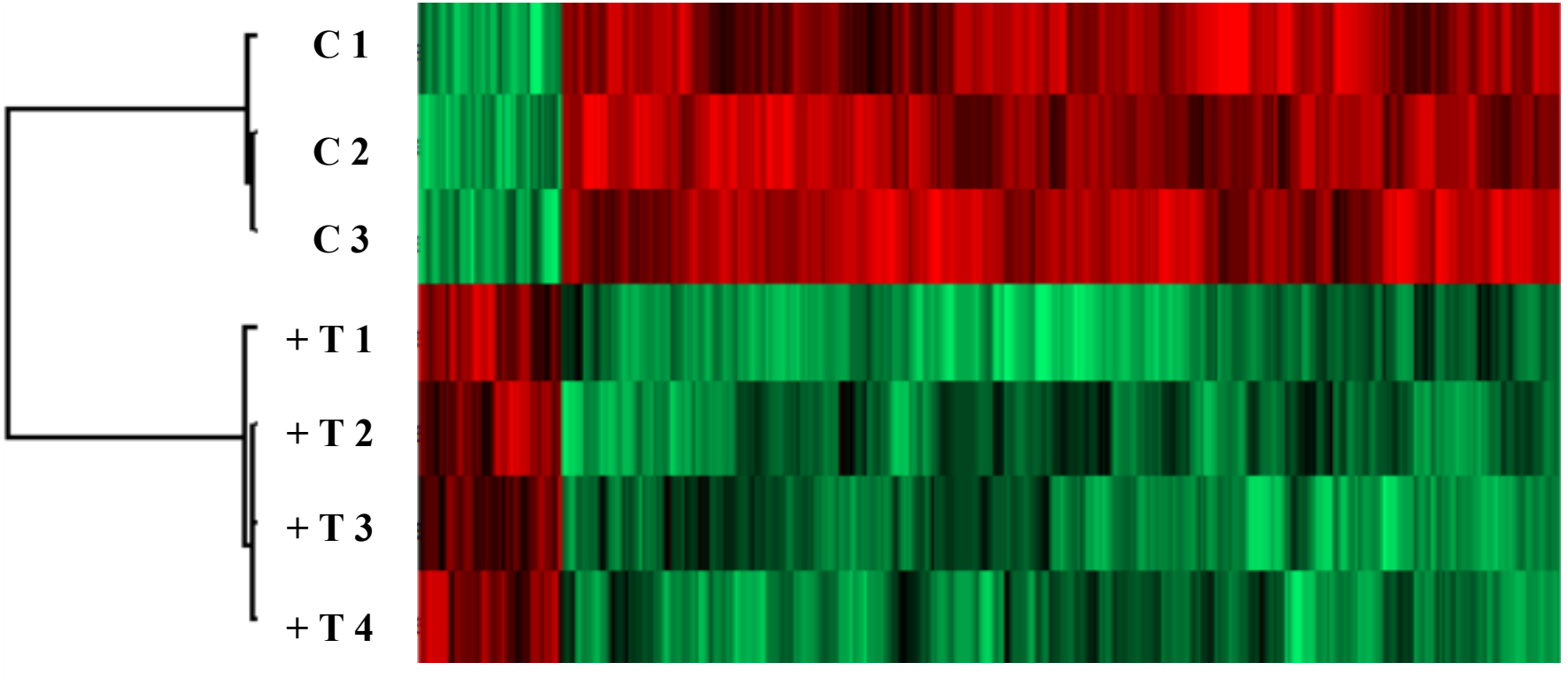

*Fig 3.4.17. Heat map of significantly differentially expressed proteins between control and testosterone treated male RIVCs***.** RVICs were grown to confluence, calcified for 48 hours and subject to LC-MS proteomics analysis. Data were transformed and normalised and t-tests performed with multiple comparison corrections (false discovery rate at 0.05). Red-significantly upregulated, green-significantly downregulated. 365 proteins were found to be differentially expressed.

Table 3.4.1 The most significantly upregulated proteins after testosterone treatment of calcified male-derived rat valve interstitial cells (RIVCs). RVICs were grown to confluence, calcified for 48 hours and subject to LC-MS proteomics analysis. Data were transformed and normalised and analysed using Student's t-tests multiple comparison corrections (false discovery rate at 0.05). This table is sorted by fold change. They also display the -log10 p values and the q values from the Student's t-test.

Gene name	Log (FC) (4s.f)	-Log Student's T-test p-value (4s.f)	Student's T-test q-value (4s.f)
Comp	2.066	4.128	0.04918
Aoc3	1.629	3.041	0.03267
Fat4	1.623	4.472	0.0720
Ndrg1	1.620	4.364	0.05634
Aox1	1.357	5.987	0.01400
Akr1c15	1.326	2.677	0.03622
Cspg4	1.306	3.600	0.03107
LOC102546963	1.288	3.039	0.03237
Eln	1.286	2.686	0.03523
Wdfy2	1.186	2.555	0.03846

Table 3.4.2 The most significantly downregulated proteins after testosterone treatment of calcified male-derived rat valve interstitial cells (RIVCs). RVICs were grown to confluence, calcified for 48 hours and subject to LC-MS proteomics analysis. Data were transformed and normalised and Student's t-tests were performed with multiple comparisons corrections (false discovery rate at 0.05). This table is sorted by fold change. They also display the -log10 p values and the q values from the Student's t-test.

Gene name	Log (FC) (4s.f)	-Log Student's T-test p-value (4s.f)	Student's T-test q-value (4s.f)
Mcam	-1.578	2.170	0.04837
Ccn3	-1.514	3.098	0.03025
Tubb3	-1.014	2.835	0.03224
Pik3c2a	-0.7505	2.348	0.04069
Fbln2	-0.7492	3.007	0.03207
Arpp19	-0.6967	2.236	0.04510
Mapkapk2	-0.6521	2.482	0.03864
Arhgef25	-0.6490	3.014	0.03161
Mmp2	-0.5667	2.520	0.03868
Shroom1	-0.5631	3.072	0.03155

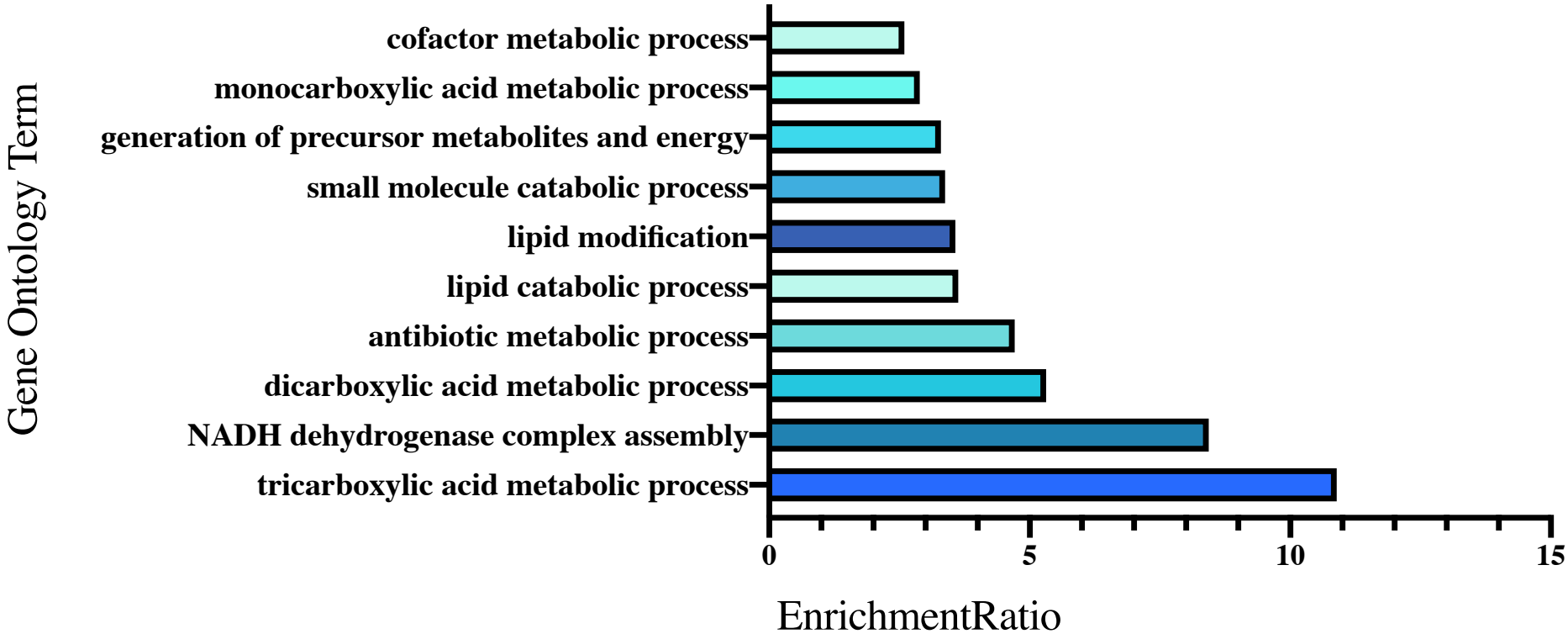

*Fig 3.4.18 Gene ontology of hits from proteomics between control and testosterone treated male-derived rat valve interstitial cells (RIVCs)***.** RVICs from male animals were grown to confluence, calcified for 48 hours and subject to LC-MS proteomics analysis. Gene ontology analysis performed on WebGestalt, Over representation analysis.

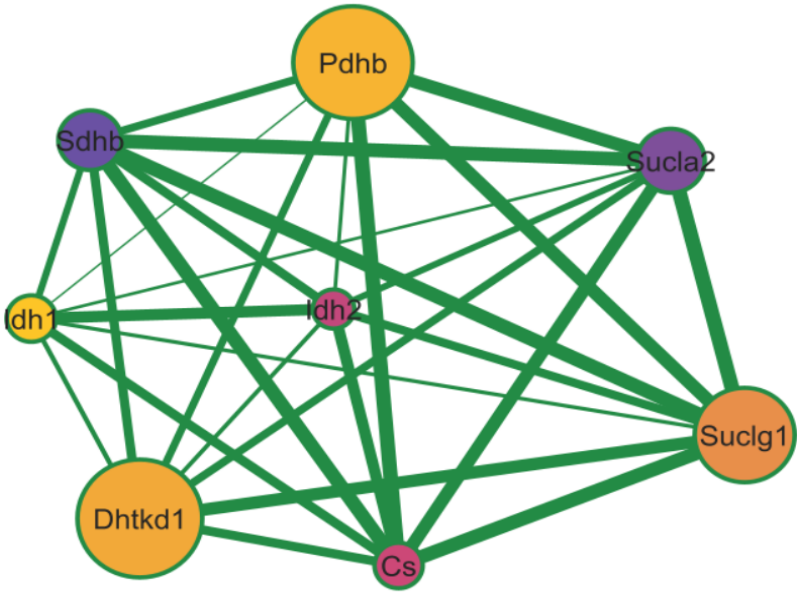

Fig 3.4.19 Protein interactions network of protein hits associated with tricarboxylic acid metabolism. M*ale-derived rat valve interstitial cells (*RVICs) were grown to confluence, calcified for 48 hours and subject to LC-MS proteomics analysis. A metabolism network map from the 8 unique tricarboxylic acid metabolism protein hits was created using STRING in Cytoscape. Associated genes were determined in STRING based on published databases and specific omics publications. The size of the node is relative to fold change; colour is relative to significance and thickness of the linking line is relative to strength of association. Tricarboxylic acid metabolism had a 10.9 enrichment ratio in this data set. Nodes represent proteins and lines represent physical interactions between them**.**

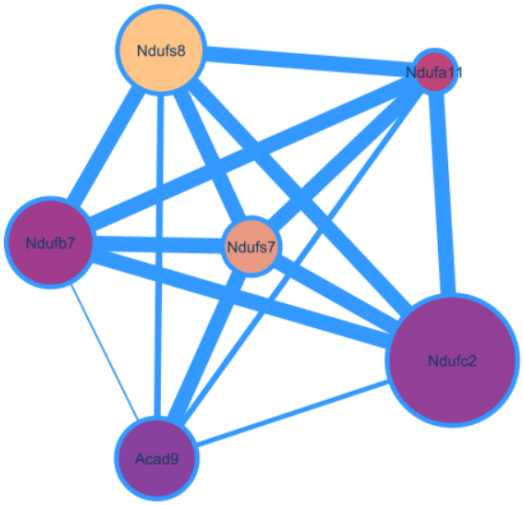

Fig 3.4.20 Protein interactions network of protein hits associated with NADH dehydrogenase assembly. M*ale-derived rat valve interstitial cells* (RVICs) were grown to confluence, calcified for 48 hours and subject to LC-MS proteomics analysis. A metabolism network map from the 6 unique protein hits that were associated with NADH dehydrogenase assembly was created using STRING in Cytoscape. Associated genes were determined in STRING based on published databases and specific omics publications. The size of the node is relative to fold change, colour is relative to significance and thickness of the linking line is relative to strength of association. NADH dehydrogenase assembly had an 8.4 enrichment ratio in this data set. Nodes represent proteins and lines represent physical interactions between them.

3.5 Discussion

In this study, it was hypothesized that: (i) testosterone drives aortic valve calcification, and (ii) oestrogen is protective against aortic valve calcification (Simard *et al.*, 2017). The intention was to investigate whether sex differences in aortic valve calcification could be modelled using isolated VICs. A combination of *in vitro* assays and proteomics analysis was used to assess whether sex hormones modulated the *in vitro* calcification of VICs. The results described in this chapter demonstrate that calcification of VICs can be induced *in vitro* and that RVICs can be used to investigate the influence of sex hormones on *in vitro* calcification. The development of this model has led to experiments demonstrating that testosterone increases calcification in RVICs and highlighting the mechanisms underpinning testosterone-enhanced aortic valve calcification. This work is important in contributing to elucidating the mechanisms of sexual dimorphism displayed in humans with CAVD (Simard *et al.*, 2017).

3.5.1 RVICs can be used as an in vitro model of valve calcification

The first experiment undertaken in this chapter showed that the RVICs Sv40 cell line expresses markers consistent with their identity as VICs. The markers of VICs that were used (vimentin and α-SMA) were selected as previously published data had demonstrated the expression of these proteins in primary RVICs (Cui *et al.*, 2017). These cells did not show immunofluorescence when stained for CD31, an endothelial cell marker references, which confirmed that they did not have features of endothelial cells. These experiments demonstrated the manufactured cell line has protein markers consistent with VICs.

There are many methods of inducing *in vitro* calcification include the addition of Calciprotein Particles (CPP) and β-Glycerophosphate (Kelynack and Holt, 2016). The protocol chosen in this thesis was high phosphate and high calcium as it produced VIC calcification *in vitro* consistent with the literature and high phosphate is a risk factor for vascular calcification in humans (Campos-Obando *et al.*, 2022). The selected media conditions were based on previously published *in vitro* calcification of RVICs and the data that was generated in this thesis produced a consistent pattern of calcium deposition with Cui *et al.* (2017).

The presence of α-SMA in the VICs indicates that under the standard culture conditions used in the lab, VICs exist in an activated/proliferative phenotype (Tan *et al.*, 2019). In a healthy valve, VICs exist in a quiescent state (Liu, Joag and Gotlieb, 2007). It was, therefore,

investigated whether different culturing conditions, which produce different cell phenotypes, would affect *in vitro* calcification. The activated-phenotype-inducing media has been previously published in the MacRae laboratory (Cui *et al.*, 2017) whilst the 'quiescent' media was based on a published protocol (Porras *et al.*, 2017; Tan *et al.*, 2019). The activating media has a higher percentage of FBS, which can induce proliferation in cells (Latif *et al.*, 2015). The different culture conditions did not produce different responses to the calcification media. The current theory behind the de-differentiation of VICs during CAVD is that VICs change from a qVICs to aVICs to finally become obVICs (Hjortnaes *et al.*, 2015). These obVICs are the phenotype that produces hydroxyapatite (Hjortnaes *et al.*, 2015). As there was no change in the calcium deposition seen between the culture conditions, the same amount of hydroxyapatite has been produced. Potentially the calcification media is inducing the same amount of differentiation into obVICs in both culture conditions.

3.5.2 RVICs can be used to investigate the effect of sex hormones on in vitro calcification

It has been shown previously that testosterone augments calcification in VSMCs (Zhu *et al*., 2016). To validate whether the protocol used in this thesis would successfully model sex-hormone enhanced calcification, the testosterone treatment was first conducted on VSMCs. This assay produced a similar pattern of calcification in response to testosterone that was seen in Zhu *et al*. (2016) so the optimisation was, therefore, repeated on VICs. After the results with the SV40 cell line where inconsistent with the previous published data on VSMCs, the testosterone assay was replicated on primary VICs from male and female rats, which produced results more consistent with the pattern generated by testosterone-augmented calcification on VSMCs in Zhu *et al*. (2016). The qRT-PCR demonstrated that *Ar* mRNA expression was lower in the RVICs SV40 cell line (derived from male rats) than in primary cells. This could explain the lack of effect of testosterone on the SV40 cell line. Therefore, it was concluded that this cell line was not appropriate for the investigation of the effect of sex hormones. There are acknowledged problems with using cell lines as opposed to primary cells, including genetic and phenotypic instability and misidentification of the cell line (Geraghty *et al.*, 2014). Therefore further development was conducted on primary RVICs.

3.5.3 Testosterone augments *in vitro* calcification of RVICs, potentially through the androgen receptor

The data presented here demonstrates that the addition of testosterone (10-200 nM over 48 hours) augments *in vitro* calcification in VICs. Given the observation that testosterone augmented calcification at a lower concentration in VICs from male, compared with female, rats, VICs from males may be more susceptible to pathological changes in serum testosterone than females. In VSMCs, a higher expression of AR has been seen in cells from males compared to females (Higashiura, Mathur and Halushka, 1997). Although there is contrasting data that shows that testosterone inhibits calcification of VSMCs (Son *et al.*, 2010). The demonstration here that testosterone stimulates calcification of VICs is consistent with clinical trials in which high testosterone has been associated with an increase in VSMC calcification (Morris and Channer, 2012); especially as the concentrations of testosterone used in this study are within the physiological range (from 7 nmol/L to 40 nmol/L in healthy male adults and >40 nmol/L is considered to be high) for circulating testosterone in humans (Handelsman, Hirschberg and Bermon, 2018).

As there was high AR mRNA expression in the RVICs and in the aorta of male rats, the calcium assay supplemented with sex hormones were repeated with DHT (an analogue of testosterone that selectively binds to the AR (Foradori, Weiser and Handa, 2008), is not metabolised by aromatase (Dušková and Pospíšilová, 2011), and has no non-genomic effects (Foradori, Weiser and Handa, 2008). The demonstration that DHT significantly increased calcification in RVICs indicates that this response is mediated by the androgen receptor, which has been previously shown in murine VSMCs (Zhu *et al.*, 2016). Although further experiments (as described in section 3.5.6) would need to be performed to confirm this finding.

In both male and female primary RIVCs, no change was recorded in calcium deposition after oestradiol administration, contrary to the initial hypothesis. The interpretation of this could be that oestrogen does not influence calcification in valve interstitial cells under the conditions of this thesis. CAVD is a disease which involves interactions between many cell types in the aortic valve therefore this observation is limited in only using VICs. In the literature there are few investigations into the influence of sex hormones on VICs. However, work on VSMCs has shown that oestrogen can both inhibit (Osako *et al.*, 2010) and augment (Balica *et al.*, 1997) calcification of VSMCs. Clinical trials have also been performed investigating the influences of oestrogens on vascular calcification with positive results. Oestrogen treatment and HRT has

been shown to reduce aortic plaque calcification burden (Shemesh *et al.*, 1997; Manson *et al.*, 2007). Therefore, our studies indicate oestrogen has no significant effect on calcification in VICS, but this needs which contradicted to the literature on oestrogens action on VSMCs.

3.5.4 Testosterone alters respiration and energy metabolism in calcified male-derived RVICs

Incubation with testosterone altered the expression of 365 proteins in calcified RVICs, over 60 % of these are proteins associated with cellular energy metabolism. Interestingly previous preclinical investigation has linked a dysregulation in metabolism during calcification. Therefore, testosterone may cause dysfunctional metabolism (shown by the proteomic data) which causes augmented calcification (shown in the *in vitro* assays). This is a preliminary finding but is supported by another preclinical investigation which have shown that inducing an osteogenic phenotype in VICs increased expression of NAD(P)H oxidase subunits including Nox2 and p22phox (Liberman *et al.*, 2008). A recent study in rabbits also demonstrated decreased valve calcification in response to lipoic acid (antioxidant) treatment, suggesting ROS and cellular metabolism maybe contributing to the development of valve calcification (Liberman *et al.*, 2008). Furthermore, a metabolic shift has been observed in patients with CAVD, including a reduction of proteins associated with oxidative phosphorylation, fatty acid transport and the TCA cycle, consistent with those observed in this study (Heather *et al.*, 2011). Another clinical study reported evidence of increased oxidative stress and uncoupling of nitric oxide synthases (NOS) in calcified valves (Miller *et al.*, 2008). Overall, the proteomics analysis indicated that testosterone may be causing a change in cellular metabolism which induces calcification (see Figure 3.5.1). To further this study, a male murine model of CAVD could be treated with testosterone, to investigate if the testosterone enhanced valve calcification *in vivo.* A following treatment with metformin could be applied, to stimulate autophagy to investigate if the metformin affects aortic valve calcification (De Santi *et al.*, 2019).

There are also indicators of immune cell function in this proteomic data set. The ontology analysis revealed pathways associated with neutrophil activation. In clinical studies, the neutrophil-lymphocyte ratio has been associated with an increase in coronary artery calcification (Serrano *et al.*, 2019). Preclinical trials have shown that calcium-phosphate mineral particles induce the release of neutrophil extracellular traps which are coupled with ROS production (Peng *et al.*, 2017). These mineral particles (which reflect microcalcification) directly interact with neutrophils and macrophages to induce a pro-inflammatory state (Peng *et al.*, 2017). This indicated that another pathway through which testosterone may augment

calcification may be through neutrophil activation and induction of inflammation, although these are preliminary observations.

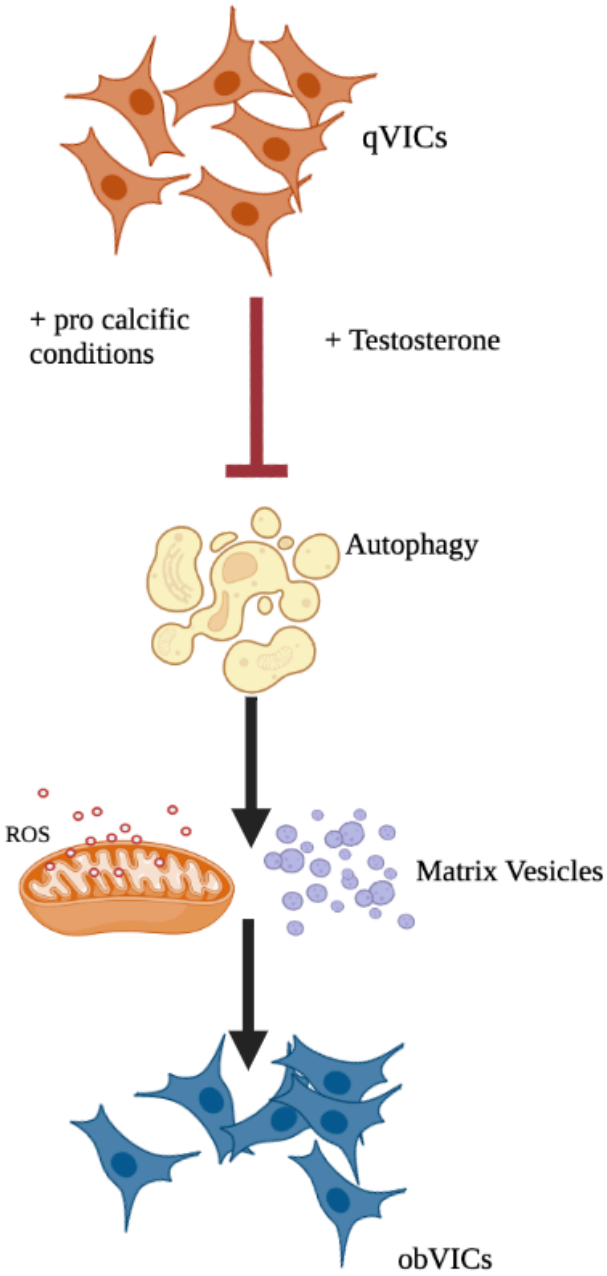

Figure 3.5.1: Potential Mechanism of Testosterone fuelling calcification. This figure shows the potential mechanism by which testosterone is augmenting calcification. qVICs- quiescent valve interstitial cells, obVICs- osteoblastic valve interstitial cells. ROS- Reactive oxygen species.

3.5.6 Limitations and future investigations

A notable limitation of the proteomics experiment was that the VICs were isolated from 5–6-week-old rats. Rats usually go through puberty between 6-8 weeks of age (Leibowitz *et al.*, 2009). These samples were therefore from pre-pubescent animals and may have had reduced endogenous sex hormone production compared to adults (where CAVD is only seen in adult humans). These experiments could therefore be repeated on samples from animals in their productive years.

In this study, it was hypothesized that testosterone-mediated calcification was through the action of testosterone on the androgen receptor in VICs. To confirm this conclusion, further experiments could be carried out to delete the AR *in vitro* using a siRNA method. These experiments were planned but problems with the protocol optimisation left insufficient time to complete this experiment. The testosterone assay would then be repeated to investigate whether the deletion of the AR blunts/reduces the effect of testosterone on calcification.

Once some of the hits from the analysis of the testosterone proteomics have been validated, pharmacological modulators could be developed for *in vitro* investigation. Testosterone is largely down-regulating proteins involved in the TCA cycle and NAPD regulation. Activators of these targets (identified by proteomics including IDH2 and CS) could be selected, and *in vitro,* functional studies carried out, for example siRNA knockdown. It would be interesting to investigate how testosterone is affecting *in vitro* cellular metabolism and mitochondrial function using a Seahorse analyser (Little *et al.*, 2020). This would include assays to investigate whether the introduction of modulators of these hits prevents testosterone-induced valvular calcification.

To extend this study, experiments should be undertaken to investigate whether testosterone is affecting valve calcification *in vivo*. This could be performed by designing an *in vivo* experiment in which a model of valve calcification was subject to orchidectomy (to stop testosterone production (Song *et al.*, 2017)) to investigate whether calcification was reduced with the abolition of testosterone production. Furthermore, testosterone (or DHT) could be administered (by injection/ minipump implantation). This would investigate whether calcification could be restored with the re-introduction of circulating androgen.

3.5.7 Conclusion

In conclusion, data reported in this chapter demonstrate that testosterone augments calcification of VICs, whilst pathway analysis revealed alterations to cellular energy metabolism. It was further demonstrated that oestrogen has no significant effect on calcification of VICs *in vitro*. This is the first study which has investigated the effect of sex hormones on VICs. This study also reports a novel pathway analysis of calcified valve interstitial cells from rats comparing testosterone to control calcified cells. These investigations could contribute to the understanding of the mechanisms of sexual dimorphism in CAVD. These findings may have implications for testosterone steroid abuse and hormonal replacement therapy (Morris and Channer, 2012). Further studies conducted on sex differences expanding from *in vitro* to *in vivo* systems follows in the next chapter.

Chapter 4: ApoE$^{-/-}$ mice display more vascular calcification and larger atherosclerotic lesions in females compared with males

Chapter 4: ApoE$^{-/-}$ mice display more vascular calcification and larger atherosclerotic lesions in females compared with males

4.1 Introduction

4.1.1 Apolipoprotein E (ApoE)

Apolipoprotein E (ApoE) is a protein involved in lipoprotein metabolism. ApoE aids lipoprotein clearance from the circulation to the liver (Marais, 2019). ApoE binds to receptors in the LDL receptor family and ApoE is present in some lipoproteins including very low-density lipoprotein (vLDLs) and LDLs (Libeu *et al.*, 2001; Nakamura *et al.*, 2003). In mice, deletion of the ApoE protein (ApoE$^{-/-}$) severely reduces lipoprotein clearance, producing a state of dyslipidaemia /hypercholesterolemia. On a chow diet, ApoE$^{-/-}$ mice have an average circulating cholesterol of 400 mg/dL (22.2 mmol/L) compared to 80 mg/dL in wild-type (WT) mice (Maeda, 2011). The dyslipidaemia in these animals is also characterised by increased plasma levels of LDLs, vLDLs and triglyceride (TG), which are risk factors for many cardiovascular diseases including aortic stenosis and valve calcification (Su and Peng, 2020). For this reason, many models of aortic valve calcification are based on insults which induce dyslipidaemia.

4.1.2 ApoE$^{-/-}$ mice as a model of aortic valve calcification

No preclinical murine model is consistent in developing cardiovascular calcification. Throughout murine models of CAVD, there is variability of between 25 and 75 % of the colony developing calcification. The reason murine models are used widely in preclinical studies is their relatively short generation time, low cost, and the abundance of available experimental resources including reagents and gene manipulation techniques (Sider, Blaser and Simmons, 2011). One of the most commonly used murine models of valve calcification is the ApoE$^{-/-}$ mouse on a high-fat diet. This is because ApoE$^{-/-}$ mice are commercially available and have been shown to more consistently present with pathologies of dyslipidaemia and aortic valve thickening and calcification, in comparison with other models (Sider, Blaser and Simmons, 2011). Calcification can develop in ApoE$^{-/-}$ mice at 8-12 months of age on a standard chow diet (McRobb *et al.*, 2017; Purroy *et al.*, 2018). Many methods can be employed to accelerate the dyslipidaemia phenotype in these mice, including supplementation with dietary fats (high fat/ high cholesterol diet), or causing additional damage with surgical intervention (such as in the 5/6 nephrectomy chronic kidney disease model (Bro *et al.*, 2003)). Another option is to

cross the ApoE$^{-/-}$ with another genetically manipulated model that is predisposed to cardiovascular disease, such as the low-density lipoprotein receptor knockout mouse (LDLR$^{-/-}$) (Langheinrich *et al.*, 2007). As more methods of inducing CAVD in murine models have developed so have the methods for detecting calcification.

4.1.3 Detection of calcification in murine models

As CAVD develops into aortic stenosis, the gold standard detection and characterisation method is echocardiography imaging in both patients and animal models. Echocardiography imaging of the heart is used to detect left ventricular remodelling whilst Doppler imaging of the aortic outflow is used to detect aortic stenosis and regurgitation (Tastet *et al.*, 2019). For macrocalcification, there are validated commercially available histological stains including alizarin red and von kossa staining (Goettsch *et al.*, 2016). As these methods only detect macrocalcification and stenosis there is a need for innovations in methodologies for the early detection of aortic valve pathologies. One of these innovative techniques is PET, a non-invasive imaging method which uses targeted radiotracers to produce a highly sensitive and specific imaging tool (Joseph and Tawakol, 2016). Radiolabelled sodium fluoride (NaF/^{18}F) can detect novel areas of bone remodelling and formation, through its binding to hydroxyapatite crystals (MacAskill *et al.*, 2020b). Therefore it can also be used to detect microcalcification (Even-Sapir *et al.*, 2006; Creager *et al.*, 2019). It has been shown previously that the radiotracer 18F-Sodium fluoride, binds specifically to hydroxyapatite and, therefore, can be used to image microcalcification (Tzolos and Dweck, 2020). This is, therefore, an important tool for investigating the development of calcification both in humans and in preclinical models. This imaging technique has been used to detect micro calcification in the ApoE$^{-/-}$ model of calcification although only in male subjects (MacAskill *et al.*, 2020b).

4.1.3 Sex differences in models of CAVD

Despite the characterisation of prominent sex differences in CAVD, most studies carried out in ApoE$^{-/-}$ mice only employ male animals (Woodward *et al.*, 2021). A small number of sex comparison studies in ApoE$^{-/-}$ mice have been carried out which focus on the sexually dimorphic development of atherosclerosis which has shown female ApoE$^{-/-}$ mice developing larger plaques and more severe dyslipidaemia (Meyrelles *et al.*, 2011). The pathology behind this sexual dimorphism is unknown. Some studies report greater calcification in arteries and atherosclerotic plaques in the aortic sinus of female mice (McRobb *et al.*, 2017; Marek *et al.*, 2017). This is opposed to the evidence that oestrogen is generally cardioprotective, with a study

reporting that oestrogen treatment prevents hyperlipidaemia and atherosclerotic plaque formation in ApoE$^{-/-}$ mice (Goetz *et al.*, 2019). This is also opposed to the sex difference seen in humans where it has been well-characterised that men develop atherosclerosis at a younger age than women (Kaplan *et al.*, 1996). Unlike in human CAVD, sex differences in ApoE$^{-/-}$ models of CAVD remain ambiguous. Characterising the sex differences of one of the most commonly used model of CAVD could be crucial to further understanding the pathogenesis of the sexual dimorphism in this disease.

4.2 Hypothesis and aims

The work described in this chapter addresses the hypothesis that ApoE$^{-/-}$ mice provide a tractable, sexually dimorphic model of calcific aortic valve disease. A combination of new imaging techniques and histological/ immunohistochemical analysis can be used to track progression of valve disease in these models.

This hypothesis will be addressed with the following aims:

1. To assess whether ApoE$^{-/-}$ mice subjected to a western diet for 12 weeks display aortic valve dysfunction and aortic valve calcification.

2. To determine whether development of CAVD is sex dependent in the ApoE$^{-/-}$ mouse.

4.3: Materials and methods

4.3.1: Mice

ApoE$^{-/-}$ mice (Charles River, Italy) were group-housed on a 12-hour light/dark cycle at 22-24 ºC. Mice were provided *ad libitum* access to water, chow, and environmental enrichment. During experiments, mice were weighed weekly. All procedures were performed in accordance with University of Edinburgh Ethics guidelines and UK Home Office guidelines and under relevant UK Home Office licences.

4.3.2: Western diet protocol

At 27 weeks of age, the standard chow diet was replaced with *ad libitum* access to western diet pellets (Research Diets, USA). Before starting the western diet, echocardiographic imaging was performed to measure baseline cardiac and aortic function, as described (Chapter 2, section 2.3). Echocardiography was repeated at 8 and 12 weeks after the start of the western diet (Figure 4.3.1).

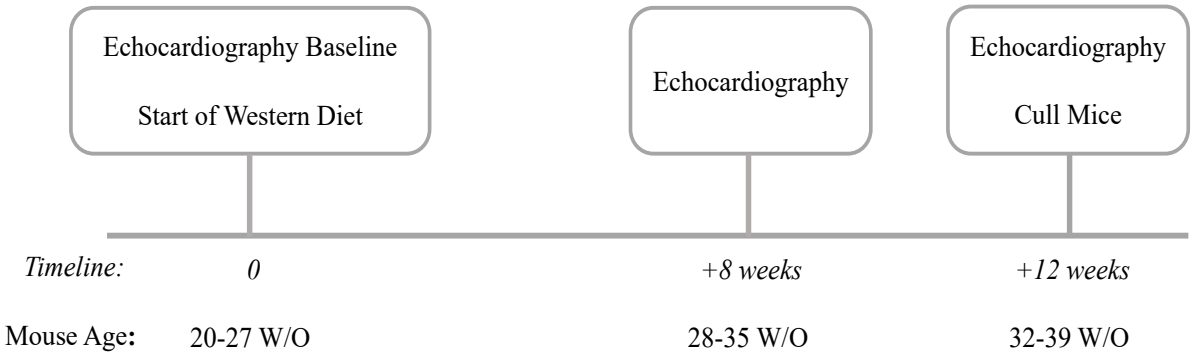

Figure 4.3.1: Timeline of ApoE$^{-/-}$ western diet study. After baseline echocardiography, male and female ApoE$^{-/-}$mice were maintained on western diet for 12 weeks with echocardiography repeated following exposure to a western diet for 8 and 12 weeks. W/O - weeks of age.

4.3.4 Tissue collection

Tissues were collected immediately after culling, as described in Chapter 2, section 2.5.2. Organs were weighed pre-fixation. Tibiae and femora had their soft tissue removed and were then measured using DigiMax digital Vernier callipers (R. S. Components Ltd, Corby, UK).

4.3.5 Echocardiography of ApoE$^{-/-}$ mice

Echocardiography was carried out as described in Chapter 2 section 2.3 to detect stenosis and regurgitation.

4.3.6 Ex-vivo PET/CT of ApoE$^{-/-}$ mice

PET/CT imaging was performed as described in Chapter 2, section 2.3. CT densities were analysed using hot average (average of the 5 hottest pixels). PET was analysed using both average uptake and hot average uptake. This method was implemented to detect hydroxyapatite (micro-calcification).

4.3.7 Autoradiography

Autoradiography of aortic root sections was carried out with 18F-Sodium fluoride (100 ± 2.35 kBq/mL) as described in Chapter 2 section 2.7.4. This was used to detect the presence of hydroxyapatite in aortic valve sections.

4.3.8 Histology

Valve embedding and sectioning were carried out as described in Chapter 2, section 2.3.2. Tissues were stained with H&E, Masson's Trichrome, Alizarin Red and Von Kossa, as described in Chapter 2, section 2.3.3. All sections were imaged on an AxioImager Z1 microscope (Zeiss, Germany).

4.3.9 Blood Lipid Analysis

Blood was collected as described in Chapter 2, section 2.5.2. Plasma was separated from whole blood by centrifugation (2000 RCF x 10 min at 4 °C) and stored at -20 °C. Assays were performed by the Biochemical Assay service at The University of Edinburgh's Shared University Research Facilities. Plasma concentrations of LDL were calculated by a formula (LDL calculation = Total Cholesterol - (Triglycerides/2.2) – HDL) from the cholesterol, HDL, and triglyceride.

4.3.11 Micro-computed tomography (μ-CT) imaging

Tibiae were fixed in 10 % formalin (Sigma) and stored at room temperature. Bones were subject to micro-CT scans, as described in Chapter 2 section 2.6.3. Analysis of the tibia was

conducted in the trabecular bone and at three points of the cortical bone. These were 37 %, 50 % and 75 % of bone length below the growth plate.

4.4 Results

4.4.1 Weight and necropsies of western diet fed ApoE$^{-/-}$ mice

There was no significant effect of sex in femur or tibia length (Figure 4.4.1A). Weekly weights were taken of the mice during the western diet regimen. Females were lighter than males at the start of the western diet. Female mice had a significantly lower body mass throughout the study (Figure 4.4.1B). Both female and male mice gained a significant amount of body mass over the course of the study, female weight increased from 23.67 ± 0.65g to 30.21 ± 1.51g (a mean increase of 6.5 g) and male weight increased from 33.82 ± 0.44g to 42.78 ± 1.68 g (a mean increase of 9 g) (Figure 4.4.1B).

Organ weights were normalised to both body mass (Table 4.1) and tibia length (Table 4.2). As a percentage of body mass, females had significantly bigger spleens and pancreas. Males had significantly bigger brown adipose tissue and gonadal white adipose tissue (Table 4.1). When normalised to tibia length, males had significantly larger gonadal white adipose tissue, brown adipose tissue, livers, kidneys, and hearts (Table 4.2).

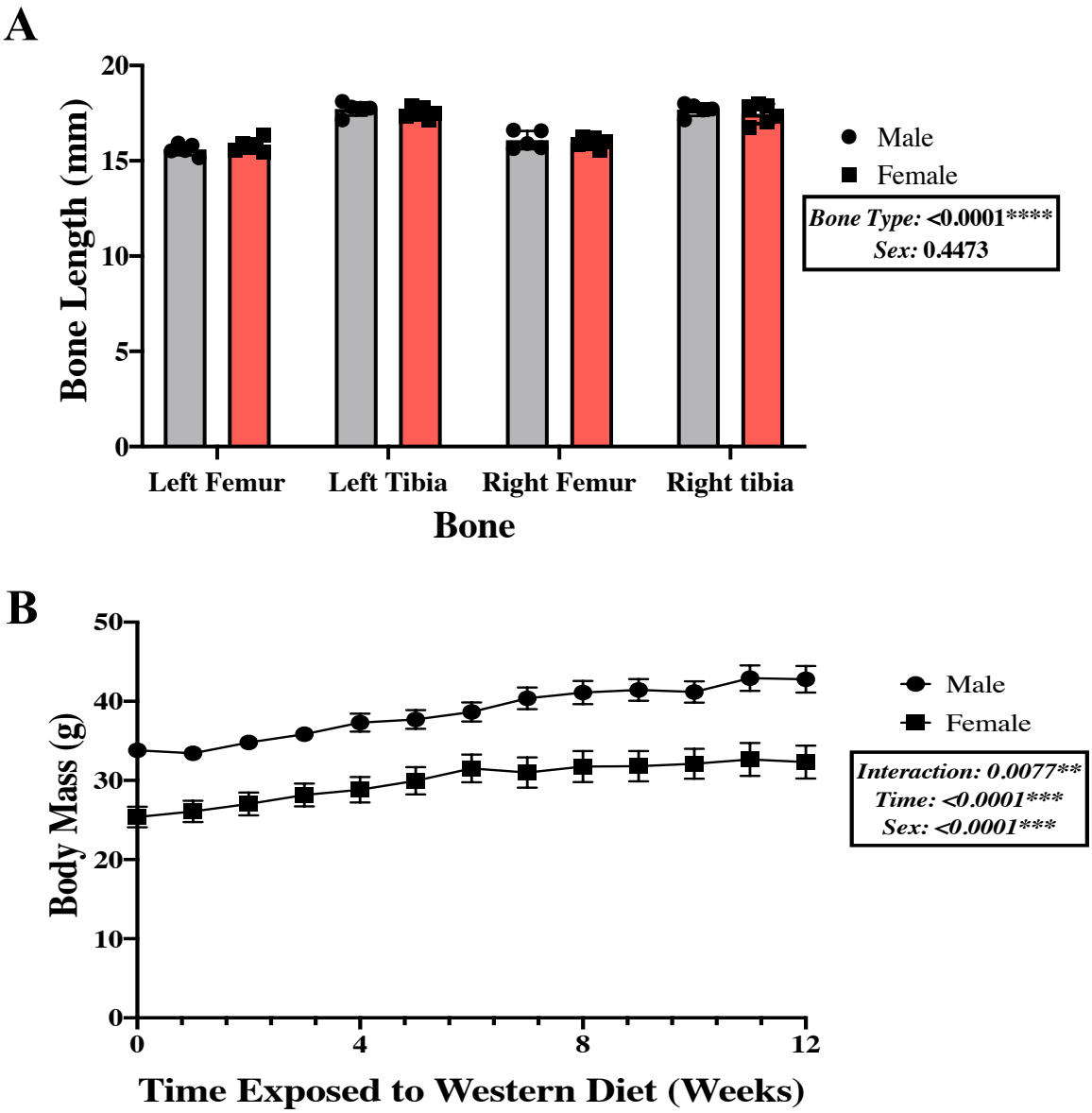

Figure 4.4.1: Body mass and bone length of western diet-fed ApoE$^{-/-}$ mice. Male and female mice were subjected to a western diet for 12 weeks and weighed weekly. Bones were taken at cull and measured. (A) Tibiae were longer than femora and there were no sex differences in lengths of either bone. Males N=5 Females N=6 (B) Male and female mice gained a significant amount of weight over the 12 weeks of western diet administration and the males were significantly heavier. Males N=12 Females N=10. Data are represented as mean ± SEM. Significance was determined with a Two-way ANOVA. **= $p<0.01$ ***= $p<0.0001$.

Table 4.1: Necropsy masses (normalised to body mass) of organs from ApoE$^{-/-}$ mice fed a western diet. The mice were subject to a western diet for 12 weeks and organs weighed pre-fixation. Organ masses are displayed as a percentage of total body mass. Data are presented as mean ± SEM to 2 decimal places. Unpaired Student's t-tests were performed to determine sex differences. Males N=10-11 Females N=7-10 *= $p<0.05$. WAT - white adipose tissue (I-inguinal, G-gonadal, M-mesenteric). BAT - Brown adipose tissue.

ORGAN	WEIGHT (g) FEMALE	WEIGHT (g) MALE	P VALUE
IWAT	2.35 ± 0.34	2.39 ± 0.16	0.91
GWAT	2.74 ± 0.48	4.06 ± 0.29	0.03*
MWAT	1.13 ± 0.19	1.05 ± 0.16	0.77
BAT	0.36 ± 0.03	0.59 ± 0.10	0.05*
LIVER	5.93 ± 0.20	6.13 ± 0.36	0.66
KIDNEY	0.91 ± 0.14	1.03 ± 0.13	0.52
SPLEEN	0.47 ± 0.07	0.31 ± 0.02	0.03*
PANCREAS	0.46 ± 0.03	0.36 ± 0.03	0.03*
HEART	0.55 ± 0.03	0.53 ± 0.03	0.67

Table 4.2: Necropsy masses (normalised to tibia length) of organs from ApoE$^{-/-}$ mice fed a western diet. Mice were subject to a western diet for 12 weeks and organs weighed pre-fixation. Organ masses have been normalised to tibia length (mg/mm). Data presented as mean±SEM to 2 decimal places. Unpaired Student's t-tests were performed to determine sex differences. Males N=9 Females N=9 *=p<0.05 **= p<0.01 ***=p<0.001 ****=p<0.0001. WAT - white adipose tissue (I - inguinal, G - gonadal, M - mesenteric). BAT - Brown adipose tissue.

ORGAN	WEIGHT (g) FEMALE	WEIGHT (g) MALE	P VALUE
IWAT	44.63 ± 7.46	54.88 ± 6.10	0.30
GWAT	53.00 ± 10.85	97.94 ± 9.16	0.006**
MWAT	20.46 ± 3.65	25.97 ± 4.72	0.37
BAT	5.90 ± 0.67	12.38 ± 2.40	0.02*
LIVER	102.50 ± 7.57	145.4 ± 11.56	0.007**
KIDNEY	13.50 ± 1.88	21.49 ± 2.72	0.03*
SPLEEN	7.36 ± 1.02	7.24 ± 0.86	0.93
PANCREAS	7.74 ± 0.72	8.63 ± 0.81	0.42
HEART	9.17 ± 0.30	12.88 ± 0.55	0.001**

4.4.2 The western diet had no significant effect on cardiac function of ApoE$^{-/-}$ mice.

To analyse health of the aortic valve, Doppler measurements were taken of the left ventricular outflow tract prior to chronic high fat challenge. These measurements were repeated at 8- and 12-weeks post-diet administration. No aortic regurgitation was observed in either sex, at any timepoint on the echocardiography scanning. Example Doppler images for both males and females across the study are shown (Figure 4.4.2). No significant effect of sex or time was observed in any measurements of aortic function taken using pulse wave Doppler across the study (Figure 4.4.3).

Other parameters of cardiac function were also measured using echocardiography throughout the study. Left ventricular mass and thickness and cardiac output were higher in males, but these did not change over the course of the study. There was also no difference in ejection fraction (Figure 4.4.4).

Cardiac function was also investigated using M-mode echocardiography (Figure 4.4.5). Males had significantly larger LVESD, LVEDD and posterior wall thickness (Figure 4.4.5). Females had larger fractional shortening percentage (Figure 4.4.5 A). The diet significantly increased posterior wall thickness in females (Figure 4.4.5 B).

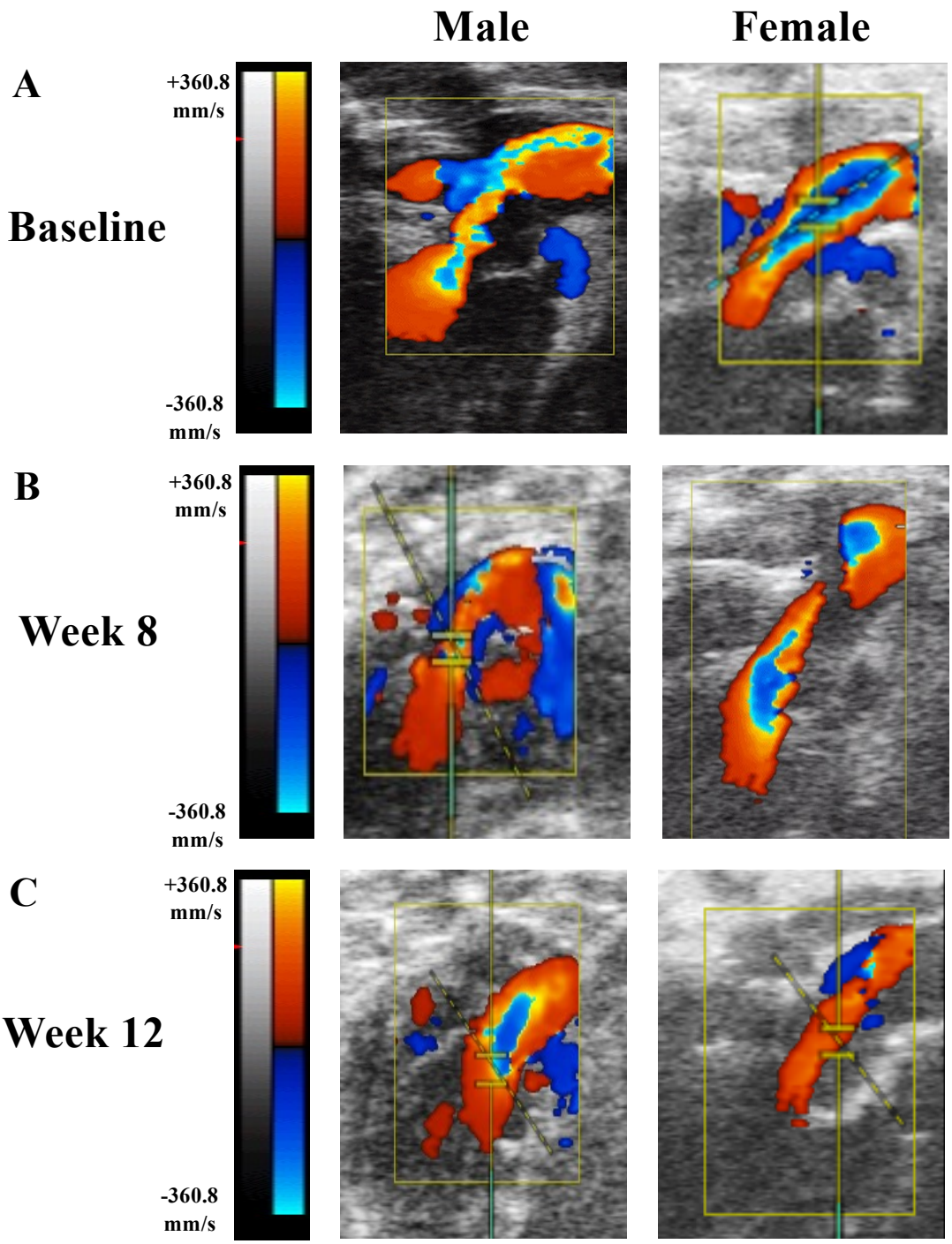

Figure 4.4.2: Colour Doppler images of blood flow in the ascending aorta of western diet-fed ApoE$^{-/-}$ mice. ApoE$^{-/-}$ mice were subject to a western diet for 12 weeks and ultrasound imaging pre-diet (baseline) and 8- and 12-weeks post-diet. This figure displays example colour Doppler images for males and females during the study. Scale describes mean velocity of blood. This figure was made using Microsoft PowerPoint.

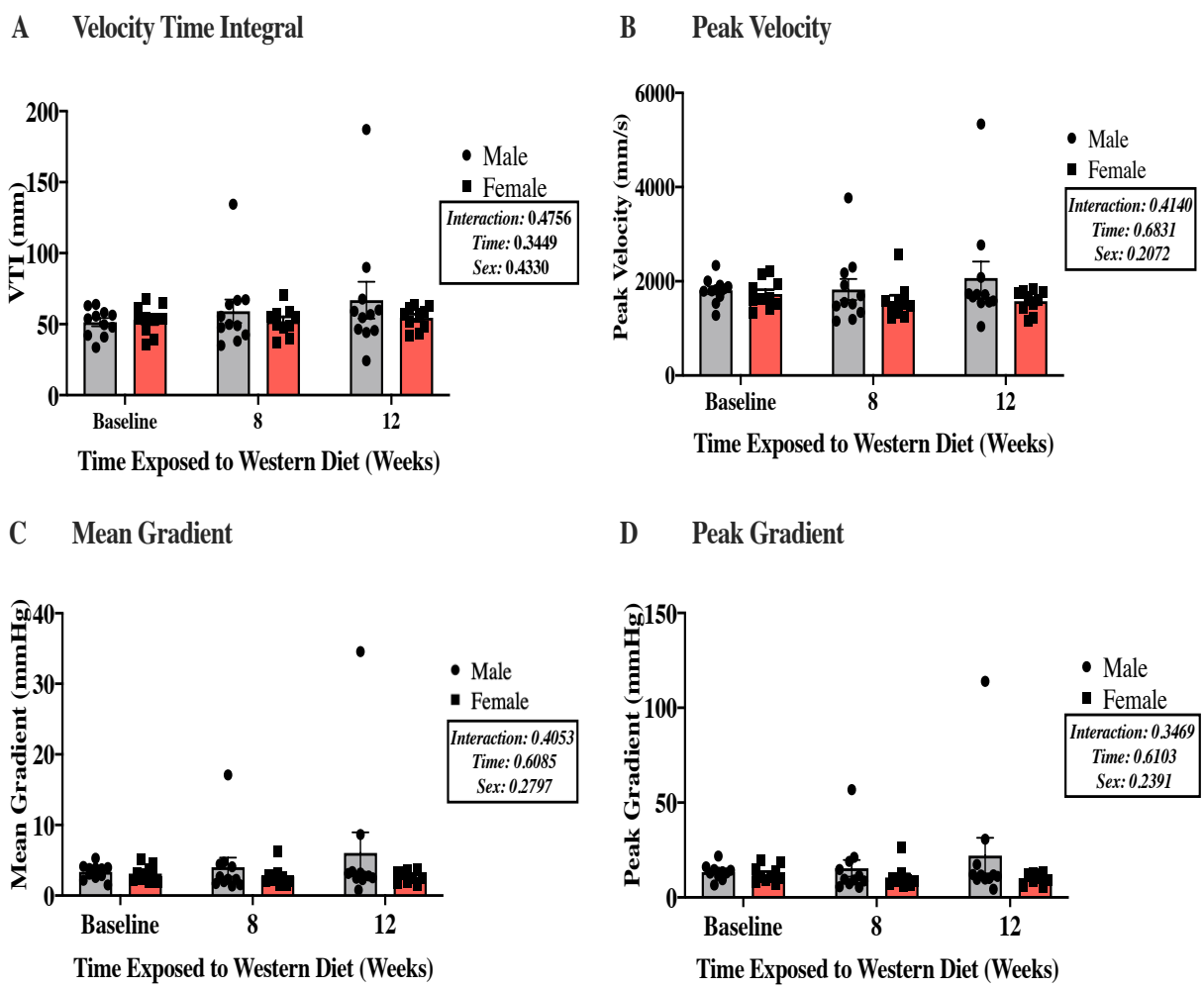

Figure 4.4.3: Aortic blood flow during exposure of male and female ApoE$^{-/-}$ mice to western diet. ApoE$^{-/-}$ mice were subject to a western diet for 12 weeks and ultrasound imaging was performed pre-diet (baseline) and 8- and 12-weeks post-diet. A) Velocity time integral (VTI) of blood velocity through the aortic valve. B) Peak velocity of aortic outflow blood. C) Mean gradient of blood flow across the aortic valve. D) Peak gradient of blood flow through the aortic valve. There were no sex or time differences for any of the parameters. Columns represent mean ± SEM, points represent single data values. Males N=11 Females N=10. Significance was assessed with two-way ANOVAs. VTI - Velocity time integral.

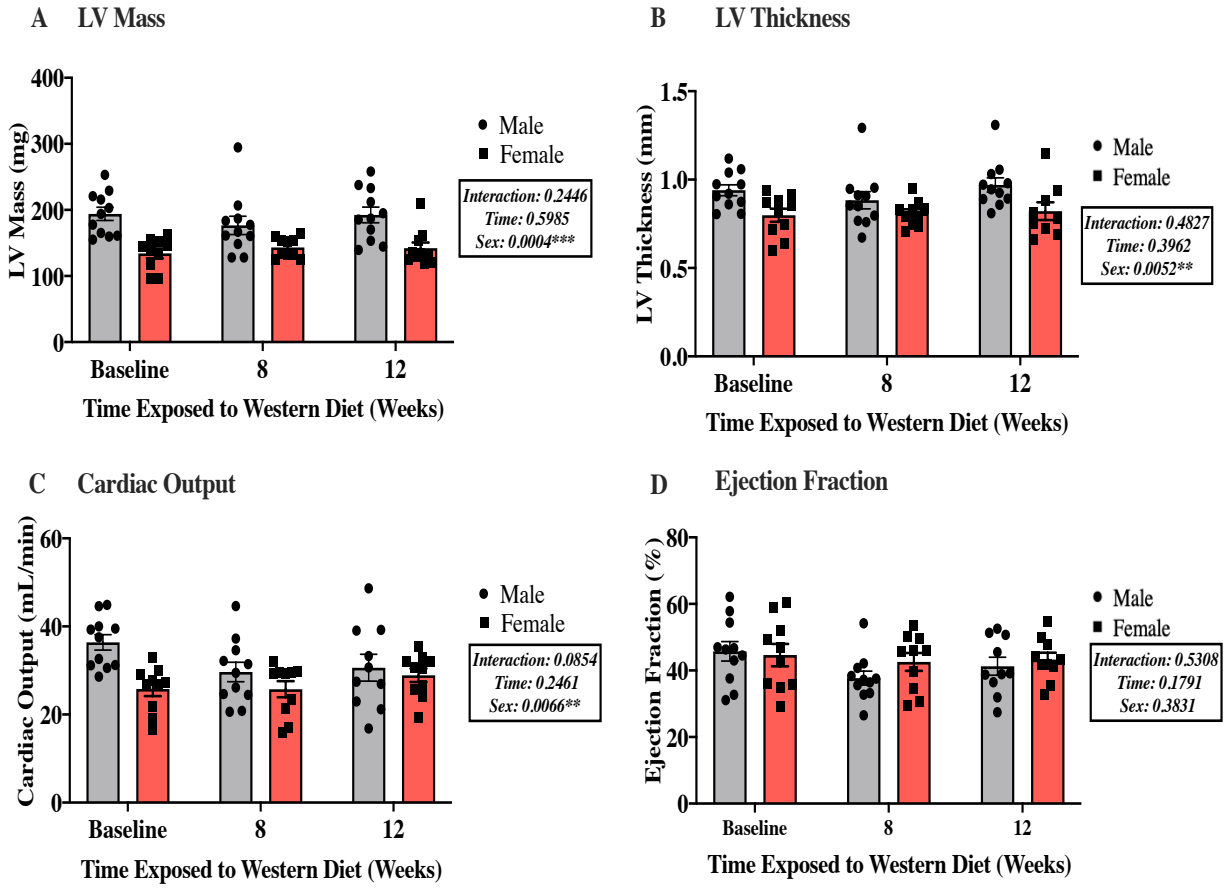

Figure 4.4.4: Cardiac function in mice exposed to western diet. ApoE$^{-/-}$ mice were subject to a western diet for 12 weeks and ultrasound imaging was performed pre-diet (baseline) and 8- and 12-weeks post-diet. Graphs display (A) LV mass (mg), (B) LV thickness (mm), (C) Cardiac Output (mL/min) and (D) Ejection Fraction (%). There were sex differences in LV mass, LV thickness and Cardiac output. There was no significant change in any measurements with addition of a western diet. Columns represent mean±SEM, points represent single data values. Males N=11 Females N=10. Significance was determined with two-way ANOVAs. *=p<0.05, **=p<0.01, **=p<0.001. LV - Left ventricle.

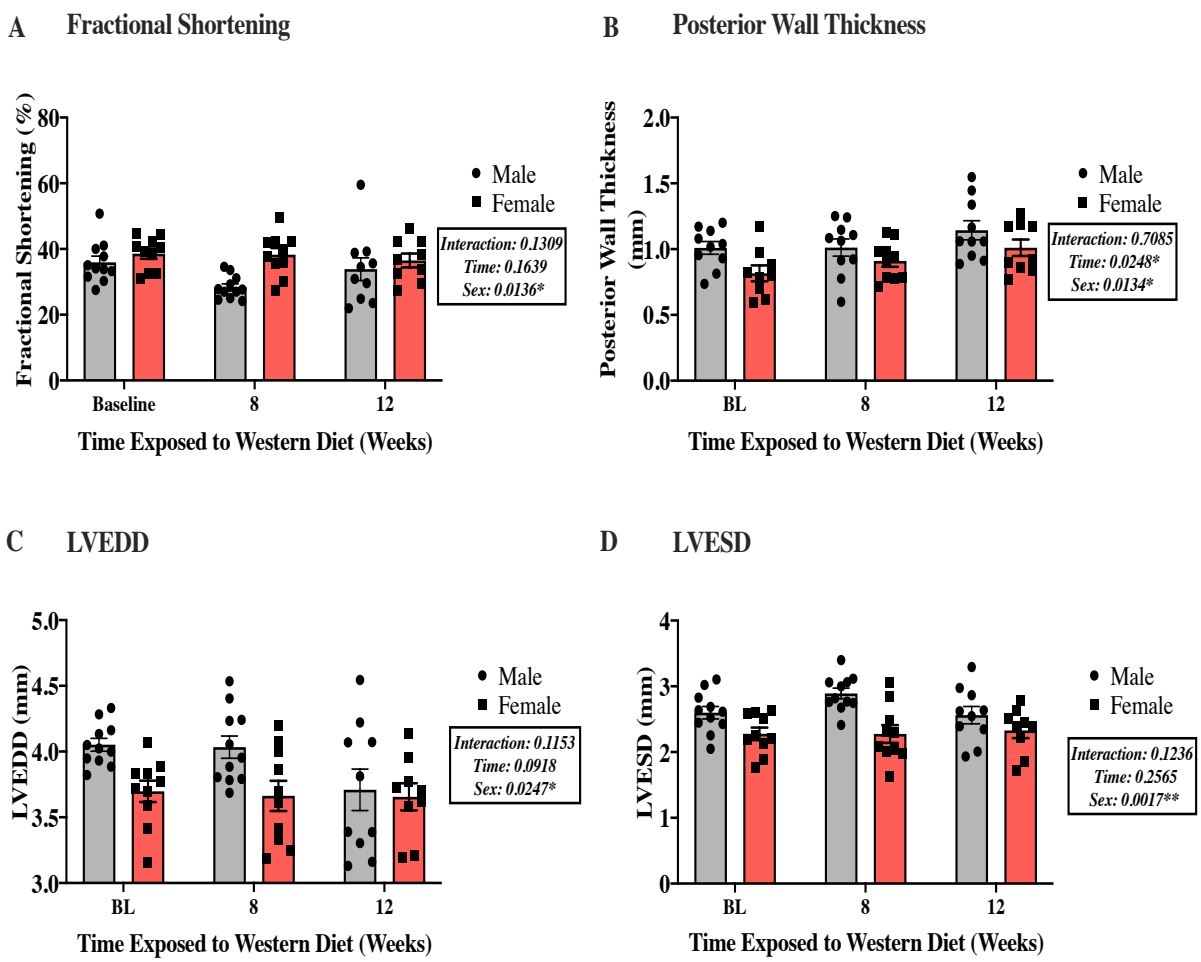

Figure 4.4.5: M-Mode measurements of cardiac function in mice fed western diet. ApoE$^{-/-}$ mice were subject to a western diet for 12 weeks and ultrasound imaging was performed pre-diet (baseline) and 8- and 12-weeks post-diet. Graphs display (A) Fractional Shortening (%), (B) Posterior Wall Thickness (mm), (C) LVEDD (mm) and (D) LVESD (mm). Males had significantly larger LVESD, LVEDD and posterior wall thickness. Females had larger fractional shortening. The diet significantly increased posterior wall thickness. Columns represent mean ± SEM, points represent single data values. Males N=11 Females N=10. Significance was determined with two-way ANOVAs. *=p<0.05, **=p<0.01. LV - Left ventricle. LVEDD - Left ventricular end diastolic diameter. LVESD - Left ventricular end systolic diameter.

4.4.3 PET/CT of western diet fed ApoE$^{-/-}$ mice

Hearts and aortas were analysed by *ex-vivo* PET/CT imaging. CT scanning was used to analyse tissue densities and observe any develop of macrocalcification. Spots of macrocalcification were observed in the CT images (Figure 4.4.6 A). In aortas, macrocalcification spots were observed in 100 % of female samples and 38 % of male samples. The CT densities in both aortas and hearts displayed no significant effect of sex (Figure 4.4.6 B/C).

The aortas and hearts of the ApoE$^{-/-}$ mice were subject to PET scanning using 18F-Sodium fluoride to determine presence of microcalcification. There was no significant difference in radiotracer binding in the aortas of male and female mice (Figure 4.4.7). In the hearts, females had significantly higher average binding (0.0891 ± 0.0126 kBq/cc:mBq/mL) than males (0.0548 ± 0.0097 kBq/cc:mBq/mL) (equivalent to 1.6 fold increase in females)(Figure 4.4.8 A). There was no significant sex difference of the hot average of 18F-Sodium fluoride binding in the hearts (Figure 4.4.8 B).

The resolution of micro-PET could not accurately determine whether there was microcalcification in the aortic valve. These tissues were, therefore, sectioned after scanning and analysed using autoradiography. This showed that there was no significant difference in 18F-Sodium fluoride binding to the aortic root sections in male and female mice (Figure 4.4.9).

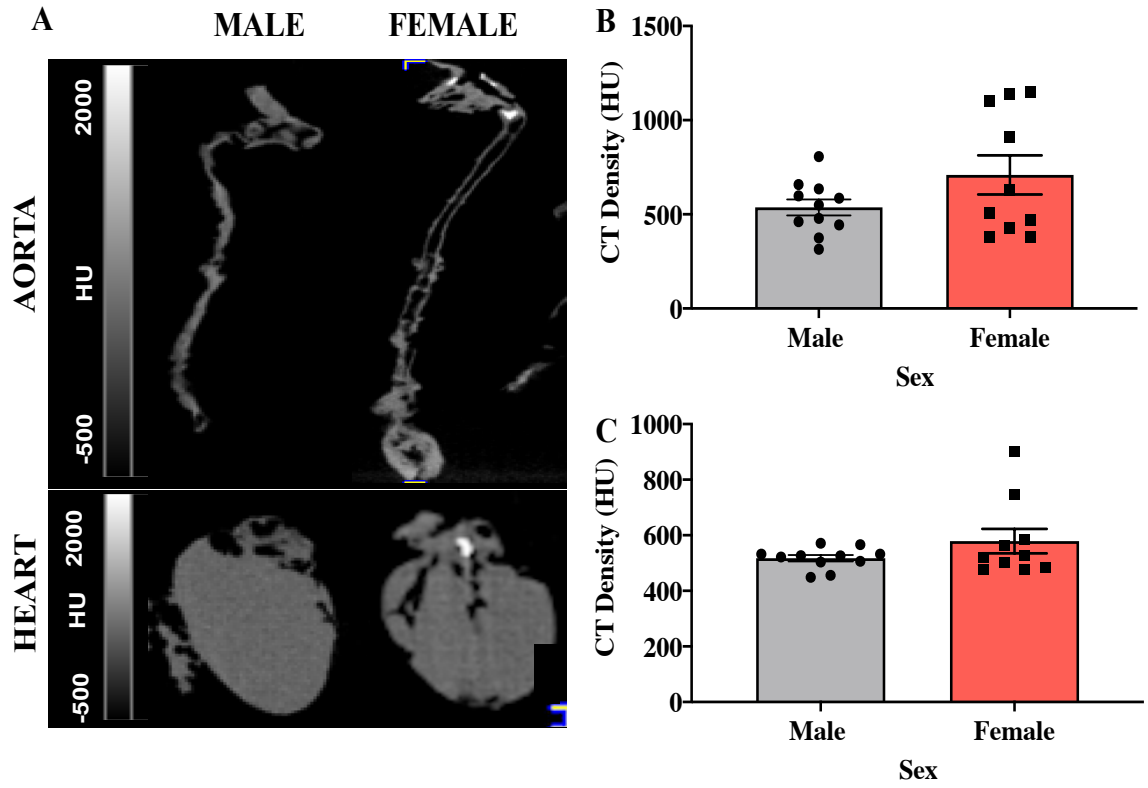

D

	Observed calcium nodules (number of mice)	
Tissue	Male	Female
Aorta	4/11	10/10
Heart	0/10	2/10

Figure 4.4.6: CT densities of aortas and hearts from western diet-fed ApoE$^{-/-}$ mice. Mice were subject to a western diet for 12 weeks; the hearts and aortas were then fixed and subject to CT scanning. A) Representative images of CT scans in tissues. Scale of HU (Hounsfield units) represents radiodensity, where the brighter the signal the denser the tissue. Bright white spots on figure show areas of 'bone-like' density. Graphs display average tissue density in the B) aortas ($p=0.1282$) and C) hearts ($p=0.1734$). There was no significant difference in tissue density for hearts and aortas between males and females. D) Rate of observed calcium nodules from the CT scans in the mouse population. Columns represent mean ± SEM, points represent single data values. Males N=11 Females N=10. Significance was determined with unpaired Student's t-tests. CT - computerised tomography. HU - Hounsfield units.

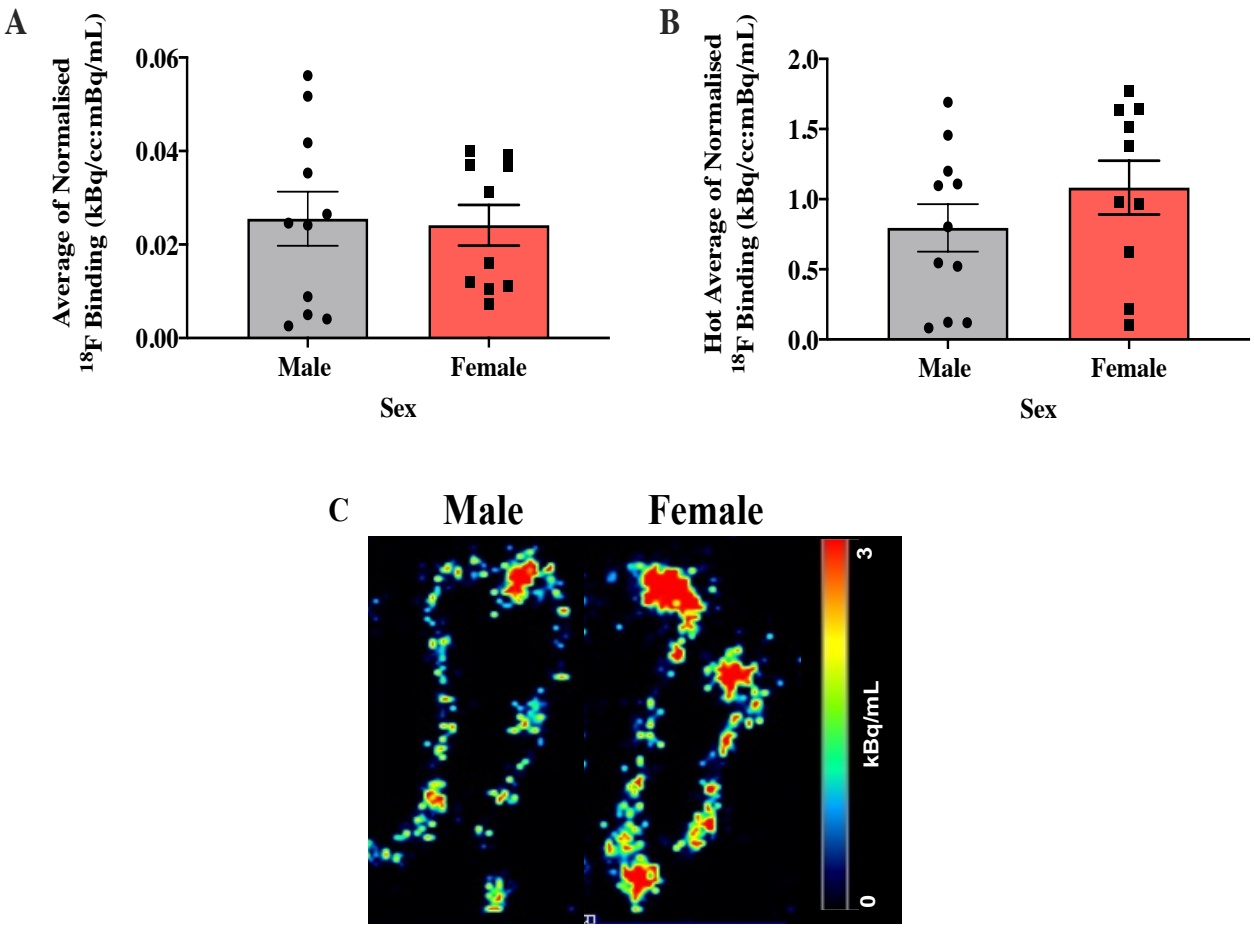

Figure 4.4.7:[18]F uptake in aortas of western diet-fed ApoE$^{-/-}$ mice. Mice were subject to a western diet for 12 weeks; the aorta were fixed and subject to PET scanning with 18F-Sodium fluoride. Graphs display A) Average 18F binding and B) Hot average of 18F binding. The hot average is the average of the 5 hottest pixels. There was no difference in uptake of 18F-Sodium fluoride between males and females. C) Representative PET images, the warmer the signal, the more 18F binding. Columns represent mean ± SEM and points represent single data values. Males N=11 Females N=10. Significance was determined with unpaired Student's t-tests. PET- Positron-emission tomography.

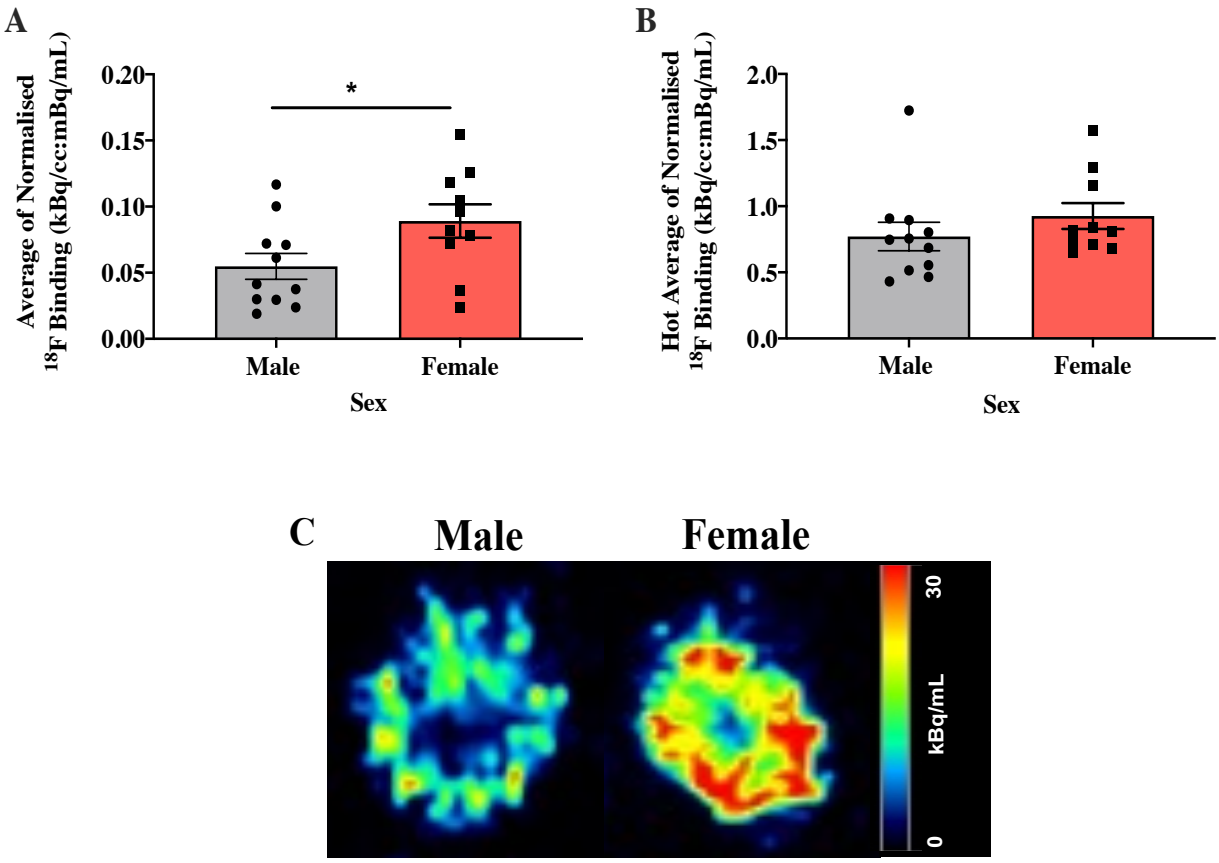

Figure 4.4.8 :[18]F uptake in hearts of western diet-fed ApoE[-/-] mice. Mice were subject to a western diet for 12 weeks; the hearts were fixed and subject to PET scanning with 18F-Sodium fluoride. Graphs display A) Average 18F binding and B) Hot average of 18F binding. The hot average is the average of the 5 hottest pixels. Females had more 18F binding then males (A). C) Representative PET images, the warmer the signal, the more 18F binding. Columns represent mean ± SEM and points represent single data values. Males N=11 Females N=10. Significance was determined with unpaired Student's t-tests. PET- Positron-emission tomography. *=$p<0.05$

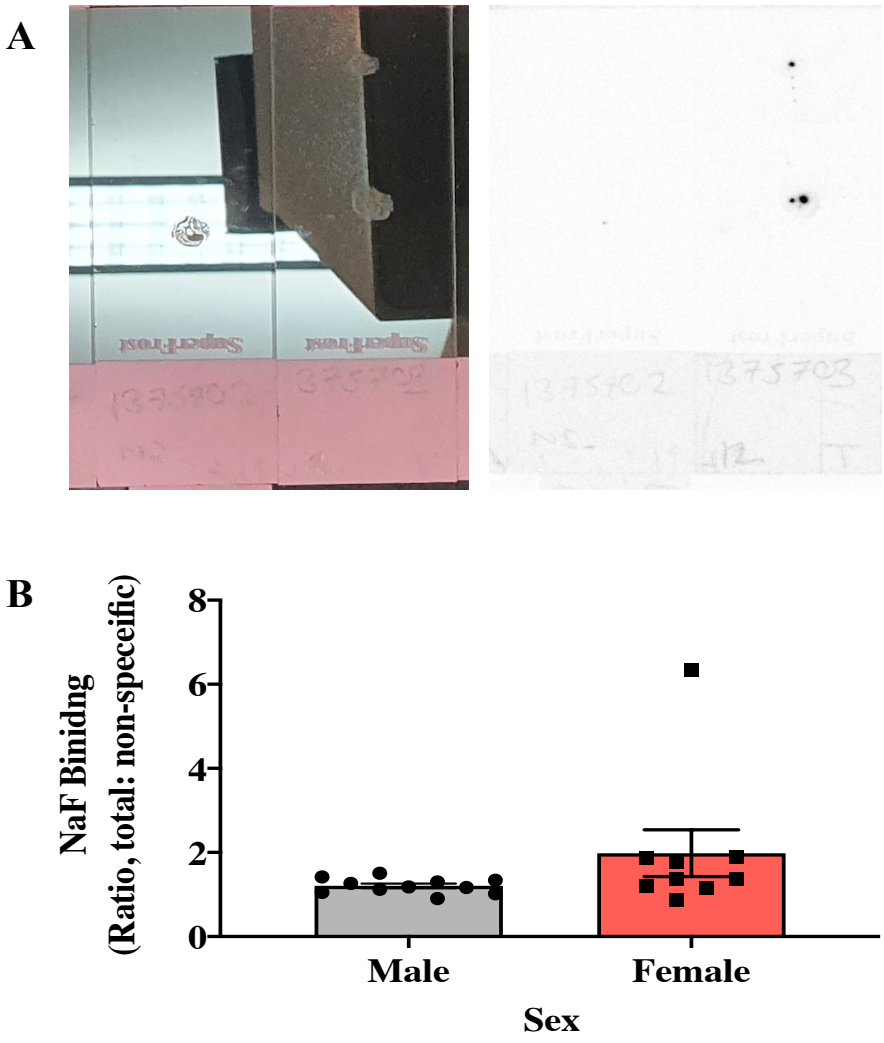

Figure 4.4.9 :^{18}F uptake in aortic root sections of western diet-fed ApoE$^{-/-}$ mice. Mice were subject to a western diet for 12 weeks; the hearts were fixed, sectioned, and subject to autoradiography imaging using 18F-Sodium fluoride. A) Examples of slides and matching autoradiography images. B) 18F binding in the aortic root sections. There was no significant difference between males and females. Columns represent mean ± SEM and points represent single data values. Males N=11 Females N=10. Significance was determined with unpaired Sudent's t-tests. PET- Positron-emission tomography.

4.4.4 Histological analysis of the aortic root of western diet fed ApoE$^{-/-}$ mice

Within the valve root, two methods of calcium staining were employed. Positive von Kossa staining was observed in the aortic valve cusps of 5/6 of the male mice and 4/4 of the female mice (Figure 4.4.10 A). Positive von Kossa staining was observed in the aortic root plaques of 2/6 of the male mice and ¼ of the female mice (Figure 4.4.10 A). There was no significant sex difference in the von Kossa stains (Figure 4.4.10 A). There was no positive alizarin red staining in the valve cusps. There was positive alizarin staining observed in the aortic root plaques, with 1/10 males staining positive and 4/9 of female mice having positive staining (Figure 4.4.10 B). There was no significant sex difference quantification of the in the staining (Figure 4.4.10 B).

H&E staining was employed to investigate structural differences in the aortic valve. There was no significant effect of sex on average cusp area (Figure 4.4.11 A). Female mice had a significantly ($p=0.0013$) larger plaque area than male mice in the aortic root (73.07 ± 5.69 µm compared to 33.92 ± 6.69 µm) (females had 2.15x larger plaques than males) (Figure 4.4.11 B). There was no significant difference in fibrosis (measured by quantification of positive Masson's trichome stain) between males and females (4.4.12 C).

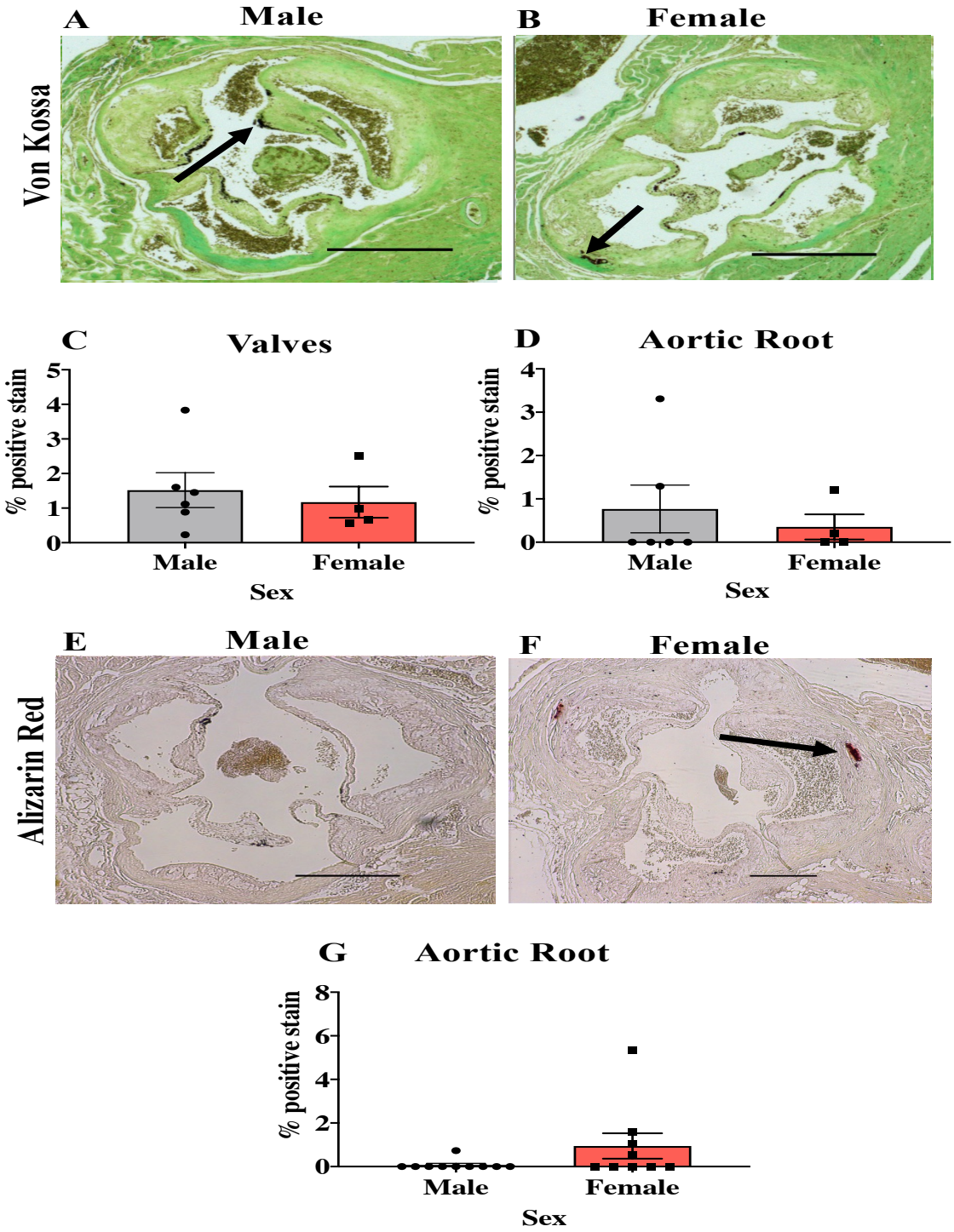

Figure 4.4.10: Calcium staining of the aortic root in western diet-fed ApoE$^{-/-}$ mice. Mice were subject to a western diet for 12 weeks; the hearts were then fixed, embedded, sectioned and subject to calcium staining. A) Example images of Von Kossa staining in male mice. B) Example images of Von Kossa staining in female mice. C) Quantification of von kossa staining in aortic valve cusps (Males N=6 Females N=4). D) Quantification of von kossa staining in atherosclerotic plaques (Males N=6 Females N=4). E) Example images of alizarin red staining in male mice. F) Example images of alizarin red staining in female mice. G) Quantification of alizarin red staining in atherosclerotic plaques (Males N=9 Females N=9). There was no significant sex difference in any measurement. Columns represents mean ± SEM; points are single data values. Significance was determined with unpaired Student's t-tests. Images were taken at x40 zoom.

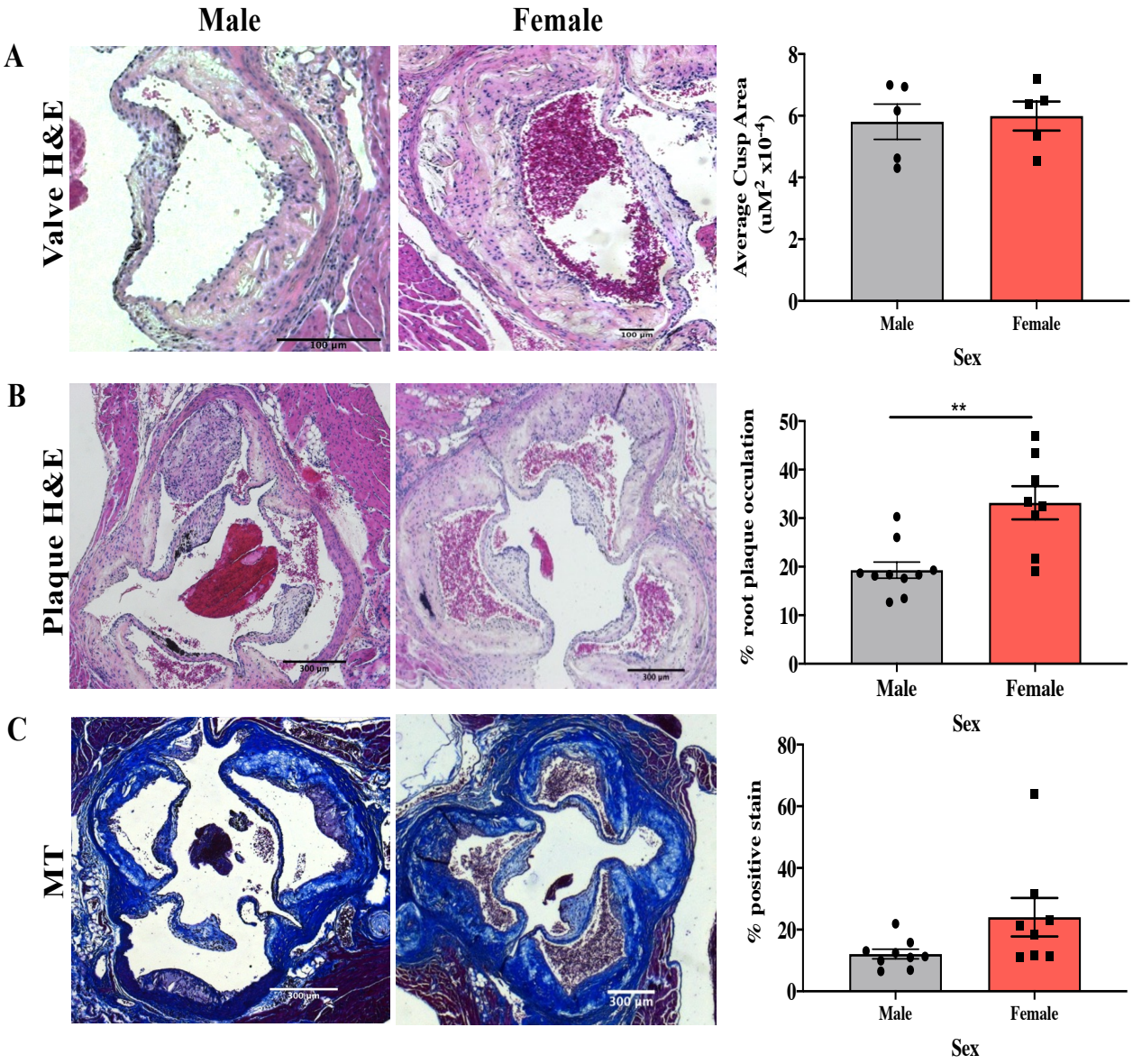

Figure 4.4.11: Histological staining of the aortic root in western diet-fed ApoE$^{-/-}$ mice. Mice were subject to a western diet for 12 weeks; the hearts were then fixed, embedded, sectioned and subject to H&E and Masson's Trichrome staining. A) Example images and analysis of mean cusp area (p=0.8080). B) Example images and analysis of plaque area (p=0.0013). C) Example images and analysis of Masson's Trichome stain (p=0.0684). Females had a significantly larger plaque in the aortic root than males. Males N=10 Females N=8. Columns represent mean ± SEM; points are single data values. Significance was determined with unpaired Student's t-tests. Images were taken at x40 zoom. MT= Masson's Trichrome. **=p<0.01

4.4.5 Micro-CT analysis of the tibia

Trabecular architecture was analysed using micro-CT. Females displayed significantly ($p<0.0001$) lower bone volume (0.04 ± 0.01 mm^2) compared to males (0.15 ± 0.01 mm^2) (Figure 4.4.12 A). Females also displayed significantly ($p<0.0001$) lower percentage bone volume (1.17 ± 0.22 %) compared to males (3.39 ± 0.30 %) (Figure 4.4.12 B). Males had a 2.71x higher trabecular number than females ($p<0.001$) (Figure 4.4.12 E). Females had a significantly ($p=0.0054$) larger Structural Model Index (SMI) than males (Figure 4.4.12 F).

Cortical measurements were taken at three points to allow for analysis of structure across the whole tibia. From the growth plate, analysis was performed 37 % of bone length below the plate and repeated at 50 and 75 % below. At 37 %, females had a higher ($p=0.0022$) percentage bone volume (60.68 ± 1.97 %) compared to males (Figure 4.4.13 B). Males had a larger ($p=0.0234$) cortical bone perimeter (16.16 ± 0.65 mm) than females (13.55 ± 0.85 mm) (Figure 4.4.13). The 50 % point of cortical bone analysis revealed females having a higher ($p=0.0159$) percentage bone volume than males (Figure 4.4.14 B). Males also had greater cortical bone area ($p=0.0125$), thickness ($p=0.0284$) and porosity ($p=0.0176$) (Figure 4.4.14). At the lowest (75 % below growth plate) point of cortical analysis, males had a ($p=0.0050$) larger bone volume (0.3990 ± 0.0064 mm^3) than females (0.3517 ± 0.0137 mm^3). Males also had a larger (0.8047 ± 0.0130 mm^2) cross-sectional bone area than females (0.6878 ± 0.0232 mm^2; $p=0.0003$) (Figure 4.4.15 C). Finally, males also had a larger ($p=0.003$) bone perimeter (Figure 4.4.15 D).

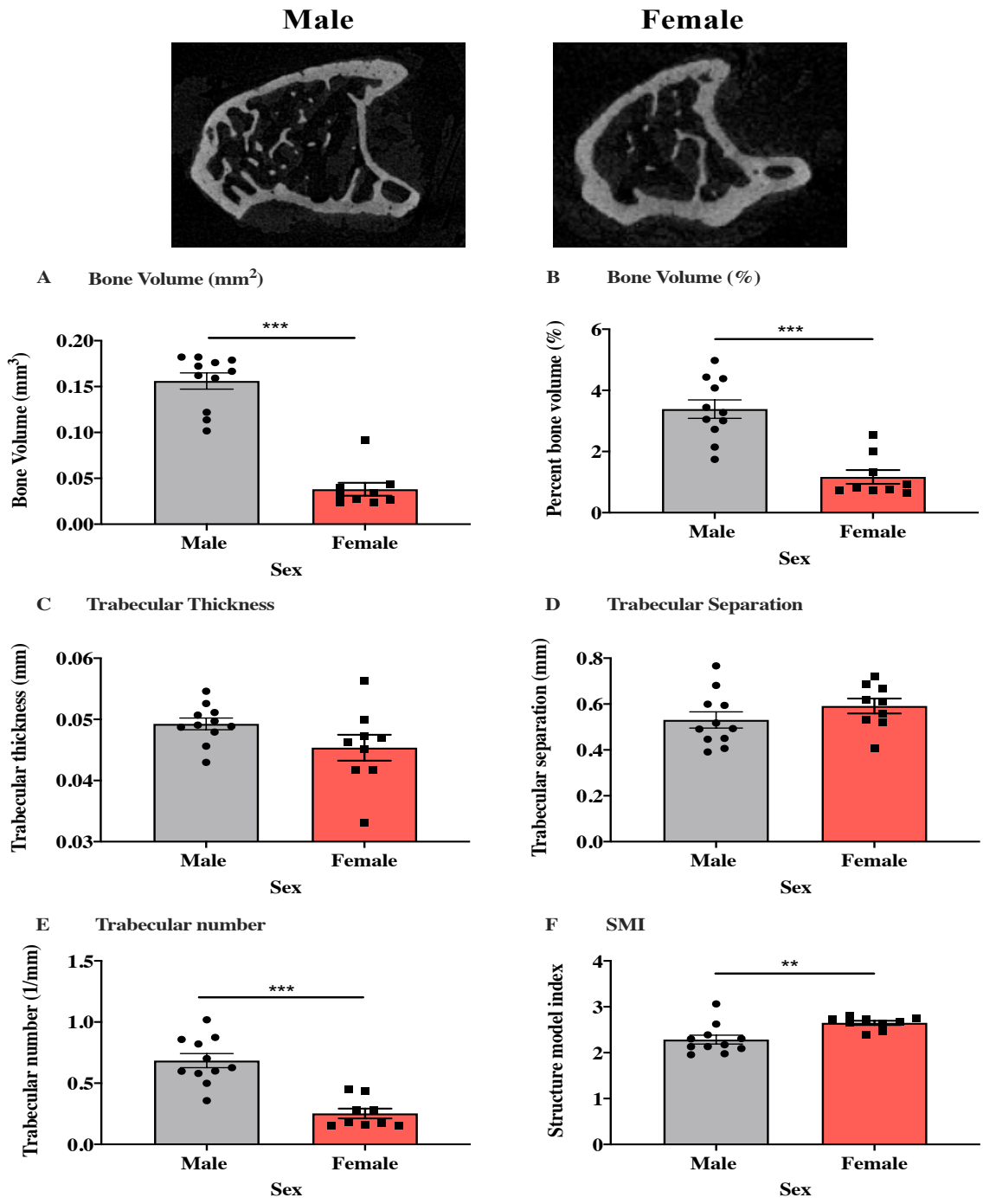

Figure 4.4.12: Trabecular architecture analysis of Western diet-fed male and female ApoE$^{-/-}$ mice. Mice were subject to a western diet for 12 weeks; tibiae were taken post-cull and analysed using a Micro-CT scanner. A) Trabecular bone volume. B) Trabecular bone volume represented as a percentage of total bone volume. C) Average thickness of the trabecular. D) Trabecular separation as calculated by mean distance between the trabeculae throughout the trabecular bone. E) Trabecular number was calculated by taking the mean number of trabeculae per mm. F) Comparison of Structure Model Index (a way of measuring rods and plates in trabecular bone) between male and female mice. Females had a significantly lower bone volume and trabecular number. Females also had a higher SMI. Males N=11 Females N=10. Columns represents mean ± SEM; points are single data values. Significance was determined with unpaired Student's t-tests. SMI- Structure Model Index. **=p<0.01, ***=p<0.001

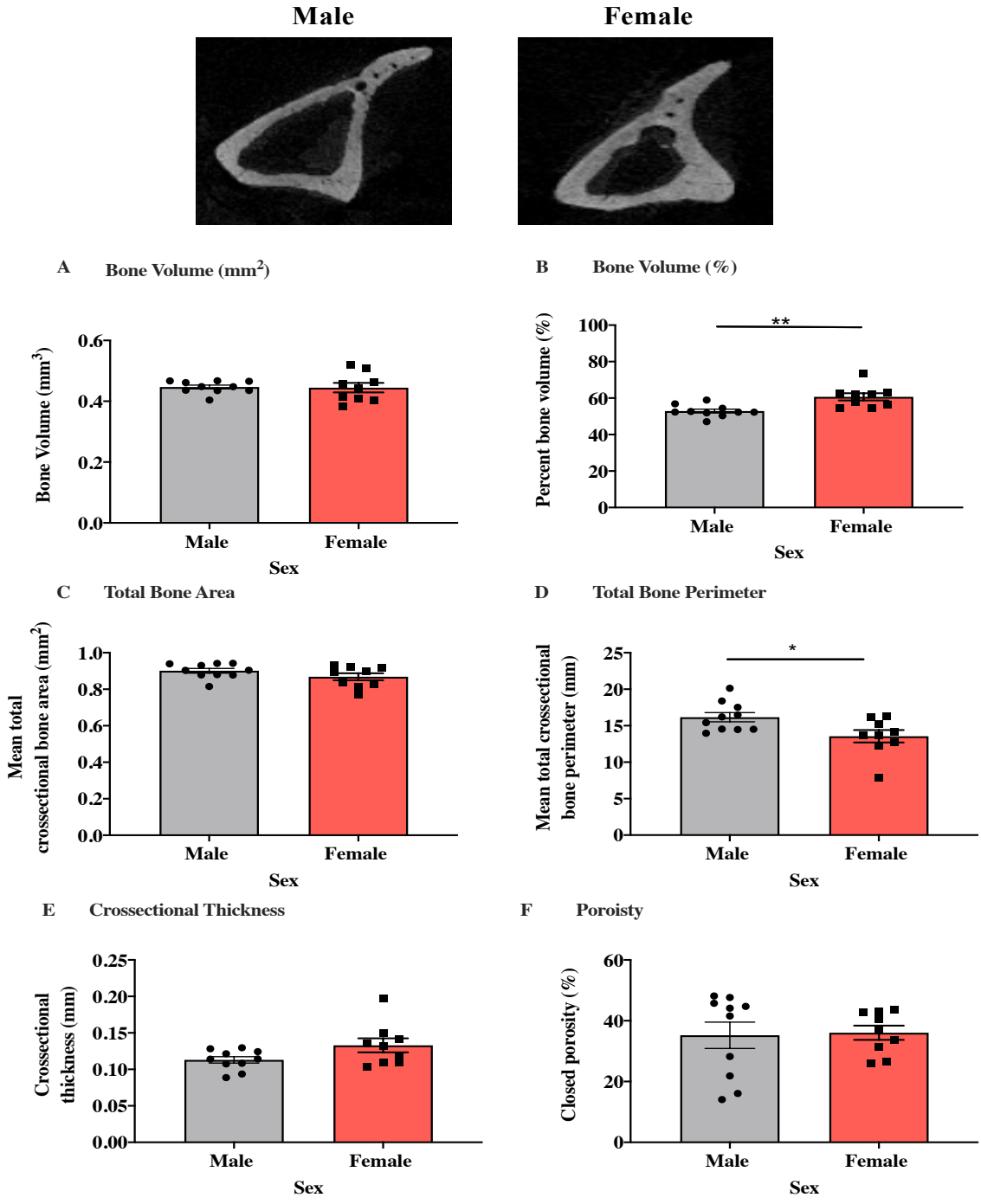

*Figure 4.4.13 Analysis of cortical region of tibiae 37 % of bone length below growth plate***.** Mice were subject to a western diet for 12 weeks; tibiae were taken post-cull and analysed using a Micro-CT scanner. A) Cortical bone volume. B) Cortical bone volume represented as a percentage of total bone volume. C) Cross-sectional tissue area in experimental groups. D) Mean cross-sectional tissue perimeter. E) Mean thickness of the cortical bone throughout the tibiae of the mice. F) Porosity (the average fraction of empty volume within the bone) analysis between the male and female mice. Females had a significantly lower bone volume and bone perimeter. Males N=11 Females N=10. Columns represents mean ± SEM; points are single data values. Significance was determined with unpaired Student's t-tests. *=$p<0.05$, **=$p<0.01$

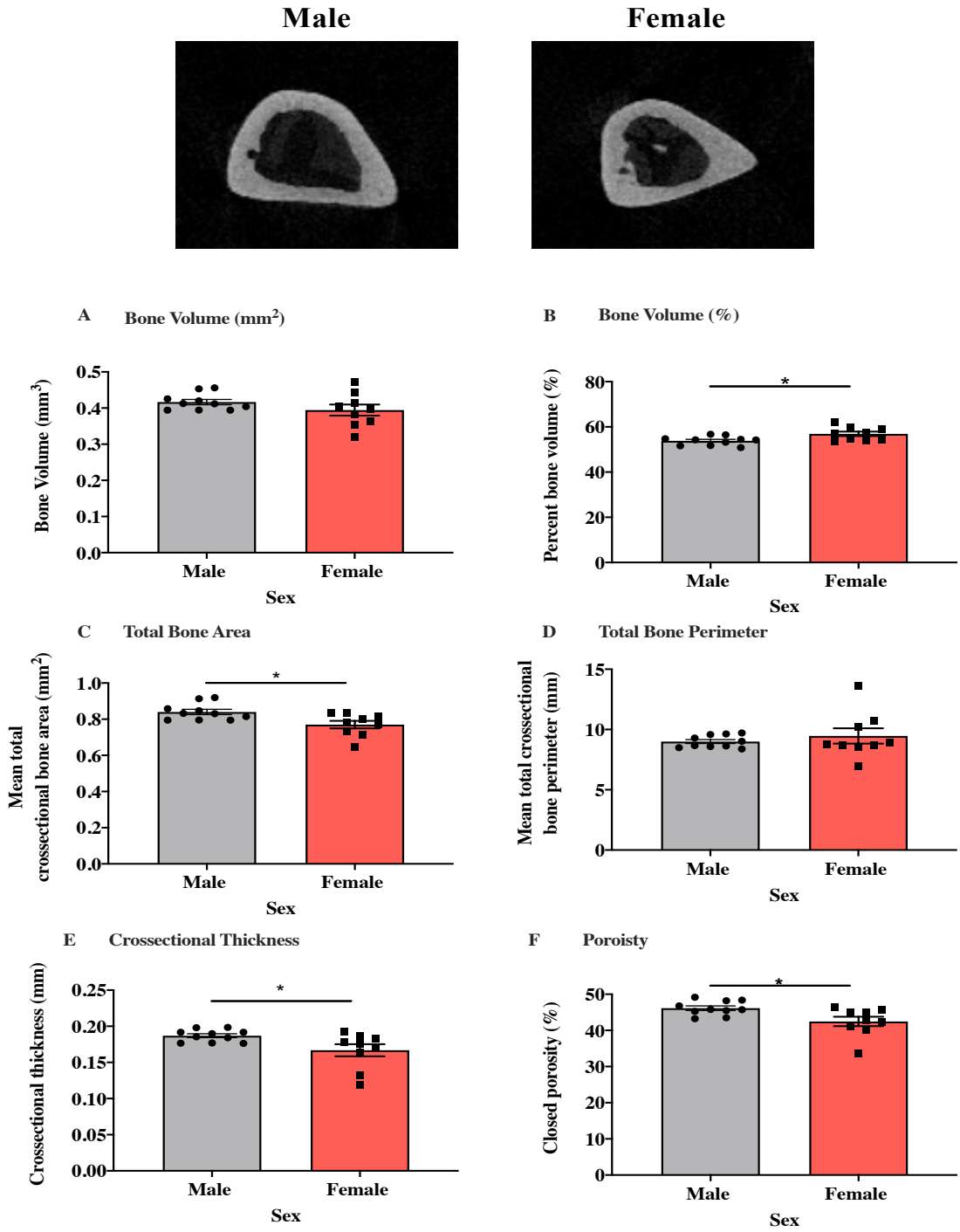

Figure 4.4.14 Analysis of the cortical region of tibiae 50 % of bone length below growth plate. Male and Female ApoE$^{-/-}$ mice were subject to a western diet for 12 weeks; tibiae were taken post-cull and analysed using a Micro-CT scanner. A) Cortical bone volume. B) Cortical bone volume represented as a percentage of total bone volume. C) Cross-sectional tissue area in experimental groups. D) Mean cross-sectional tissue perimeter. E) Mean thickness of the cortical bone throughout the tibiae of the mice. F) Porosity (the mean fraction of empty volume within the bone) analysis between the male and female mice. Females had a significantly higher bone volume. Males had greater cortical area, cross-sectional thickness, bone perimeter and porosity. Males N=11 Females N=10. Columns represents mean ± SEM; points are single data values. Significance was determined with unpaired Student's t-tests. *=$p<0.05$

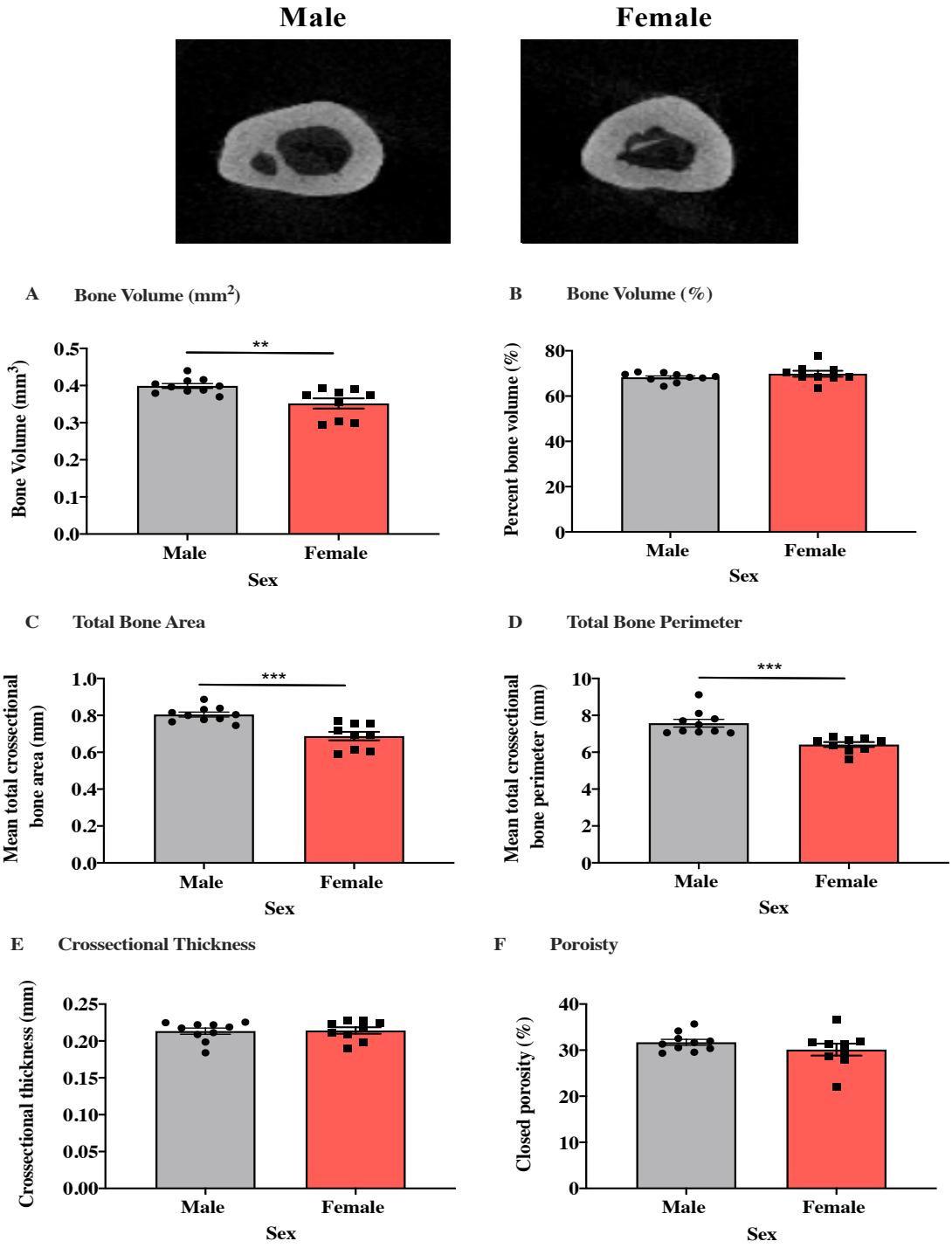

Figure 4.4.15 Analysis of cortical region of tibiae 75 % of bone length below growth plate. Male and female ApoE$^{-/-}$ mice were subject to a western diet for 12 weeks; tibiae were taken post-cull and analysed using a Micro-CT scanner. A) Cortical bone volume. B) Cortical bone volume represented as a percentage of total bone volume. C) Cross-sectional tissue area in experimental groups. D) Mean cross-sectional tissue perimeter. E) Mean thickness of the cortical bone throughout the tibiae of the mice. F) Porosity (the mean fraction of empty volume within the bone) analysis between the male and female mice. Females had a significantly lower bone volume, cross-sectional bone area and bone perimeter. Males N=11 Females N=10. Columns represents mean ± SEM; points are single data values. Significance was determined with unpaired Student's t-tests. **=p<0.01, ***=p<0.001

4.4.6 Plasma lipid levels.

In order to determine whether these mice had sexually dimorphic dyslipidaemia, plasma lipid levels were analysed at cull. Males had a 1.41-fold higher circulating cholesterol levels compared to females (p=0.009) (Figure 4.4.16 A). Males also had a higher (1.52-fold; p=0.0023) plasma HDL (Figure 4.4.16 B) and LDL (1.54-fold; p=0.0039; Figure 4.4.16 C) concentrations. There was no significant effect of sex on circulating triglyceride concentrations (Figure 4.4.16 D).

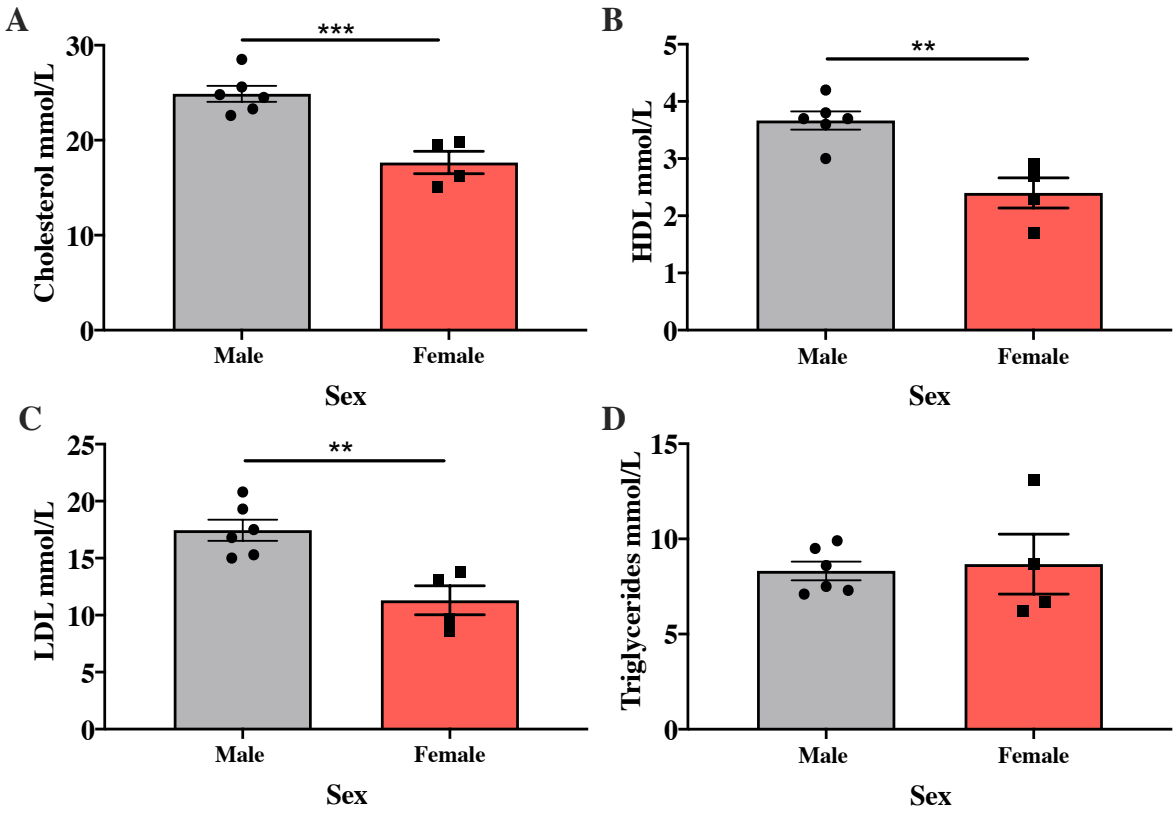

Figure 4.4.16 Analysis of plasma levels in western diet-fed male and female ApoE$^{-/-}$ mice. Mice were subject to a western diet for 12 weeks and blood was taken at cull and subject to lipid analysis. A) Plasma cholesterol concentrations. B) Plasma High Density Lipoprotein (HDL) concentrations. B) Plasma Low Density Lipoprotein (HDL) concentrations. D) Plasma triglyceride concentrations. Males had significantly higher concentrations of cholesterol, HDL, and LDL in their plasma. Males N=6 Females N=4. Columns represents mean ± SEM; points are single data values. Significance was determined with unpaired Student's t-tests. **=p<0.01, ***=p<0.001

4.5 Discussion

It was hypothesised ApoE$^{-/-}$ mice fed a western diet for 12 weeks would provide a tractable, sexually dimorphic model of calcific valve disease. It was also hypothesised that the western diet would accelerate CAVD pathology which would be more severe in males. The data presented here demonstrated that there was no evidence of CAVD present in western-fed ApoE$^{-/-}$ mice. ApoE$^{-/-}$ on a western diet did develop both micro and macrocalcification which was predominately intimal vascular calcification in atherosclerotic plaques. This work builds on Macaskill *et al.* (2020a) work by showing that cardiovascular microcalcification is detectable through micro-PET imaging in both females and males. The data in this chapter also demonstrates the novel finding that females develop more microcalcification in the hearts and have a higher incidence of vascular intimal macrocalcification than male ApoE$^{-/-}$ mice fed a western diet for 12 weeks.

4.5.1 ApoE$^{-/-}$ mice fed a western diet for 12 weeks do not develop aortic stenosis or aortic valve calcification

The data presented here demonstrates that ApoE$^{-/-}$ mice do not develop the haemodynamic changes associated with CAVD: with no aortic regurgitation and no significant changes in the aortic blood velocity. Haemodynamic changes around the aortic valve are usually only present when there is severe thickening/remodelling of the aortic valve (Balachandran, Sucosky and Yoganathan, 2011). Therefore, it is unsurprising that the mild-moderate thickening of the valve cusps seen in this study did not cause sufficient stenosis to produce haemodynamic changes detectable with echocardiography. In humans, severe chronic stenosis causes a pressure overload which can result in left ventricular hypertrophy as a compensatory mechanism to maintain cardiac output (Grossman, Jones and McLaurin, 1975). As no aortic stenosis was observed in this model it follows that there was no indication of changes to the left ventricular wall and no change in cardiac function, although LV wall measurements were made using echocardiography and would have to be confirmed by histology.

There are previous methodologies in the literature which have been tested to induce aortic stenosis in ApoE$^{-/-}$ mice, including a range of dietary supplementation, breeding with another knockout line and mice used at a range of ages. The reports are inconsistent regarding whether ApoE$^{-/-}$ mice develop aortic stenosis. ApoE$^{-/-}$ mice on a standard chow diet at 52 weeks (13 months) have shown mild increases in aortic outflow velocity but not prominent stenosis

(Hartley *et al.*, 2000). When aged to 103 weeks (25.75 months) on a chow diet, ApoE$^{-/-}$ display significant stenosis and blood velocity reached 4 m/s (which is similar to stenosis seen in humans) (Tanaka *et al.*, 2005). However this study only saw regurgitation in 9/30 mice over 70 weeks of age (Tanaka *et al.*, 2005). It is hypothesised the development of the CAVD pathology can be accelerated using a high cholesterol/ high-fat diet. In 8-week-old ApoE$^{-/-}$ mice on western diet for 16 weeks there was no change in aortic velocity (Y. Liu *et al.*, 2022). When the cholesterol-rich diet is extended to 24 weeks, there is a significant increase in aortic velocity, but did not reach high enough blood velocities to be classed as stenosis in humans (Saikrishnan *et al.*, 2014; Wang *et al.*, 2021; Liu *et al.*, 2022). Until ApoE$^{-/-}$ mice have the diet regime extended to 40 weeks was significant stenosis observed (Yang *et al.*, 2021). This indicated that the mice used in this study were not old enough and potentially were not on the dietary supplementation long enough to observe significant aortic stenosis.

There was also no evidence of macrocalcification in the aortic valve cusps of male or female ApoE$^{-/-}$ mice, measured by histology and autoradiography. C57Bl/6 mice have melanocytes in the aortic valve cusps which can produce a black stain during histological analysis (Mjaatvedt *et al.*, 2005; Yajima and Larue, 2008). As von kossa stains calcium black is it impossible to determine whether the black staining produced in the von kossa is calcium or melanin. This positive staining was therefore validated using alizarin red which showed no positive calcium staining in the valve cusps. The histology saw similar aortic valve cusps areas compared to wild-type non-stenosis aortic valves and smaller valves than have been reported in other ApoE$^{-/-}$ studies (Niepmann *et al.*, 2019; Jannasch *et al.*, 2021). Without remodelling, calcium or stenosis it is unlikely that 27-week-old ApoE$^{-/-}$ mouse on a western diet for 12 weeks produces a robust model of CAVD. To further this study the mice may have to be aged for much longer or subject to longer diet alterations. Possibly ApoE$^{-/-}$ mice on a high-fat diet could be combined with another insult, such as the recently published CAVD surgical model (Honda *et al.*, 2014).

4.5.2 ApoE$^{-/-}$ mice fed a western diet for 12 weeks develop, vascular but not valvular, calcification with a sexual dimorphism.

The PET-CT imaging in this chapter demonstrates that ApoE$^{-/-}$ mice exposed to an atherogenic diet for 12 weeks develop microcalcification in the aortas with more microcalcification in the females. Also, a higher proportion of female mice had positive alizarin red staining in the aortic root atheromas when compared with males. Clinically, males present with more coronary artery calcification than females, especially during the female reproductive years when they are

believed to be protected against coronary calcification (Nakao *et al.*, 2018). Interestingly as female mice developed large plaques in the aortic sinus, which were more prone to calcification, this indicates that in this model females have a high propensity to develop advanced atheroma. Again, this is contrary to the sexual dimorphism observed in humans where men tend to develop atherosclerosis younger than women (Mathur *et al.*, 2015).

The larger plaques observed in females in this study are consistent with the literature. In previous studies on ApoE$^{-/-}$ mice, females have displayed larger plaques in the aortic root than males, although the reason for this is unclear (McRobb *et al.*, 2017). It has been shown that male and female mice on an ApoE$^{-/-}$ background have significantly different lipid responses: where females have higher plasma concentrations of cholesterol and LDL (Marek *et al.*, 2017). Female ApoE$^{-/-}$ mice have also been shown to have a higher proportion of CD3+CD4+ T-cells compared with males and oestrogens have been shown to enhance the proliferative capacity of spleen cells in response to LDLs (Caligiuri *et al.*, 1999). This may indicate that female ApoE$^{-/-}$ mice are more prone to inflammation. Interestingly, when normalised to body mass the spleens were bigger in females in this study. Therefore, female ApoE$^{-/-}$ mice subject to a western diet may have increased inflammation compared to males, which may contribute to atheroma. Unfortunately, due to the limited amount of plasma that could be viably taken from the mice, only plasma lipids were measured. Plasma immune cell measurements would be needed to confirm this hypothesis. Therefore, there is evidence in the literature and this thesis that females develop larger atherosclerotic plaques than males in high-fat diet fed ApoE$^{-/-}$ mice. This is a significant limitation of the model and the method that is used to induce calcification.

When exposed to a western diet, both male and female ApoE$^{-/-}$ mice gained significant mass, which was consistent with the mass gained in Williams *et al.*, (2015). Despite no differences in tibia length, male mice were heavier. Interestingly the males and females showed the same percentage of weight gain, yet males did have bigger white and gonadal adipose tissue, which indicated males are gaining more fat mass.

4.5.3 Western diet -fed ApoE$^{-/-}$ female mice have less bone mass than males

Pathological ectopic calcification can disrupt calcium homeostasis and lead to osteoporosis (Persy and D'Haese, 2009). Females have lower bone densities in both humans and mice (Yao *et al.*, 2013; Alswat, 2017). The trabecular analysis displays less bone mass in females compared with males. Compared to the wild-type mice in Matsumoto *et al.* (2018), the female

ApoE$^{-/-}$ mice in this cohort has severely reduced percentage bone volume and trabecular number. This could suggest the female have some demineralisation in their tibias. Although the numbers generated in trabecular analysis for both males and females vary in the literature, meaning it cannot be concluded whether the females are undergoing demineralisation from the data in this study alone (Yee *et al.*, 2016).

The cortical data displayed females having a lower bone area and smaller perimeter than males. This is again consistent with female mice have lower bone densities. The females in this study consistently displayed a lower cortical bone area, and higher porosity compared to the literature (Sapra *et al.*, 2021). Chande *et al.* (2019) analysed cortical bone volume in wild-type mice and found higher cortical bone volume than in this study in males. However, Hong *et al.* (2020) performed micro-CT on male ApoE$^{-/-}$ mice of a similar age to this study and found similar measurements, suggesting the lower bone volume may be an aspect of the age and genotype of the mice used in this study. In (Hjortnaes *et al.*, 2010) it was demonstrated that male ApoE$^{-/-}$ develop cardiovascular calcification and loose bone mass compared to WT mice. And other models of vascular calcification, such as the OPG$^{-/-}$ mouse has shown both vascular calcification and osteoporosis (Bucay *et al.*, 1998). This suggests that potentially there is some bone loss in these mice, but this would have to be investigated further for confirmation. The higher rates of bone demineralisation in females may contribute to the increased rate of vascular calcification seen in the females.

4.4.5 Differences in Dyslipidaemia did not correlate with sexual dimorphism in atheroma.

To investigate whether these mice had dyslipidaemia and whether this dyslipidaemia contributed to the sexual dimorphism displayed in the atheroma, plasma lipid concentrations were measured. The serum lipid concentrations suggest these mice have hyperlipidaemia with larger serum cholesterol and LDL concentrations compared to WT mice (Yin *et al.*, 2012; Hinder *et al.*, 2013). The cholesterol and LDL measurements are consistent with previously reported dyslipidaemia ApoE$^{-/-}$ mice, although the LDL levels in this data set were higher than those seen in Yin *et al.* (2012).

A previous study which found female ApoE$^{-/-}$ mice developing larger atherosclerotic lesions than male mice also found more dyslipidaemia in the female mice, suggesting the larger levels of atheroma can be attributed to higher concentrations of circulating cholesterol. As the dyslipidaemia was higher in males the larger lesions observed in females cannot simply be

attributed to higher concentrations of circulating cholesterol. As HDL is believed to be cardioprotective (Grundy *et al.*, 2019), the elevated HDL in males may contribute to why they developed smaller lesions and less calcification. The evidence for HDL being cardioprotective is controversial, though, and newer investigations believe that HDL may have more of a U-shaped relationship with cardiac health; where either too much or too little is detrimental (Rodriguez, 2021).

4.4.6 Future investigations

The main issue with this study design is that the ApoE$^{-/-}$ mice did not produce valve calcification. To induce valve calcification, mice could be used at an older age or exposed to a western diet for longer. Another option would be to combine the western-fed ApoE$^{-/-}$ mouse with a surgical model which produces valve calcification such as the wire injury model of CAVD (Honda *et al.*, 2014) or the 5/6 nephrectomy model of CKD (Aikawa *et al.*, 2009). Another option would be to combine the ApoE$^{-/-}$ with another genetically modified murine line which is predisposed to developing valve calcification, for example, the LDLR$^{-/-}$ or the ApoEB^{100} mouse (Fleury *et al.*, 2022).

To further this study experiments should be undertaken to address whether sex hormones contribute to the development calcification observed in this study. To do this, female and male mice could be subject to ovariectomy or orchiectomy, respectively, which would remove the production of sex hormones (Goetz *et al.*, 2019). It could then be investigated whether loss of sex hormones affects the valve function and development of calcification in these mice.

It would also be interesting to assess the pathogenesis of the valve in this study. The valves do not display macrocalcification but could be subject to CAVD disease pathologies which come earlier than macrocalcification. One of the limitations of this study is it did not investigate all the pathologies associated with CAVD development. I would therefore go on to investigate the phenotype of the VICs in the valve and the expression of osteogenic markers in the valve using IHC and western blot. I would also investigate the disruption of the endothelial layer and lipid deposition in the valve.

4.4.7 Conclusions

In conclusion, data from this chapter demonstrates that ApoE$^{-/-}$ mice fed a western diet for 12 weeks do not produce CAVD. This study also demonstrated that females develop larger atherosclerotic lesions and more calcification which is opposite to the sexual dimorphism that humans display. No studies have previously examined the sexual dimorphism of the development of calcification in atherogenic ApoE$^{-/-}$ mice before. Understanding the mechanism behind these differences could lead to a better understanding of what is contributing to the sexual dimorphism in humans. If the sexual dimorphism cannot be modelled using the ApoE$^{-/-}$ mouse then other routes could be used to investigate.

5.0 Development of the Wire Injury Model of CAVD

5.0 Development of the Wire Injury Model of CAVD

5.1 Introduction

Following my findings in Chapter 5, that 40-week-old western diet-fed ApoE$^{-/-}$ mice did not produce aortic valve calcification, it was decided to investigate an alternative *in vivo* model with the aim of developing valve calcification.

5.1.1 Limitations with models of CAVD

One of the current problems with models of CAVD is that the models don't produce consistent valve calcification and don't reproduce all of the pathophysiological aspects of the disease. The different murine models of CAVD, as reviewed by Sider *et al.* (2011), each demonstrate different components of the disease (such as dyslipidaemia, inflammation, calcification and neovascularisation), but none exhibit all of these features (Sider, Blaser and Simmons, 2011). Furthermore, murine models vary in severity and pathophysiology between cohorts so are not consistently reproducible (Sider, Blaser and Simmons, 2011). It is possible that human CAVD is not accurately modelled in these *in vivo* preclinical studies because of the limitations in the methods that are currently used to induce the disease in mice. CAVD does not happen spontaneously in murine models and is often induced by genetic mutations that do not exist in humans such as LDLr$^{-/-}$ mouse (Lin *et al.*, 2021). Also, CAVD is a feature of ageing and is, therefore, hard to replicate without ageing mice. With the current lack of pharmaceutical interventions for CAVD being, in part, due to the lack of translatable murine models, there is a need to review the methods through which CAVD is induced preclinically.

5.1.2 The currently used murine models of CAVD

The largest group of mouse models of CAVD are those that induce dyslipidaemia, through genetic deletion of the LDLr, ApoE and/or ApoB genes (Summarised in section 1.9.2) (Fleury *et al.*, 2022). One limitation of these murine models, highlighted in Chapter 4, is that some publications demonstrate aortic root calcification as opposed to aortic valve calcification (Yang *et al.*, 2018). Atherosclerotic plaque calcification occurs when VSMCs, at the site of the plaque, become osteogenic and therefore represents intimal vascular calcification rather than valve calcification (Sorokin et al., 2020). As valve calcification originates from VICs and not VSMCs, atherosclerotic plaque calcification should not be used interchangeably with valve calcification, despite occurring in the aortic root. This lack of calcification in the valve leaflets

may also contribute to the observation that these models do not always produce haemodynamic changes, which do not usually occur until ApoE$^{-/-}$ are over 100 weeks old (Tanaka *et al.*, 2005). Therefore, it is unlikely that models of CAVD based on induction of dyslipidaemia will be able to fully replicate CAVD, and, therefore, alternative models should be explored.

Other models of CAVD exist which are generated by genetic manipulation of genes which don't produce dyslipidaemia. Models of congenital malformations of the aortic valve are also used to model CAVD, these include models of congenital bicuspid aortic valve (as opposed to a healthy tricuspid valve) as a congenital bicuspid aortic valve is associated with an increased risk of developing CAVD (Hoffman and Kaplan, 2002). This is modelling in mice with NOTCH suppression; mutations in NOTCH have been shown to increase the risk of a bicuspid aortic valve. These models of calcification have shown a more constant ability to develop stenosis but as they have a congenic defect which causes a bicuspid valve, there are limitations to the conclusions that can be drawn from them (Tkatchenko et al., 2009; Hakuno et al., 2010).

5.1.3. The wire injury model of calcification

The first surgical model of CAVD was developed by Honda *et al.* (2014) in Japan in 2014. This model is based on direct physical insult to the aortic valve. In mice the insult is artificial, whereas in humans, CAVD is partially caused by mechanical damage over a long period. Therefore, wire injury may induce valve remodelling through the activation of similar repair mechanisms to those that contribute to the condition in patients. The surgery consists of inserting a guidewire into the right common carotid artery and forwarding the wire into the left ventricle under echocardiographic guidance. The wire is then used to abrade the aortic valve leaflets causing direct injury (Honda et al., 2014). The two most important factors of this new model are: (1) that the surgery can be performed on wild-type mice, and (2) that the model develops all the physiological characteristics of calcific valve stenosis. These include valve fibrosis, calcification, valve thickening, the presence of osteogenic markers in the valve cusps and hemodynamic changes in aortic outflow leading to stenosis (Honda et al., 2014). Niepmann *et al.* (2019) further developed this procedure to achieve either mild, moderate, or severe cusp injury to enable the modelling of different stages of CAVD. Another group has also published this model but without inducing calcification (Artiach *et al.*, 2020). Currently, no laboratory in the UK is using this model and it has not been established whether there is a sexual dimorphism in the remodelling response to wire injury of the aortic valve.

5.2 Aims and hypothesis

The work outlined in this chapter addresses the hypothesis that direct injury to the aortic valve will result in the development of calcific aortic valve disease in C57Bl/6 mice. This will be achieved by establishing the original methodology published by Honda *et al.* (2014) and modified by Niepmann *et al.* (2019).

Project aims

1. To perform a pilot study to ensure the surgery and echocardiography imaging can be performed without excess mortality.

2. To cause sufficient damage to the aortic valve to induce both valve calcification and aortic stenosis.

3. To determine whether there is a sexually dimorphic response to the aortic valve wire injury.

5.3 Materials and methods

5.3.1 Mice

Adult male and female C57BL6/J (Harlan Ltd., UK) mice were maintained on a standard chow diet as outlined in Section 2.4. Adult ApoE$^{-/-}$ mice were obtained from Charles River (Trenant, UK). All procedures were performed in accordance with the UK Home Office, under Home Office licences and the University of Edinburgh Ethics guidelines.

5.3.2 Wire injury surgery

Wire injury surgery was performed on 10–14-week-old C57Bl6 mice and 25-week-old ApoE$^{-/-}$ mice, as outlined in Section 2.4.3. The mice were culled at various time points depending on the aims of the study.

5.3.2.1 Development of the wire injury protocol

This was the first time that wire injury of the aortic valve (as described by Honda et al. 2014) protocol was performed in the UK, so method development was performed. This included four separate studies. First, a pilot study was conducted to ensure the surgeries were safe to perform, and then three subsequent studies, incrementally increasing the amount of damage to the valve.

Study 1: Pilot Study

For the pilot study, seven male mice were used. During the surgery, the wire was rubbed against the valve up to 20 times. Sham mice followed the same surgical protocol except the wire was not advanced over the valve. The details of the timeline of the study can be seen in Figure 5.3.1.

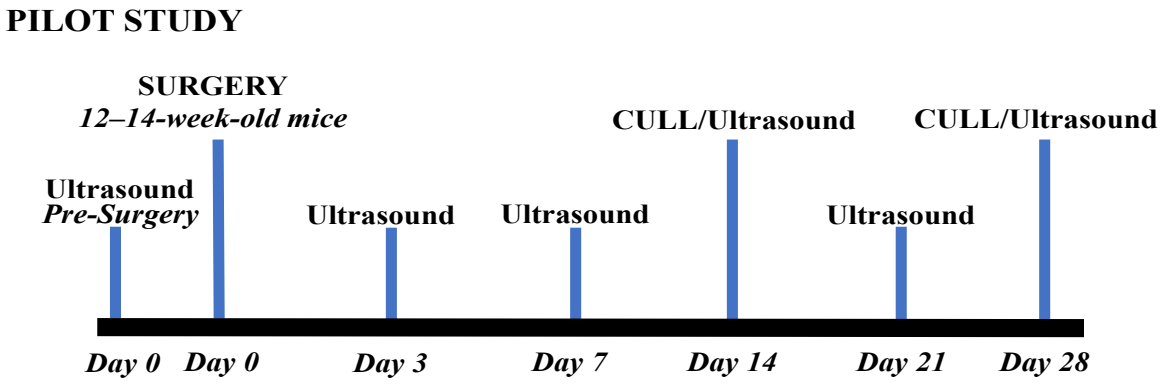

Figure 5.3.1: Timeline of pilot study. Timeline of the pilot study completed for the development of the wire injury model.

Study 2: Mild injury study

For the mild injury study, 6 male and 6 female mice were studied. The wire was rubbed against the valve up to 50 times and twisted up to 20 times, the details of the timeline of the study can be seen in Figure 5.3.2.

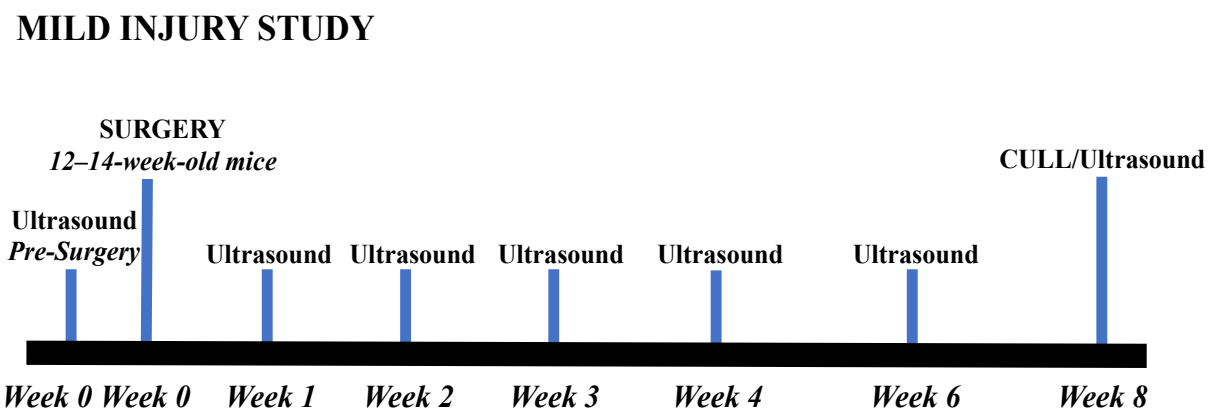

Figure 5.3.2: Timeline of mild injury study. Timeline of the mild injury study completed for the development of the wire injury model.

Study 3: Moderate injury study

For the moderate injury study, 4 male and 4 female mice were included. The wire was rubbed against the valve up to 50 times and twisted up to 50 times, the details of the timeline of the study can be seen in Figure 5.3.3.

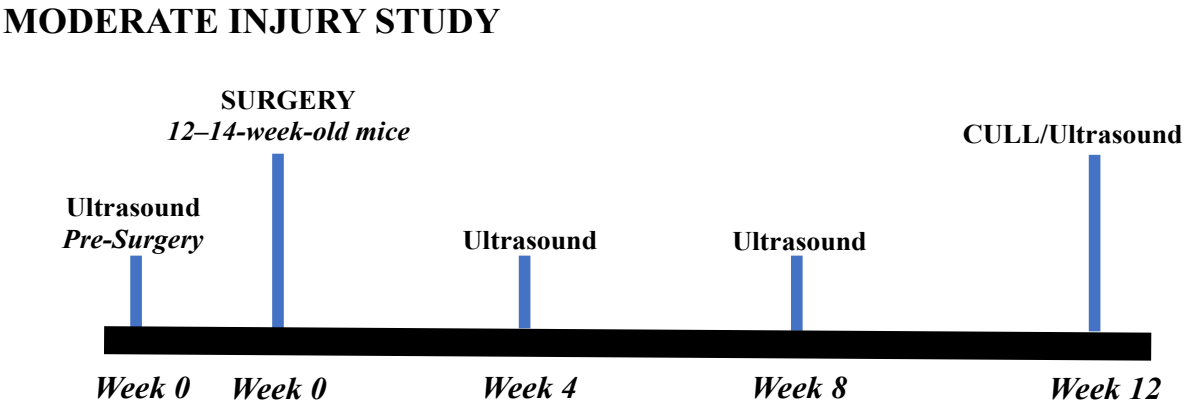

Figure 5.3.3: Timeline of moderate injury study. Timeline of the moderate injury study completed for the development of the wire injury model.

Study 4: Wire injury on ApoE$^{-/-}$ background mice

The moderate injury protocol was also performed on 25-week-old ApoE$^{-/-}$ male and female mice (mouse details in section 2.2). This study aimed to determine whether the wire injury surgery performed on ApoE$^{-/-}$ mice with additional risk factors would increase the likelihood of calcification.

5.3.2.2 Tissue collection

Tissues were collected immediately after culling, as described in Chapter 2, section 2.5.2.

5.3.3 Echocardiography of wire injury mice to determine haemodynamic changes.

Echocardiography scans were performed pre-surgery and at subsequent time points after surgery. These scans aimed to determine whether the wire injury would cause aortic stenosis and haemodynamic changes in the aorta. Furthermore, these scans would determine whether injury to the aortic valve caused changes in cardiac function. Echocardiography scanning was carried out as described in Chapter 2 section 2.3.

5.3.4 Aortic valve pathology

Valve embedding and sectioning were performed as described in Chapter 2, section 2.3.2. Tissues were stained with H&E to allow for quantification of valve thickness, and with Masson's Trichrome to investigate collagen deposition. As it has been previously reported that the aortic valve has melanin deposits, which can cause a false positive calcium stain with Von Kossa staining (Mjaatvedt *et al.*, 2005), both Alizarin Red and von kossa staining were used to detect calcium in the valve. Alizarin red was used to validate any von kossa stains. Immunohistochemistry was carried out as described in section 2.7.4. Calcium staining was carried out as described in Chapter 2, section 2.3.3. All sections were imaged on an AxioImager Z1 microscope (Zeiss, Germany).

5.4 Results

5.4.1 Pilot Study

5.4.1.1 Low mortality and weight loss following wire injury surgery.

The initially study was performed to confirm that wire injury to the mouse aortic valve could be carried out under ultrasound guidance without excessive mortality. Ultrasound images from the surgery can be seen in Figure 5.4.1 A and B. Only one mouse had to be killed due to post-surgery morbidity (symptoms included hunched back, eyes partially closed and rigid movements) and no mice died under anaesthetic (Figure 5.4.1 C). For displaying the mouse weight during the study, mice were grouped separately, into mice that were culled after 2 weeks (n=3; Figure 5.4.1 D) and mice that were culled after 4 weeks (n=1; Figure 5.4.1 E). The biggest weight loss recorded was -12.1 % of total body weight, although this mouse recovered body weight by week 2 (Figure 5.4.1 E). The loss of body mass was not statistically significant.

5.4.1.2 Investigating morbidity of the culled mice from the pilot study

One mouse had to be culled 4 days post-surgery and a detailed investigation of the cause was undertaken. During surgery in this mouse, the guidewire was accidentally inserted into the ventricle soft tissue (seen in Figure 5.4.2 B). Dysfunction of the systole was observed on the ultrasound of this mouse (Figure 5.4.2 A). Histological imaging of the left ventricle (Figure 5.4.2 C) demonstrated damage to the left ventricle wall. The cardiac function measurements displayed a decrease in fractional shortening, ejection fraction, left ventricular thickness, left ventricular mass and cardiac output (Figure 5.4.2 D).

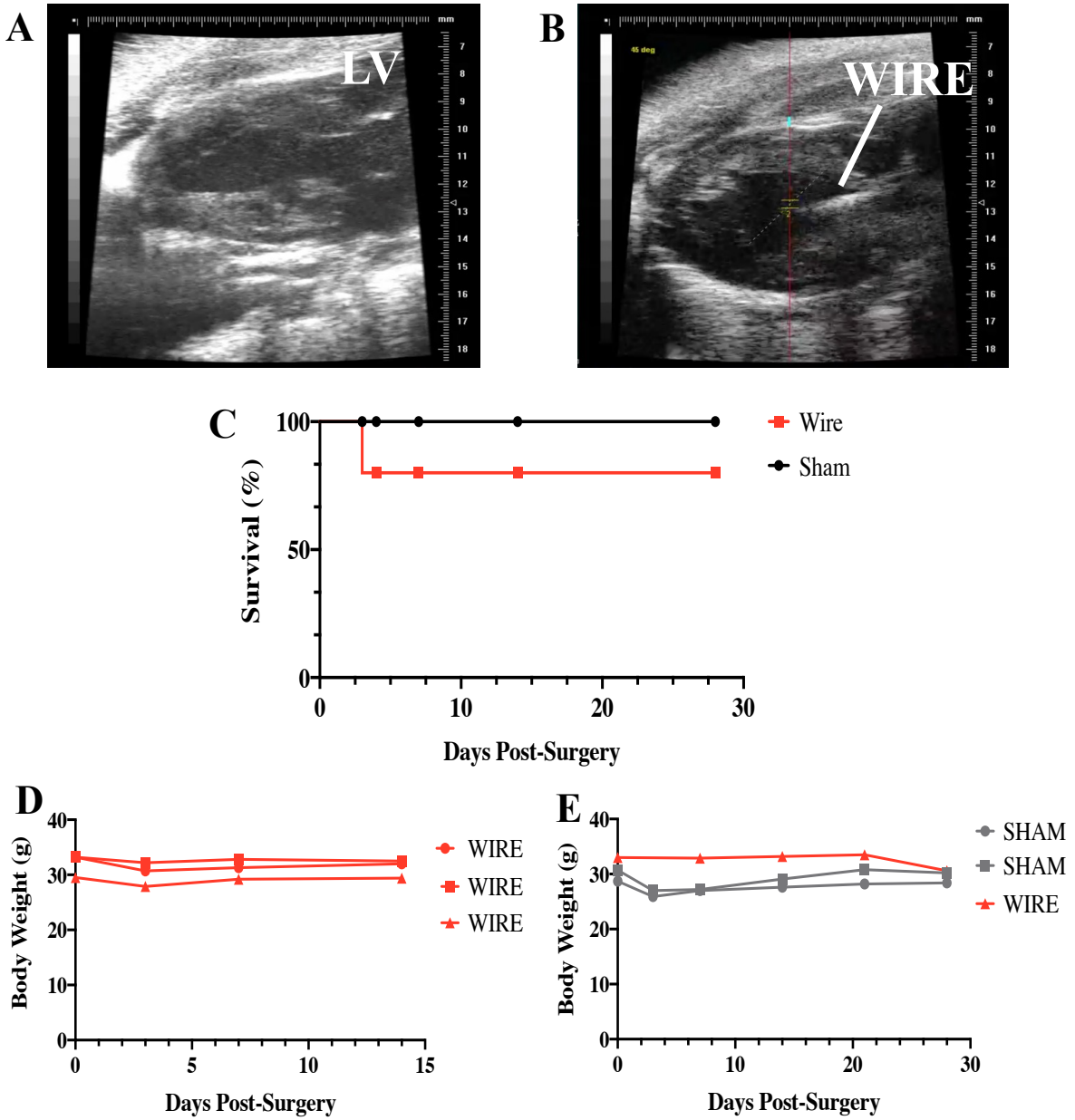

*Figure 5.4.1: Pilot study survival and body weight***.** Mice had a guidewire inserted into the left ventricle (LV) and rotated up to twenty times across the aortic valve, under ultrasound guidance. Weights were recorded pre surgery, then every 7 days until 28-days post-surgery. A) Long-axis ultrasound scans of the heart (B) were used to confirm guidewire placement. C) There was low mortality after the WI surgery. D) Wire injury had little effect on body weight in mice maintained for 2 weeks. E) Wire injury had little effect on body weight in mice maintained for 4 weeks. Panel C shows survival for 7 mice (n= 4 wire; n=2 sham) that underwent surgery. Panels D and E, display individual lines for individual mice

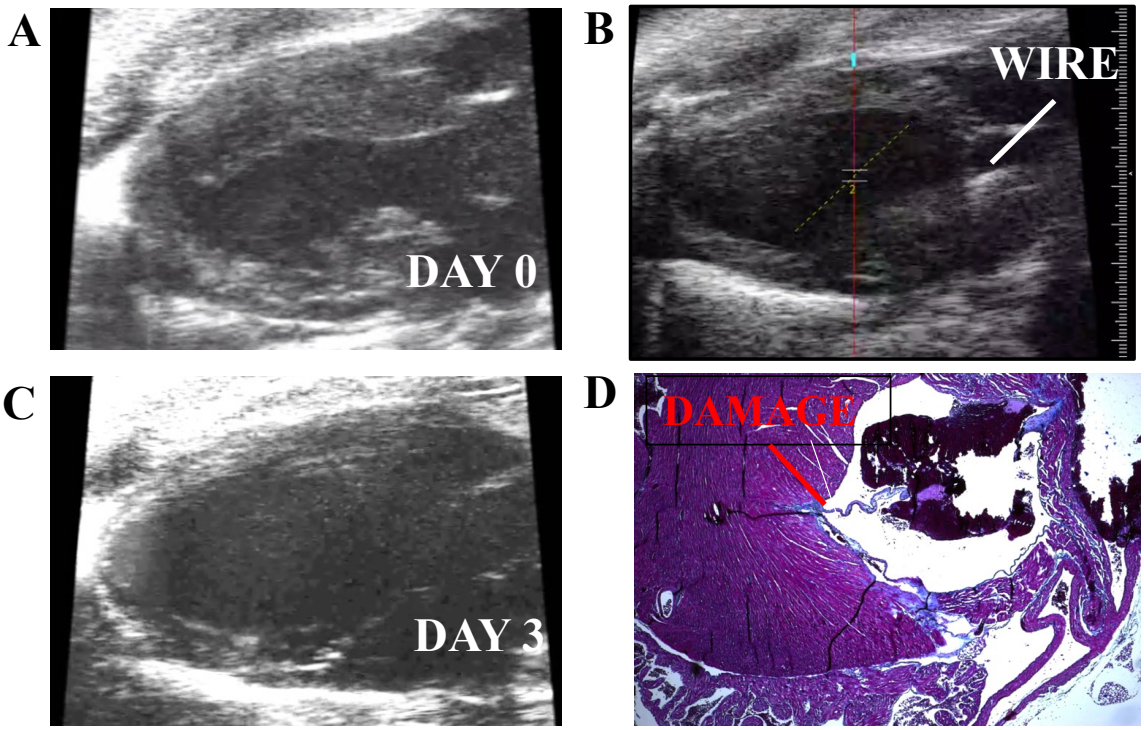

E

	Baseline	3 Days
Fractional Shortening (%)	41.51	29.08
Ejection Fraction (%)	77.29	43.08
LVESD (mm)	2.42	2.71
LVEDD (mm)	4.14	3.83
LV Thickness (mm)	0.92	0.79
LV Mass (mg)	205.06	197.13
Cardiac Output (mL/min)	29.84	24.29

*Figure 5.4.2: Case study of mouse morbidity***.** This mouse had a guidewire inserted into the left ventricle and rotated up to twenty times across the aortic valve, under ultrasound guidance. The mouse had to be culled 4 days post-surgery due to morbidity, symptoms included hunched back, eyes partially closed and rigid movements. A) Ultrasound of the heart before wire injury. B) Ultrasound displaying wire-insertion. C) Images of systole after 3 days of surgery. D) Masson's trichrome staining of left ventricle. Scale bar 800μM. E) Table of cardiac function measurements of the mouse, at base line and 3 days post-surgery. LVEDD- left ventricular end diastolic diameter. LVESD- left ventricular end systolic diameter.

5.4.1.3 Aortic velocity and cardiac function were unaltered during the pilot study.

During the pilot study, assessments of aortic and cardiac function were performed to determine whether the wire injury caused any aortic valve damage. Readings following wire injury were compared with baseline measurements and demonstrated no significant change in peak aortic outflow velocity (Figure 5.4.3 A) or velocity time integral (VTI) (Figure 5.4.3 B) up to 14 days post-surgery. There were also no significant changes seen in cardiac measurements, including left ventricular thickness or ejection fraction (Figures 5.4.3 C and 5.4.3 D). To investigate further whether the wire influenced cardiac function, additional echocardiography measurements were taken (Table 1). None of the cardiac function measurements were significantly different post-wire injury compared with baseline measurements.

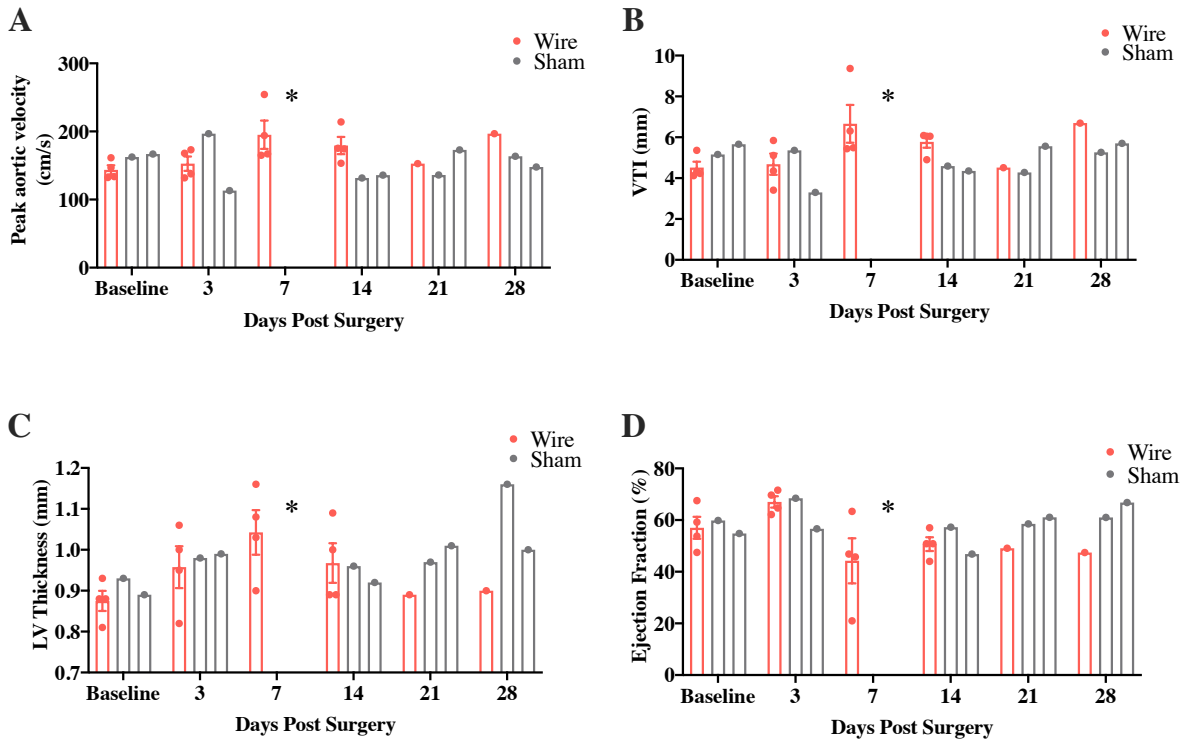

Figure 5.4.3: Cardiovascular consequences of wire injury surgery. Mice had a guidewire inserted into the left ventricle and rotated up to twenty times across the aortic valve, under ultrasound guidance. Rubbing the aortic valve with the wire did not change (A) peak aortic velocity (cm/s) or (B) VTI (mm). Cardiac measurements such as (LV) thickness (mm) (C) or ejection fraction (%) (D) also did not change. One-Way ANOVAs were performed with post-hoc Dunnett's tests (only performed on WI mice (up to 14 days) not shams). Columns represent mean±SEM, points represent single data values. Bar charts for sham mice display individual mice. Sham N=2, Wire injury (0-14 days N=4) (21-28 days N=1). VTI= Velocity time integral, LV= Left ventricle. * Due to a technical error the scans for sham mice could not be performed at the 7-day time-point.

Table 5.4.1: Cardiovascular functional measurements of wire injury pilot study. Mice had a guidewire inserted into the left ventricle and rotated up to twenty times across the aortic valve, under ultrasound guidance. Data displays mean±SEM of wire injury mice and was analysed using One-way ANOVA with post-hoc Dunnett's tests. N=4. The statistical analysis was only performed on WI mice between baseline and day 14. LVESD- left ventricular end systolic diameter, LVEDD- left ventricular end diastolic diameter, LV mass- left ventricular mass.

	Baseline (Day 0)	**Day 3**	**Day 7**	**Day 14**
Fractional Shortening (%)	36.88 ± 7.91	34.05 ± 1.25	27.62 ± 8.75	33.34 ± 3.12
Aortic Wall (mm)	1.13 ± 0.21	0.96 ± 0.11	0.88 ± 0.07	1.03 ± 0.12
Posterior Wall (mm)	0.98 ± 0.09	0.91 ± 0.10	1.13 ± 0.11	0.94 ± 0.04
LVEDD (mm)	4.08 ± 0.36	4.22 ± 0.13	4.40 ± 0.09	4.38 ± 0.20
LVESD (mm)	3.56 ± 0.47	2.74 ± 0.11	2.87 ± 0.18	3.13 ± 0.10
LV Mass (mg)	211.30 ± 5.24	225.00 ± 12.81	239.52 ± 16.78	226.01 ± 12.64
Cardiac Output (mL/min)	20.48 ± 0.64	19.57 ± 4.02	12.97 ± 1.96	17.25 ± 1.16

5.4.1.4 Valve cusps display evidence of remodelling after wire injury

Post-necropsy, valves were taken from sham and wire injury mice and subjected to staining. Images of H&E stained sections revealed that valves looked thicker post-wire injury, compared with sham mice (Figure 5.4.4 A, B, C and D). These stains were not quantified due to the low N numbers of the sham mice. The Masson's Trichrome indicated that the thickened valves were formed, in part, from collagen (Figure 5.4.4 C & D). Alizarin red and von Kossa staining indicated that the aortic valve was negative for calcium deposition (Figure 5.4.5).

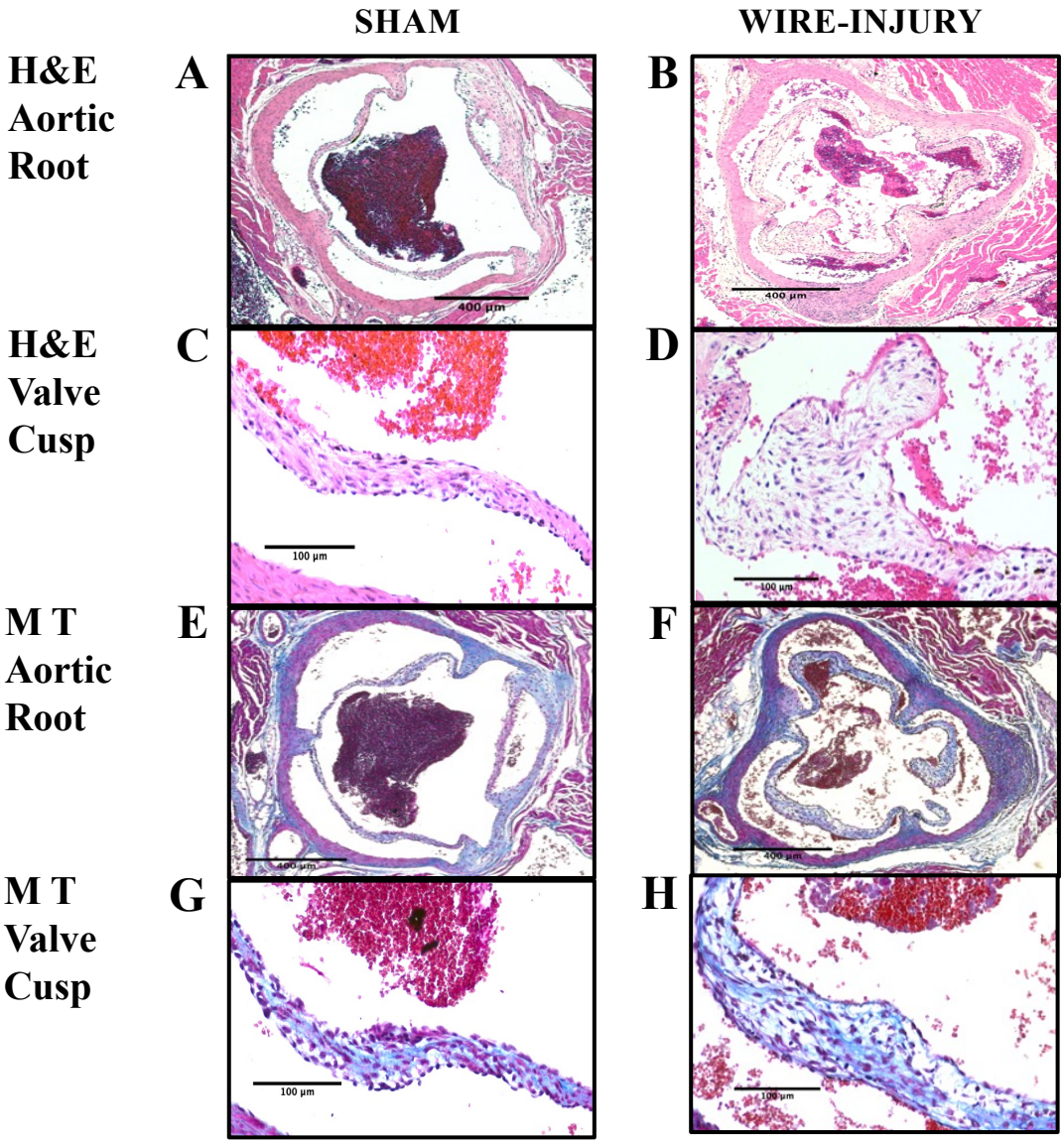

Figure 5.4.4: Histological staining of the aortic root after the pilot study. Mice had a guidewire inserted into the left ventricle and rotated up to twenty times across the aortic valve, under ultrasound guidance. A-D display H&E staining of A) aortic root of sham B) aortic root of wire Injury C) higher magnification of sham D) higher magnification of wire injury. E-H display Masson's trichrome (MT) staining of E) aortic root of sham and F) aortic root of wire injury G) higher magnification of sham and H) higher magnification of wire injury.

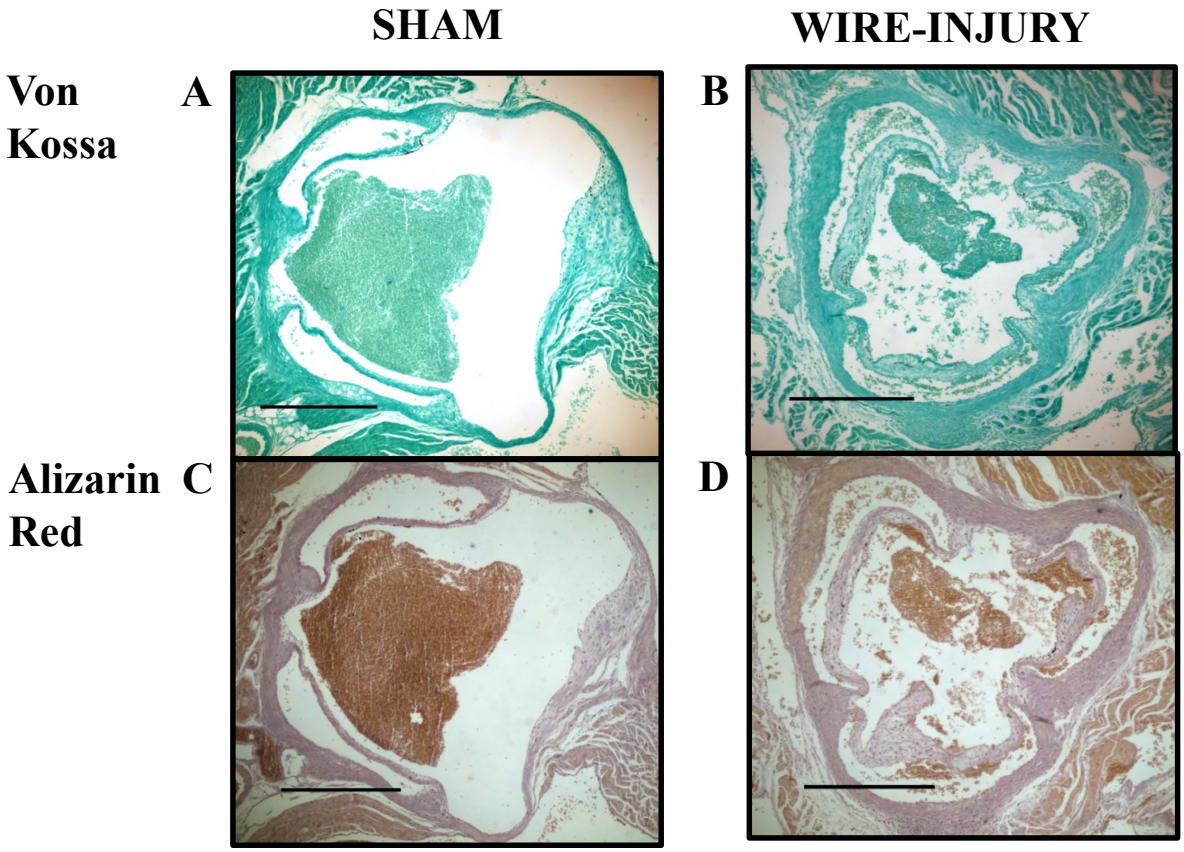

Figure 5.4.5: Calcium staining of mouse aortic root in sections obtained from the pilot study. Mice had a guidewire inserted into the left ventricle and rotated up to twenty times across the aortic valve, under ultrasound guidance. A) Representative von kossa image from a sham mouse B) Representative von kossa image from a wire injury mouse C) Representative alizarin red image from a sham mouse E) Representative alizarin red image from a wire injury mouse. All calcium stains were negative. Scale bar - 400 μM

5.4.2 Mild injury study

5.4.2.1 Mild wire injury surgery led to mortality in male mice.

The next study sought to increase the damage to the aortic valve and determine whether the damage caused by the wire was different between males and females. The surgical protocol was altered by increasing the number of rubs and rotations of the wire across the valve. This produced more mortality in males (3/6) than females (1/5), which were all due to technical issues during surgery (Figure 5.4.6 A). All mice that survived the surgical procedure survived for the entire 56-day recovery period. After the surgery, females had a significantly greater increase in body weight, compared to males, across all time points (Figure 5.4.6 B, $p<0.05$).

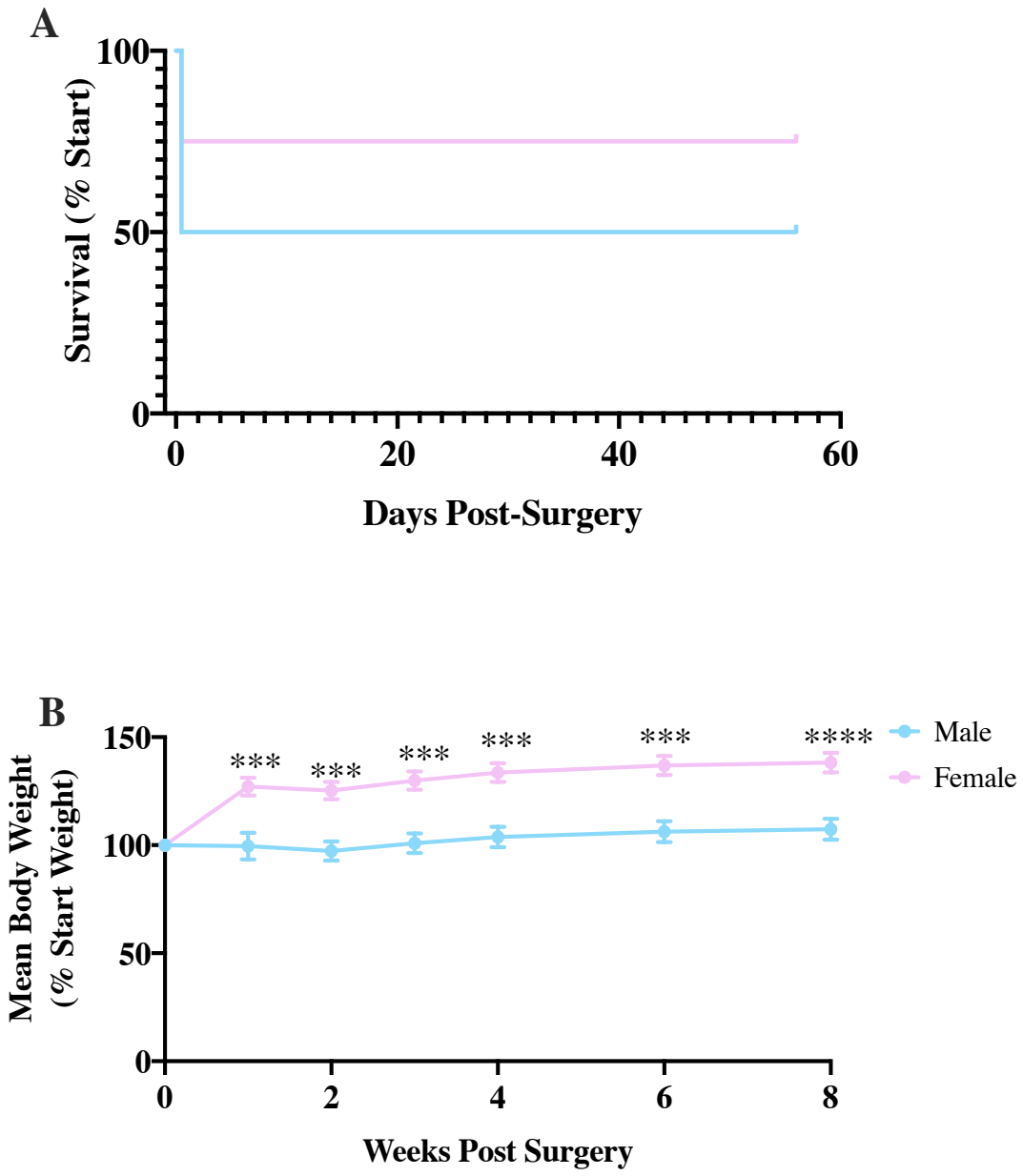

Figure 5.4.6: Investigating the sex differences in survival after mild wire injury. Mice had a guidewire inserted into the left ventricle and rotated up to twenty times across the aortic valve, under ultrasound guidance. A) Survival after wire injury surgery (all deaths were caused by non-recovery from surgery) B) Female mice gained significantly more weight post-surgery. Males N=3 Females N=4. In B, significance was determined with a Two-Way ANOVA. ***=p<0.001 ****=p<0.0001 Blue-Male, Female-Pink.

5.4.2.2 Study to investigate sex-differences in cardiac function after the mild wire injury surgery

VTI did not show a sexual dimorphism pre-surgery (Figure 5.4.7 A). Immediately post-surgery female VTI increased, this was sustained over the course of the 8 weeks post-surgery. The VTI recorded in males did not change after the WI surgery and there was a significant difference between male and female response to the surgery in VTI measurements ($p=0.0026$, Figure 5.4.7 A). Peak velocity was not significantly different between males and females before the WI surgery Figure 5.4.7 B). There was no significant effect of the surgery on peak velocity measurements across any time point in either males or females (Figure 5.4.7 B). Before surgery, male mice had a larger ejection fraction than female mice (Figure 5.4.7 C). After surgery, the ejection fraction in males declined whereas the ejection fraction in females did not change ($p=0.0038$, Figure 5.4.7 C). LV thickness was significantly larger in males compared to females $p=0.0126$, Figure 5.4.7 D). The surgery did not have a significant effect on LV thickness in males or females (Figure 5.4.7 D).

Further measurements of cardiac function were also assessed using echocardiography in M (motion) mode. Before surgery, males had a larger LV mass ($p=0.0031$ Figure 5.4.8 A) and cardiac output ($p=0.0126$ Figure 5.4.8 B). The surgery had no significant effect on LV Mass or cardiac output on male or female mice across any time point post-surgery Figure 5.4.8 A/B). There was no change in posterior wall thickness between males and females across any timepoint pre- and post-surgery (Figure 5.4.8 C). Males had larger LVEDD measurements before surgery ($p=0.0293$, Figure 5.4.8 E). The surgery did not significantly affect the LVEDD measurements in male or female mice (Figure 5.4.8 E). LVESD was not significantly different between male and female mice before the surgery. The surgery did not significantly affect LVESD measurements in either male or female mice (Figure 5.4.8 F).

After cull, aortic roots were sectioned and subject to histological staining. H&E staining of valves from the male (Figure 5.4.9 A) and female (Figure 5.4.9 B) mice 56 days after injury indicated little valve remodelling. Quantification of valve area demonstrated no significant difference in the thickness of the aortic valve cusps between male and female mice (Figure 5.4.9 C). Quantification of Masson's trichrome (Figure 5.4.9 D&E) staining demonstrated that there was no significant difference in collagen staining between male and female WI mice 56 days post-surgery (Figure 5.4.9 F). The aortic root was also subject to two types of calcium

staining, alizarin red (Figure 5.4.10 A/B) and von Kossa stains (5.4.10 C/D). Dark spots identified on the valves cusps (indicated by a blue star in the figure) were originally thought to be calcium deposition, although this was questioned when the dark spots were consistent (in location and distribution) in both alizarin red and von Kossa stained sections (where spot appeared black on alizarin red, which stains calcium red). After consultation with a pathologist (Dr. Jorge del Pozo, East Bush Pathology, RDSVS, University of Edinburgh), it was noted that C57Bl/6 mice are prone to melanin deposition in their valves, and the dark spots seen in the histology from these mice were consistent with the presence of melanin (Yajima and Larue, 2008). In light of this information, I, therefore, concluded that there was no calcium deposition in the histological sections examined.

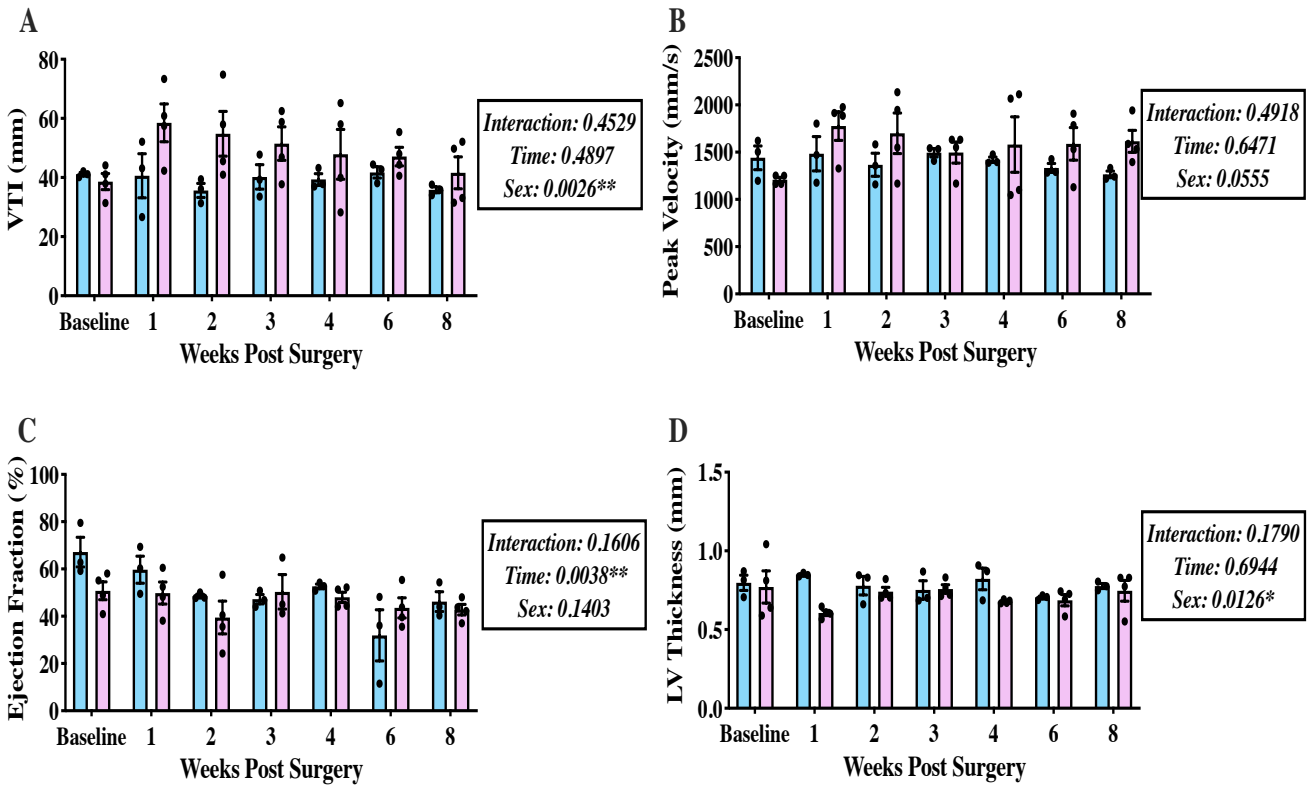

Figure 5.4.7: Investigating the sex differences after mild wire injury. Mice had a guidewire inserted into the left ventricle and rotated up to twenty times across the aortic valve, under ultrasound guidance. Males had bigger measurements for VTI (mm) (A) and peak velocity (mm/s) (B). VTI (mm) (A), peak velocity (mm/s) (B) and LV thickness (mm) (D) measurements did not change from pre- to post-surgery in either males or females. C) Ejection fraction (%) decreased from baseline (pre-surgery) across the 8 weeks post-surgery in both males and females. There was no sex difference in this loss of ejection fraction. Columns represent mean±SEM, points represent single data values. Males N=3 Females N=4. In A, B, C and D significance was determined using a Two-Way ANOVA. *=p<0.05, **=p<0.00. Blue-Male, Female-Pink. VTI=velocity time integral, LV thickness= left ventricular thickness.

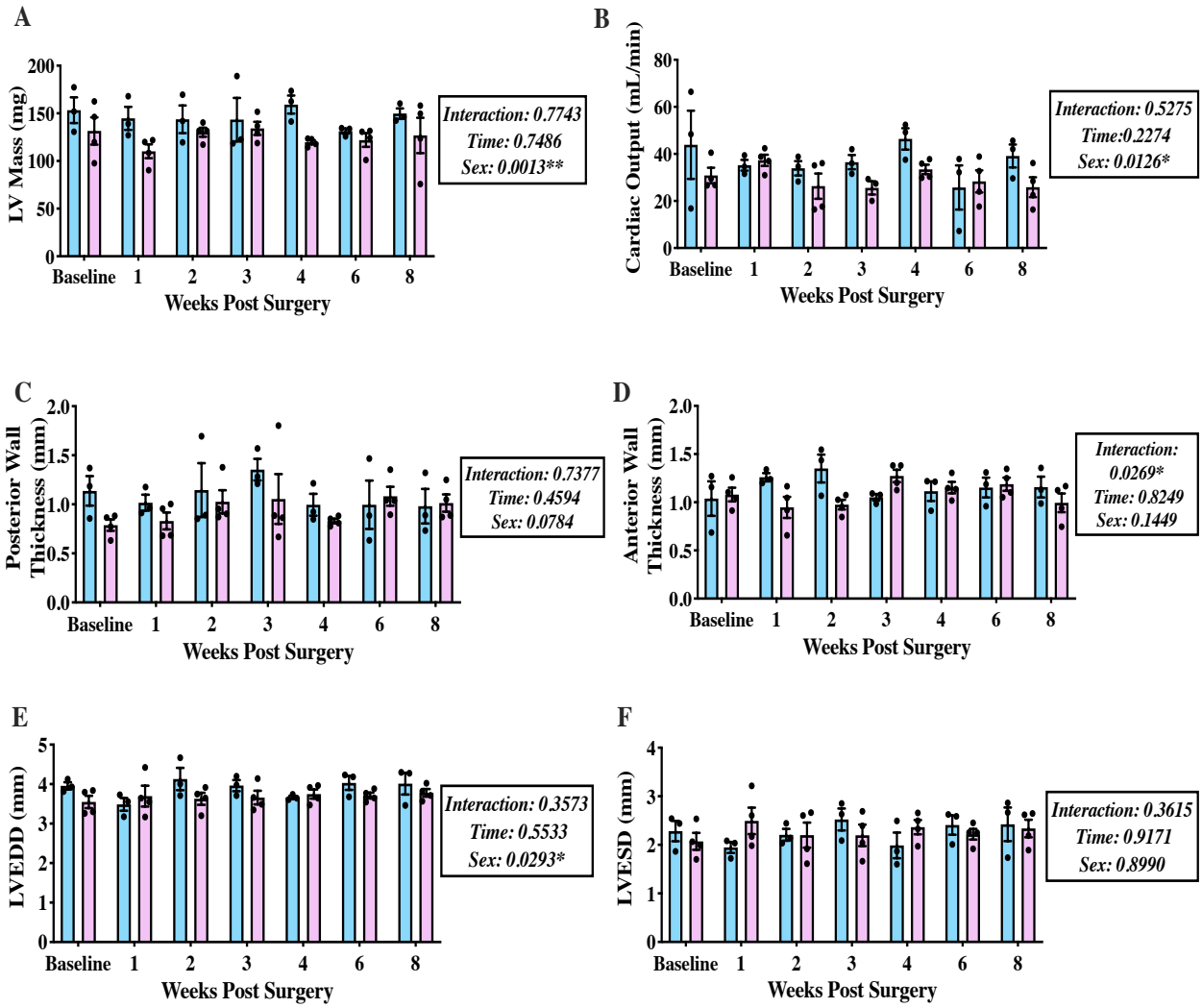

Figure 5.4.8: Investigating the sex differences in cardiac function after mild wire injury, measured using M-mode echocardiography. Mice had a guidewire inserted into the left ventricle and rotated up to twenty times across the aortic valve, under ultrasound guidance. Males had greater left ventricular mass (LV Mass (mg)) (A), cardiac output (mL/m) (B) and left ventricular end diastolic diameter (LVEDD (mm)) (E) pre-surgery. Male and female did not have significant differences in (C) posterior wall thickness (mm) (D) anterior wall thickness (mm) or (F) LVESD (mm) pre-surgery. None of the measurements significantly changed from baseline (pre-surgery) to post-surgery in either males or females. Columns represent mean±SEM, points represent single data values. Males N=3 Females N=4. Statistical Significance was determined using Two-Way ANOVA. *=$p<0.05$, **=$p<0.001$. Blue-Male, Female-Pink. LVESD- left ventricular end systolic volume.

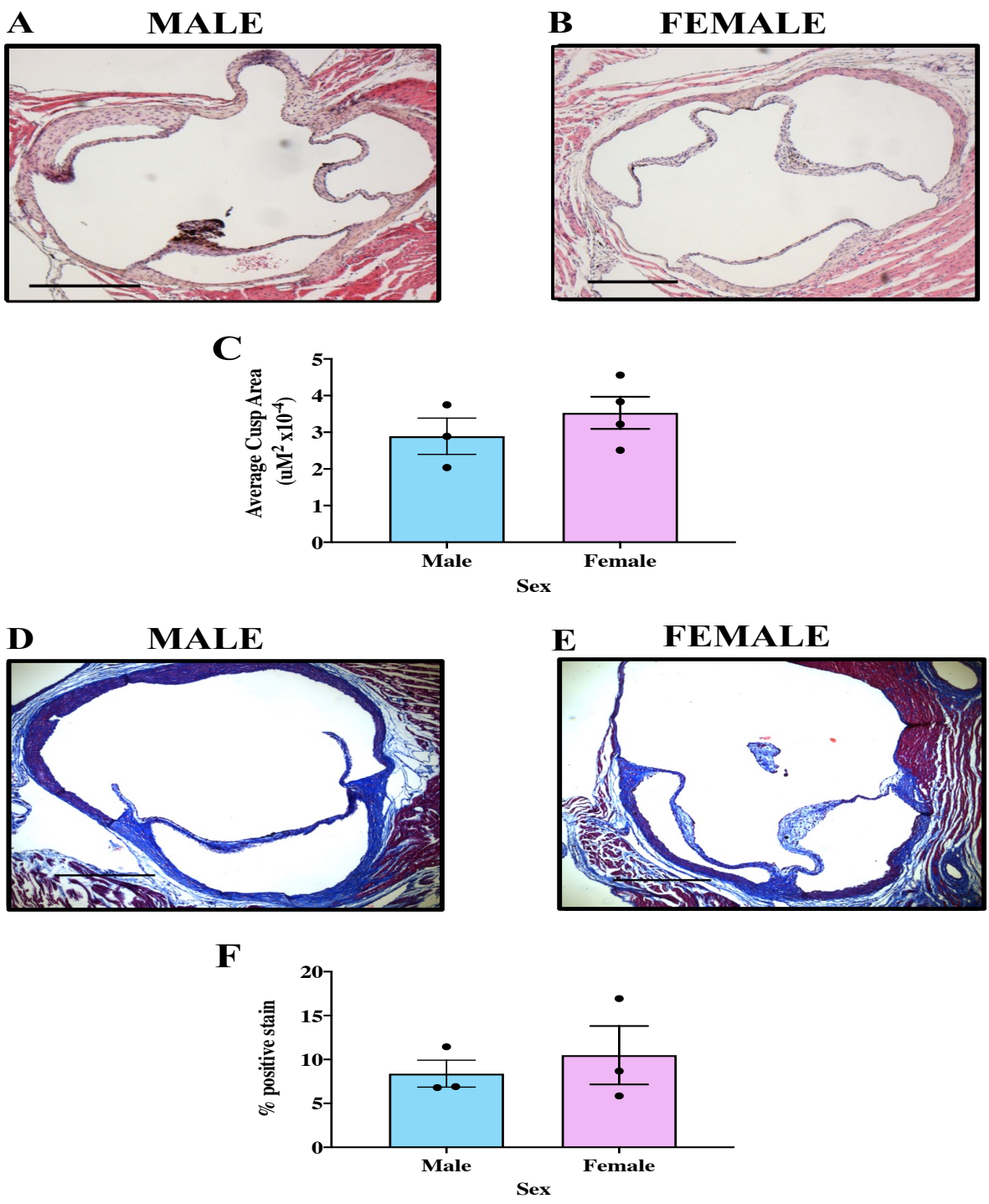

*Figure 5.4.9: Histological staining of the aortic root after mild injury***.** Mice had a guidewire inserted into the left ventricle and rotated up to twenty times across the aortic valve, under ultrasound guidance. A) Representative H&E image from a male mouse B) Representative H&E image from a female mouse C) Quantification of the valve cusp area from the H&E staining D) Representative MT image from a male mouse E) Representative MT image from a female mouse F) Quantification of the MT staining. H&E- haematoxylin and eosin, MT- Masson's trichrome. Quantification was tested for significance with Student's unpaired t-test, columns represent mean±SEM, points represent single data values. Males N=3 Females N=3. Blue-Male, Female-Pink. Scale bar - 400 µM

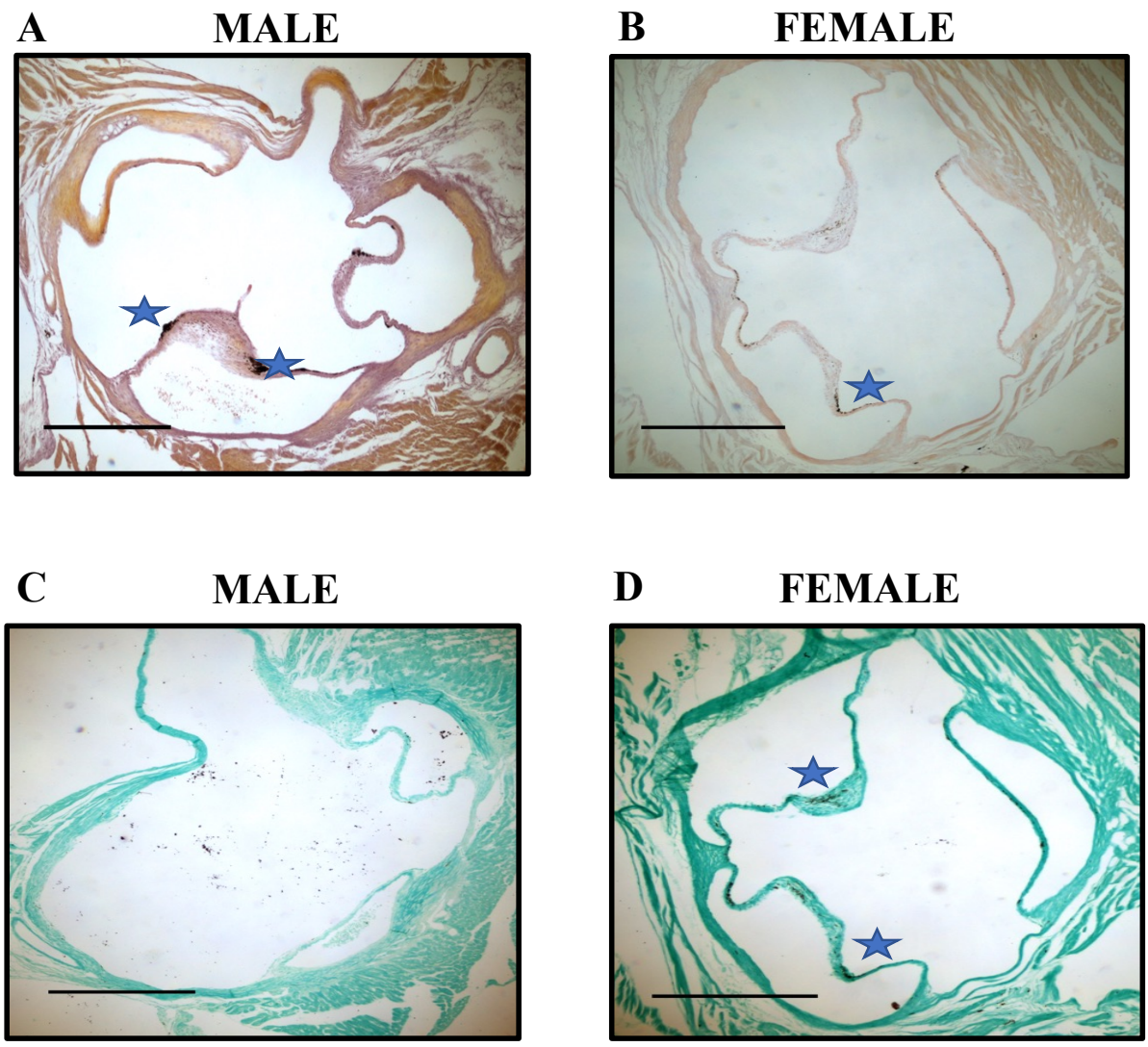

*Figure 5.4.10: Calcium staining of aortic root after the mild injury study***.** Mice had a guidewire inserted into the left ventricle and rotated up to twenty times across the aortic valve, under ultrasound guidance. A) Representative alizarin red image from a male mouse B) Representative alizarin red image from a female mouse C) Representative von Kossa image from a male mouse D) Representative von Kossa image from a female mouse. All calcium stains were negative. Scale bar - 400 µM**.** Blue starts indicate areas of melanin**.**

5.4.3 Moderate injury study

5.4.3.1 Mortality observed in females after moderate injury

Analysis of the mild injury study demonstrated that, whilst mortality and morbidity were low in mice that survived the surgery, the damage induced in the aortic valves was not sufficient to cause either the haemodynamic changes described in previous studies (Honda *et al.*, 2014; Niepmann *et al.*, 2019) or deposition of calcium in the valve leaflets. To address this, the method was adapted in an attempt to increase the damage caused to the aortic valve. The surgical protocol was altered by increasing the number of times the wire was advanced across the valve and rotated (based on the previously published protocol) to determine (i) whether this would replicate the features of CAVD reported in previous studies (Honda *et al.*, 2014; Niepmann *et al.*, 2019) and (ii) whether there was a sexual dimorphism in the response to the wire injury.

The first group of surgeries were performed successfully without any technical issues during surgery (N=4 females and N=4 males). These mice recovered from surgery well. To increase the N numbers the next group of mice had surgery performed on them. In this next study the mortality was surprisingly high both in males (2/4) and in females (3/3). One of those females died due to surgical complications. The other mice all had to be culled due to health reasons post-surgery having failed to recover fully from anaesthesia. The adverse symptoms in these mice were strikingly consistent and strikingly different from symptoms observed in the previous investigations. In all cases, the mice appeared to be recovering from anaesthesia but then relapsed into unconsciousness. Over a period of approximately 40 minutes, they then exhibited barrel rolling and unilateral loss of movement with unilateral ptosis (one eye partially closed). Overall, 6/8 males survived, and 4/7 females survived (Fig 5.4.11 A). All of the mice that survived surgery did not lose significant amounts of weight post-surgery across any time point (Figure 5.4.11 B).

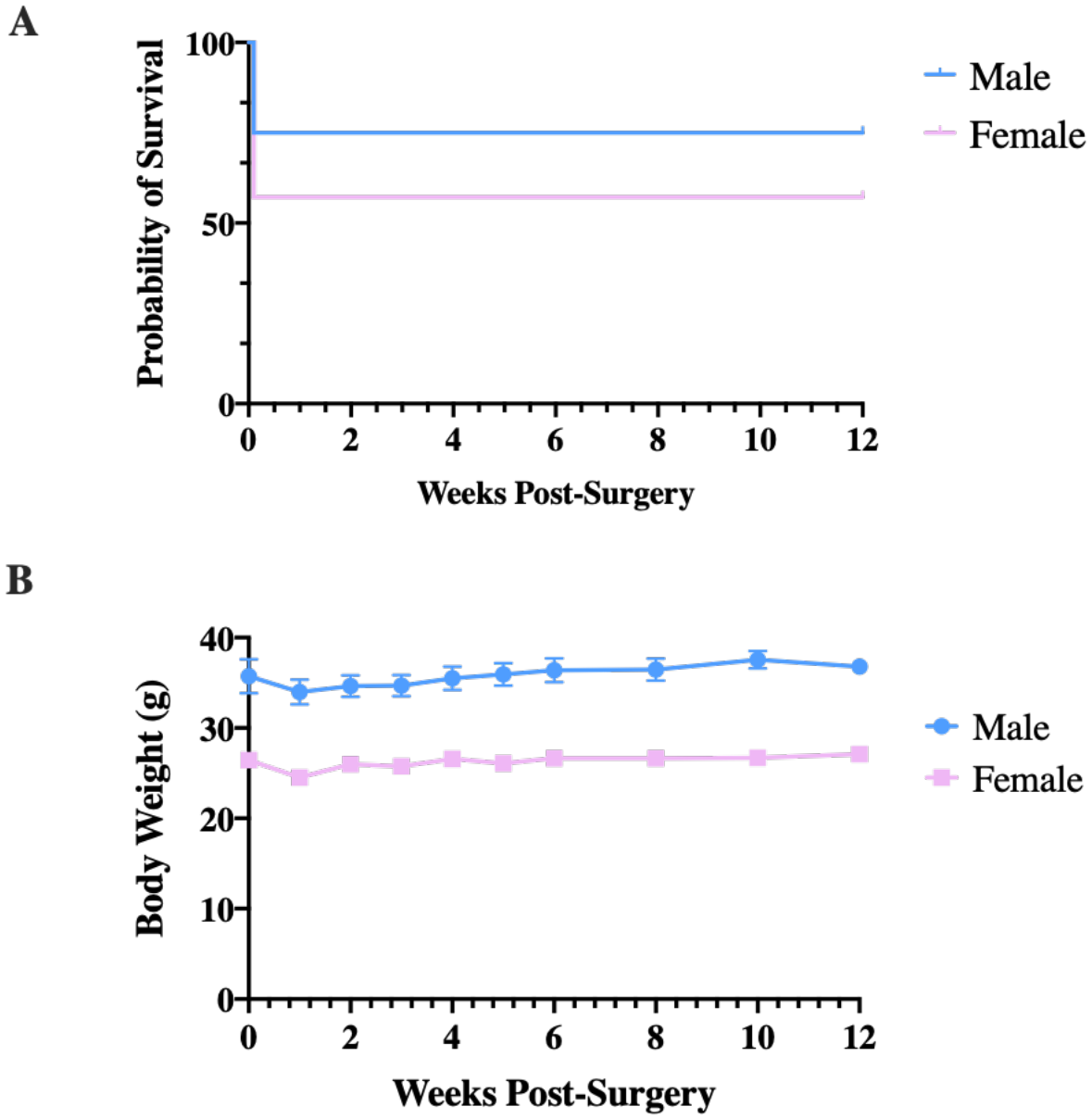

Figure 5.4.11: Investigating the sex differences in weight and survival after moderate wire injury. Mice had a guidewire inserted into the left ventricle and rotated up to fifty times across the aortic valve, under ultrasound guidance. (A) Both males and females lost minimal amounts of weight after surgery. Males N=5 Females N=4. (deaths females N=4/8, Males N=2/7). Blue-Male, Female-Pink

5.4.3.2 Study to determine sex-differences in cardiac function after the moderate wire injury surgery

There were no sex differences in VTI (Figure 5.4.12 A) or Peak Velocity (Figure 5.4.12 B) measurements pre-surgery and no effect of the surgery on this measurement in either male or female mice at any time-point post-surgery. Ejection fraction showed no significant change over time, although a significant interaction ($p=0.0153$) between time and sex was noted, highlighting that male and female mice had significantly different effects recovering from the surgery. Females reached their lowest ejection fraction at week 8 whereas males reached their lowest ejection fraction at week 12 (Figure 5.4.12 C). Left ventricular thickness (LV thickness) was slightly higher in males pre-surgery and continue to be significantly higher post-surgery compared to females ($p=0.0022$, Figure 5.4.12 D). There was no effect of surgery on LV thickness in females.

Other measurements of cardiac function were made using echocardiography in M-mode. Cardiac output (Figure 5.4.13 A), LV mass (Figure 5.4.13 B), LVEDD (Figure 5.4.13 C) and LVESD (Figure 5.4.13 D) displayed no sex differences pre-surgery and no effect of the surgery in either male or female mice across any time-point post-surgery Fractional shortening measurements were not significantly different between male and female mice pre-surgery. Post-surgery, FS in male mice increased whereas females slightly decreased causing a significant sex effect ($p=0.0306$, Figure 5.4.13 E). Anterior wall diameter (Figure 5.4.13 F) was larger in males pre-surgery, but there was no change over time from baseline (pre-surgery) to post-surgery in males. (Figure 5.4.13 F)

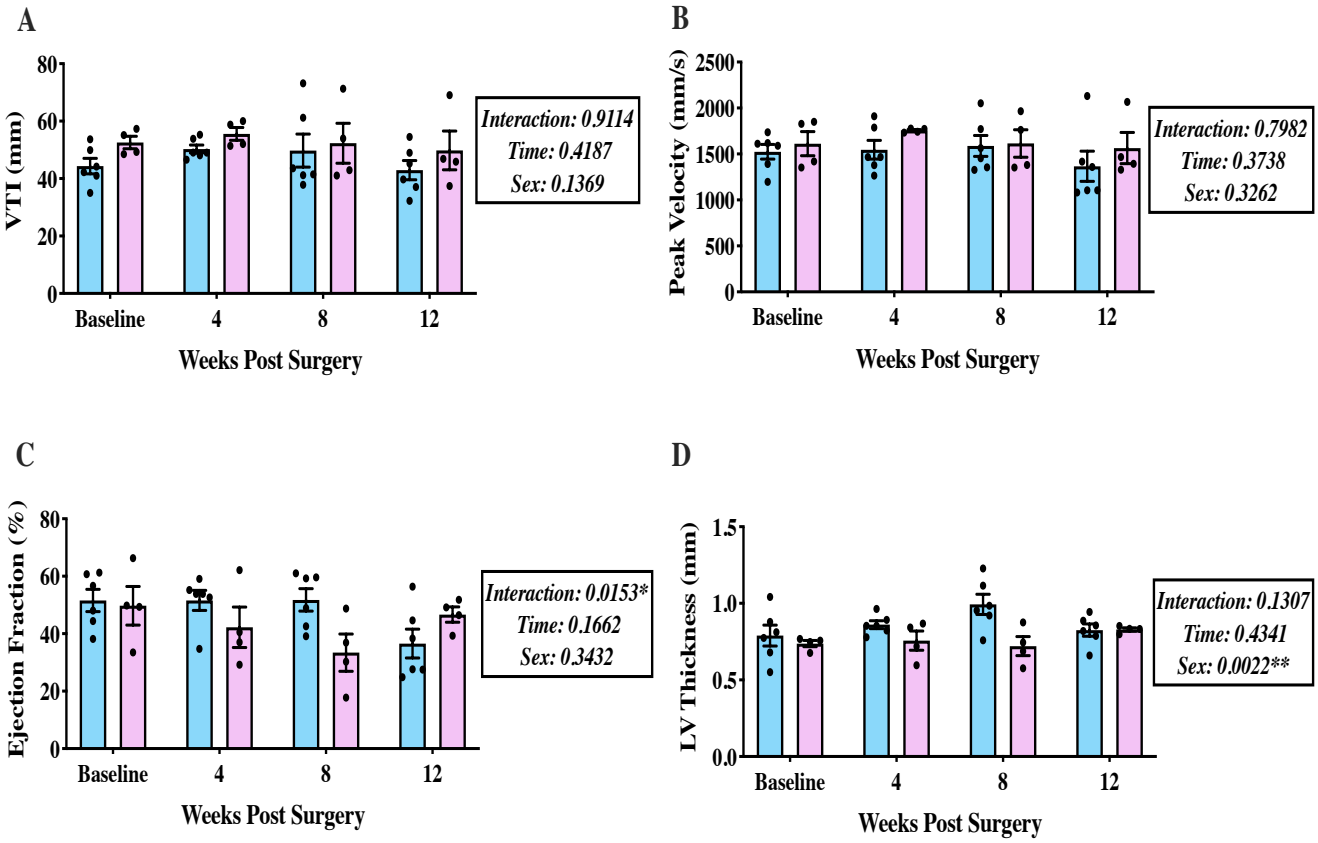

Figure 5.4.12: Investigating the sex differences in echocardiography measurements after moderate wire injury. Mice had a guidewire inserted into the left ventricle and rotated up to fifty times across the aortic valve, under ultrasound guidance. There was no sex difference pre-surgery or change in aortic valve function after surgery as measured by A) VTI (mm) and B) Peak velocity (mm/s) in either males and females. C) Ejection fraction showed no sex differences or significant change over time, although there was a significant interaction between time and sex. (D) Left ventricle thickness pre-surgery (LV thickness (mm, D) was greater in males but this measurement was unchanged after wire injury in both male and female mice. Columns represent mean±SEM, points represent single data values. Males N=5 Females N=4. Significance was determined with a Two-Way ANOVA. *=p<0.05, **=p<0.00. Male-Blue, Female-Pink. VTI=velocity time integral, LV thickness= left ventricular thickness.

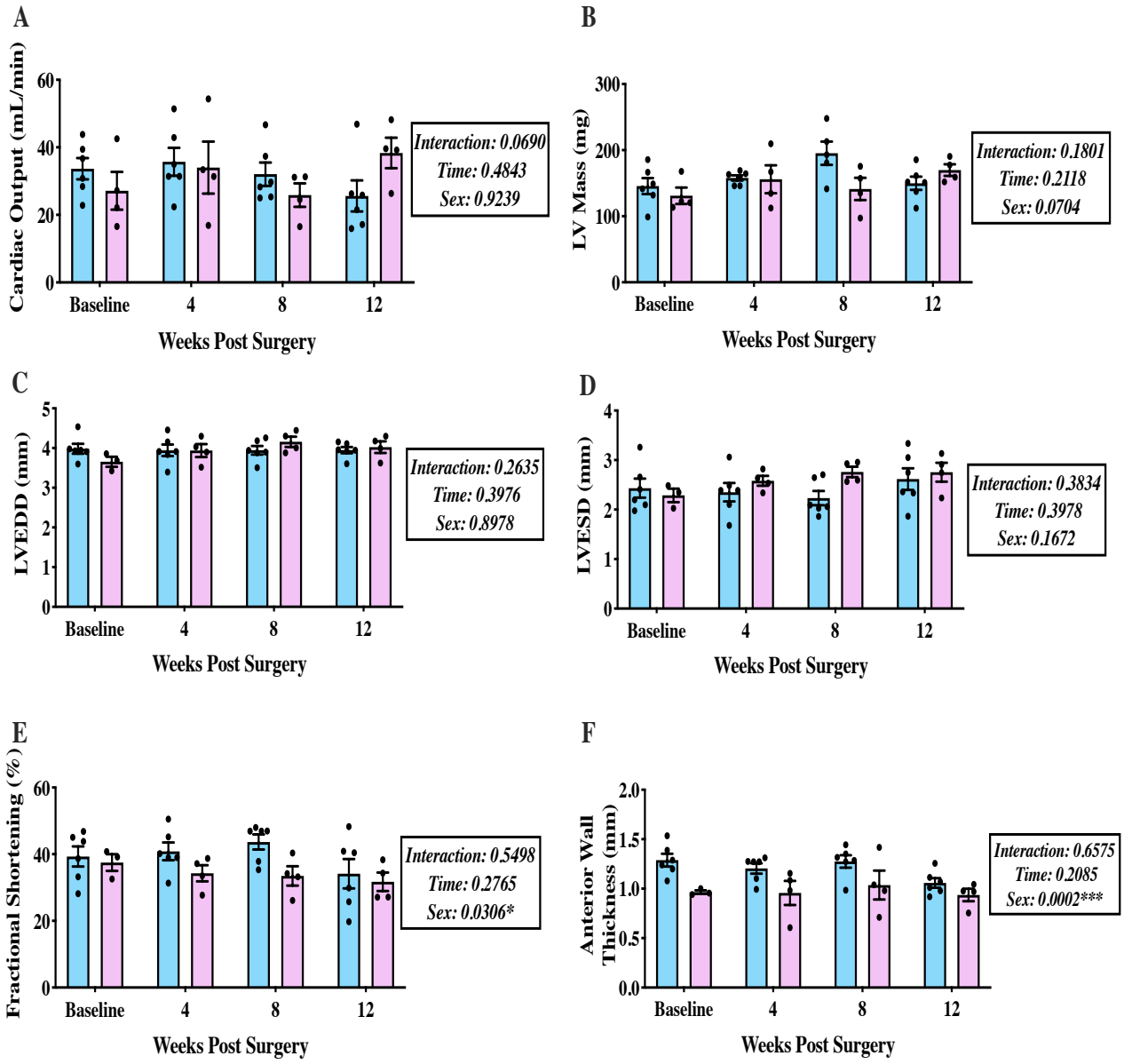

*Figure 5.4.13: Investigating the sex differences in cardiac function after moderate wire injury, measured using M-mode echocardiography***.** Mice had a guidewire inserted into the left ventricle and rotated up to fifty times across the aortic valve, under ultrasound guidance. There was no sex difference pre-surgery, no effect of the surgery and no sex difference post-surgery in A) cardiac output (mL/min), B) LV mass (mg), C) LVEDD (mm) or D) LVESD (mm). Males had bigger measurements for fractional shortening post-surgery (%, E) and anterior wall thickness (mm, F) pre-surgery but these measurements did not change post-surgery in either males or females. Columns represent mean±SEM, points represent single data values. Males N=5 Females N=4. Statistical Significance was determined using Two-Way ANOVAs. *=p<0.05, ***=p<0.0001. Male-Blue, Female-Pink. LVESD- left ventricular end systolic volume, LVEDD- left ventricular end diastolic volume, LV mass- left ventricular mass.

5.4.3.3 Histopathology to assess sexual dimorphic changes in valve pathology following moderate wire injury

H&E staining (Figure 5.4.14 A&B) showed that the valve cusps thickness was not significantly different between males and females (Figure 5.4.14 C). Masson's trichrome (Figure 5.4.14 E&E) staining displayed evidence of fibrosis which was not significantly different between males and females (Figure 5.4.14 F).

The aortic root was also subject to two types of calcium staining: alizarin red (Figure 5.4.15 A/B) and von Kossa stains (5.4.15 C/D). The calcium stains were negative and dark spots on the stain are likely to be caused by pigmentation, as explained in section 5.4.2.2.

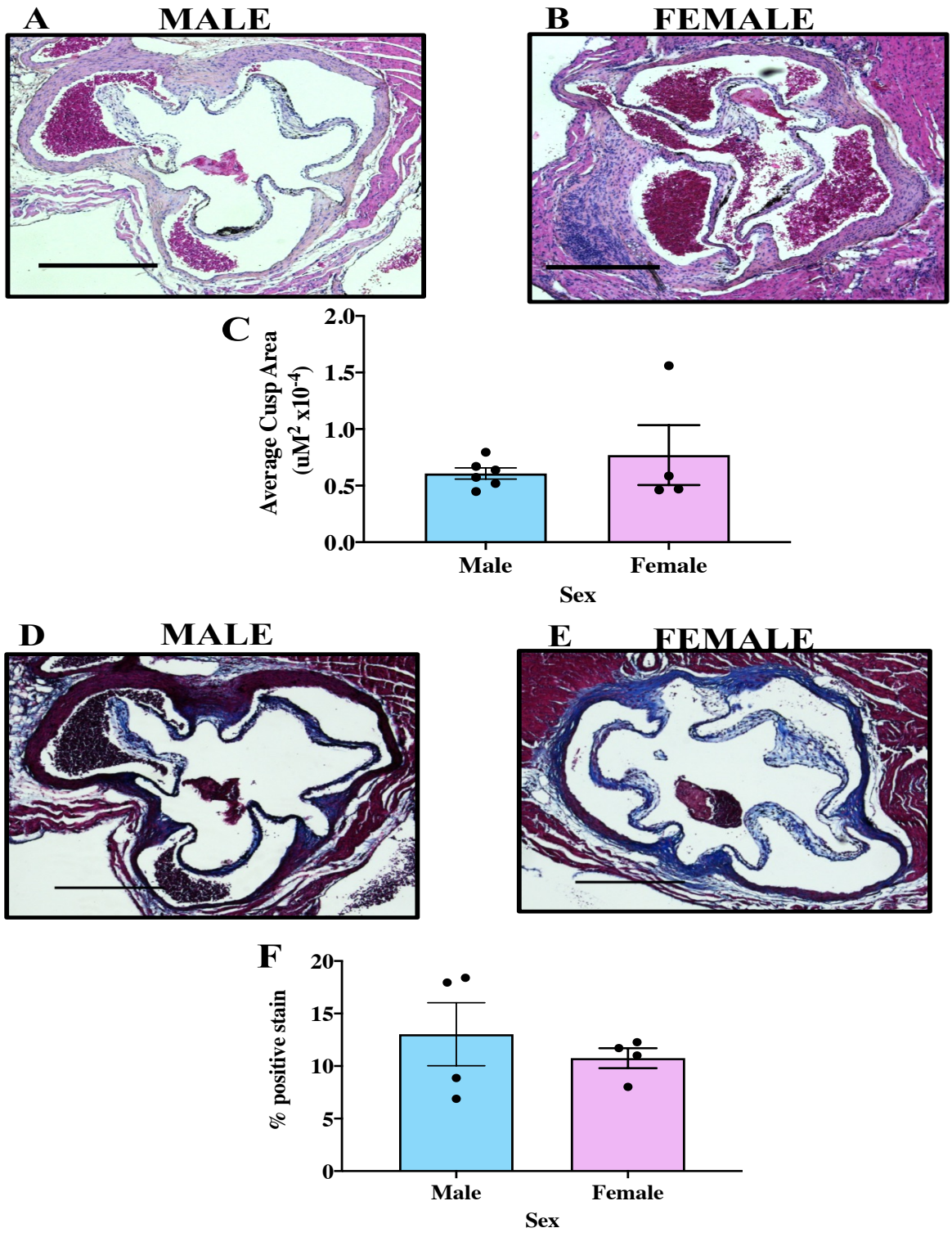

Figure 5.4.14: Investigating the sex differences in thickness and fibrosis after moderate wire injury. Mice had a guidewire inserted into the left ventricle and rotated up to fifty times across the aortic valve, under ultrasound guidance. Hearts were paraffin embedded, sectioned, and stained with H&E and Masson's Trichome. A) Representative H&E-stained aortic root from male mice. B) Representative H&E-stained aortic root from female mice. C) There was no significant difference in cusp area in samples from male and female mice. D) Representative Masson's Trichrome-stained aortic root from male mice. E) Representative Masson's Trichome stained aortic root from female mice. F) There was no significant difference in collagen deposition between sections from male and female mice. Columns represent mean±SEM, points represent single data values. Males N=4-5 Females N=4. Statistical significance was determined using Student's unpaired t-tests. H&E- Haematoxylin and eosin. Blue-Male, Female-Pink. Scale bar - 400 μM.

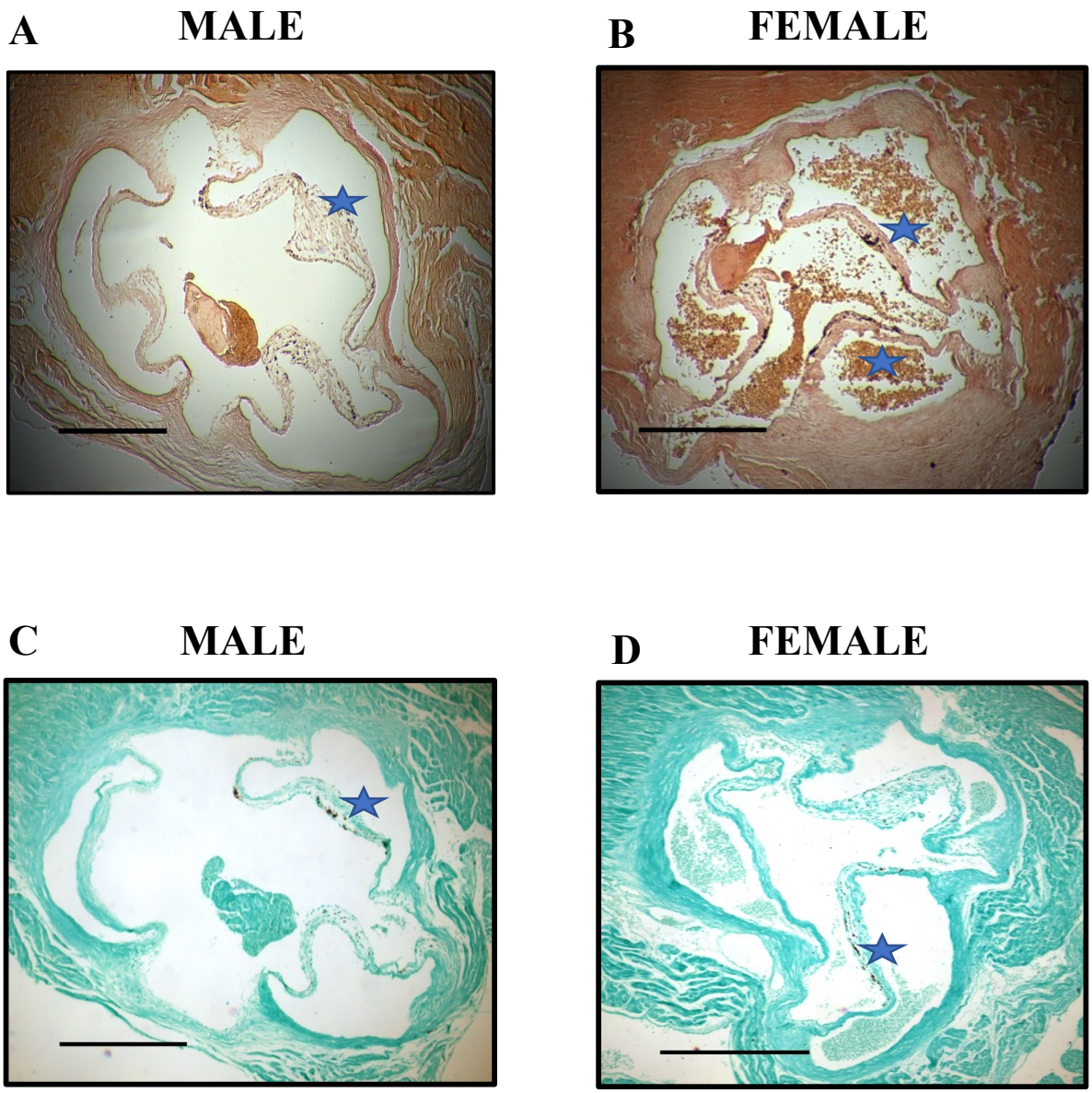

Figure 5.4.15: Calcium staining of aortic root after moderate injury. Mice had a guidewire inserted into the left ventricle and rotated up to fifty times across the aortic valve, under ultrasound guidance. A) Representative alizarin red image from a male mouse. B) Representative alizarin red image from a female mouse. C) Representative von Kossa image from a male mouse. D) Representative von Kossa image from a female mouse. There was no indication of calcium deposition in the aortic valves. Scale bar - 400 µM**.** Blue stars indicate areas of suspected melanin.

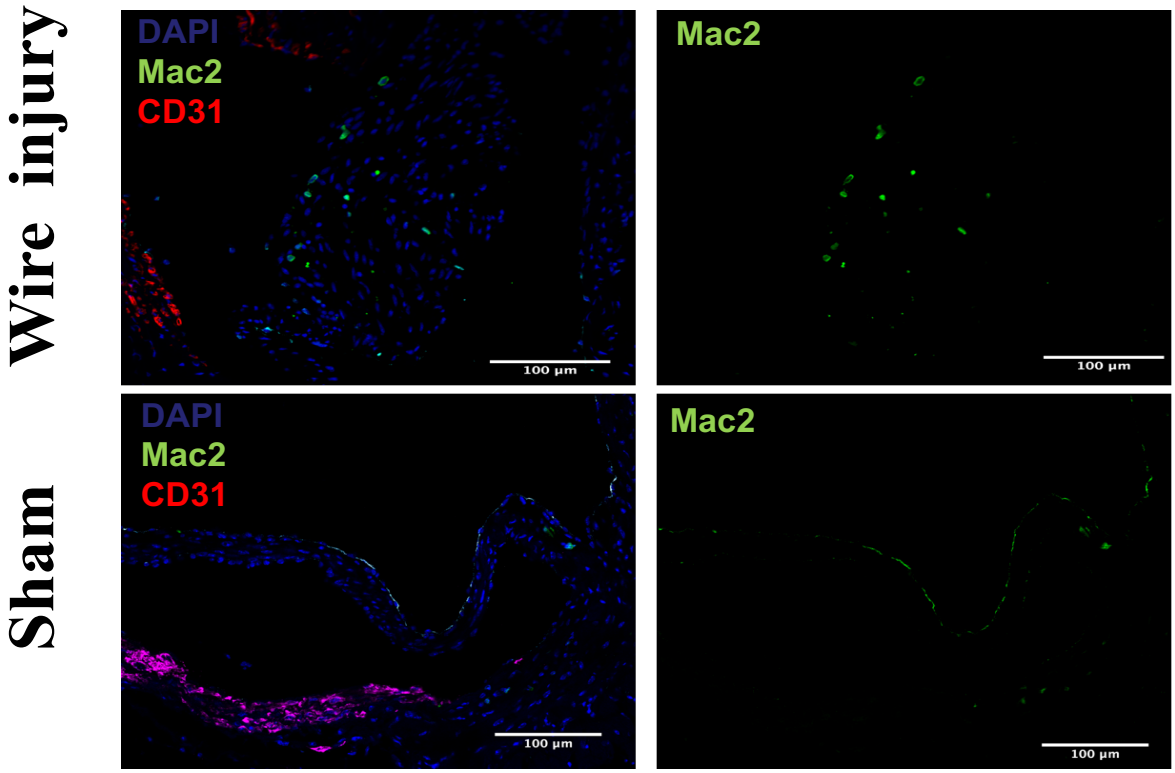

Figure 5.4.16: Mac2 immunohistochemistry staining in the aortic valve of mice subject to the moderate injury surgery. Mice had a guidewire inserted into the left ventricle and rotated up to fifty times across the aortic valve, under ultrasound guidance. Dapi is pictured in blue, Mac2 staining in green and CD31 in red. Top line represents wire injury mice, bottom line represents sham mice. The representative image was from a male mouse.

5.4.4 Identifying the cause of unexpectedly high mortality post-operative morbidity/ mortality in response to wire injury surgeries

Due to the lack of haemodynamic changes and calcification of the aortic valve, a further, severe injury experiment was designed. Both Honda *et al.* (2014) and Niepmann *et al.* (2019) only saw valve calcification when a 15º bend in the guidewire was made. Therefore, the next experiment would follow the protocol exactly, with a 15º bend in the guidewire.

Unfortunately, the mice used in this set of experiments developed severe unexpected reactions to the surgery. The consistent symptoms with these mice were that they started to recover from anaesthetic, then seemed to relapse and never truly regained consciousness; as a result, they

had to be euthanised. Investigations into the cause of the problems were conducted as shown in Figure 5.4.17. Initial feedback from the Named Vet suggested a problem with the anaesthetic. This suggestion was investigated systematically. One mouse (male, C57Bl/6 12-14 weeks old) was anaesthetised as for the normal surgical protocol but allowed to recover without undergoing surgery. This animal recovered from the anaesthetic without any apparent ill effects. A second mouse from the same cohort was anaesthetised and subject to carotid artery ligation without insertion or advancement of the guidewire. This mouse exhibited the same symptoms as the mice that had failed to recover after the wire injury and had to be euthanised.

These observations indicated that the symptoms observed were a result of right carotid artery ligation rather than of a side-effect of the anaesthesia or an adverse response to wire injury. This was unexpected as none of the mice previously used for this surgery had exhibited this reaction. The symptoms displayed by these mice during recovery from anaesthesia (summarised in Figure 5.4.18 A) were constant with cerebral ischemia. Consultation with colleagues using preclinical stroke models (Prof Karen Horsburgh, University of Edinburgh) suggested that this complication was due to a congenital malformation of blood supply to the brain that had been reported in some sub-strains of C57Bl/6 mice (McColl *et al.*, 2004). These sub-strains have been shown to have an incomplete Circle of Willis (Figure 5.4.18 B). The consequence of this abnormality is that occlusion of the carotid artery during surgery causes excessive interruption of blood supply to the brain, resulting in ischaemic stroke; there is no straightforward method for ascertaining a complete Circle of Willis before surgery.

Following consultation with the named Vets, it was agreed that the model of wire injury would have to be discontinued in C57Bl/6 mice as the outcomes were too unpredictable.

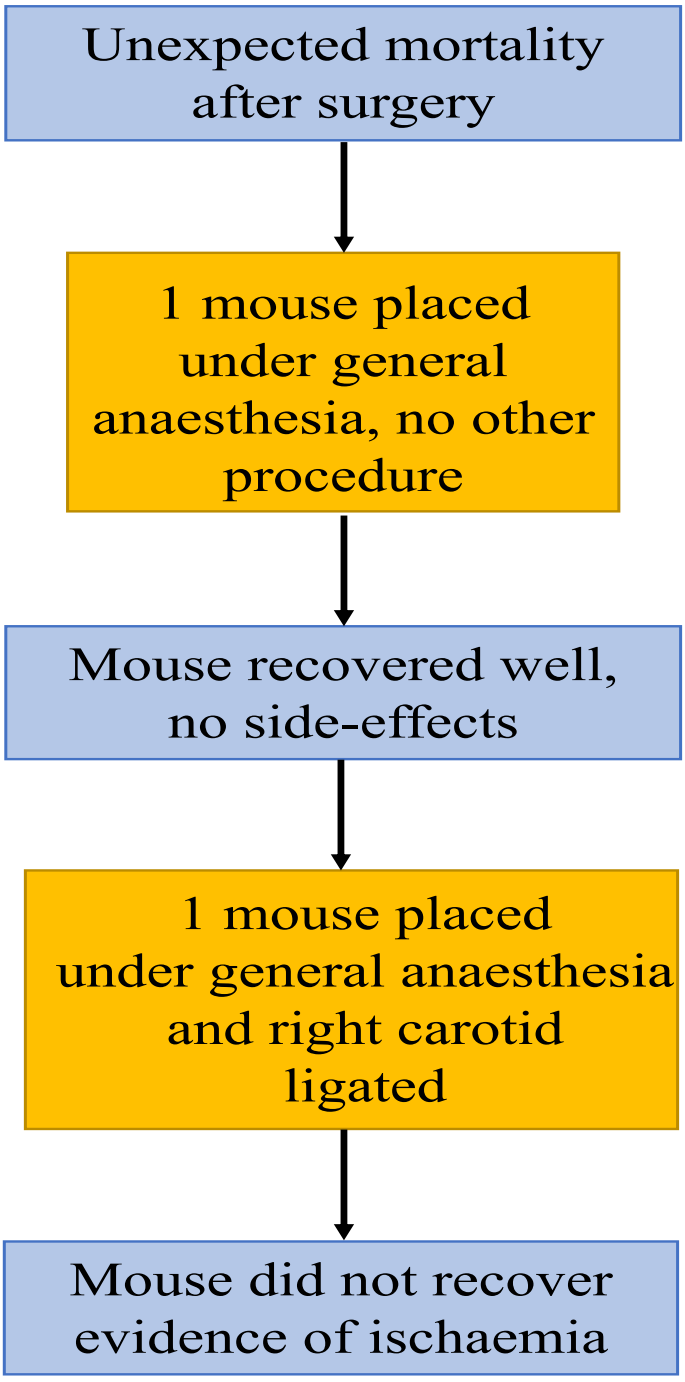

Figure 5.4.17: Trouble shooting the unexpected reactions of the C57Bl/6 mouse strain to the wire injury protocol. This flow chart shows the trouble-shooting steps performed to identify the cause of post-operative morbidity in mice subjected to wire injury surgery.

A

Observed behaviours
One eye partially closed
Barrel-rolling
Rigid postures and tails
Slow, rigid movements (continuing 1-hour post-surgery)

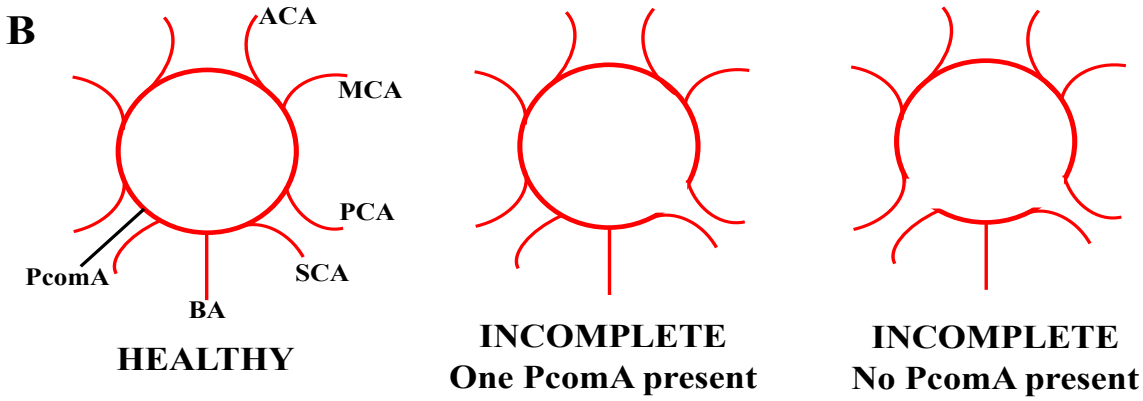

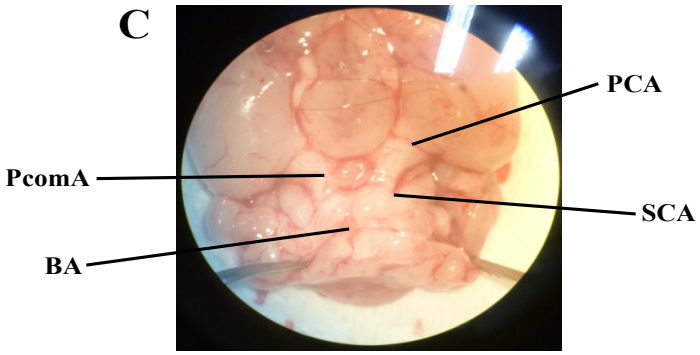

Figure 5.4.18: Mortality in the wire injury surgeries which led to discontinuation of the protocol. A) Behaviours after surgery which were consistent with cerebral ischemia. B) Diagram displaying incomplete Circle of Willis which has been previously observed in C57Bl/6 mice. (based on (McColl *et al.*, 2004). C) Image of the Circle of Willis of the brain in a normal C57Bl/6 mouse (taken from a different stock than ours). PComA- posterior communicating artery, ACA- anterior cerebral artery, PCA- posterior cerebral artery, SCA- superior cerebellar artery, BA-basilar artery

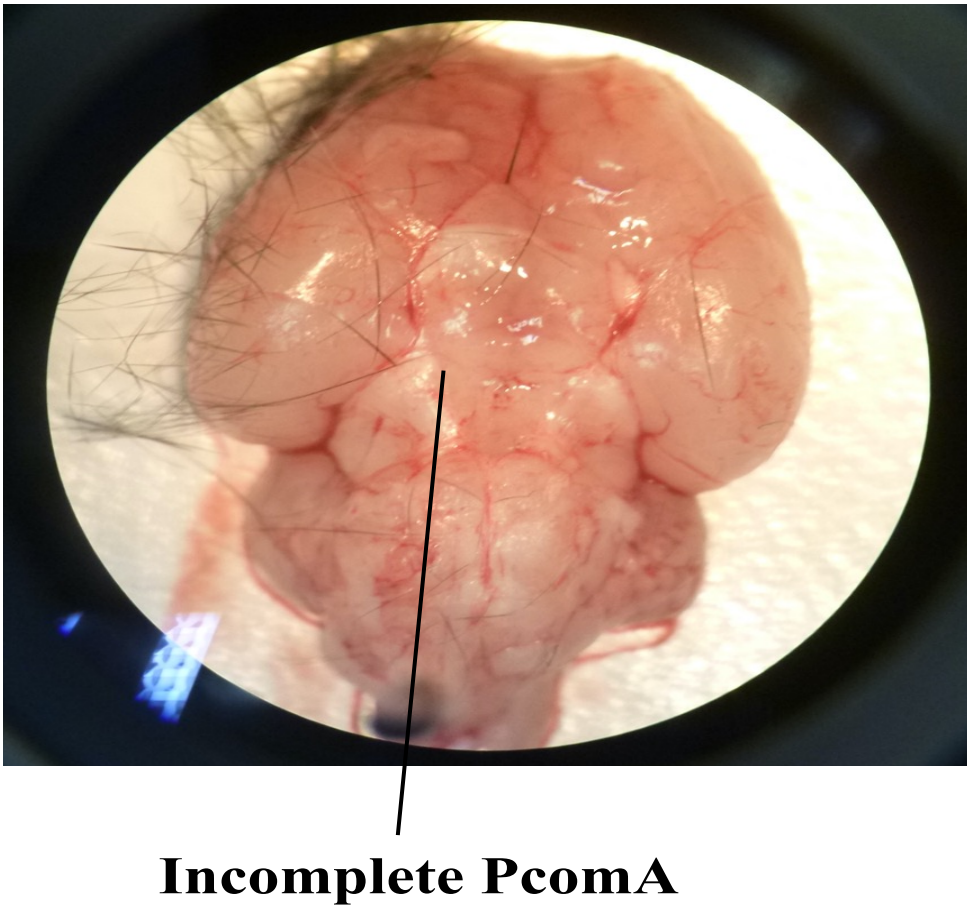

Figure 5.4.19: Photograph of the incomplete Circle of Willis observed in the mice used in this study. PcomA- posterior communicating artery

5.4.5 Wire injury surgeries in ApoE$^{-/-}$ mice

With the failure of mild or moderate injury to induce aortic regurgitation or valve calcification in C57Bl/6 mice it was postulated that CAVD may be accelerated by combining wire injury with systemic cardiovascular risk factors. Consequently, wire injury was attempted on atherosclerosis-prone ApoE$^{-/-}$ mice. Delays in shipping these mice from the supplier in Italy meant that they were older than the C57Bl/6 mice used for wire injury (25 weeks old, male and female) and were subsequently shown to have lesions in their aorta and aortic branches (Figure 5.4.20). These lesions caused technical difficulty in advancing the wire while performing the surgery and led to a high intraoperative failure/ mortality (Figure 5.4.20). Echocardiography measurements could not be analysed because of the low N numbers but have been plotted in Figure 5.4.21. No notable change was seen in the thickness of the aortic valve cusps in the

histology (Figure 5.4.22). This study demonstrated that it is not sustainable to attempt the WI surgery in ApoE$^{-/-}$ mice with pre-existing lesions and there was no evidence of significant aortic regurgitation in these mice (as measured by the echocardiography).

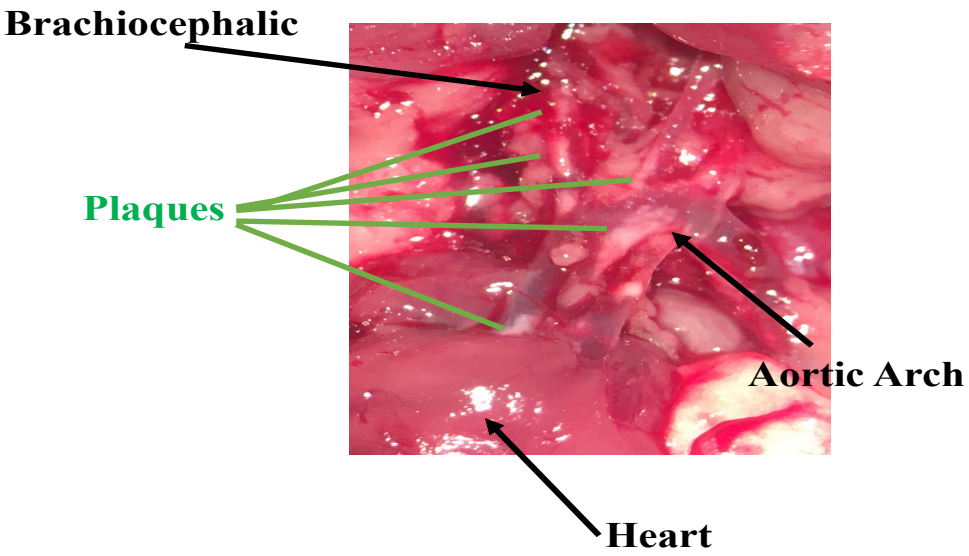

Mouse	Outcome
Male	
1004286	Unable to get past lesions-used as sham
1004287	Died during surgery
1004288	Successful Surgery
1004289	Died during surgery
1004290	Successful Surgery
1004291	Successful Surgery
Female	
1004301	Successful Surgery
1004302	Successful Surgery
1004303	Found dead day after surgery
1004304	Health problems and culled
1004305	Died during surgery

Figure 5.4.20: Mortality in the wire injury surgeries on ApoE$^{-/-}$ mice. This diagram displays the cause of the high mortality in the ApoE$^{-/-}$ WI mice. (A) Mice had atherosclerotic plaques (marked by a green arrow) prior to WI surgery. (B) This led to high mortality rates due to technical difficulties during surgery. The table details each mouse and the outcome of the wire injury surgery.

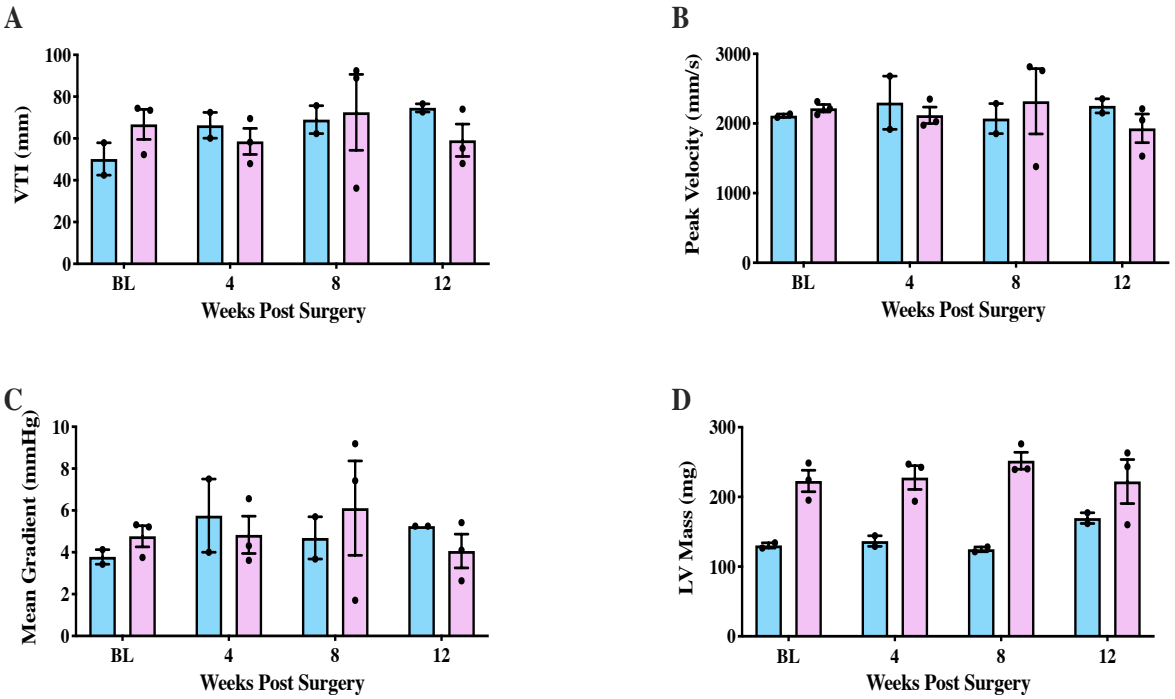

Figure 5.4.21: Sex differences in echocardiography measurements after wire injury on ApoE$^{-/-}$ mice. ApoE$^{-/-}$ mice had a guidewire inserted into the left ventricle and rotated up to fifty times across the aortic valve, under ultrasound guidance. A) VTI and B) Peak Velocity or C) Mean gradient D) LV mass Points represent single data values. Males N=2 Females N=3. Male-Blue-, Female-Pink. BL-baseline. LV-left ventricle

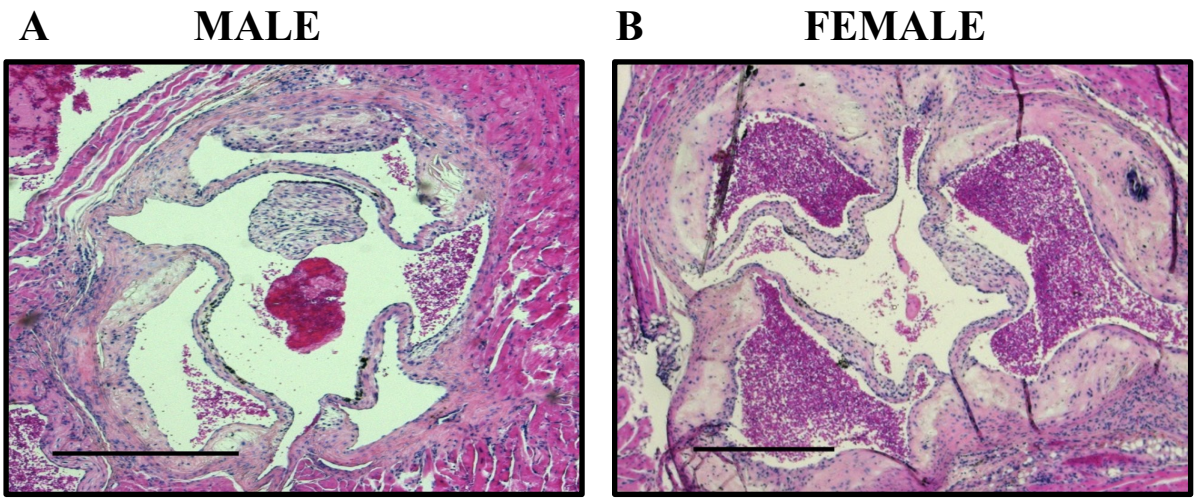

Figure 5.4.22: Histology of the aortic root after WI surgery. ApoE$^{-/-}$ mice had a guidewire inserted into the left ventricle and rotated up to fifty times. Hearts were paraffin embedded, sectioned, and stained with H&E A) Representative H&E-stained aortic root from male mice. B) Representative H&E-stained aortic root from female mice. Scale bar - 400 μM

5.5 Discussion

The need for new models of aortic valve calcification is a pressing issue in the preclinical investigation of CAVD. This is primarily because no current pharmaceutical interventions are available for CAVD, which has been linked to a lack of translatability of murine models (Tsang *et al.*, 2016). Secondly, many of the current murine models produce inconsistent calcification that does not always appear on the aortic valve cusps and is, therefore, not true valve calcification. Finally, many of these models are based on genetic manipulation and it is expensive to maintain the colonies and generate mixed backgrounds. The data in this chapter presents the first time that the WI model of CAVD (by Honda et al., (2014)) has been developed in the U.K. The studies described were designed to systematically introduce the wire injury to ensure compliance with animal welfare regulations. It was successfully demonstrated that the wire injury surgery, combined with ultrasound guidance which requires the transfer of the mouse to the imaging suite during the procedure, can be performed without excess mortality. This study also extends the previously published model by including female subjects and showing that wire injury to the aortic valve does not cause significantly different amounts of damage between male and female mice (Honda et al., 2014; Niepmann et al., 2019). Despite significant unexpected challenges during this model development, it was also demonstrated that the cause of the unexpected mortality in C57Bl/6 mice could be attributed to congenital abnormalities in the cerebral circulation. Preliminary investigations showed that application if the wire injury surgery to $ApoE^{-/-}$ mice required use of mice before they developed substantial atherosclerotic lesions in their vasculature.

5.5.1 The wire injury surgery method is safe to perform.

The pilot study aimed to establish whether the wire injury procedure could be performed under ultrasound guidance without excessive mortality. The surgical procedure had a number of challenges. In particular, the insertion of the guidewire into the right carotid artery must be followed by the transfer of the mouse to the ultrasound scanner in the imaging lab, for observation of the advancement of the wire across the aortic valve. After the injury, the mouse must be moved back to the surgical table for completion of the surgery. Moving an anaesthetised mouse with an open conduit (right carotid) artery brings a number of risks, including uncontrolled bleeding. As there were no deaths during surgery in the pilot study, it was established that these surgeries could be performed successfully and safely in our unit.

This study also demonstrated fewer actual deaths than the originally published method ((Honda et al., 2014) which reported deaths to intra-operative bleeding and during the weeks after surgery, which was not seen in this pilot study (Honda et al., 2014). Although the mild and moderate injury in (Niepmann *et al.*, 2019) only saw a 4 % mortality rate, which used a similar protocol to that used in the pilot study. Only one mouse in the pilot study in this thesis needed to be culled post-surgery for health reasons and this resulted from a surgical error in which the wire damaged the left ventricle.

A further aim was to assess whether the wire injury would result in valve remodelling and valve calcification. Given the echocardiography and negative calcium stains, after the pilot study, there was limited evidence of sustained damage to the aortic valve. The echocardiography displayed similar baseline measurements to Honda *et al.*, but by 1-week post-surgery, the aortic outflow velocity in the Honda study had risen to 371 cm/s, whereas the pilot study did not show a significant increase in aortic outflow velocity after the surgery (Honda et al., 2014). Niepmann *et al.* (2019) reported aortic velocities of ~1500 mm/s 1-week post-surgery similar to the results described in this chapter in their 'mild' wire injury phenotype. Stenosis does not usually occur in CAVD until there is a large amount of established valve calcification (Lerman, Prasad and Alotti, 2015). Therefore, without the presence of calcification and significant remodelling, it was unlikely these mice would develop stenosis. The lack of haemodynamic changes observed in the echocardiography was consistent with the histological analysis of the valves which only displayed mild-moderate valve thickening (similar to the mild phenotype described by Niepmann et al. 2019). This suggests more damage needs to be inflicted on the valve to produce sustained injury which would result in remodelling and calcification of the aortic valve and cause haemodynamic changes to the aortic outflow.

5.5.2 The mild-moderate injury was not sufficient to produce CAVD.

The next study (the mild injury study) attempted to inflict greater injury than the pilot study and use a protocol similar to the ‘mild injury’ characterised by Niepmann *et al.* (2019). This study aimed to determine whether, by increasing the number of ‘turns and rubs’ of the wire, further damage could be induced to the valve (as seen in Niepmann *et al.* (2019)) to create the necessary haemodynamic changes to induce valve calcification. In addition, these studies would make the first attempt to identify the influence of sex on the response to wire injury. These surgeries produced higher mortality than seen in the pilot study but in all cases, this could be attributed to surgical error. In the surviving mice, there was no evidence of aortic

regurgitation, stenosis, or valve remodelling in the histology. In the previous publications only the moderate-severe surgical protocol saw significant valve thickening in the histology (Honda *et al.*, 2014; Niepmann *et al.*, 2019). This indicated that although the surgery could be performed, the injury was not sufficient to cause aortic regurgitation and the subsequent cardiac remodelling. This was consistent with the mild valve-injury phenotype described by Niepmann *et al.* (2019). These results demonstrate that, whilst the WI surgery is safe to perform with increasing amounts of damage (if technical errors are avoided), more damage to the valve is needed to induce aortic regurgitation and valve calcification in this model.

In the mild injury study, the greater VTI (1-2 weeks post-surgery) observed in female mice compared with males could be due to a sex difference in response to the injury. Previous literature has shown greater neointimal proliferation in response to femoral artery injury in female mice, although those differences in remodelling did not cause a significant difference in blood velocities between males and females in the vessels. (Roque et al., 2000). However, this study also identified a potential source of systematic error. when comparing males and females using this protocol; female mice are significantly smaller than age-matched males (with smaller hearts and blood vessels). Therefore, the wire, which was the same size for both sexes, is likely to cause more damage to the valve in females. To mitigate this limitation, instead of using age-matched mice, future studies may need to consider using weight-matched mice groups. Alternatively, a proportionally smaller wire could have been used.

The moderate injury study produced little evidence of CAVD and did not replicate the stenosis, calcification or valve remodelling reported by Honda *et al.* (2019). In the previous publications, to achieve a severe injury, including stenosis and calcification, a 15^{o} bend was put in the tip of the guidewire (Honda et al., 2014; Niepmann et al., 2019) to cause more initial damage to the valve. However, not all of Honda's injured mice, even with the bend in the wire, developed calcification in the valve aortic root. It was therefore planned to perform a final, severe injury surgery. This protocol would involve putting a 15^{o} bend in the wire. The wire would be then rubbed against the valve up to 50 times and twisted up to 50 times, although this protocol could never be performed due to the unexpected morbidity that was experienced with the new cohort of mice.

5.5.3 Identifying the cause of morbidity/ mortality in later studies

Ligation of the common carotid artery is a common procedure in C57Bl/6 mice, not just in this model but in a variety of disease models. In other studies (and in the pilot and mild injury studies reported here), this ligation has been performed without severe mortality (Honda et al., 2014; Brown et al., 2018). However, the development of the model of wire injury was dramatically and unexpectedly interrupted, during the attempts to increase group sizes in the moderate injury study, by the (previously unseen but consistent) failure of mice to recover from surgery. The presentation of symptoms of cerebral ischemia (barrel rolling, one eye partially closed and unilateral loss of movement) required euthanasia and, eventually, the discontinuation of this protocol. Systematic troubleshooting confirmed that these symptoms were not caused by the anaesthetic or by the injury (or potential embolism) in response to the insertion of the wire but were a result of carotid artery ligation. This is consistent with these mice having a congenital defect in the blood supply to the brain (Bertrand, Dygert and Toborek, 2017). Indeed, it has been reported that C57Bl/6 have a congenital defect in their Circle of Willis with only one in ten C57Bl/6 mice having a complete Circle of Willis which can only be detected at necropsy (McColl et al., 2004a). In the absence of a complete Circle of Willis, right carotid artery occlusion would be predicted to cause cerebral ischaemia/ stroke. This has important welfare implications for all murine models which require carotid artery ligation in C57BL/6 mice. For any further model development, an alternative strain should be considered.

5.5.4 Wire injury to the aortic valve cannot be performed on 25-week-old ApoE$^{-/-}$ mice.

Straight guidewires have been used in previous studies (both in the studies described in this thesis and in Niepmann *et al.*, (2019)) to induce mild increases in the aortic blood velocity without valve calcification. It was hypothesised that combining the moderate surgery protocol with a murine model which is susceptible to cardiovascular calcification would enhance the likeliness of the mouse to develop valve calcification. This is because ApoE$^{-/-}$ mice are prone to inflammation (Zhang, Wu and Wu, 2011) and dyslipidaemia (de Freitas *et al.*, 2015), which are risk factors for developing atherosclerosis and CAVD (Chen, Engert and Thanassoulis, 2019). However, the lack of change in the aortic velocity post-surgery and valve histology (showing little remodelling) indicates that the surgery did not cause CAVD in these mice. This possibly means that only a limited amount of damage can be performed with a straight-sprung guidewire to the aortic valve of a mouse, and this is not sufficient to induce valve calcification even in the presence of cardiovascular risk factors. The aortic output velocities were higher

than those seen in previous studies conducted on C57Bl/6 mice, even before the injury, which indicates an underlying effect on the aortic outflow velocity of the ApoE genetic deletion. This could also be due to the older age of the ApoE$^{-/-}$ mice. Studies in younger ApoE$^{-/-}$ mice have shown lower aortic blood velocities than this study, further suggesting an age effect (Jung *et al.*, 2015). However, the present study did not show an increase in aortic outflow velocity over the 12-week study period, indicating that the WI did not cause stenosis in 25-week-old ApoE$^{-/-}$ mice.

Wire injury to the aortic valves of ApoE$^{-/-}$ mice was associated with a very high mortality rate compared to the previous studies conducted in C57Bl6/J mice. These ApoE$^{-/-}$ mice were 25 weeks old when they underwent surgery which meant they had pre-existing lesions in their arteries. The original experimental design planned use of younger mice but complications with availability and shipping, led to the mice being older than intended. At the 25 weeks of age, these mice had developed substantial atherosclerotic lesions causing technical difficulties in inserting the wire and advancing it across the aortic valve without snapping the right carotid artery. There was also the risk while the wire was being advanced through the carotid artery that it could have disrupted a lesion, potentially causing embolization and/ or thrombosis, leading to ischaemic injury. Due to the high mortality, this study is underpowered. There was no attempt to increase group sizes as it was anticipated that changes were need both in the age of the mice used and the amount of damage inflicted by the wire. The wire injury surgery, therefore, cannot be performed consistently safely on 25-week-old ApoE$^{-/-}$ mice with established lesions. Further studies could be performed on younger mice which would not have atherosclerotic lesions. Alternatively, the wire injury could be combined with a different murine model of vascular calcification, for example, the AAV-PCSK9 model of induced atherosclerosis (Goettsch *et al.*, 2016). As these mice have addition risk factors for developing remodelling it might increase the likelihood of the surgery causing valvular remodelling and therefore valvular calcification.

5.5.5 Limitations of these studies

As this was a method development process, and due to the level of peri-operative deaths, some of the investigations described in this chapter, do not have sufficient statistical power to allow detailed interpretation of the impact of injury on aortic valve remodelling or the impact of sex on the remodelling process. It was recognised that this would be an issue in the pilot and mild injury studies but, since it was clear that the injury produced was not causing aortic

regurgitation or calcification, it was not appropriate to increase group sizes in these studies. Similarly, attempting to increase group sizes in the ApoE$^{-/-}$ mouse study would have been inappropriate since the major outcomes form this cohort were the demonstrations that (i) the wire injury was not producing enough damage to cause aortic regurgitation and valve calcification (even in atherosclerosis-prone mice) and (ii) surgical success was considerably reduced in mice with pre-existing atherosclerotic lesions. With more time available this study would have been repeated in younger ApoE$^{-/-}$ mice before the development of vascular lesions. In the moderate injury study, the intention to increase group sizes was thwarted by the mortality resulting from the development of ischaemic stroke in response to carotid artery ligation. This is a considerable issue which can only be solved by changing mouse strains which the surgery was performed on. Another issue with the use of C57BL/6J mice is that their valve leaflets contain black pigment in the interstitium, which has been identified to be melanocytes (Mjaatvedt et al., 2005). These dark pigments can be mistaken for a positive von Kossa stain in the valve, which was cause a false positive therefore staining in the aortic valve needed to be confirmed by alizarin red (Mjaatvedt et al., 2005).

A major limitation of the studies reported in this chapter is that the injury induced in the aortic valve was insufficient to produce either haemodynamic changes in the aorta or subsequent aortic valve calcification. Therefore, the aim of introducing a model of consistent, reproducible valve calcification was not met. The published papers only show calcification in a subset of mice, even when performing the severe injury (Honda et al., 2014; Niepmann et al., 2019). This severe injury is also associated with a high mortality and morbidity post-operatively. This could potentially explain why Artiach *et al.* (2020) used the moderate, not severe, injury protocol in their study. There may be microcalcification in present in the aortic valve of these mice although this was not assessed.

There are also limits when using mice to model human disease. One of the main limitations when applying this model is that acute endothelial damage via a coronary guide wire does not directly mimic the prolonged mechanical injury that is responsible for humans developing CAVD (Towler, 2013). Furthermore, the structure of the aortic valve differs between mice and humans (Hinton *et al.*, 2008). This means that any finding which uses this model will have to be confirmed in large animals (which have the same valve structure as humans), and ultimately in humans.

5.5.6 Further studies

As macrocalcification usually occurs later in CAVD development, there is a need for innovations in imaging methods for the early detection of aortic valve microcalcification in *vivo*. Positron emission tomography (PET) is a non-invasive method of imaging with target radiotracers providing a highly sensitive and specific probes (Joseph and Tawakol, 2016). Radiolabelled sodium fluoride (NaF/18F) can detect novel areas of bone remodelling and formation, through its binding to hydroxyapatite crystals. Consequently, it can also be used to detect microcalcification, as it was used in this thesis in Chapter 4 (Even-Sapir et al., 2006; MacAskill *et al.*, 2020). This is therefore an important tool for investigating the development of calcification in the WI model of CAVD. These imaging techniques could be applied to the mild/moderate protocol to detect the presents of microcalcification.

The unexpected mortality, caused by the incomplete Circle of Willis in these mice had not been reported before in the WI model of aortic stenosis but had been noted in other mouse surgical models (McColl *et al.*, 2004). This brings into question whether to continue to development of this model. There is a strong argument that development of this model should continue for two reasons. Firstly, the cause of the morbidity was identified and there is a reasonable solution in changing the strain of mice that the surgery is performed on. Secondly, the protocol for severe valve injury described in the literature by Honda et al. (2014) (and achieved by putting a 15^{o} bend in the guidewire) has been shown by others to produce valve calcification (Niepmann *et al.*, 2019). Mechanical injury is an important risk factor for people to develop AVS, and as this model is also based on mechanical injury it has potential to clarify mechanisms that contribute to CAVD and help identify new therapeutic regimens.

5.5.7 Conclusion

The protocol to establish the wire injury model of aortic stenosis in the mouse went through significant development. This chapter displayed the first study conducted in the United Kingdom to successfully perform the wire injury model of aortic stenosis. The data generated has provided important background information for subsequent refinement of the model. However, it would not be possible to conclude from this work whether consistent, reproducible valve calcification can be induced by wire injury without significant peri- and post-operative mortality. It was demonstrated that wire injury of the aortic valve can be induced in both male and female mice, but in the data generated there was no consistent evidence that the response

to this injury was different in male, compared with female, mice. Further developing a model of valve calcification is crucial to improving our understanding of the mechanisms involved in CAVD and the influence of sex on the development of this condition.

6.0 General Discussion

6.0 General discussion

6.1 Recapitulation

Calcific aortic valve disease (CAVD) is the most common valve disease in the western world (Yutzey *et al.*, 2014). It causes aortic regurgitation and, if untreated, heart failure (Lindman *et al.*, 2016). There are currently no pharmaceutical interventions available for treating CAVD, and surgery to replace the diseased aortic valve has significant risks, especially in patients with comorbidities including CKD and diabetes (Porras, McCoy and Masters, 2017). Key reasons underpinning the lack of drug development to prevent or treat CAVD could include not only our limited mechanistic understanding of calcification as a disease but also the sex differences associated with soft tissue calcification in humans. Thorough clinical research has characterised the sexual dimorphism in valvular calcification, highlighting how male patients are more susceptible to the disease earlier in life whereas female patients do not typically tend to develop aortic valve calcification until after menopause (Simard *et al.*, 2017). Currently, there is no mechanistic understanding of this observation. Despite this clinical observation, very limited preclinical research in murine models of CAVD has been conducted using female subjects, with males being the default choice. This problem is embedded throughout medical research and in 2014 the national NIH created a policy to include females in preclinical investigations (Clayton and Collins, 2014). Despite this policy, less than 20 % of preclinical medical research is currently conducted using females (Sundari Ravindran *et al.*, 2020). This thesis presents novel, preclinical investigations designed to address the influence of sex hormones on valve calcification. These interrogate the following questions: (1) does the action of sex hormones stimulate calcification of isolated VICs *in vitro*? (2) Is aortic valve calcification more evident in male atherosclerosis-prone ($ApoE^{-/-}$) mice? (3) Is calcification more evident in male mice following wire injury to the aortic valve (Honda *et al.*, 2014)?

6.2 Key findings

6.2.1 Testosterone augments the calcification of valve interstitial cells

Pérez-López *et al.*, (2010) proposed that sex hormones may influence cardiovascular calcification. Men develop calcification earlier than women; this suggests male sex is a risk factor for calcification; therefore, it has been proposed that testosterone may augment the process of calcification (Mohan *et al.*, 2021). This proposition is supported by the demonstration that testosterone augments vascular calcification in preclinical models (Zhu *et*

al., 2016). This discovery in vascular calcification is significant but it cannot be assumed that testosterone will demonstrate the same behaviour in valve cells as vascular and valvular calcification do not have the same pathophysiology. However, the augmentation of testosterone in vascular calcification could indicate a relationship between testosterone and calcification in the valves. The first aim of this thesis was, therefore, to determine whether sex hormones regulate calcification in valve interstitial cells. To enable these investigations, it was necessary to optimise the *in vitro* conditions for stimulating the calcification of VICs. As vascular and valvular calcification are not the same disease the conditions which evoke calcification in VSMCs cannot be assumed to evoke calcification in VICs (Cui *et al.*, 2017). The demonstration that testosterone augments calcification in cultured VICs from both male and female rats is novel. This data also demonstrates that oestrogen did not induce notable differences in the calcification of VICs from male or female rats, suggesting that oestrogen does not affect the calcification of VICs under the conditions used in this thesis. The effects of oestrogens on valvular health are currently highly controversial. Oestrogens have been shown to have both a protective and antagonistic effect on calcification (Osako *et al.*, 2010; Hu *et al.*, 2021). ER alpha knockdown has been shown to inhibit calcification of valve interstitial cells which suggests oestrogens augment calcification which is opposing to the results in this study. This may indicate that oestrogens do not have a similar linear relationship with valve calcification. To conclude, this thesis presents the development of an *in vitro* system for investigating the influence of sex hormones on valve calcification. This system generated the novel finding that testosterone augments calcification in isolated VICs from both male and female rats. This has implications for the cardiovascular safety of exogenous androgens.

As it was found that testosterone augments *in vitro* VIC calcification, subsequent studies were designed to identify testosterone-mediated pathways responsible for the augmented calcification. It was decided that proteomics would be performed between male calcified VICs and male calcified VICs treated with testosterone. Proteomics was chosen as it provides an unbiased screen of protein expression and because unlike RNA sequencing, proteomics accounts for post-translational modifications (Wang, Liu and Zhang, 2014). Pathways analysis of the significantly differentially expressed proteins between male calcified VICs and male calcified VICs treated with testosterone reveal proteins associated with mitochondrial energy metabolism. One of the protein families identified in the screen, The NDUF family (a complex in the mitochondrial ETC) has been shown to induce the mitochondrial unfolded protein response (UPR), causing a prolonged pathological lifespan and increased ROS production

(Rauthan *et al.*, 2015). Increased ROS is associated with augmented valve calcification in humans (Phadwal *et al.*, 2021; Greenberg *et al.*, 2022). Disruption to fatty acid and oxidative metabolism (gene ontologies which were highlighted in this analysis) has also been shown in patients with aortic stenosis (Heather *et al.*, 2011). Therefore, increased ROS and mitochondrial dysfunction is a potential pathway for testosterone-augmented valve calcification which has the potential for pharmacological modulation.

6.1.2. ApoE$^{/-}$ mice on a western-fed diet do not develop valve calcification and have more vascular calcification in females compared with mice

The second research aim of this thesis was to investigate sexual dimorphism in the ApoE$^{-/-}$ mouse model of valve calcification. The ApoE$^{-/-}$ mouse was selected as it is one of the most commonly used models of CAVD in the literature and develops aortic stenosis, as well as valvular and vascular calcification (Tanaka *et al.*, 2005; Aikawa *et al.*, 2009). Despite being one of the most widely used models of CAVD, the presence/absence of a sexually dimorphic valve calcification phenotype in this model was yet to be characterised. This study used advanced micro-PET/CT to demonstrate the presence of microcalcification both in male and in female western-diet fed ApoE$^{-/-}$ mice. For the first time, haemodynamic changes were compared between male and female mice over the course of exposure to a western diet. In this study, neither male nor female 40-week-old ApoE$^{-/-}$ mice fed a western diet for 12 weeks developed aortic stenosis. The presence of aortic stenosis in ApoE$^{-/-}$ mice is reported in older animals, which may be why it was not observed in this study (Tanaka *et al.*, 2005). Interestingly, detailed histological assessment of the aortic root in these mice revealed positive macrocalcification staining (using alizarin red); but it was notable that this was within atherosclerotic plaque in the root of the aorta and not on the valve cusps themselves. This is an important observation and highlights the possibility that previous reports may have mistakenly identified atherosclerotic aortic root calcification as aortic valve calcification.

The female ApoE$^{-/-}$ mice in this study had larger plaques which were more prone to vascular calcification. The sexual dimorphism of the development of vascular calcification in this model is clearly at variance with the sexual dimorphism seen in humans, in which men characteristically have larger, earlier, and more extensively calcified vascular lesions than women (Newman *et al.*, 2001). The findings in this study that female ApoE$^{-/-}$ mice develop more atheroma than males is consistent with the sexually-dimorphic atheroma development of ApoE$^{-/-}$ mice seen in Smith *et al.* (2010). This suggests that ApoE$^{-/-}$ mice may not be an

appropriate model of sexual dimorphism. Indeed, rats might provide a more suitable model of sexual dimorphism in CAVD, since it has been reported that exposure to vitamin D induces more extensive valve calcification in male rats than in females (Nakamura *et al.*, 2003). These results highlight the need for further consideration of sex and species when selecting an *in vivo* model to study CAVD.

6.1.3. The wire injury model of CAVD is safe to perform on male and female mice and produces valvular remodelling

As discussed in Section 1.9.2, there are many murine models of CAVD although all of these have individual limitations. The first surgical wire injury (WI) model of CAVD was published in 2014 (Honda *et al.*, 2014). This model is notably translational displaying valvular calcification, stenosis, and increased osteogenic markers in the aortic valve, something which not many of the previous murine models did (Woodward *et al.*, 2021). Since the development of the WI model, laboratories have investigated this model in more detail, including characterising different variations of the wire injury insult, however, these subsequent studies were limited to male mice (Niepmann *et al.*, 2019; Artiach *et al.*, 2020). The last aim of the thesis was therefore to establish the wire injury surgical model of calcific aortic valve disease and investigate the resulting sexual dimorphism phenotype. As the first laboratory in the UK to develop this model, an initial pilot study was necessary to establish that the wire injury was safe to perform, assessing whether the surgery and the imaging could be performed successfully without excess mortality (compared to mortality in the Honda *et al.* paper), which was successful. This study confirmed that the wire injury caused remodelling in the aortic valve. Significant progress was made in conducting the mild and moderate valve injury in both sexes. The study was also important in developing and establishing new models and new protocols for murine CAVD.

Data generated in this thesis demonstrated the mild and moderate injury protocols did not produce valve calcification. Although in the original publication by Honda *et al.* (2014) more extensive damage was implemented on the valve, than in the protocols that were used in this thesis. As the protocol in Honda *et al.* (2014) produced calcification and the ones in this thesis did not, it suggests the injury performed in these studies did not elicit sufficient damage to mimic CAVD. To resolve this, more injury would be needed to be inflicted during the surgery in the form of the ‘severe’ protocol defined by Niepmann *et al.*, (2019). My findings highlight further development of this surgical model would have to be conducted on a different strain of

mice due to the welfare issues in C57Bl/6 mice, for example, BLAB/c mice. An alternative to adjusting the protocol would be to perform the WI surgery on a mouse line which is prone to soft tissue calcification, for example, Enpp1$^{-/-}$ or Klotho$^{-/-}$ mice (Zhu *et al.*, 2011; Hu *et al.*, 2011). This would increase the likelihood of the surgery producing valve calcification. Overall, there were unexpected difficulties in developing a model of calcification, but this thesis presents significant progress in establishing the wire injury model protocol.

6.3 Future directions and limitations

The results presented here have increased our knowledge of the association of sex hormones and aortic VIC calcification as well as characterising the sexual dimorphism in calcification of western-fed ApoE$^{-/-}$ mice. Nevertheless, many aspects have yet to be examined and, therefore, there are numerous opportunities for further research in this area.

Despite evidence that sex hormones can influence not only CAVD but also all cardiovascular diseases, the medical community is looking for alternatives to pharmacologically targeting sex hormones directly. This is because of previously harmful side effects of direct pharmacological modulation of serum sex hormones. Examples of this include prostate cancer treatment, where patients are treated with gonadotropin-releasing hormone (GnRH) agonists which cause androgen deprivation, but also caused unwanted cardiovascular toxicity, increased serum insulin resistance and increased serum lipid concentrations (George *et al.*, 2022). Similarly, oestrogen replacement in the form of HRT increases the patient's risk of developing breast cancer (Group on Hormonal Factors in Breast Cancer, 2019). As oestrogen had no direct effect on VICs calcification in this study, the 'protection' of females against valve calcification in their reproductive years may not be mediated by oestrogen or may not have a simple linear relationship with oestrogen. Future studies on the sexual dimorphism between male and female mice could elucidate other potential mechanisms. Proteomics comparing the proteome between male and female calcified VICs could provide an unbiased detection method to direct future studies. These studies were started and the changes in the proteome between male and female calcified RVICs can be seen in Figure 6.1.

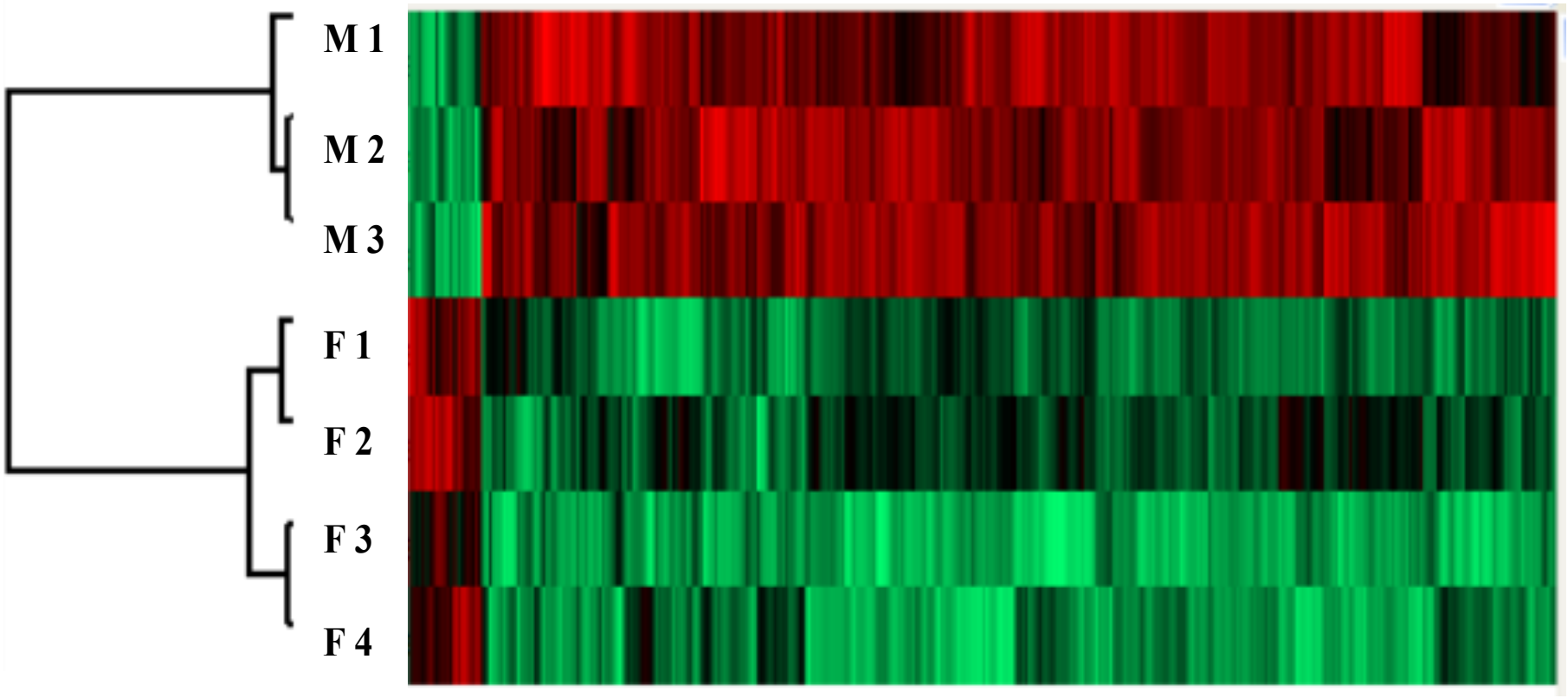

Figure 6.1. Heat map of significantly differentially expressed proteins calcified RVICs from male and female mice. RVICs were grown to confluence, calcified for 48 hours and subjected to LC-MS proteomics analysis. Data were transformed and normalised and t-tests were performed with multiple comparison corrections (false discovery rate at 0.05). Red-significantly upregulated, green-significantly downregulated. 939 proteins were found to be differentially expressed. M-male, F-female

The proteomics on testosterone treatments in VICs gave a downstream analysis of the potential mechanisms through which testosterone is augmenting calcification. This could provide insights into new therapeutic targets. The proteomics analysis in this thesis has provided preliminary insights into the pathways in which testosterone is augmenting VIC calcification and further interrogation of these downstream pathways is warranted, in particular the potential role of apoptosis and cellular metabolism in augmenting calcification. As these were highlighted in our pathway analysis and have been shown in other calcification studies (Heather *et al.*, 2011; Rogers *et al.*, 2017).

The proteomics data presented in this thesis identified over 350 protein hits, which have been previously reported to regulate cardiovascular calcification. Focusing on future investigations, the proteomics highlighted cellular metabolism which should be continued to be investigated using functional studies including CRISPR/siRNA knockout of potential protein targets. This is necessary as the change in protein identified by proteomics doesn't always cause a change in function. Another method of functional studies would be to carry out metabolic flux assays using a Seahorse Bioanalyzer to investigate if the testosterone treatment is dysregulating metabolic function (Little *et al.*, 2020). Upon any successful elucidation of a functional role, novel modulators would be tested on *in vivo* models of calcification. An exciting area to focus on would be modulators of energy metabolism. Current pharmaceutical interventions which focus on oxidative stress and mitochondrial function have been explored but with limited success. Clinical trials investigating the effect of dietary sources of antioxidants on cardiovascular outcomes have also had mixed results (Fotherby *et al.*, 2000; Lagowska-Lenard, Stelmasiak and Bartosik-Psujek, 2010; Duffy *et al.*, 2001). Other treatment options that have been explored include cysteine donors and JP4-039 (a novel mitochondrion-targeted ROS scavenger) (Orsucci *et al.*, 2019). With many available antioxidants, it would be interesting to investigate whether any of these antioxidants blunted testosterone-induced calcification. There is a transgenic mouse- the *mito*-QC mouse that has fluorescent reporters on the mitochondrial membranes and is able to detect mitophagy (Rosignol *et al.*, 2020). It would be interesting to combine the *mito*-QC mouse with a model of aortic valve calcification in investigations of mitochondrial function during CAVD pathogenesis.

The results presented here also indicated that the action of testosterone may be mediated through the androgen receptor, although functional studies on the AR proved to be challenging during my thesis. Genetic modification is a preferred method used by many to achieve

successful knockdown of target genes, especially when conducting *in vivo* and *in vitro* studies. These methods could be used to investigate further potential mechanisms by knocking down the AR in VICs using siRNA. If the deletion of the AR causes a reduction in testosterone-augments calcification in VICs. It would suggest that testosterone-augmented calcification is mediated by the AR.

This thesis has demonstrated significant progress in developing the wire injury model of CAVD, including performing pilot studies and method development to produce 'moderate valve injury' consistent with that reported by Niepmann *et al.* (2019). This model benefits from not displaying a sexual dimorphism in vascular calcification towards females, unlike the ApoE$^{-/-}$ mouse seen here. To model human CAVD more extensive damage needs to be induced, using a strain which is not prone to mutations in the circle of Willis. There is an argument for combining wire injury surgery with a mouse strain which is more prone to developing CVD, which could potentially lead to the model developing CAVD. This was attempted in Chapter 5, where the WI surgery was performed on ApoE$^{-/-}$ mice. Conclusions could not be drawn on whether these mice developed CAVD as this study had to be stopped due to a combination of mortality and the inability to forward the wire through the right carotid due to the presence of atherosclerotic lesions. Further studies could be conducted on younger ApoE$^{-/-}$ mice as these mice would not have developed atherosclerotic lesions so the wire injury surgery would be in theory, safer to perform. An alternative would be combining the wire injury with a different murine model that has been shown to have risk factors for developing ectopic calcification such as the AAV-PCSK9 model or the 5/6 nephrectomy model (Bro *et al.*, 2003; Goettsch *et al.*, 2016).

Murine models are extremely useful due to the ease of genetic manipulation of mice and the tools that have available to investigate signalling in murine tissues. As well as the relatively inexpensive cost of the studies compared to other *in vivo* models as well as their fast reproduction rates. Indeed, murine models have helped advanced medical research significantly, but mice have different valve structures to large mammals (not having the three-layered aortic valve structure encountered in humans) which may limit the translatability of results generated in murine models of CAVD. These findings could be extended by investigating sexual dimorphism in rabbit models, such as rabbits fed with a high-fat diet supplemented with vitamin D, as rabbits have a tri-layered valve leaflet as humans do and, interestingly, both males and females develop calcification (Chen *et al.*, 2020). Rabbits provide

a more physiologically translational model of CAVD. Pigs are arguably a better model as their heart valve physiology is so close to humans that porcine valves are used as replacements for human aortic valves (Manji *et al.*, 2012). Moreover, with innovation in CRISPR/Cas gene editing technology in porcine models, we could further investigate the role of AR and cellular energy metabolism in CAVD development (Ryczek *et al.*, 2021). A disadvantage of large animal models is that there are fewer laboratory reagents available meaning there is a limit to the experiments that can be conducted on these models. To conclude, despite the limitations of murine models of CAVD, murine models have significant use in deducing mechanisms of disease.

One consideration with longitudinal *in vivo* projects is the time limit of the PhD programme. During the production of this thesis, this became even more limited due to the COVID-19 pandemic. Unfortunately, the *in vivo* studies had to be terminated at the beginning of the pandemic because of access restrictions in the animal house. During the year following the outbreak of COVID-19, there was very limited access to the laboratory and extensive challenges in obtaining reagent supplies and importing animals delayed key investigations. However, this thesis has laid out significant groundwork for investigating and modelling sexual dimorphism in CAVD.

6.4 Conclusion

In conclusion, the findings of this thesis have built on and extended the current literature investigating sex differences in valve calcification. It has shown, for the first time, that testosterone augments the calcification of VICs, from male and female mice *in vitro*. The novel proteomic findings demonstrate molecular changes that testosterone induces in valve interstitial cells, which could help elucidate potential drug targets to impede testosterone-augmented calcification. The lack of knowledge surrounding the mechanisms responsible for sex differences in CAVD is partly attributable to the lack of appropriate murine models. This is further demonstrated in this thesis with the novel characterisation of the sex differences in more than one murine model of CAVD. Furthermore, developing models of valve calcification in which both calcification and aortic stenosis are present is challenging. Importantly, this study opens pathways to understanding mechanisms behind sexual dimorphism in calcification as well as highlighting important issues in the translation of sexual dimorphism in models of CAVD which needs to be considered for future research in aortic valve disease.

7.0 References

Adingupu, D. D. *et al.* (2016) 'Hyperglycemia Induced by Glucokinase Deficiency Accelerates Atherosclerosis Development and Impairs Lesion Regression in Combined Heterozygous Glucokinase and the Apolipoprotein E-Knockout Mice', *Journal of diabetes research*. 2016, 8630961

Aikawa, E. *et al.* (2009) 'Arterial and Aortic Valve Calcification Abolished by Elastolytic Cathepsin S Deficiency in Chronic Renal Disease', *Circulation*. 119, 13, pp. 1785-1794.

Ali, M. A. and Chowdhury, Y. S. (2022) 'Stentless Autograft/Homograft Aortic Valve Replacement', *StatPearls*. StatPearls Publishing.

Amann, K. (2008) 'Media Calcification and Intima Calcification Are Distinct Entities in Chronic Kidney Disease', *Clinical journal of the american society of nephrology*. 3, 6, pp. 1599–1605.

Anderson, H. C. (2003) 'Matrix Vesicles and Calcification.', *Current rheumatology reports*, 5, 3, pp. 222–6.

Arenas-Jal, M., Suñé-Negre, J. M. and García-Montoya, E. (2020) 'Coenzyme Q10 Supplementation: Efficacy, Safety, and Formulation Challenges', *Comprehensive reviews in food science and food safety*, 19, 2, pp. 574–594.

Arjunon, S. *et al.* (2013) 'Aortic Valve: Mechanical Environment and Mechanobiology', *Annals of biomedical engineering*. 41, 7, p. 1331-1347.

Aronow, W. S. *et al.* (2001) 'Association of Coronary Risk Factors and Use Of Statins with Progression of Mild Valvular Aortic Stenosis in Older Persons', *The American journal of cardiology*. 88, 6, pp. 693–695.

Arsenault, B. J. *et al.* (2014) 'Lipoprotein(a) Levels, Genotype, and Incident Aortic Valve Stenosis', *Circulation: cardiovascular genetics*. 7, 3, pp. 304–310.

Aslam, A. K. *et al.* (2007) 'Prosthetic Heart Valves: Types and Echocardiographic Evaluation', *International journal of cardiology*. 122, 2, pp. 99–110.

Avci, A. *et al.* (2014) 'The Relationship between Neutrophil/Lymphocyte Ratio and Calcific Aortic Stenosis', *Echocardiography*. 31, 9, pp. 1031–1035.

Ayers, J. *et al.* (2018) 'Recent Developments in the Role of Coenzyme Q10 for Coronary Heart Disease: a Systematic Review', *Current atherosclerosis reports*. 20, 6, pp. 1–7.

Badin, J. K. *et al.* (2019) 'Effect of Age on Diabetogenicity of Alloxan in Ossabaw Miniature Swine', *Comparative medicine*. 69, 2, pp. 114–122.

Bakhshian Nik, A., Hutcheson, J. D. and Aikawa, E. (2017) 'Extracellular Vesicles As Mediators of Cardiovascular Calcification', *Frontiers in cardiovascular medicine*. 4, 78.

Balachandran, K., Sucosky, P. and Yoganathan, A. P. (2011) 'Hemodynamics and mechanobiology of aortic valve inflammation and calcification', *International journal of inflammation*. pp. 1–15.

Bardeesi, A. S. A. *et al.* (2017) 'A Novel Role of Cellular Interactions in Vascular Calcification', *Journal of translational medicine*.15, 1, p. 95.

Barrett, H. E. *et al.* (2019) 'Calcifications in Atherosclerotic Plaques and Impact on Plaque Biomechanics', *Journal of biomechanics*. 87, pp. 1–12.

Benton, J. A., Fairbanks, B. D. and Anseth, K. S. (2009) 'Characterization of Valvular Interstitial Cell Function in Three Dimensional Matrix Metalloproteinase Degradable PEG Hydrogels', *Biomaterials*. 30, 34, pp. 6593-6603.

Bentzon, J. F. *et al.* (2014) 'Mechanisms of Plaque Formation and Rupture', *Circulation research*.114, 12, pp. 1852–1866.

Boffa, M. B. and Koschinsky, M. L. (2019) 'Oxidized Phospholipids as a Unifying Theory for Lipoprotein(a) and Cardiovascular Disease', *Nature reviews cardiology*. 16, 5, pp. 305–318.

Boonrungsiman, S. *et al.* (2012) 'The Role of Intracellular Calcium Phosphate in Osteoblast-ediated Bone Apatite Formation', *Proceedings of the national academy of sciences of the united states of america*. 109, 35, pp. 14170–14175.

Bosch, G. *et al.* (2008) 'Comprehensive Proteomics of Methylobacterium Extorquens AM1 Metabolism Under Single Carbon and Nonmethylotrophic Conditions', *Proteomics*. 8, 17, pp. 3494–3505.

Bouchareb, R. *et al.* (2015) 'Carbonic Anhydrase XII in Valve Interstitial Cells Promotes The Regression of Calcific Aortic Valve Stenosis', *Journal of molecular and cellular cardiology*. 82, pp. 104–115.

Bro, S. *et al.* (2003) 'Chronic Renal Failure Accelerates Atherogenesis in Apolipoprotein E-deficient Mice', *Journal of the american society of nephrology:JASN*. 14, 10, pp. 2466–2474.

Bucay, N. *et al.* (1998) 'Osteoprotegerin-deficient Mice Develop Early Onset Osteoporosis and Arterial Calcification', *Genes & development*. 12, 9, pp. 1260–1268.

Byon, C. H., Heath, J. M. and Chen, Y. (2016) 'Redox Signaling In Cardiovascular Pathophysiology: A Focus on Hydrogen Peroxide and Vascular Smooth Muscle Cells', *Redox biology*. 9, pp. 244-253.

Calderon-Margalit, R. *et al.* (2014) 'Prospective Association of Polycystic Ovary Syndrome With Coronary Artery Calcification and Carotid-Intima-Media Thickness', *Arteriosclerosis, thrombosis, and vascular biology*. 34, 12, pp. 2688–2694.

Caligiuri, G. *et al.* (1999) 'Effects of Sex and Age on Atherosclerosis and Autoimmunity in ApoE-deficient Mice', *Atherosclerosis*. 145, 2, pp. 301–308.

Castellan, R. F. P. *et al.* (2020) 'Electrocardiogram-gated Kilohertz Visualisation (EKV) Ultrasound Allows Assessment of Neonatal Cardiac Structural and Functional Maturation and Longitudinal Evaluation of Regeneration After Injury', *Ultrasound in medicine & biology*. 46, 1, pp. 167–179.

Chan, K. L. *et al.* (2010) 'Effect of Lipid Lowering with Rosuvastatin on Progression of Aortic Stenosis: Results of the Aortic Stenosis Progression Observation: Measuring Effects Of Rosuvastatin (ASTRONOMER) trial', *Circulation*. 121, 2, pp. 306–314

Chande, S. *et al.* (2019) 'Transgenic Mouse Model for Conditional Expression of Influenza Hemagglutinin-tagged Human SLC20A1/PIT1', *PLOS ONE*. 14, 10, p. e0223052.

Chaturvedi, P. *et al.* (2015) 'Differential miRNA Expression in Cells and Matrix Vesicles in Vascular Smooth Muscle Cells from Rats with Kidney Disease', *PLOS ONE*. 10, 6, p. e0131589.

Chen, H. Y., Engert, J. C. and Thanassoulis, G. (2019) 'Risk Factors for Valvular Calcification', *Current opinion in endocrinology, diabetes, and obesity*. 26, 2, pp. 96-102.

Chen, J. H. *et al.* (2009) 'Identification and Characterization of Aortic Valve Mesenchymal Progenitor Cells with Robust Osteogenic Calcification Potential', *The American journal of pathology*. 174, 3, pp. 1109–1119.

Chen, Y. *et al.* (2020) 'Macrophage-derived MMP-9 Enhances The Progression of Atherosclerotic Lesions and Vascular Calcification in Transgenic Rabbits', *Journal of cellular and molecular medicine*. 24, 7, pp. 4261–4274.

Chen, Y., Zhao, X. and Wu, H. (2020) 'Arterial Stiffness: A Focus on Vascular Calcification and its Link to Bone Mineralization', *Arteriosclerosis, thrombosis, and vascular biology*. 40, 5, pp. 1078-1093.

Chen, Z. *et al.* (2021) 'Zinc Ameliorates Human Aortic Valve Calcification Through GPR39 Mediated ERK1/2 Signalling Pathway', *Cardiovascular research*. 117, 3, pp. 820–835.

Choi, B. *et al.* (2017) 'Dipeptidyl peptidase-4 Induces Aortic Valve Calcifcation By Inhibiting Insulin-like Growth Factor-1 Signaling in Valvular Interstitial Cells', *Circulation*. 135, 20, pp. 1935–1950.

Cipollone, F. *et al.* (2011) 'A Unique MicroRNA Signature Associated with Plaque Instability in Humans', *Stroke*. 42, 9, pp. 2556–2563.

Clark, P. R. *et al.* (2007) 'Increased ICAM-1 Expression Causes Endothelial Cell Leakiness, Cytoskeletal Reorganization and Junctional Alterations', *Journal of investigative dermatology*. 127, 4, pp. 762–774.

Clarke, E. M. *et al.* (2014) 'Is Atherosclerosis Fundamental to Human Aging? Lessons from Ancient Mummies', *Journal of cardiology*. 63, 5, pp. 329–334.

Clayton, J. A. and Collins, F. S. (2014) 'NIH to Balance Sex in Cell and Animal Studies', *Nature*. 509, 7500, pp. 282-283.

Collaborative Group on Hormonal Factors in Breast Cancer 'Type and Timing of Menopausal Hormone Therapy and Breast Cancer Risk: Individual Participant Meta-Analysis of the Worldwide Epidemiological evidence' (2019) *The lancet*. 394, 1020, pp. 1159–1168.

Creager, Michael D. *et al.* (2019) '18F-fluoride Signal Amplification Identifies Microcalcifications Associated with Atherosclerotic Plaque Instability in PET/CT Images', *Circulation. Cardiovascular imaging*. 12, 1, p. e007835.

Cui, L. *et al.* (2017) 'End Stage Renal Disease-induced Hypercalcemia May Promote Aortic Valve Calcification via Annexin VI Enrichment of Valve Interstitial Cell Derived-Matrix vesicles', *Journal of cellular physiology*. 232, 11, pp. 2985–2995.

Dai, X. Y. *et al.* (2013) 'Phosphate-induced Autophagy Counteracts Vascular Calcification by Reducing Matrix Vesicle Release', *Kidney international*. 83, 6, pp. 1042–1051.

Davey, R. A. and Grossmann, M. (2016) 'Androgen Receptor Structure, Function and Biology: From Bench to Bedside', *The clinical biochemist reviews*. 37, 1, pp. 3-15.

Dellgren, G. *et al.* (2002) 'Late Hemodynamic and Clinical Outcomes of Aortic Valve Replacement with the Carpentier-Edwards Perimount Pericardial Bioprosthesis', *The journal of thoracic and cardiovascular surgery*. 124, 1, pp. 146–154.

Desjardin, J. T. *et al.* (2022) 'Sex Differences and Similarities in Valvular Heart Disease', *Circulation research*. 130, 4, pp. 455–473.

van Ditzhuijzen, N. S. *et al.* (2016) 'Serial Coronary Imaging of Early Atherosclerosis Development in Fast-Food-Fed Diabetic and Nondiabetic Swine', *JACC: Basic to translational science*. 1, 6, pp. 449-460.

Dorrington, J. H., Moon, Y. S. and Armstrong, D. T. (1975) 'Estrodiol-17β Biosynthasis in Cultured Granuloma cells from Hypophysectomized Immature Rats; Stimulation by Follicle-Stimulating Hormone1',*Endocrinology*. 97, 5, pp. 1328–1331.

Driscoll, K., Cruz, A. D. and Butcher, J. T. (2021) 'Inflammatory and Biomechanical Drivers of Endothelial-Interstitial Interactions in Calcific Aortic Valve Disease', *Circulation research*. 128, 9, pp. 1344-1370.

Duffy, S. J. *et al.* (2001) 'Effect of Ascorbic Acid Treatment on Conduit Vessel Endothelial Dysfunction in Patients with Hypertension', *American journal of physiology. Heart and circulatory physiology*. 280, 2, pp. 528-34

Durham, Andrew L. *et al.* (2018) 'Role of Smooth Muscle Cells in Vascular Calcification: Implications in Atherosclerosis and Arterial Stiffness', *Cardiovascular research*. 114, 4, p. 590-600.

Dutta, P. and Lincoln, J. (2018) 'Calcific Aortic Valve Disease: a Developmental Biology Perspective', *Current cardiology reports*. 20, 4, pp.21

Dweck, M. R., Boon, N. A. and Newby, D. E. (2012) 'Calcific Aortic Stenosis: A Disease of the Valve and the Myocardium', *Journal of the american college of cardiology*. 60, 19, pp. 1854–1863.

Eacker, S. M. *et al.* (2008) 'Hormonal Regulation of Testicular Steroid and Cholesterol Homeostasis', *Molecular endocrinology*. The Endocrine Society, 22, 3, p. 623-35.

Even-Sapir, E. *et al.* (2006) 'The Detection of Bone Metastases in Patients with High-Risk Prostate Cancer: 99mTc-MDP Planar Bone Scintigraphy, Single- and Multi-field-of-view SPECT, 18F-Fluoride PET, and 18F-Fluoride PET/CT', *Journal of nuclear medicine*. 47, 2, pp. 287–297.

Fang, M. *et al.* (2020) 'AntagomiR-29b Inhibits Vascular and Valvular Calcification and Improves Heart Function in Rats', *Journal of cellular and molecular medicine*. 24, 19, pp. 11546-11557.

Fang, Q. Q. *et al.* (2018) 'Angiotensin-converting Enzyme Inhibitor Reduces Scar Formation by Inhibiting Both Canonical and Noncanonical TGF-β1 Pathways', *Scientific reports*. 8, 1, p. 3332.

Ferdous, Z., Jo, H. and Nerem, R. M. (2013) 'Strain Magnitude-Dependent Calcific Marker Expression in Valvular and Vascular Cells', *Cells tissues organs*. 197, 5, pp. 372–383.

Fisher, C. I., Chen, J. and Merryman, W. D. (2013) 'Calcific Nodule Morphogenesis by Heart Valve Interstitial Cells is Strain Dependent', *Biomechanics and modeling in mechanobiology*.12, 1, pp. 5-17.

Florencio-Silva, R. *et al.* (2015) 'Biology of Bone Tissue: Structure, Function, and Factors That Influence Bone Cells', *BioMed research international*, 2015, 421747.

Foradori, C. D., Weiser, M. J. and Handa, R. J. (2008) 'Non-genomic Actions of Androgens', *Frontiers in neuroendocrinology*. 29, 2, pp. 169-81.

Fotherby, M. D. *et al.* (2000) 'Effect of Vitamin C on Ambulatory Blood Pressure and Plasma Lipids in Older Persons', *Journal of hypertension*. 18, 4, pp. 411–415.

Furmanik, M. *et al.* (2021) 'Endoplasmic Reticulum Stress Mediates Vascular Smooth Muscle Cell Calcification via Increased Release of Grp78 (Glucose-Regulated Protein, 78 kDa)-Loaded Extracellular Vesicles', *Arteriosclerosis, thrombosis, and vascular biology*. 41, pp. 898–914.

García-Rodríguez, C. *et al.* (2018) 'Toll-Like Receptors, Inflammation, and Calcific Aortic Valve Disease', *Frontiers in physiology*. 9, p. 201.

George, G. *et al.* (2022) 'Qualitative Analysis of Interviews and Focus Groups Exploring Factors Contributing to Adherence to GnRH Agonists in Men with Prostate Cancer', *Seminars in oncology nursing*. 38, 4, p. 151236.

Gerdts, E. *et al.* (2010) 'Impact of Baseline Severity of Aortic Valve Stenosis on Effect of Intensive Lipid Lowering Therapy (from the SEAS study)', *The American journal of cardiology*. 106, 11 , pp. 1634–1639.

Goettsch, C. *et al.* (2011) 'miR-125b Regulates Calcification of Vascular Smooth Muscle Cells', *The american journal of pathology*. 179, 4, pp. 1594-600.

Goettsch, C., Hutcheson, J. D. and Aikawa, E. (2013) 'MicroRNA in Cardiovascular Calcification: Focus on Targets and Extracellular Vesicle Delivery Mechanisms', *Circulation research*. 112, 7, pp. 1073-84.

Goetz, L. G. *et al.* (2019) 'Addition of Estradiol to Cross-Sex Testosterone Therapy Reduces Atherosclerosis Plaque Formation in Female ApoE-/- Mice', *Endocrinology*. 159, 2, pp. 754–762.

Gould, A. L. *et al.* (1998) 'Cholesterol Reduction Yields Clinical Benefit: Impact of Statin Trials', *Circulation*. 97, 10, pp. 946–952.

Grim, J. C. *et al.* (2020) 'Secreted Factors from Pro-inflammatory Macrophages Promote an Osteoblast-like Phenotype in Valvular Interstitial Cells', *Arteriosclerosis, thrombosis, and vascular biology*. 40, 11, p. e296.

Grossman, W., Jones, D. and McLaurin, L. P. (1975) 'Wall Stress and Patterns of Hypertrophy in the Human Left Ventricle', *Journal of clinical investigation*. 56, 1, pp. 56–64.

Grundy, S. M. *et al.* (2019) '2018 Guideline on the Management of Blood Cholesterol: A Report of the American College of Cardiology/American Heart Association Task Force on Clinical Practice Guidelines', *Circulation*. 139, 25, pp. E1082–E1143.

Habas, K. and Shang, L. (2018) 'Alterations in Intercellular Adhesion Molecule 1 (ICAM-1) and Vascular Cell Adhesion Molecule 1 (VCAM-1) in Human Endothelial Cells', *Tissue and cell*. 54, pp. 139–143.

Hakuno, D. *et al.* (2010) 'Periostin Advances Atherosclerotic and Rheumatic Cardiac Valve Degeneration by Inducing Angiogenesis and MMP Production in Humans and Rodents', *The journal of clinical investigation*. 120, 7, pp. 2292-302.

Hammad, S. K. *et al.* (2021) 'Resveratrol Ameliorates Aortic Calcification in Ovariectomized Rats via SIRT1 Signaling', *Current issues in molecular biology*. 43, 2, pp. 1057-1071.

Handelsman, D. J. (2020) 'Androgen Physiology, Pharmacology, Use and Misuse', *Endocrinology: adult and pediatric*. 2–2, pp. 2368-2393.

Handelsman, D. J., Hirschberg, A. L. and Bermon, S. (2018) 'Circulating Testosterone as the Hormonal Basis of Sex Differences in Athletic Performance', *Endocrine reviews*. 39, 5, pp. 803-829.

Hartley, C. J. *et al.* (2000) 'Hemodynamic Changes in Apolipoprotein E-knockout Mice', *American journal of physiology - heart and circulatory physiology*. 279, 5, pp. 48-5.

He, P. *et al.* (2020) 'Hdac9 Inhibits Medial Artery Calcification Through Down-Regulation of Osterix', *Vascular pharmacology*. 132, p. 106775.

Heather, L. C. *et al.* (2011) 'Changes in Cardiac Substrate Transporters and Metabolic Proteins Mirror the Metabolic Shift in Patients with Aortic Stenosis', *PloS one*. 6, 10, p. e26326

Helske, S. *et al.* (2004) 'Induction of Local Angiotensin II-Producing Systems in Stenotic Aortic Valves', *Journal of the american college of cardiology*. 44, 9, pp. 1859–1866.

Henein, M. *et al.* (2015) 'High Dose and Long-term Statin Therapy Accelerate Coronary Artery Calcification', *International journal of cardiology*. 184, 1, pp. 581–586.

Hinder, L. M. *et al.* (2013) 'Apolipoprotein E Knockout as the Basis for Mouse Models of Dyslipidemia-induced Neuropathy', *Experimental neurology*. 39, 1, pp. 102–110.

Hinton, R. B. *et al.* (2008) 'Mouse Heart Valve Structure and Function: Echocardiographic and Morphometric Analyses from the Fetus Through the Aged Adult', *American journal of physiology. Heart and circulatory physiology*. 294, 6, pp. H2480-8

Hjortnaes, J. *et al.* (2015) 'Valvular Interstitial Cells Suppress Calcification of Valvular Endothelial Cells.', *Atherosclerosis*. 242, 1, pp. 251–260.

Ho, C. Y. and Shanahan, C. M. (2016) 'Medial Arterial Calcification: An Overlooked Player in Peripheral Arterial Disease', *Arteriosclerosis, thrombosis, and vascular biology*. 36, 8, pp. 1475–1482.

Hoffman, J. I. E. and Kaplan, S. (2002) 'The Incidence of Congenital Heart Disease', *Journal of the american college of cardiology*. 39, 12, pp. 1890–1900.

Holdcroft, A. (2007) 'Gender Bias in Research: How Does it Affect Evidence Based Medicine?', *Journal of the royal society of medicine*. 100, 1, pp. 2-3.

Honda, S. *et al.* (2014) 'A Novel Mouse Model of Aortic Valve Stenosis Induced by Direct Wire Injury', *Arteriosclerosis, thrombosis, and vascular biology*, 34, 2, pp. 270–278.

Honda, Y. *et al.* (2009) 'The Effect of Microstructure of Octacalcium Phosphate on the Bone Regenerative Property', *Tissue engineering part a*, 15, 8, pp. 1965–1973.

Horvath, K. A. *et al.* (2011) 'Transapical Aortic Valve Replacement under Real-time Magnetic Resonance Imaging Guidance: Experimental Results with Balloon-Expandable and Self-Expanding Stents', *European journal of cardio-thoracic surgery : official journal of the european association for cardio-thoracic Surgery*. 39, 6, p. 822-8.

Hsu, Y. J. *et al.* (2015) 'Hyperphosphatemia Induces Protective Autophagy in Endothelial Cells Through the Inhibition of Akt/mTOR Signaling', *Journal of vascular surgery*. 62, 1, pp. 210-221.e2.

Hu, M. C. *et al.* (2011) 'Klotho Deficiency Causes Vascular Calcification in Chronic Kidney Disease', *Journal of the mmerican society of nephrology : JASN*. 22, 1, pp. 124-36.

Hulley, S. *et al.* (2002) 'Noncardiovascular Disease Outcomes During 6.8 years of Hormone Therapy: Heart and Estrogen/progestin Replacement Study Follow-up (HERS II)', *JAMA*, 288, 1, pp. 58–66.

Hutcheson, J. D. *et al.* (2012) 'Intracellular Ca2+ Accumulation is Strain-Dependent and Correlates with Apoptosis in Aortic Valve Fibroblasts', *Journal of biomechanics*. 45, 5, pp. 888-94.

Hutcheson, J. D. *et al.* (2013) 'Cadherin-11 Regulates cell-cell Tension Necessary for Calcific Nodule Formation by Valvular Myofibroblasts', *Arteriosclerosis, thrombosis, and vascular biology*. 33, 1, pp. 114-20.

Ishibashi, S. *et al.* (1993) 'Hypercholesterolemia in Low Density Lipoprotein Receptor Knockout Mice and its Reversal by Adenovirus-mediated Gene Delivery.', *Journal of clinical investigation*. 92, 2, pp. 883-93.

Johansson, M. E. *et al.* (2005) 'Haemodynamically Significant Plaque Formation and Regional Endothelial Dysfunction in Cholesterol-fed ApoE-/- Mice', *Clinical science*. 108, 6, pp. 531–538.

Joseph, P. and Tawakol, A. (2016) 'Imaging Atherosclerosis with Positron Emission Tomography.', *European heart journal*, 37, 39, pp. 2974–2980.

Joshi, N. V. *et al.* (2014) 'Will 18F-sodium Fluoride PET-CT Imaging be the Magic Bullet for Identifying Vulnerable Coronary Atherosclerotic Plaques?', *Current cardiology reports*. 16, 9, p.521

Jung, J. J. *et al.* (2015) 'Multimodality and Molecular Imaging of Matrix Metalloproteinase Activation in Calcific Aortic Valve Disease', *Journal of nuclear medicine*. 56, 6, pp. 933–938.

Kaden, J. J. *et al.* (2003) 'Interleukin-1 beta Promotes Matrix Metalloproteinase Expression and Cell Proliferation in Calcific Aortic Valve Stenosis.', *Atherosclerosis*, 170, 2, pp. 205–11.

Kaden, J. J. *et al.* (2005) 'Tumor Necrosis Factor Alpha Promotes an Osteoblast-like Phenotype in Human Aortic Valve Myofibroblasts: a Potential Regulatory Mechanism of Valvular Calcification.', *International journal of molecular medicine*, 16, 5, pp. 869–72.

Kalil, R. S. *et al.* (2015) 'Effect of Extended Release Niacin on Cardiovascular Events and Kidney Function in Chronic Kidney Disease: A Post-Hoc Analysis of the AIM-HIGH Trial', *Kidney international*. 87, 6, pp. 1250-7.

Karagianni, A. E. *et al.* (2021) 'Application Across Species of a One Health Approach to Liquid Sample Handling for Respiratory Based -Omics Analysis', *Scientific reports*, 11, 1, pp. 1–12.

Kearns, A. E., Khosla, S. and Kostenuik, P. J. (2008) 'Receptor Activator of Nuclear Factor κB Ligand and Osteoprotegerin Regulation of Bone Remodeling in Health and Disease', *Endocrine reviews*. 29, 2, pp. 155-92.

Kelynack, K. J. and Holt, S. G. (2016) 'An In Vitro Murine Model of Vascular Smooth Muscle Cell Mineralization', *Methods in molecular biology* 1397, pp. 209–220.

Kirkby, N. S. *et al.* (2011) 'Quantitative 3-Dimensional Imaging of Murine Neointimal and Atherosclerotic Lesions by Optical Projection Tomography', *PLOS ONE*. 6, 2, p. e16906.

Kirkby, N. S. *et al.* (2015) 'Generation and 3-Dimensional Quantitation of Arterial Lesions in Mice Using Optical Projection Tomography', *Journal of visualized experiments : JoVE*. 2015, 99, p. e50627.

Kohn, M. H., Price, R. E. and Pelz, H. J. (2008) 'A cardiovascular Phenotype in Warfarin-Resistant Vkorc1 Mutant Rats', *Artery research*. 2, 4, pp. 138-147.

Kousteni, S. *et al.* (2001) 'Nongenotropic, Sex-nonspecific Signaling Through the Estrogen or Androgen Receptors: Dissociation from Transcriptional Activity', *Cell*. 104, 5, pp. 719–730.

Ku, C. H. *et al.* (2006) 'Collagen Synthesis by Mesenchymal Stem Cells and Aortic Valve Interstitial Cells in Response to Mechanical Stretch', *Cardiovascular research*. 71, 3, pp. 548–556.

Kutryb-Zajac, B. *et al.* (2020) 'Nucleotide ecto-enzyme Metabolic Pattern and Spatial Distribution in Calcific Aortic Valve Disease; its Relation to Pathological Changes and Clinical Presentation', *Clinical research in cardiology*. 109, 2, pp. 137-160.

Lagowska-Lenard, M., Stelmasiak, Z. and Bartosik-Psujek, H. (2010) 'Influence of Vitamin C on Markers of Oxidative Stress in the Earliest Period of Ischemic Stroke', *Pharmacological reports* 62, 4, pp. 751–756.

Lai, J. *et al.* (2015) 'Low Serum Testosterone Level was Associated with Extensive Coronary Artery Calcification in Elderly Male Patients with Stable Coronary Artery Disease', *Coronary artery disease*. 26, 5, pp. 437–441.

Langheinrich, A. C. *et al.* (2007) 'Vasa Vasorum Neovascularization and Lesion Distribution Among Different Vascular Beds in ApoE−/−/LDL−/− Double Knockout Mice', *Atherosclerosis*. 191, 1, pp. 73–81.

Lanzer, P. *et al.* (2014) 'Medial Vascular Calcification Revisited: Review and Perspectives', *European heart journal*. 35, 23, pp. 1515–1525.

Latif, N. *et al.* (2015) 'Modulation of Human Valve Interstitial Cell Phenotype and Function Using a Fibroblast Growth Factor 2 Formulation', *PLOS ONE*. 10, 6, p. e0127844.

Lee, H.-R., Kim, T.-H. and Choi, K.-C. (2012) 'Functions and Physiological Roles of Two Types of Estrogen Receptors, ERα and ERβ, Identified by Estrogen Receptor Knockout Mouse', *Laboratory animal research*. 28, 2, pp. 71-6.

Lee, S. H. and Choi, J. H. (2018) 'Involvement of Inflammatory Responses in the Early Development of Calcific Aortic Valve Disease: Lessons from Statin Therapy', *Animal cells and systems*. 22, 6, pp. 390-399.

Leopold, J. A. (2015) 'Vascular Calcification: Mechanisms of Vascular Smooth Muscle Cell Calcification', *Trends in cardiovascular medicine*. 25, 4, pp. 267-74.

Lerman, D. A., Prasad, S. and Alotti, N. (2015) 'Calcific Aortic Valve Disease: Molecular Mechanisms and Therapeutic Approaches.', *European cardiology*. 10, 2, pp. 108–112.

Li, Q. *et al.* (2017) 'Abcc6 Knockout Rat Model Highlights the Role of Liver in PPi Homeostasis in Pseudoxanthoma Elasticum', *Journal of investigative dermatology*. 137, 5, pp. 1025–1032.

Li, T. *et al.* (2022) 'Matrix Vesicles as a Therapeutic Target for Vascular Calcification', *Frontiers in cell and developmental biology*. 10, 825622

Li, Z. *et al.* (2017) 'Impaired Bone Formation in Ovariectomized Mice Reduces Implant Integration as Indicated by Longitudinal in vivo Micro-computed Tomography', *PLoS ONE*. 12, 9, p. e 0184835

Libby, P. and Aikawa, M. (2003) 'Mechanisms of Plaque Stabilization with Statins', *The american journal of cardiology*. 91, 4, pp. 4–8.

Libby, P. and Pasterkamp, G. (2015) 'Requiem For The "vulnerable plaque"', *European heart journal*. 36, 43, pp. 2984–2987

Liberman, M. *et al.* (2008) 'Oxidant Generation Predominates Around Calcifying Foci and Enhances Progression of Aortic Valve Calcification', *Arteriosclerosis, thrombosis, and vascular biology*. 28, 3, pp. 463–470.

Libeu, C. P. *et al.* (2001) 'New Insights into the Heparan Sulfate Proteoglycan-binding Activity of Apolipoprotein E', *Journal of biological chemistry*. 276, 42, pp. 39138–39144.

Lim, S. V. *et al.* (2015) 'Excessive Growth Hormone Expression in Male GH Transgenic Mice Adversely Alters Bone Architecture and Mechanical Strength', *Endocrinology*. 156, 4, pp. 1362-71.

Lin, C. *et al.* (2017) 'Isolation and Characterization of Primary Rat Valve Interstitial Cells: A New Model to Study Aortic Valve Calcification', *JoVE (Journal of Visualized Experiments)* 2017, 129, p. e56126.

Lindman, B. R. *et al.* (2016) 'Calcific Aortic Stenosis', *Nature reviews disease primers*. 2, p. 16006.

Lindsey, L. M. et al. (2018) Guidelines for measuring cardiac physiology in mice. *Heart and Circulatory Physiology*. 314, 4, pp. H733-H752

López, J. *et al.* (2012) 'Viral and Bacterial Patterns Induce TLR-mediated Sustained Inflammation and Calcification in Aortic Valve Interstitial Cells.', *International journal of cardiology*. 158, 1, pp. 18–25.

Luo, G. *et al.* (1997) 'Spontaneous Calcification of Arteries and Cartilage in Mice Lacking Matrix GLA Protein', *Nature*. 386, 6620, pp. 78–81.

Ma, W. Q. *et al.* (2019) 'Restoring Mitochondrial Biogenesis with Metformin Attenuates β-GP-induced Phenotypic Transformation of VSMCs into an Osteogenic Phenotype via Inhibition of PDK4/Oxidative Stress-Mediated Apoptosis', *Molecular and cellular endocrinology*. 479, pp. 39–53.

MacAskill, M. G. *et al.* (2020) 'Characterisation of an Atherosclerotic Micro-Calcification Model Using ApoE−/− Mice and PET/CT', *IJC Heart & Vasculature*. 31, p. 100672.

Maeda, N. (2011) 'Development of Apolipoprotein E-deficient Mice', *Arteriosclerosis, thrombosis, and vascular biology*. 31, 9, pp. 1957–1962.

Manson, J. E. *et al.* (2007) 'Estrogen Therapy and Coronary-Artery Calcification', *New england journal of medicine*. 356, 25, pp. 2591–2602.

Manzoor, S. *et al.* (2018) 'Progression of Medial Arterial Calcification in CKD', *Kidney international reports*. 3, 6, pp. 1328–1335.

Maor, G., Segev, Y. and Phillip, M. (1999) 'Testosterone Stimulates Insulin-Like Growth Factor-I and Insulin-Like Growth Factor-I-Receptor Gene Expression in the Mandibular Condyle—A Model of Endochondral Ossification', *Endocrinology*. 140, 4, pp. 1901–1910.

Marais, A. D. (2019) 'Apolipoprotein E in Lipoprotein Metabolism, Health and Cardiovascular disease', *Pathology.* pp. 165–176.

Marek, I. *et al.* (2017) 'Sex Differences in the Development of Vascular and Renal Lesions in Mice with a Simultaneous Deficiency of Apoe and the Integrin Chain Itga8', *Biology of sex differences*. 8, 1.

Marinko, J. T. *et al.* (2019) 'Folding and Misfolding of Human Membrane Proteins in Health andDisease: From Single Molecules to Cellular Proteostasis', *Chemical reviews*. 119, 9, pp. 5537-5606.

Masjedi, S. *et al.* (2017) 'Sex-related Differences in Matrix Remodeling and Early Osteogenic Markers in Aortic Valvular Interstitial Cells', *Heart and vessels*. 32, 2, pp. 217–228.

Mathieu, P., Bouchareb, R. and Boulanger, M.-C. (2015) 'Innate and Adaptive Immunity in Calcific Aortic Valve Disease.', *Journal of immunology research*. 2015, p. 851945.

Matsumoto, S. *et al.* (2018) 'Effects of Polymethoxyflavonoids on Bone loss Induced by Estrogen Deficiency and by LPS-dependent Inflammation in Mice', *Pharmaceuticals*. 11, 1, p7.
Matsumoto, Y. *et al.* (2010) 'Regular Exercise Training Prevents Aortic Valve Disease in Low-density Lipoprotein-receptor-deficient Mice', *Circulation*. 121, 6, pp. 759–767.

McColl, B. W. *et al.* (2004) 'Extension of Cerebral Hypoperfusion and Ischaemic Pathology Beyond MCA Territory after Intraluminal Filament Occlusion in C57Bl/6J Mice', *Brain research*. 997, 1, pp. 15–23.

McRobb, L., Handelsman, D. J. and Heather, A. K. (2009) 'Androgen-Induced Progression of Arterial Calcification in Apolipoprotein E-Null Mice Is Uncoupled from Plaque Growth and Lipid Levels', *Endocrinology*, 150, 2, pp. 841–848.

McRobb, L. S. *et al.* (2017) 'Estrogen Receptor Control of Atherosclerotic Calcification and Smooth Muscle Cell Osteogenic Differentiation', *Arteriosclerosis, thrombosis, and vascular biology*. 37, 6, pp. 1127–1137.

Mecadon, K. (2021) 'Managing Side Effects of Immunosuppressants', *Rhode island medical journal*, 104, 1, pp. 31–33.

Mendelsohn, M. E. (2000) 'Nongenomic, ER-Mediated Activation of Endothelial Nitric Oxide Synthase':, *Circulation research*. 87, 11, pp. 956–960.

Mendelsohn, M. E. and Karas, R. H. (1999) 'The Protective Effects of Estrogen on the Cardiovascular System', *The new england journal of medicine*. 340, 23, pp. 1801–1811.

Meng, X. *et al.* (2008) 'Expression of Functional Toll-like Receptors 2 and 4 in Human Aortic Valve Interstitial Cells: Potential Roles in Aortic Valve Inflammation and Stenosis', *American journal of physiology-cell physiology*. 294, 1, pp. C29–C35.

Menon, V. and Lincoln, J. (2018a) 'The Genetic Regulation of Aortic Valve Development and Calcific Disease', *Frontiers in cardiovascular medicine*. 5, 162.

Meyrelles, S. S. *et al.* (2011) 'Endothelial Dysfunction in the Apolipoprotein E-deficient Mouse: Insights into the influence of diet, gender and aging', *Lipids in health and disease*. 10, p. 211.

Miller, J. D. *et al.* (2008) 'Dysregulation of Antioxidant Mechanisms Contributes to Increased Oxidative Stress in Calcific Aortic Valvular Stenosis in Humans', *Journal of the american college of cardiology*. 52, 10, pp. 843-50.

Miller, T. R. (1980) ' Quantitative Cardiovascular Studies: Clinical and Research Applications of Engineering Principles , edited by N. H. C. Hwang, D. R. Gross, and D. J. Patel ', *Medical physics*. 7, 5, pp. 579–579.

Miller, V. M. and Duckles, S. P. (2008) 'Vascular Actions of Estrogens: Functional Implications', *Pharmacological reviews*. 60, 2, pp. 210-41.

Mjaatvedt, C. H. *et al.* (2005) 'Normal Distribution of Melanocytes In the Mouse Heart', *The anatomical record. Part A, Discoveries in molecular, cellular, and evolutionary biology*. 285, 2, pp. 748–757.

Moesgaard, S. G. *et al.* (2014) 'Matrix metalloproteinases (MMPs), Tissue Inhibitors of Metalloproteinases (TIMPs) and Transforming Growth Factor-β (TGF-β) in Advanced Canine Myxomatous Mitral Valve Disease', *Research in veterinary science*. 97, 3, pp. 560–567.

Mohan, J. *et al.* (2021) 'Coronary Artery Calcification', *StatPearls,* Stat Pearl Publishing, Treasure Island, US*A*.

Moreau, K. L. *et al.* (2007) 'Oxidative Stress Contributes to Chronic Leg Vasoconstriction in Estrogen-Deficient Postmenopausal Women', *Journal of applied physiology.* 102, 3, pp. 890–895.

Morris, P. D. and Channer, K. S. (2012) 'Testosterone and Cardiovascular Disease in Men', *Asian journal of andrology*. 14, 3, p. 428.

Moura, L. M. *et al.* (2007) 'Rosuvastatin Affecting Aortic Valve Endothelium to Slow the Progression of Aortic Stenosis', *Journal of the american college of cardiology*. 49, 5, pp. 554-61.

Muller, A. M. *et al.* (2000) 'Expression of Endothelial Cell Adhesion Molecules on Heart Valves: Up-regulation in Degeneration as Well as Acute Endocarditis', *The journal of pathology*.191, 1, pp. 54–60.

Nakamura, T. *et al.* (2007) 'Estrogen Prevents Bone Loss via Estrogen Receptor α and Induction of Fas Ligand in Osteoclasts', *Cell*. 130, 5, pp. 811–823.

Nakao, Y. M. *et al.* (2018) 'Sex Differences in Impact of Coronary Artery Calcification to Predict Coronary Artery disease', *Heart*. 104, 13, pp. 1118–1124.

Nanao-Hamai, M. *et al.* (2016) 'Protective Effects of Estrogen Against Vascular Calcification via Estrogen Receptor α-Dependent Growth Arrest-Specific Gene 6 Transactivation', *Biochemical and biophysical research communications*. 480, 3, pp. 429–435.

Ng, K. *et al.* (2011) 'Angiotensin-Converting Enzyme Inhibitor Limits Pulse-Wave Velocity and Aortic Calcification in a Rat Model of Cystic Renal Disease', *American journal of physiology - renal physiology*. 301, 5, pp. 959–966.

Niepmann, S. T. *et al.* (2019) 'Graded Murine Wire-Induced Aortic Valve Stenosis Model Mimics Human Functional and Morphological Disease Phenotype', *Clinical research in cardiology*. 108, 8, pp 847-856.

Nkomo, V. T. *et al.* (2006) 'Burden of Valvular Heart Diseases: a Population-Based Study', *The lancet*, 368, 9540, pp. 1005–1011.

Node, K. *et al.* (1997) 'Roles of NO and Ca2+-activated K+ Channels in Coronary Vasodilation Induced By 17β-Estradiol in Ischemic Heart Failure', *The FASEB journal*. 11, 10, pp. 793–799.

O'Brien, J. *et al.* (2018) 'Overview of microRNA Biogenesis, Mechanisms of Actions, and Circulation', *Frontiers in Endocrinology*. 9, 402.

O'Brien, K. D. *et al.* (2002) 'Association of Angiotensin-Converting Enzyme with Low-Density Lipoprotein in Aortic Valvular Lesions and in Human Plasma', *Circulation*. 106, 17, pp. 2224–2230.

Okazaki, M. *et al.* (1994) 'Molecular Cloning and Characterization of OB-cadherin, a New Member of Cadherin Family Expressed in Osteoblasts.', *Journal of biological chemistry*. 269, 16, pp. 12092–12098.

Oliveira, J. C. C. *et al.* (2019) 'Effect of Testosterone on Proliferation Markers and Apoptosis in Breasts of Ovariectomized Rats', *Revista brasileira de ginecologia e obstetricia : revista da Federacao Brasileira das Sociedades de Ginecologia e Obstetricia*. 41, 12, pp. 703–709.

Olsen, M. H. *et al.* (2004) 'Effect of Losartan Versus Atenolol on Aortic Valve Sclerosis (a LIFE substudy)', *The american journal of cardiology*. 94, 8, pp. 1076–1080.

.

Orsucci, D. *et al.* (2019) 'Mitochondrial Disorders and Drugs: What Every Physician Should Know', *Drugs in context*. 8, 212588.

Osako, M. K. *et al.* (2010) 'Estrogen Inhibits Vascular Calcification via Vascular RANKL System: Common Mechanism of Osteoporosis and Vascular Calcification.', *Circulation research*, 107, 4, pp. 466–75.

Otsuka, F. *et al.* (2014) 'Has our Understanding of Calcification in Human Coronary Atherosclerosis Progressed?', *Arteriosclerosis, thrombosis, and vascular biology*. 34, 4, pp. 724–736.

Paigen, B. *et al.* (1987) 'Comparison of Atherosclerotic Lesions and HDL-lipid Levels in Male, Female, and Testosterone-treated Female Mice from Strains C57BL/6, BALB/c, and C3H', *Atherosclerosis*. 64, 2–3, pp. 215–221.

Park, B. J. *et al.* (2012) 'Inverse Relationship Between Bioavailable Testosterone and Subclinical Coronary Artery Calcification in Non-obese Korean Men', *Asian journal of andrology*, 14, 4, pp. 612–615

Parra-Izquierdo, I. *et al.* (2018) 'Calcification Induced by Type I Interferon in Human Aortic Valve Interstitial Cells Is Larger in Males and Blunted by a Janus Kinase Inhibitor', *Arteriosclerosis, thrombosis, and vascular biology*, 38, 9, pp. 2148–2159.

Parra-Izquierdo, I. *et al.* (2019) 'Lipopolysaccharide and Interferon-γ Team up to Activate HIF-1α via STAT1 in Normoxia and Exhibit Sex Differences in Human Aortic Valve Interstitial Cells', *Biochimica et Biophysica Acta (BBA) - Molecular basis of disease*. 1865, 9, pp. 2168-2179.

Parzych, K. R. and Klionsky, D. J. (2014) 'An Overview of Autophagy: Morphology, Mechanism, and Regulation', *Antioxidants & redox signaling*. 20, 3, pp. 460-73.

Passmore, M. *et al.* (2015) 'Osteopontin Alters Endothelial and Valvular Interstitial Cell Behaviour in Calcific Aortic Valve Stenosis Through HMGB1 Regulation', *European journal of cardio-thoracic surgery*. 48, 3, pp. e20–e29.

Paterni, I. *et al.* (2014) 'Estrogen Receptors Alpha (ERα) and Beta (ERβ): Subtype-Selective Ligands and Clinical Potential', *Steroids*. NIH Public Access, 90, pp. 13-29.

Peeters, F. E. C. M. *et al.* (2020) 'Biomarkers Associated With Aortic Valve Calcification: Should We Focus on Sex Specific Processes?', *Frontiers in cell and developmental biology*. 8, 604.

Peng, H. H. *et al.* (2017) 'Mineral Particles Stimulate Innate Immunity Through Neutrophil Extracellular Traps Containing HMGB1', *Scientific reports,* 7, 1, pp. 1–16.

Persy, V. and D'Haese, P. (2009) 'Vascular Calcification and Bone Disease: the Calcification Paradox', *Trends in molecular medicine*. 15, 9, pp. 405–416.

Petitti, D. B. (2002) 'Hormone Replacement Therapy for Prevention: More Evidence, More Pessimism', *JAMA*. 288, 1, pp. 99–101.

Phadwal, K. *et al.* (2020) 'Autophagy as a Novel Therapeutic Target in Vascular Calcification', *Pharmacology & therapeutics*. 206, p. 107430.

Phadwal, K. *et al.* (2021) 'Mitochondrial Dysfunction: Cause or Consequence of Vascular Calcification?', *Frontiers in cell and developmental biology*. 9, 611922 p. 336.

Proudfoot, D. *et al.* (2000) 'Apoptosis Regulates Human Vascular Calcification in Vitro: Evidence For Initiation of Vascular Calcification by Apoptotic Bodies', *Circulation research*. 87, 11, pp. 1055–1062.

Purroy, A. *et al.* (2018) 'Matrix Metalloproteinase-10 Deficiency Delays Atherosclerosis Progression and Plaque Calcification', *Atherosclerosis*. 278, pp. 124–134.

Qiao, J. H. *et al.* (1994) 'Pathology of Atheromatous Lesions in Inbred and Genetically Engineered Mice. Genetic determination of arterial calcification.', *Arteriosclerosis and thrombosis: A journal of vascular biology*. 14, 9, pp. 1480–1497.

Rabkin, E. *et al.* (2001) 'Activated Interstitial Myofibroblasts Express Catabolic Enzymes and Mediate Matrix Remodeling in Myxomatous Heart Valves', *Circulation*. 104, 21, pp. 2525–2532.

Rajamannan, N. M. *et al.* (2005) 'Atorvastatin Inhibits Calcification and Enhances Nitric Oxide Synthase Production in the Hypercholesterolaemic Aortic Valve'. *Heart*. 91, 6, pp. 806-8120.

Rattazzi, M. *et al.* (2008) 'Clones of Interstitial cells from Bovine Aortic Valve Exhibit Different Calcifying Potential when Exposed to Endotoxin and Phosphate', *Arteriosclerosis, thrombosis, and vascular biology*., 28, 12, pp. 2165–2172.

Rauthan, M. *et al.* (2015) ‘A Mutation in Caenorhabditis elegans NDUF-7 Activates the Mitochondrial Stress Response and Prolongs Lifespan via ROS and CED-4’, *G3 (Bethesda)*, 5, 8, pp. 1639–1648

Robb, J. D. *et al.* (2012) ‘An Ovine Model of Pulmonary Insufficiency and Right Ventricular Outflow Tract Dilatation’, *The journal of heart valve disease*. 21, 2, pp. 247-52.

Robinson, L. J. *et al.* (2009) ‘Estrogen Inhibits RANKL-stimulated Osteoclastic Differentiation of Human Monocytes through Estrogen and RANKL-regulated Interaction of Estrogen Receptor-α with BCAR1 and Traf6’, *Experimental cell research*. 315, 7, pp. 1287-301.

Rodriguez, A. (2021) ‘High HDL-Cholesterol Paradox: SCARB1-LAG3-HDL Axis’, *Current Atherosclerosis Reports*. 23, 1, p. 5.

Roijers, R. B. *et al.* (2011) ‘Microcalcifications in Early Intimal Lesions of Atherosclerotic Human Coronary Arteries’, *The american journal of pathology*. 178, 6, pp. 2879-87.

Rosenbaugh, E. G. *et al.* (2013) ‘Antioxidant-based therapies for angiotensin II-associated cardiovascular diseases’, *American journal of physiology - regulatory, integrative and comparative physiology*. 304, 11, pp. R917-28.

Rossouw, J. E. *et al.* (2002) ‘Risks and Benefits of Estrogen Plus Progestin in Healthy Postmenopausal Women: Principal Results From the Women’s Health Initiative Randomized Controlled Trial’, *JAMA*. 288, 3, pp. 321–333.

Rutkovskiy, A. *et al.* (2017) ‘Valve Interstitial Cells: The Key to Understanding the Pathophysiology of Heart Valve Calcification’, *Journal of the american heart association: Cardiovascular and cerebrovascular disease*. 6, 9, p. e006339.

Santavy, P. (2011) 'Aortic Valve Stenosis- Current Views on Diagnostics and Treatements', *IntechOpen* published 22 Sept. 2011.

Santos, G. M., Fairall, L. and Schwabe, J. W. R. (2011) ‘Negative Regulation by Nuclear Receptors: a Plethora of Mechanisms’, *Trends in endocrinology and metabolism*. 22, 3, pp. 87-93.

Sapra, L. *et al.* (2021) ‘Lactobacillus rhamnosus attenuates Bone Loss and Maintains Bone Health by Skewing Treg-Th17 Cell Balance in Ovx Mice’, *Scientific reports.* 11, 1, pp. 1–18.

Lo Sasso, G. *et al.* (2016) ‘The Apoe−/− Mouse Model: a Suitable Model to Study Cardiovascular and Respiratory Diseases in the Context of Cigarette Smoke Exposure and Harm Reduction’, *Journal of translational medicine*. 14, 1, p. 146.

Sathyamurthy, I. and Alex, S. (2015) ‘Calcific Aortic Valve Disease: is it Another Face of Atherosclerosis?’, *Indian heart journal*. 67, 5, pp. 503–6.

Schmidt, M. *et al.* (2006) ‘Inflammation and Sex Hormone Metabolism’, *Annals of the new york academy of sciences*. 1069, 1, pp. 236–246.

Schwartz, C. J. and Mitchell, J. R. (1962) ‘Observations on Localization of Arterial Plaques’, *Circulation research*. 11 pp. 63–73.

Serrano-Teruel, M. E. *et al.* (2019) ‘Mitochondrial DNA Haplogroups Influence the Risk of Aortic Stenosis’, *Asian cardiovascular & thoracic annals*. 27, 1, pp. 5–10.

Serrano, C. V. *et al.* (2019) ‘Association between Neutrophil-Lymphocyte and Platelet-Lymphocyte Ratios and Coronary Artery Calcification Score among Asymptomatic Patients: Data from a Cross-Sectional Study’, *Mediators of inflammation*. 2019, 6513847

Shah, T. A. *et al.* (2019) ‘Post-Transcriptional Bone Morphogenetic Protein 2 (BMP2) Gene Regulation in Aorta’, *bioRxiv*. *pre print*

Shi, X. *et al.* (2020) 'Calcification in Atherosclerotic Plaque Vulnerability: Friend or Foe?', *Frontiers in physiology*.11, 56.

Shioi, A. and Ikari, Y. (2018) 'Plaque Calcification During Atherosclerosis Progression and Regression', *Journal of atherosclerosis and thrombosis*. 25, 4, pp. 294-303.

Sider, K. L. *et al.* (2014) 'Evaluation of a Porcine Model of Early Aortic Valve Sclerosis', *Cardiovascular pathology.* 23, 5, pp. 289–297.

Sider, K. L., Blaser, M. C. and Simmons, C. A. (2011) 'Animal models of calcific aortic valve disease.', *International journal of inflammation*. 2011, p. 364310.

Simard, L. *et al.* (2017) 'Sex-Related Discordance Between Aortic Valve Calcification and Hemodynamic Severity of Aortic Stenosis', *Circulation research*. 120, 4, pp. 681–691.

Simmons, C. A. *et al.* (2005) 'Spatial Heterogeneity of Endothelial Phenotypes Correlates With Side-Specific Vulnerability to Calcification in Normal Porcine Aortic Valves', *Circulation research*. 96, 7, pp. 792-9.

Singh, A., Tandon, S. and Tandon, C. (2021) 'An Update on Vascular Calcification and Potential Therapeutics', *Molecular biology reports*. 48, 1, pp. 887–896.

Small, E. M., Frost, R. J. A. and Olson, E. N. (2010) 'MicroRNAs Add a New Dimension to Cardiovascular disease', *Circulation*. 121, 8, pp. 1022-32.

Smith, D. D. *et al.* (2010) 'Increased Aortic Atherosclerotic Plaque Development in Female Apolipoprotein E-null Mice is Associated with Elevated Thromboxane A2 and Decreased Prostacyclin Production', *Journal of physiology and pharmacology*. 61, 3, pp. 309–316.

Son, B.-K. *et al.* (2010) 'Androgen Receptor-dependent Transactivation of Growth Arrest-Specific Gene 6 Mediates Inhibitory Effects of Testosterone on Vascular Calcification.' 285, 10, pp. 7537–44.

Sorokin, V. *et al.* (2020) 'Role of Vascular Smooth Muscle Cell Plasticity and Interactions in Vessel Wall Inflammation', *Frontiers in immunology*. 11, p. 3053.

Speer, M. Y. *et al.* (2009) 'Smooth Muscle Cells Give Rise to Osteochondrogenic Precursors and Chondrocytes in Calcifying Arteries', *Circulation research*. 104, 6, pp. 733–741.

Sritharen, Y. *et al.* (2017) 'Pathophysiology of Aortic Valve Stenosis: Is It Both Fibrocalcific and Sex Specific?', *Physiology.* 32, 3, pp. 182–196.

Staines, K. A. *et al.* (2020) 'Conditional Deletion of E11/Podoplanin in Bone Protects Against Ovariectomy-induced Increases in Osteoclast Formation and Activity', *Bioscience reports*. 40, 1.

Su, X. and Peng, D. (2020) 'The Exchangeable Apolipoproteins in Lipid Metabolism and Obesity', *Clinica chimica acta*. 503, pp. 128–135.

Subramanya, V. *et al.* (2019) 'Association of Endogenous Sex Hormone Levels with Coronary Artery Calcium Progression Among Post-Menopausal Women in the Multi-Ethnic Study of Atherosclerosis (MESA)', *Journal of cardiovascular computed tomography*. 13, 1, pp. 41-47.

Sullivan, J. M. and Fowlkes, L. P. (1996) 'The Clinical Aspects of Estrogen and the Cardiovascular System', *Obstetrics & gynecology*. 87, 2, pp. 36S-43S.

Sullivan, M. L. *et al.* (1998) 'The Cardiac Toxicity of Anabolic Steroids', *Progress in cardiovascular diseases*. 41, 1, pp. 1–15.

Summerhill, V. I. *et al.* (2020) 'Sex-Specific Features of Calcific Aortic Valve Disease', *International journal of molecular sciences*. 21, 16, pp. 1–19.

Sun, J. *et al.* (2015) 'Role of Bone Morphogenetic Protein-2 in Osteogenic Differentiation of Mesenchymal Stem Cells', *Molecular medicine reports*. 12, 3, pp. 4230–4237.

Sun, Y. *et al.* (2017) 'Dietary Potassium Regulates Vascular Calcification and Arterial Stiffness'. *American society for clinical investigation*, 2, 19, p. e94920.

Synetos, A. *et al.* (2014) 'Catheter Based Inhibition of Arterial Calcification by Bisphosphonates in an Experimental Atherosclerotic Rabbit Animal Model', *International journal of cardiology*. 176, 1, pp. 177–181.

Tan, K. *et al.* (2019) 'Evaluation of Canine 2D Cell Cultures as Models of Myxomatous Mitral Valve Degeneration', *PLoS ONE*. 14, 8, p. e0221126.

Tanaka, K. *et al.* (2005) 'Age-Associated Aortic Stenosis in Apolipoprotein E-Deficient Mice', *Journal of the American college of cardiology*. 46, 1, pp. 134–141.

Tang, Y. *et al.* (2020) 'MicroRNA Profiles in Calcified and Healthy Aorta Differ: Therapeutic Impact of miR-145 and miR-378', *bioRxiv*. *pre print*

Tastet, L. *et al.* (2019) 'Staging Cardiac Damage in Patients With Asymptomatic Aortic Valve Stenosis', *Journal of the american college of cardiology*. 74, 4, pp. 550–563.

Thanassoulis, G. *et al.* (2013) 'Genetic Associations with Valvular Calcification and Aortic Stenosis.', *The new england journal of medicine*. 368, 6 pp. 503-512.

Thomassen, H. K. *et al.* (2017) 'Echocardiographic Aortic Valve Calcification and Outcomes in Women and Men With Aortic Stenosis.', *Heart.* 103, 20, pp. 1619–1624.

Tkatchenko, T. V. *et al.* (2009) 'Lack of Periostin Leads to Suppression of Notch1 Signaling and Calcific Aortic Valve Disease', *Physiological genomics*. 39, 3, pp. 160-168.

Travison, T. G. *et al.* (2016) 'Circulating Sex Steroids and Vascular Calcification in Community-Dwelling Men: The Framingham Heart Study', *The journal of clinical endocrinology & metabolism*. 101, 5, pp. 2160–2167.

Tsang, H. *et al.* (2017) 'Exploiting Novel Valve Interstitial Cell Lines to Study Calcific Aortic Valve Disease', *Molecular medicine reports*. 17, 2, pp. 2100–2106.

Tsang, H. G. *et al.* (2020) 'Expression of Calcification and Extracellular Matrix Genes in the Cardiovascular System of the Healthy Domestic Sheep (Ovis aries)', *Frontiers in genetics*. 11, 919.

Tseng, H. and Grande-Allen, K. J. (2011) 'Elastic fibers in the Aortic Valve Spongiosa: a Fresh Perspective on its Structure and Role in Overall Tissue Function', *Acta biomaterialia*. 7, 5, pp. 2101-8.

Tyson, J. *et al.* (2020) 'Mechanisms of the Osteogenic Switch of Smooth Muscle Cells in Vascular Calcification: WNT Signaling, BMPs, Mechanotransduction, and EndMT', *Bioengineering*, 7, 3, pp. 1–23.

Tzolos, E. and Dweck, M. R. (2020) '18F-Sodium Fluoride (18F-NaF) for Imaging Microcalcification Activity in the Cardiovascular System', *Arteriosclerosis, thrombosis, and vascular biology*. 40, pp. 1620–1626.

Vancheri, F. *et al.* (2019) 'Coronary Artery Microcalcification: Imaging and Clinical Implications', *Diagnostics*. 9, 4, p. 125.

Vinhas M. et al. (2013) Transthoracic echocardiography reference values in juvenile and adult 129/Sv mice. *Cardiovascular ultrasound.* 11, 12

Vossen, L. M. *et al.* (2020) 'Pharmacological and Nutritional Modulation of Vascular Calcification', *Nutrients*. 12, 1.

Walker, G. A. *et al.* (2004) 'Valvular Myofibroblast Activation by Transforming Growth Factor-beta: Implications for Pathological Extracellular Matrix Remodeling in Heart Valve Disease', *Circulation research*. 95,

3, pp. 253–260.

Wang, G. *et al.* (2015) 'Origin and Differentiation of Vascular Smooth Muscle Cells', *The journal of physiology*. 593, 14, pp. 3013-30.

Wang, H. *et al.* (2013) 'Characterization of Cell Subpopulations Expressing Progenitor Cell Markers in Porcine Cardiac Valves', *PLoS ONE*. 8, 7, p. e69667.

Wang, H., Leinwand, L. A. and Anseth, K. S. (2014) 'Cardiac Valve Cells and Their Microenvironment—Insights From In Vitro Studies', *Nature reviews. Cardiology*. 11, 12, pp. 715-27.

Wang, S. S. *et al.* (2009) 'Disruption of the Aortic Elastic Lamina and Medial Calcification Share Genetic determinants in mice', *Circulation.* 2, 6, pp. 573–582.

Weiss, R. M. *et al.* (2006) 'Calcific Aortic Valve Stenosis in Old Hypercholesterolemic Mice', *Circulation* 114, 19, pp. 2065–2069.

Whitsel, E. A. *et al.* (2001) 'Intramuscular Testosterone Esters and Plasma Lipids in Hypogonadal Men: a Meta-analysis', *The American journal of medicine*. 111, 4, pp. 261–269.

Williams, J. *et al.* (2015) 'BSN723T Prevents Atherosclerosis and Weight Gain in ApoE Knockout Mice Fed a Western Diet.', *WebmedCentral*. 6, 12.

Wingard, D. L., Suarez, L. and Barrett-Connor, E. (1983) 'The Sex Differential in Mortality from All Causes and Ischemic Heart Disease', *American journal of epidemiology*. 117, 2, pp. 165–172.

Woodward, H. J. *et al.* (2021) 'Regulatory Role of Sex Hormones in Cardiovascular Calcification', *International Journal of molecular sciences.* 22, 9, p 4620.

Wu, M., Rementer, C. and Giachelli, C. M. (2013) 'Vascular Calcification: an Update on Mechanisms and Challenges in Treatment', *Calcified tissue international*. 93, 4, p. 365.

Wu, X. *et al.* (2020) 'Estrogen Inhibits Vascular Calcification in Rats via Hypoxia-Induced Factor-1α Signaling', *Vascular*. 28, 4, pp. 465-474.

Xiao, F. *et al.* (2017) 'Sex-dependent Aortic Valve Pathology in Patients with Rheumatic Heart Disease', *PLOS ONE*. 12, 6, p. e0180230.

Yee, C. S. *et al.* (2016) 'Sclerostin Antibody Treatment Improves Fracture Outcomes in a Type I Diabetic Mouse Model', *Bone*. 82, pp. 122-34.

Yetkin, E. and Waltenberger, J. (2009) 'Molecular and Cellular Mechanisms of Aortic Stenosis', *International journal of cardiology*, 135, 1, pp. 4–13.

Yin, W. *et al.* (2012) 'Plasma Lipid Profiling Across Species for the Identification of Optimal Animal Models of Human Dyslipidemia', *Journal of lipid research*. 53, 1, pp. 51-65.

Zeadin, M. *et al.* (2009) 'Effect of Leptin on Vascular Calcification in Apolipoprotein E–Deficient Mice', *Arteriosclerosis, thrombosis, and vascular biology*. 29, 12, pp. 2069–2075.

Zechner, R., Madeo, F. and Kratky, D. (2017) 'Cytosolic Lipolysis and Lipophagy: Two Sides of the Same Coin', *Nature reviews molecular cell biology.* 18, 11, pp. 671–684.

Zeng, Z. *et al.* (2007) 'Macromolecular Transport in Heart Valves. I. Studies of Rat Valves with Horseradish Peroxidase', *American journal of physiology - heart and circulatory physiology*. 292, 6, pp. 2664–2670.

Zhang, Y. *et al.* (2011) 'A Program of MicroRNAs Controls Osteogenic Lineage Progression by Targeting Transcription Factor Runx2', *Proceedings of the national academy of sciences of the united states of america*. 108, 24, pp. 9863–9868

Zhou, Q. *et al.* (2021) 'Midkine Prevents Calcification of Aortic Valve Interstitial Cells via Intercellular Crosstalk', *Frontiers in cell and developmental biology*. 9, 794058.

Zhu, D. *et al.* (2011b) 'The Appearance and Modulation of Osteocyte Marker Expression during Calcification of Vascular Smooth Muscle Cells', *PLoS ONE*. 6, 5, p. e19595.

Zhu, D. *et al.* (2015) 'BMP-9 regulates the Osteoblastic Differentiation and Calcification of Vascular Smooth Muscle cells Through an ALK1 Mediated Pathway', *Journal of cellular and molecular medicine*. 19, 1, pp. 165–174.

Zhu, D., Hadoke, Patrick W. F., *et al.* (2016) 'Ablation of the Androgen Receptor From Vascular Smooth Muscle Cells Demonstrates a Role for Testosterone in Vascular Calcification', *Scientific reports*. 6, 1, p. 24807.

Zhu, Y. *et al.* (2019) 'Lactate Accelerates Calcification in VSMCs Through Suppression of BNIP3-Mediated Mitophagy', *Cellular signalling*. 58, pp. 53–64.

Ziegler, A., Gonzalez, L. and Blikslager, A. (2016) 'Large Animal Models: The Key to Translational Discovery in Digestive Disease Research', *Cellular and molecular gastroenterology and hepatology*. 2, 6, pp. 716-724.

Your PIPS student feedback will be uploaded on the EASTBIO website to share with others. **PLEASE INCLUDE AN IMAGE** FROM YOUR PIPS TO UPLOAD WITH THIS

PhD Student	**Holly Woodward, 2018, University of Edinburgh**		
Organisation	ECSA	Website	https://ecsa.citizen-science.net
What I did during my internship	During my internship I helped with organising the company conference. I also chaired sessions at the conference and writing the report on the conference afterwards.		
What I learned during my internship	I learnt about event advertising on social media and other platforms. I learnt how to write a structured report for a communication event.		
One thing I particularly enjoyed, found surprising or challenging during my internship	I enjoyed working with people a lot, I enjoyed the conference and the positive feedback we got from it.		
One output or achievement from my internship that can be shared with future employers	A successful conference		
Any wider long term benefit I expect from my internship	To be more confident in public speaking and hosting communication events.		

APPENDIX II

Primary Antibodies			
Target	Species	Manufacturer	Concentration
Vimentin (IF)	Mouse	Sigma	1 in 900
α-SMA (IF)	Rabbit	Abcam	1 in 200
CD31 (IF/IHC)	Rabbit	Abcam	1 in 50
IGG (IF)	mouse	Sigma	1 in 900
ENPP1 (Western)	Rabbit	Pierce	1 in 1000
RUNX2 (Western)	Rabbit	abcam	1 in 1000
BMP2 (Western)	Rabbit	Abcam	1 in 1000
β-actin (Western)	Mouse	Cell signalling	1 in 1000
α-SMA-cy3 direct conjugate (IHC)	Mouse	Sigma	1 in 1250
Mac2 (IHC)	Rat	Cedarline	1 in 800

Secondary Antibodies			
Target	Species	Manufacturer	Concentration
Anti mouse (IF)	Goat	Thermo Fisher	1 in 100
Anti rabbit (IF)	Donkey	Thermo Fisher	1 in 100
Anti rat (IHC)	Goat	Abcam	1 in 500
Anti rabbit (IHC)	Goat	Life Technologies	1 in 500
Dapi (IHC)		Abcam	1 in 1000
Anti Rabbit (Western)	Goat	Dako	1 in 500
Anti Mouse (Western)	Goat	Invitrogen	1 in 500

APPENDIX III

Diagrams of how measurements are taken and calculated in murine *in vivo* echocardiography are shown in *Figure 1 appendix III.* These measurements are used in the equations to calculate echocardiography measurements, shown in *table 1 appendix II.*

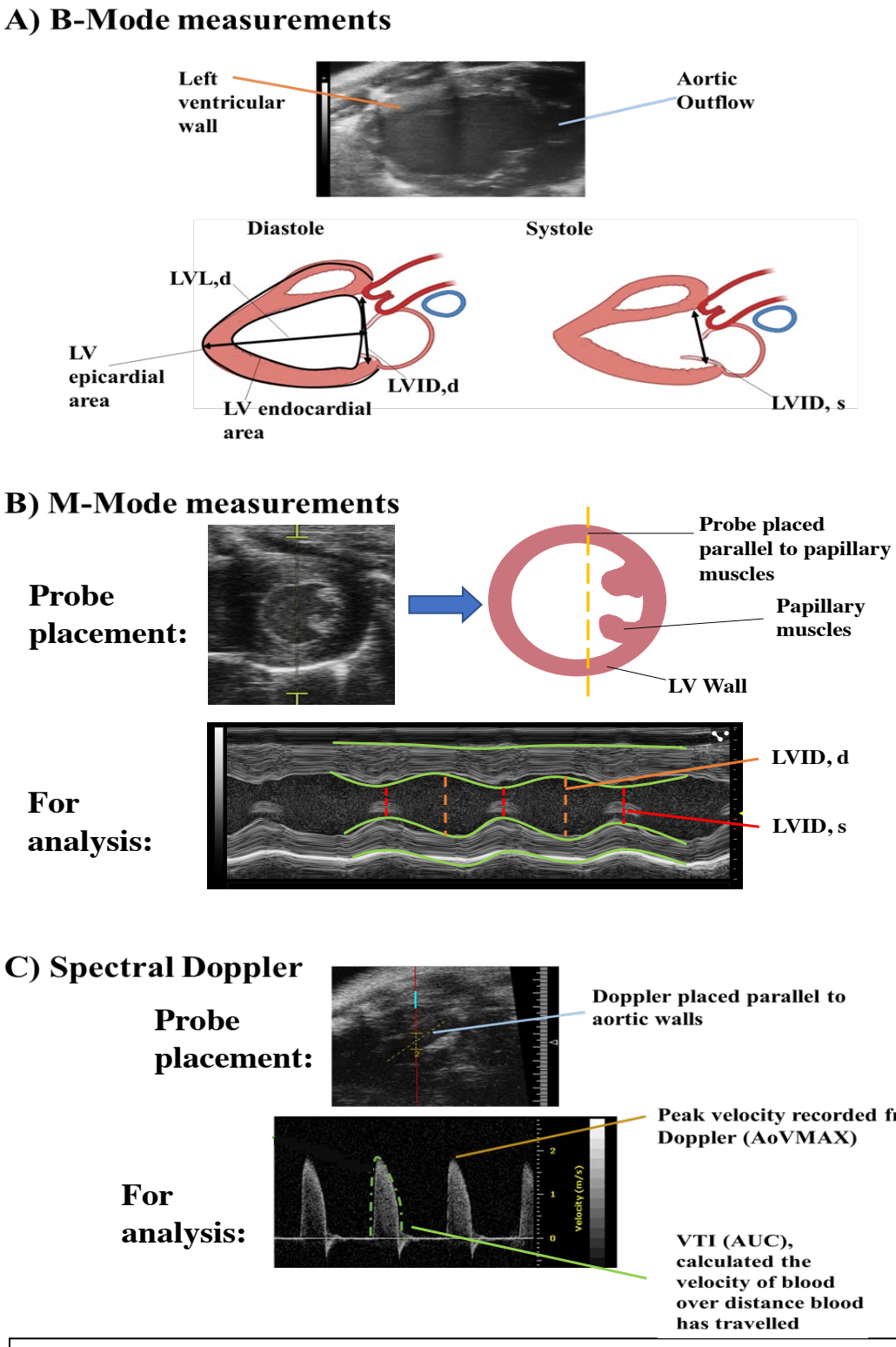

Figure 1 appendix III: Diagrams of echocardiography measurements. This figure shows how measurements were made in each mode of imaging, A) B-mode, B) M-mode and C) Spectral Doppler. These measurements were used to calculate parameters defined in table 1.

Table 1 appendix III: Echocardiography calculation. This tables displays the equations used to calculate echocardiography parameters that were used in this thesis. Each measurement was taken from echocardiography images, as shown in *figure 1*.

Parameter	Equation
B mode calculations	
LV Mass	$1.05 \text{ x } (\frac{5}{6} \text{ x } LVAEPI \text{ x } (LVL; d + \text{T}) - (\frac{5}{6} \text{ x } LVAEND \text{ x } LVL; d)$
LV Wall Thickness	$\frac{\sqrt{\frac{LV\ Area\ Epicardial\ Border; d}{\pi}} - \sqrt{\frac{LV\ Area\ Endocardial\ Border; d}{\pi}}}{\sqrt{\frac{LV\ Area\ Endocardial\ Border; d}{\pi}}}$
Cardiac Output	$Left\ Ventricular\ Stroke\ Volume\ x\ Heart\ Rate$
Ejection Fraction	$\frac{Left\ Ventricular\ \ Stroke\ Volume}{Left\ Ventricular\ \ Volume; d} x100$
M mode calculations	
LV Mass	$1.05\ LVID\ (d+\ LVPW;\ d+\ IVS;\ d^3 -\ LVID;\ d^3$
Fractional Shortening	$\frac{LVID; d - LVID; s}{LVID; d}\ x100$
Fractional Area Change	$\frac{Left\ Ventricular\ Area; d - Left\ Ventricular\ \ Area; s}{Left\ Ventricular\ Area; d} x100$
Ejection Fraction	$\frac{Left\ Ventricular\ \ Stroke\ Volume}{Left\ Ventricular\ \ Volume; d} x100$
Fractional Shortening	$\frac{LVID; d - LVID; s}{LVID; d}\ x100$
Pulse Wave Doppler Calculations	
Peak Gradient	$\frac{1.053}{2}\ x\ \frac{Ao\ Vmax^2}{100}$

Abbreviations:
LVAEPI= Epicardial area, LVAEND= endocardial area, LVL; d = Left ventricle length diastole, LVID; d= diastolic left ventricular internal diameter, LVID; s= systolic left ventricular internal diameter, LVPW; d= Left Ventricle Posterior Wall; Diastole, IVS; d = Intra-Ventricular Septum; Diastole, AoVmax= Aortic Maximum Velocity

Assumptions
The B-Mode and M-Mode calculations assume that the associated measurements have been made at end diastole or end systole, as appropriate. Density is assumed to be consistent in all measurements. These calculations also assume the volume of the ventricle is elliptical. Finally, the software interpolates between the points drawn in the analysis software (shown in Figure 1, appendix III).

Table 2 appendix III: Table of typical echocardiography measurements from a healthy adult male mouse. Numbers taken from Lindsey *et al.* (2018), Vinhas *et al.* (2013) and Tufan *et al.* (2010).

Parameter	Typical value in healthy male mice
B mode	
Left ventricular mass (mg)	80
Left ventricular wall thickness (mm)	0.8
Cardiac output (mL/min)	30
Ejection fraction (%)	60-70
M Mode	
Fractional shortening (FS) (%),	40
Posterior wall thickness (mm, PWT),	0.64
Left ventricular end-diastolic diameter (LVEDD) (mm)	3.4
Left ventricular end-systolic diameter (LVESD) (mm)	2.1
PW Doppler	
Velocity time integral (VTI) (mm)	5.5
Peak velocity (mm/s)	1500
Mean gradient (mmHg)	2
Peak gradient (mmHg)	4

International Journal of
Molecular Sciences

MDPI

Review

Regulatory Role of Sex Hormones in Cardiovascular Calcification

Holly J. Woodward [1,*], Dongxing Zhu [2,*], Patrick W. F. Hadoke [3] and Victoria E. MacRae [1]

[1] The Roslin Institute & R(D)SVS, University of Edinburgh, Easter Bush, Midlothian EH25 9RG, UK; vicky.macrae@roslin.ed.ac.uk
[2] Guangzhou Institute of Cardiovascular Disease, Guangdong Key Laboratory of Vascular Diseases, State Key Laboratory of Respiratory Disease, the Second Affiliated Hospital, Guangzhou Medical University, Guangzhou 510260, China
[3] University/BHF Centre for Cardiovascular Science, University of Edinburgh, Edinburgh, 47 Little France Crescent, Edinburgh EH16 4TJ, UK; patrick.hadoke@ed.ac.uk
* Correspondence: s1791143@ed.ac.uk (H.J.W.); dongxing.zhu@gzhmu.edu.cn (D.Z.); Tel.: +44-1316519158 (H.J.W.); +86-020-37103613 (D.Z.)

Abstract: Sex differences in cardiovascular disease (CVD), including aortic stenosis, atherosclerosis and cardiovascular calcification, are well documented. High levels of testosterone, the primary male sex hormone, are associated with increased risk of cardiovascular calcification, whilst estrogen, the primary female sex hormone, is considered cardioprotective. Current understanding of sexual dimorphism in cardiovascular calcification is still very limited. This review assesses the evidence that the actions of sex hormones influence the development of cardiovascular calcification. We address the current question of whether sex hormones could play a role in the sexual dimorphism seen in cardiovascular calcification, by discussing potential mechanisms of actions of sex hormones and evidence in pre-clinical research. More advanced investigations and understanding of sex hormones in calcification could provide a better translational outcome for those suffering with cardiovascular calcification.

Keywords: calcification; testosterone; estrogen; atherosclerosis; aortic valve

check for updates

Citation: Woodward, H.J.; Zhu, D.; Hadoke, P.W.F.; MacRae, V.E. Regulatory Role of Sex Hormones in Cardiovascular Calcification. *Int. J. Mol. Sci.* **2021**, *22*, 4620. https://doi.org/10.3390/ijms22094620

Academic Editors: Elena Bonanno, Virginia Tancredi, Manuel Scimeca, Rita Bonfiglio and David Magne

Received: 3 February 2021
Accepted: 26 April 2021
Published: 28 April 2021

Publisher's Note: MDPI stays neutral with regard to jurisdictional claims in published maps and institutional affiliations.

Copyright: © 2021 by the authors. Licensee MDPI, Basel, Switzerland. This article is an open access article distributed under the terms and conditions of the Creative Commons Attribution (CC BY) license (https://creativecommons.org/licenses/by/4.0/).

1. Clinical Consequences of Cardiovascular Calcification

Cardiovascular calcification describes the regulated deposition of mineral in blood vessels (vascular calcification) and heart valves (valvular calcification). Calcification is considered a predictor of risk associated with vascular disease [1], with more than 60% of people over 65 years of age displaying calcification in their cardiovascular system [2]. If left untreated, calcification can lead to a number of significant clinical consequences, including coronary insufficiency, aortic stenosis, and, in severe cases, heart failure. Vascular calcification was previously considered the consequence of passive precipitation of calcium and phosphate in the vascular system due to ageing. However, over the past decades, studies have revealed that cardiovascular calcification is indeed an actively regulated process that shares many similarities with physiological bone formation [3]. Despite extensive characterization of cardiovascular calcification in patients, the precise mechanisms that initiate and regulate calcification are still unclear. There is also a distinct sex difference in patients, with males having a tendency to acquire calcification earlier in life, and females developing calcification post-menopause [4]. Although the mechanism(s) behind this sex difference remain(s) to be fully elucidated, current evidence suggests a strong link between the specific actions of individual sex hormones and cardiovascular calcification. In this review, we seek to complement the recent excellent publication by Zhang et al. [5] by discussing the current understanding of the underlying mechanisms through which estrogens and androgens regulate calcification in blood vessels and valves, including a focus on the role for pre-clinical models in this research.

2. Types of Cardiovascular Calcification

According to its location, cardiovascular calcification can be divided into three major types: atherosclerotic intimal vascular calcification, medial vascular calcification, and aortic valve calcification. Within the scientific literature, cardiovascular and vascular calcification terms are frequently used interchangeably, however it is important to recognize that these are separate processes. The following section addresses these different types of calcification in more detail (Figure 1).

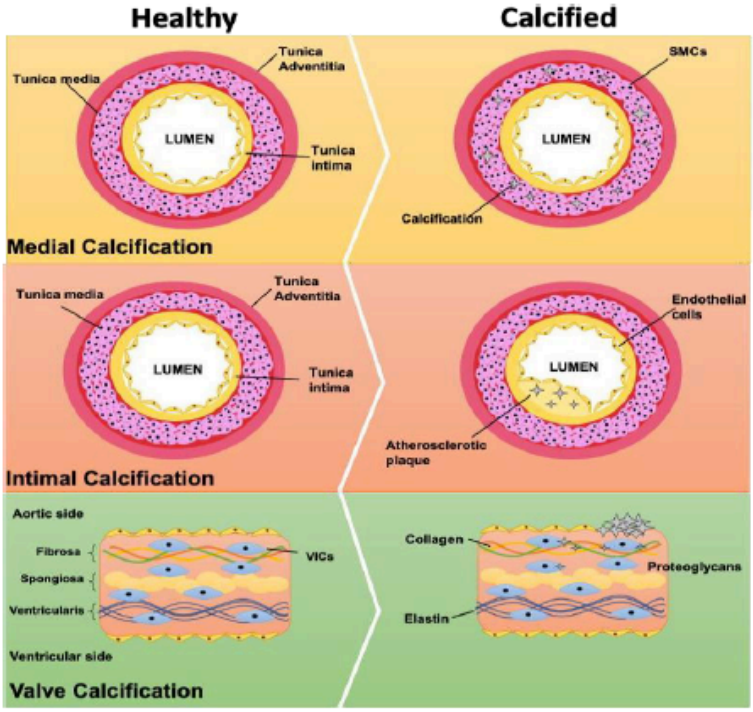

Figure 1. Comparison of types of cardiovascular calcification. The most common types of cardiovascular calcification are medial, intimal and valve. This figure displays both the normal and disease state for each of these diseases. Medial calcification occurs in the tunica media of the aorta, around the smooth muscle cells. Intimal calcification occurs within an atherosclerotic plaque in the intima of the artery. Valve interstitial cells, which could have a role in valve calcification, mostly accumulate in the aortic side of the valve.

2.1. *Atherosclerotic Intimal Calcification*

There are two types of calcification—intimal or medial—that occur in large arteries. Intimal calcification occurs as a result of atherosclerotic plaque development [6]. During blood vessel calcification, vascular smooth muscle cells (VSMCs) lose their contractile phenotype and become osteogenic, depositing matrix vesicles that enhance calcification [7]. Intimal calcification in atherosclerotic plaques can either stabilise or destabilise the plaque depending on the pattern of deposition and plaque composition. There is evidence that macrocalcification stabilises the fibrous cap covering the atherosclerotic plaque, whereas microcalcification destabilises the plaque, provoking a pro-inflammatory response causing increased susceptibility to plaque rupture [8]. Plaque rupture is considered a major cause of blood vessel stenosis and ischemia in patients, directly leading to thrombus formation and myocardial infarction [9]; although it has been suggested that superficial erosion of plaques may be more significant than plaque rupture as a cause of thrombosis [10]. Within blood vessels, VSMCs in the media, myofibroblasts in the adventitia and pericytes in the micro vessels can also become calcified [11].

2.2. Medial Calcification

Medial calcification is linked to altered bone and mineral metabolism and is a clinical predictor of coronary artery disease [2]. Additionally, it is highly prevalent in patients with end stage renal disease (ESRD) and diabetes [12]. Medial calcification occurs in vessels without inflammatory or lipid cell infiltration into the vessel wall and occurs along the elastic fibres of blood vessels causing vessel stiffening and decreased compliance [13]. Medial calcification can also occur in rare diseases such as Mönckeberg's Arteriosclerosis and Kawasaki disease [14]. The blood vessel stiffening (sclerosis) associated with medial calcification can result in increased blood pressure, local ischaemia and a high risk of vascular mortality [15,16]. Furthermore, medial calcification can lead to heart failure due to loss of aortic elasticity [17].

2.3. Valvular Calcification

Calcific aortic valve disease (CAVD) is the most common valve disease in the western world, affects up to 25% of the older population, and currently has no pharmaceutical interventions [18]. The pathogenesis of valve disease is not completely understood and there is a debate as to whether it is a feature of atherosclerosis or is independent of traditional CV risk factors. Endothelial cell disruption and basement membrane damage are evident in early-stage valve disease; one theory proposes that this could be caused by mechanical injury as a result of valve movement [19].

Clinically, progression of valve disease is well-characterised. Initial stages involve endothelial cell damage, infiltration of lipids and macrophages, as well as lipid oxidisation [20]. In later stages fibrosis and calcification cause obstruction of the aortic valve opening [20]. Valve interstitial cells (VICs) have been proposed to play a role in valve calcification. Quiescent VICs (qVICs) are the main cell type in a normal valve and function to maintain physiological valve structure and inhibit angiogenesis. If VICs are injured these cells can become activated. These activated VICs (aVICs) have the capacity to adapt to a dynamic environment through their activation and secretion of proteolytic enzymes mediating extracellular matrix remodelling followed by a normalization of phenotype [19]. When VICs are cultured in osteoblastic culture medium, they differentiate to osteoblastic cells (obVICs). Proteins associated with osteogenesis (including osteopontin, bone sialoprotein, alkaline phosphatase and bone morphogenetic protein (BMP)-2 and -4) have been identified by in vitro studies [21]. ObVICs also produce matrix vesicles which deposit calcium in the valves in the form of hydroxyapatite (HA) crystals. Development of macrocalcification and large calcium nodules is extremely damaging in valves. These nodules appear on the aortic side of the valve and restrict valve movement, causing stenosis and aortic regurgitation [22].

2.4. Pharmaceutical Strategies

Numerous pharmaceutical interventions against medial and intimal vascular calcification have been interrogated, ranging from statins to phosphate binders, with little therapeutic effect [15]. Vascular calcification is difficult to treat due to calcification having multiple causes, some of which are idiopathic. Furthermore, common diseases such as hypertension, chronic kidney disease, osteoporosis and hyperlipidaemia accelerate the progression of vascular calcification (reviewed in Lu et al. [23]). Therefore, future treatment approaches may need to be personalized, and reflect the other co-morbidities of the patient [24].

There are currently no pharmaceutical interventions for valve calcification. Clinically, severe stenosis can only be treated with either a mechanical or bioprosthetic valve replacement. Without surgery patient prognosis is between 2–3 years [25]. Synthetic valves characteristically have a 20-year lifespan, bringing increased mortality risks for patients requiring subsequent valve replacements [26,27]. Following surgery, patients are typically prescribed anticoagulants and/or immunosuppressants although their effectiveness on clinical outcomes and patient haemodynamic is debated [28].

3. Current Understanding of Cardiovascular Calcification

3.1. Calcification Is Similar to Physiological Bone Formation

Accumulating evidence shows that cardiovascular calcification is an active, cell-mediated process that shares many similarities with physiological bone formation [29] (Figure 2). Indeed, mature, lamellar bone, with hematopoietic elements and active bone remodelling, has been identified in up to 15% of calcified arteries [16]. Consistent with these findings, bone specific genes (including alkaline phosphatase (*ALP*), osteocalcin (*OCN*), runt-related transcription factor 2 (*RUNX2*), msh homeobox 2 (*MSX2*), and SRY-box transcription factor 9 (*SOX9*)) are significantly induced in calcified human arteries [30]. VSMCs, the predominant cell type in blood vessels, can undergo osteochondrogenic/osteocytic differentiation in the presence of calcifying conditions [31,32]. In vitro studies have demonstrated that high phosphate conditions mimicking the hyperphosphataemia seen in ESRD patients induces VSMC calcification and osteochondrogenic transition [31,33], in which the sodium-dependent phosphate cotransporter PiT1 plays a role. Knockdown of PiT1 expression in VSMCs in vitro significantly reduces phosphate uptake, expression of the osteogenic marker RUNX2, and calcium deposition [33].

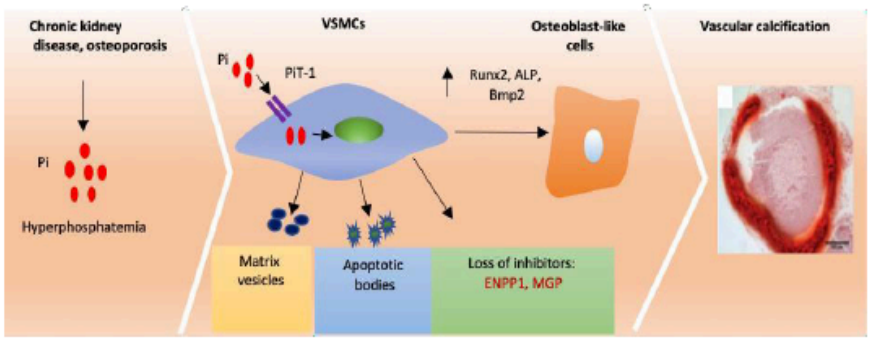

Figure 2. Vascular calcification mechanisms. In individuals with chronic kidney disease (CKD) high serum phosphate induces osteogenic transition and calcification of vascular smooth muscle cells (VSMCs) through the sodium-dependent phosphate cotransporter, Pit-1. In addition, normal blood vessels express a number of calcification inhibitors including ectonucleotide pyrophosphatase/phosphodiesterase 1 (ENPP1) and matrix Gla protein (MGP). Loss of these inhibitors promotes osteogenic transition and calcification of VSMCs. RUNX2, ALP and BMP2 become elevated which promotes osteoblast-like redifferentiation in SMCs. Matrix vesicles and apoptotic bodies also play a role in vascular calcification. Pi-phosphate RUNX2- runt-related transcription factor 2, ALP-alkaline phosphatase Bmp2-bone morphogenic protein 2.

Bone morphogenic proteins (BMPs) are regulators of physiological bone formation and have also been proposed to regulate vascular calcification. Previous reports, including studies from our laboratory, have shown that serum levels of BMP2 and BMP9 are elevated in patients with ESRD [34,35]. BMP2 enhances high phosphate-induced VSMC calcification in vitro and osteochondrogenic differentiation through up-regulation of RUNX2 [36]. Suppression of phosphate uptake using a sodium-dependent phosphate cotransporter inhibitor, phosphonoformic acid (PFA), attenuates BMP2-induced VSMC calcification in vitro [36]. To note, there is also evidence that PFA can inhibit calcium phosphate deposition independently of phosphate transport, potentially through a physicochemical mechanism [37].

BMP9 induces VSMC osteogenic differentiation and calcification through the orphan activin receptor-like kinase 1 (ALK1)-mediated pSmad1/5/8 signalling pathway [35]. The Wnt/β-catenin pathway is also involved in BMP9-induced VSMC calcification [38]. Consistent with these observations, pharmacological inhibition of BMP signalling reduces vascular calcification in a murine atherosclerotic model [39]. In contrast, BMP7 treatment efficiently reduces arterial calcification in murine models of atherosclerosis and ESRD [40].

3.2. Loss of Endogenous Inhibitors Induces Vascular Calcification

VSMCs within normal arteries have been shown to express a number of inhibitors, including matrix Gla protein (MGP) and ectonucleotide pyrophosphatase/phosphodiesterase 1 (ENPP1), which protect against ectopic calcification [19]. MGP is a secreted carboxyglutamic acid modified protein [41]. Mice that lack *Mgp* show arterial calcification [42]. Homozygous loss-of-function of MGP in humans is associated with Keutel's syndrome, in which patients exhibit excessive calcification of cartilaginous tissues and diffuse arterial calcification [43]. A possible mechanism through which MGP abrogates vascular calcification is by antagonism of BMP signalling. MGP can directly bind to BMP2 and BMP4, thus inhibiting their downstream signalling [44,45]. In accordance with these data, inhibition of BMP signalling using LDN-193189 or ALK3-Fc reduces vascular calcification in *Mgp* null mice [46]. MGP undergoes γ-glutamate carboxylation, in a vitamin-k dependent mechanism, to fully exert its protective effect on arterial calcification [47]. The vitamin K antagonist warfarin rapidly induces arterial calcification through inactivation of MGP in rodents, which can be rescued by a vitamin K-enriched diet [48].

ENPP1 is an ecto-enzyme that hydrolyzes ATP to generate pyrophosphate (PPi), which acts as a calcium phosphate crystallization inhibitor when high levels of PPi are produced. ENPP1 is widely expressed in various cells including chondrocytes, osteoblasts and VSMCs [49,50]. Tiptoe-walking (ttw/ttw) mice with a natural occurring nonsense truncation mutation in *Enpp1*, or *Enpp1* null mice, develop extensive peri-articular and arterial calcifications, and progressive ectopic ossification of the spinal ligaments [51,52]. Loss-of-function ENPP1 mutations in humans have been associated with Generalized Arterial Calcification of Infancy (GACI) [53,54]. Functional characterization of these ENPP1 mutations demonstrates a complete loss or partial reduction of its enzymatic activity, thereby reducing the generation of PPi [55]. Beyond the regulation of vascular calcification, ENPP1 also plays a role in the pathogenesis of osteoarthritis, atherosclerosis, insulin resistance and diabetes through mechanisms including the production of high levels of PPi [56–58].

3.3. Matrix Vesicles and Apoptotic Bodies Promote Cardiovascular Calcification

Matrix vesicles (MVs) are extracellular membrane-derived microparticles (approximately 100 nm in diameter). MVs have been implicated in bone mineralization, where they serve as the initial nucleation sites for hydroxyapatite formation [59]. Over recent years, the role of MVs in the regulation of cardiovascular calcification has attracted extensive attention. Previous work, including data from our laboratory, has reported the accumulation of MVs in calcified human aortic valves [60], aortic medial tissue, and atherosclerotic plaques [61]. These MVs are released by VSMCs, macrophages and valve interstitial cells, which play a role in initiating vascular calcification [60,62,63]. Proteomic analysis demonstrates that MVs released by cardiovascular cells during calcification show up-regulation of the calcium-binding Annexins but reduced expression of calcification inhibitors, including MGP and fetuin A [60,64]. Of note, vascular cell-secreted MVs contain a large amount of microRNAs, which also play a role in regulating vascular calcification [65]. A number of microRNAs identified in MVs released by vascular cells are involved in osteogenic differentiation. For example, miR-30 identified in MVs regulates the expression of osteogenic genes including *RUNX2* and *SMAD1*, and VSMC calcification [66]. In addition, MVs can be taken up by recipient VSMCs, leading to altered MAPK signalling and calcium metabolism that further drives vascular calcification [67].

Apoptosis, also termed programmed cell death, is a tightly regulated, energy dependent process which is mainly regulated by caspases [68]. Apoptotic cells exhibit blebbing, cell shrinkage, and nuclear and DNA fragmentation. Previous studies have shown apoptosis to increase during VSMC [69] and VIC calcification [70] in vitro. Induction of apoptosis using anti-Fas IgM and cycloheximide enhances VSMC calcification, while inhibition of apoptosis using the caspase inhibitor z-VAD-FMK attenuates VSMC calcification in vitro [69]. Furthermore, activation of the Gas6/Axl/Akt survival pathway reduces

VSMC calcification [71]. PiT1 is required for high phosphate-induced apoptosis in both VICs [72] and VSMCs [73]. Mechanistically, apoptotic bodies may expose phosphatidylserine on the outer membranes and generate a potential calcium-binding site suitable for HA deposition [69]. In this review we have focused on activation of calcification but it is important to note that calcification is a balance of both continuous activation and lack of resolution of calcification (reviewed in Carracedo et al. [74]).

4. The Role of Sex and Sex Hormones in Cardiovascular Calcification

4.1. Sex difference Exists in Cardiovascular Calcification

Sex differences and effects of sex hormones have been associated with cardiovascular calcification. Men have a 2-fold increased risk, compared with women, of developing CAVD [75]. Clinical studies of CAVD have demonstrated that for the same degree of stenosis, male patients have more calcification than females, whereas female patients have more fibrosis [76,77]. Furthermore, studies have shown that valve disease does not develop until after menopause in women [4].

Males also develop vascular disease, including atherosclerosis, earlier than females [78]. Circulating levels of testosterone, the predominant sex hormone in men, are positively associated with vascular calcification [79]. In elderly male patients with stable coronary artery disease, serum testosterone levels are inversely associated with vascular calcification [80]. Additionally, females with polycystic ovary disease (PCD) develop elevated levels of testosterone and have an increased risk of cardiovascular disease [81]. Over the past decades, it has become accepted that women are protected against cardiovascular disease; however, these protective effects are lost post-menopause. The most established hormonal change in postmenopausal women is the decline of estrogen levels [82], which is considered a causal factor for the increased incidence of vascular disease [83]. Serum levels of estrogen are negatively associated with vascular calcification [84]. Whilst established dogma highlights testosterone as a risk factor for calcification and estrogen as cardioprotective, the specific pathways underpinning how these sex hormones induce calcification have yet to be fully elucidated. Our current knowledge on the mechanisms through which sex hormones and their receptors interact with calcification, is summarised below.

4.2. Estrogen and Activation of the Estrogen Receptor Prevents Calcification

Clinical studies have demonstrated that estrogen replacement therapy (ERT) reduces cardiovascular disease in postmenopausal women [85] and that the effectiveness of ERT may be dependent on the "timing" of estrogen delivery relative to the age of menopause onset (within 6 years of menopause onset) [86]. Recently, the controlled Women's Health Initiative Study reported that long-term estrogen therapy reduced vascular calcification in postmenopausal women aged 50 to 59 years [87], consistent with a protective role. Studies employing estrogen replacement in ovariectomy-induced vascular calcification and osteoporosis in *Apoe*$^{-/-}$ mice further corroborate these data [88].

In VSMCs, the expression of estrogen receptor α (ERα) is greater than that of estrogen receptor β (ERβ). Estrogen mainly acts through ERα (Figure 3) to inhibit RANKL signalling, thereby reducing the osteogenic differentiation and calcification of VSMCs by upregulating BMP and downregulating MGP [88]. In addition, estrogen can inhibit vascular calcification through regulation of a range of molecular and cellular events, including hypoxia-induced factor-1α signalling [89], autophagy [90] and estrogen receptor α-dependent growth arrest-specific gene 6 transactivation [91]. Conversely, exogenous estrogen application has been reported to enhance vascular calcification in bovine aortic medial cells (in vitro) [92] and in aged male and female *ApoE*$^{-/-}$ mice (in vivo) [93]. These studies suggest a complex role of estrogen in vascular calcification. Estrogen can be generated in blood vessels by aromatase-mediated conversion of testosterone [94] and therefore, the activity of aromatase in blood vessels may also have a role in mediating the effects of estrogen on vascular calcification and warrants future investigation.

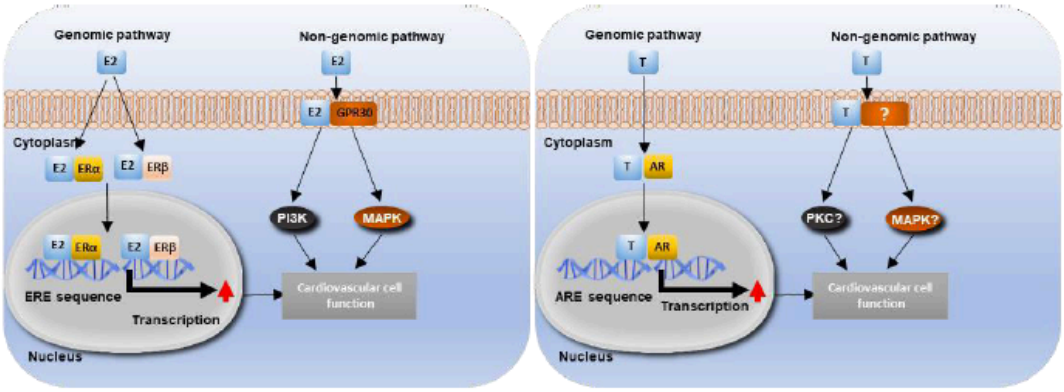

Figure 3. Estrogen binds to estrogen receptors (ERs), which act as transcription factors to regulate the expression of genes containing estrogen response elements (ERE). In addition, estrogen also rapidly induces phosphoinositide 3-kinase (PI3K) and mitogen-activated protein kinase (MAPK) signaling through the orphan G-protein coupled receptor (GPR30). Through genomic and non-genomic pathways, estrogen regulates a wide range of vascular cell functions, including proliferation, migration and senescence. E2- Estradiol. Testosterone acts in a similar mechanism, binding to the androgen receptor (AR), which act as transcription factors to regulate the expression of genes containing the androgen response elements (ARE). Testosterone is also believed to have non-genomic effects, although these pathways are less clear than estrogens.

4.3. Testosterone Is a Risk Factor for Cardiovascular Calcification

Low levels of circulating testosterone have been associated with increased coronary artery calcification in non-obese Korean men [95]. However, the recent Framingham Heart Study reports no significant association between testosterone and vascular calcification after model adjustment for other vascular risk factors in community-dwelling men [96]. In post-menopausal women, higher free serum testosterone is associated with coronary artery calcium progression [97]. Experimental studies show conflicting results on the effect of testosterone in calcification. In both male and female *Apoe*$^{-/-}$ mice, testosterone administration increases atherosclerotic calcification, which involves both androgen receptor- and estrogen receptor-mediated pathways [98]. Consistent with these results, our laboratory has previously shown that deletion of androgen receptor in VSMCs prevents testosterone-induced VSMC calcification in vitro [99]. Contrasting studies report an inhibitory effect of testosterone on VSMC calcification, which is mediated through androgen receptor-dependent transactivation of growth arrest-specific gene 6 signalling [100]. This discrepancy may reflect the complex actions of testosterone within different in vitro models. Clinical studies have shown that, in men, low endogenous testosterone levels are associated with cardiovascular disease [101] but also that high testosterone (for example with anabolic steroid use) has adverse cardiovascular effects [102]. This type of U-shaped relationship has been recognized with other hormones: for example, with corticosteroids where insufficiency causes Addison's disease but excess causes Cushing's syndrome [103].

5. Sex Hormones Mediate Cellular Signalling Pathways in the Cardiovascular System

5.1. Estrogen Signalling and Cardiovascular Function

Estrogen regulates cardiovascular function through several ERs, including ER α, ER β and the orphan G-protein-coupled receptor (GPR30) (Figure 3) [104,105]. Upon binding to estrogen, ERs undergo conformational change, leading to ER dimerization and binding to consensus (5^{t}GGTCAnnnTGACC 3^{t}) estrogen response element (ERE) sites on nuclear DNA. Co-regulators are then recruited to the estrogen-ER complex to activate or inhibit gene expression [106]. Estrogen also has the capacity to regulate gene expression indirectly by altering the activity of other transcription factors (such as AP1 and Sp1) [107,108]. In the absence of estrogen, ER at specific serine sites can be phosphorylated by Epidermal

Growth Factor (EGF), thereby mediating the stimulatory effects of EGF [109]. In addition to its genomic action, estrogen also induces acute non-genomic signalling pathways. Estrogen can bind to cell membranes to rapidly induce PI3K signalling. Furthermore, estrogen activates PI3K and MAPK through binding to GPR30 [110]. Functional classical ERs and non-classical GPR30 are widely expressed by vascular cells, including endothelial cells, VSMCs and cardiomyocytes [111]. Through estrogen's genomic and non-genomic mechanisms, regulation of a wide range of cardiovascular processes has been reported, such as: cardiac hypertrophy and failure, ischemic heart diseases, vascular injury and atherosclerosis [112,113].

5.2. Testosterone Signalling and Cardiovascular Function

Testosterone can regulate a range of cardiovascular functions and phenotypes, including vasodilation and vasoconstriction and intima-media thickness [114]. Similar to estrogen, testosterone induces both genomic and non-genomic actions. Testosterone binds to the androgen receptor (AR) to regulate gene expression through binding with the androgen response element (ARE) [115]. It also induces rapid non-genomic effects through binding to membrane androgen receptors or sensors, leading to the activation of a range of intracellular signalling molecules including calcium (Ca^{2+}), nitric oxide (NO), PKA, PKC, and MAPK [116]. The AR is expressed in several vascular cell types, including VSMCs and endothelial cells [117], and has been shown to be by expressed within the aortic valve (although the identity of valve cells expressing AR remains unclear). Testosterone can also be converted to 5 α-dihydrotestosterone (DHT; which has a higher binding activity to the AR) by the cytochrome P-450 enzyme, 5 α-reductase [118]. As testosterone can be converted into estrogen through aromatase, AR activation is also regulated by the cell-specific profile of metabolic products of testosterone [94]. Aromatase has been observed in vascular endothelial cells and 5 α-reductase has been shown to be expressed in VSMCs [119,120]. Aromatase expression has been observed in the aortic sinus of mice, but the cell-type expressing the enzyme is unknown [98].

6. Animal Models Offer Insights into Sex Differences in Cardiovascular Calcification

Females are typically under-represented in pre-clinical studies. Indeed, there is concerning evidence that within biological and medical research, 80% of studies that specified sex used only male subjects [121]. This lack of inclusion of female models likely contributes to the poorer treatment outcomes for women and a reduced understanding of sex differences in the calcification process [122]. In this section we discuss the use of both male and female in vivo models in calcification research.

6.1. Rodent Models

The human cardiovascular system comprises a complex arrangement of specialized structures with distinct functions. The current use of small rodents as the main model of human diseases is widespread. They are relatively cost effective and easy to maintain. Furthermore, rodent models offer opportunities for genetic manipulation and pre-clinical imaging techniques, making them indispensable for elucidating the mechanisms underpinning cardiovascular disease [123]. Nonetheless, limitations do exist, and significant vascular differences are apparent between humans and rodents.

Rodent models are highly resistant to vascular calcification. In order to investigate cardiovascular calcification in rodents, the pathological process has to be artificially induced, typically through diet, genetic manipulation or mechanical injury [124]. The most commonly used model of vascular and valvular calcification is the *Apoe*$^{-/-}$ mouse model fed a "western" diet [125]. However, calcification does not present uniformly across all animals within a cohort. Additional genetic models of calcification include mice lacking low density lipoprotein receptor (*Ldlr*) (intimal calcification) [126], *Enpp1*(medial) [127], *Mgp* (medial) [42] and ATP binding cassette subfamily C Member 6 (*Abcc6*) (medial) [128,129]. These models primarily display aortic calcification but valvular calcification has also been

observed in the *Ldlr*$^{-/-}$ and *Apoe*$^{-/-}$ mice [130]. Vascular calcification is a clinical consequence of ESRD, therefore it is reassuring that many models of this condition (including dietary addition of adenine, vitamin D administration and surgical induction of kidney insufficiency through 5/6 nephrectomy) have also been developed to interrogate the process of vascular calcification [131].

Exposure of rats to warfarin also produces calcification in the aorta and aortic valves [132]. However, inconsistent levels of calcification are typically observed in these rodent models, highlighting the requirement for more refined options [133].

A number of approaches can be employed to investigate the sex hormone effect on cardiovascular calcification in vivo. Sex hormone receptors can be ablated; the *Ar*$^{-/-}$ mouse has been utilized to investigate the effect of testosterone in vascular calcification [99]. Furthermore, studies involving mice lacking ERα and ERβ, have elucidated that these receptors are necessary for estrogen-mediated inhibition of the vascular injury response [134]. A physiological approach to investigating the effects of sex hormone involves the surgical removal (ovariectomy or castration) of sexual organs. Indeed, ovariectomised mice have been used to investigate bone calcification and show impaired bone formation [135].

Interestingly, sex differences in the atherosclerotic phenotype observed in *Apoe*$^{-/-}$ mice have been well-defined, whereby females tend to have larger plaques and increased calcification in those plaques [136]. Conversely, in human patients, females typically have smaller plaques and less calcification within the plaques [137]. Whilst investigations are frequently limited by the focus on a single sex, those rodent studies that have employed males and females to interrogate cardiovascular calcification pathways (Table 1), have produced divergent findings; highlighting the constraints of these animal models, and the importance of investigating both sexes in pre-clinical studies.

Table 1. Sex differences in rodent cardiovascular calcification studies. This table summarises key findings of cardiovascular calcification studies that have investigated both sexes, including the model and sex difference. In mice, increased calcification has typically been reported in females compared to males whereas in rats lower calcification has been observed in females. ApoE—Apolipoprotein E, DHT—Dihydrotestosterone, ↑—increased.

Model	Method of Calcification Induction	Type of Calcification	Sex Differences in Calcification	Treatment	Ref
Mouse					
ApoE$^{-/-}$	Aged to 36 weeks	Vascular and valvular	↑ calcification in females (aortic sinus)	17β-estradiol	[93]
ApoE$^{-/-}$	Crossed with *Itga8*$^{-/-}$	Vascular	↑ calcification in females		[93]
Klotho$^{-/-}$		Vascular	None	MicroRNA-145 and microRNA-378a	[138]
Klotho$^{-/-}$		Vascular	None	None	[139]
ApoE$^{-/-}$		Vascular, aortic sinus	↑ calcification in females	Testosterone and DHT	[98]
ApoE$^{-/-}$	18 months	Vascular	More vascular calcification in males		[140]
ApoE$^{-/-}$	Uraemia	Vascular	↑ calcification in females		[141]
C57BL/6J		Vascular	None		[141]
ApoA-II		Vascular	None		[141]
ApoE$^{-/-}$		Vascular	↑ calcification in females		[141]
ApoE$^{-/-}$	Hyperlipidaemic diet	Vascular	↑ calcification in females (medial arteries)		[142]
Rat					
Fisher	1α-Hydroxyvitamin D3	Vascular	↑ calcification in males		[143]
Wistar		Vascular	↑ calcification in males		[144]
Lewis Polycystic Kidney		Vascular	None	Perindopril	[145]

6.2. Large Animal Models

An inherent resistance to the development of cardiovascular calcification offers a crucial limitation to the employment of small animal models to investigate pathways underpinning this pathological process [146,147]. Subsequently novel therapeutic interventions for vascular or valvular calcification require pre-clinical testing in both small and large animal models to assess their suitability for clinical application.

Rabbits are a frequently employed, and highly appropriate, animal model of valvular calcification, due to the tri-layered composition of their valve leaflets (similar composition to humans) [148]. Methods of inducing calcification in rabbits include diet (e.g., vitamin D and long-term cholesterol treatment), genetic manipulation (e.g., LDLR mutated Watanabe rabbits), and surgical intervention (e.g., aortic balloon injury) [149–152]. However, studies have typically focused on male rabbits, with an extremely limited number of calcification studies including female animals. A recent study assessing both sexes in a matrix metallopeptidase 9 (MMP-9) overexpression model of atherosclerosis, revealed that both male and female rabbits developed calcified lesions in the aortic arch, with qualitative assessment suggesting greater calcification in males [153].

Porcine and ovine models are commonly used in investigations of aortic stenosis, with the majority of these studies examining synthetic or bioprosthetic valve replacements. An advantage of these larger animal models is the relative size of the vascular structures compared to humans, which permits the implementation of surgical procedures routinely employed in the clinic. Indeed, porcine valves have been an established option for human valve replacement for over 20 years [154]. Porcine models are highly appropriate due to the closely comparable valve anatomy, haemodynamic profiles and lipid composition to human patients [155]. They also show age-dependent insulin resistance [155] and are susceptible to the development of calcified plaques through exposure to a high fat diet [156]. The fibrosa layer in porcine aortic valves has similar features to the human fibrosa, including regions rich in collagen, elastin and proteoglycans [157]. As in humans, porcine aortic valves are more vulnerable to calcification on the aortic side, with molecular investigations confirming that valve endothelial cells (VECs) derived from the aortic side express osteogenic regulators including BMP4 [158]. Indeed, porcine VICs have been used to elucidate genetic sexual dimorphism, with recent microarray analysis of bovine cells highlighting the over-representation of cell pathways including cell death, proliferation, cell-to-cell signalling and movement in male-derived VICs compared to female-derived VICs [159,160]. Future aortic calcification studies are, however, required to confirm these findings in vivo. Due to their size and husbandry needs, when compared to smaller models, employing large animals will involve higher costs. Despite this, their importance in the field of human diseases is evident and will undoubtedly illuminate new biological pathways and mechanisms to facilitate the refinement of therapeutic strategies against cardiovascular calcification.

7. Future Perspectives

Despite testosterone being an established risk factor for cardiovascular calcification (and many other vascular diseases) its clinical impact is unclear and its mechanism of action in cardiovascular calcification remains to be fully understood. Whilst females are believed to be 'cardio-protected', pre-menopausal patients are severely under-represented in pre-clinical studies, which may contribute to our lack of understanding of the mechanisms underpinning the cardioprotective role of estrogens. Whether these sex hormones directly contribute to the increased vascular calcification observed in postmenopausal women remains to be investigated. Furthermore, elucidating these mechanisms is hampered not only by the limitations of pre-clinical models, but also by the severe under-representation of the female sex in pre-clinical research. Further research is essential to bridge the knowledge gap between the cellular mechanisms of calcification and the clinical sex risk factors, in order to ensure equitable treatment approaches for patients of both sexes.

Funding: H.J.W is supported by funding from the Biotechnology and Biological Science Research Council (BBSRC, no. BB/M010996/1) in the form of an EASTBIO Studentship Grant. V.E.M is supported by funding from the BBSRC in the form of an Institute Strategic Programme Grant ((BB/J004316/1). D.Z is supported by funding from the National Natural Science Foundation for Young Scientists of China (No. 81800428), The 'Yangcheng Scholar' Grant of Guangzhou (No. 202032768), The Innovation Project of Department of Education of Guangdong Province (No. 2017KTSCX158) and Guangdong Natural Science Foundation (No. 2018A030310178) and Science and Technology Projects of Guangzhou (No. 201904010289). P.W.F.H.'s research is supported by finding from the MRC (Confidence in Concept; MRC/CIC7/68), British Heart Foundation (RG/20/5/34796; PG/16/90/32518; REA3200409) and NC3Rs (NC/V001302/1).

Conflicts of Interest: The authors declare no conflict of interest.

References

1. Liu, W.; Zhang, Y.; Yu, C.-M.; Ji, Q.-W.; Cai, M.; Zhao, Y.-X.; Zhou, Y.-J. Current understanding of coronary artery calcification. *J. Geriatr. Cardiol.* **2015**, *12*, 668–675.
2. Chen, Q.; Wang, Z.-Y.; Chen, L.-Y.; Hu, H.-Y. Roles of High Mobility Group Box 1 in Cardiovascular Calcification. *Cell. Physiol. Biochem.* **2017**, *42*, 427–440. [CrossRef] [PubMed]
3. Shanahan, C.M.; Cary, N.R.B.; Salisbury, J.R.; Proudfoot, D.; Weissberg, P.L.; Edmonds, M.E. Medial Localization of Mineralization-Regulating Proteins in Association with Mönckeberg's Sclerosis. *Circulation* **1999**, *100*, 2168–2176. [CrossRef] [PubMed]
4. Christian, R.C.; Harrington, S.; Edwards, W.D.; Oberg, A.L.; Fitzpatrick, L.A. Estrogen Status Correlates with the Calcium Content of Coronary Atherosclerotic Plaques in Women. *J. Clin. Endocrinol. Metab.* **2002**, *87*, 1062–1067. [CrossRef] [PubMed]
5. Zhang, B.; Miller, V.M.; Miller, J.D. Influences of Sex and Estrogen in Arterial and Valvular Calcification. *Front. Endocrinol.* **2019**, *10*, 622. [CrossRef]
6. Amann, K. Media Calcification and Intima Calcification Are Distinct Entities in Chronic Kidney Disease: Figure 1. *Clin. J. Am. Soc. Nephrol.* **2008**, *3*, 1599–1605. [CrossRef]
7. Steitz, S.A.; Speer, M.Y.; Curinga, G.; Yang, H.-Y.; Haynes, P.A.; Aebersold, R.; Schinke, T.; Karsenty, G.; Giachelli, C.M. Smooth Muscle Cell Phenotypic Transition Associated with Calcification. *Circ. Res.* **2001**, *89*, 1147–1154. [CrossRef]
8. Nadra, I.; Mason, J.C.; Philippidis, P.; Florey, O.; Smythe, C.D.; McCarthy, G.M.; Landis, R.C.; Haskard, D.O. Proinflammatory Activation of Macrophages by Basic Calcium Phosphate Crystals via Protein Kinase C and MAP Kinase Pathways. *Circ. Res.* **2005**, *96*, 1248–1256. [CrossRef]
9. Bentzon, J.F.; Otsuka, F.; Virmani, R.; Falk, E. Mechanisms of Plaque Formation and Rupture. *Circ. Res.* **2014**, *114*, 1852–1866. [CrossRef]
10. Libby, P.; Pasterkamp, G. Requiem for the 'vulnerable plaque'. *Eur. Heart J.* **2015**, *36*, 2984–2987. [CrossRef]
11. Bardeesi, A.S.A.; Gao, J.; Zhang, K.; Yu, S.; Wei, M.; Liu, P.; Huang, H. A novel role of cellular interactions in vascular calcification. *J. Transl. Med.* **2017**, *15*, 1–8. [CrossRef]
12. Manzoor, S.; Ahmed, S.; Ali, A.; Han, K.H.; Sechopoulos, I.; O'Neill, A.; Fei, B.; O'Neill, W.C. Progression of Medial Arterial Calcification in CKD. *Kidney Int. Rep.* **2018**, *3*, 1328–1335. [CrossRef]
13. Ho, C.Y.; Shanahan, C.M. Medial Arterial Calcification. *Arter. Thromb. Vasc. Biol.* **2016**, *36*, 1475–1482. [CrossRef]
14. Lanzer, P.; Boehm, M.; Sorribas, V.; Thiriet, M.; Janzen, J.; Zeller, T.; Hilaire, C.S.; Shanahan, C. Medial vascular calcification revisited: Review and perspectives. *Eur. Heart J.* **2014**, *35*, 1515–1525. [CrossRef]
15. Wu, M.; Rementer, C.; Giachelli, C.M. Vascular Calcification: An Update on Mechanisms and Challenges in Treatment. *Calcif. Tissue Int.* **2013**, *93*, 365–373. [CrossRef]
16. Mohler, E.R.; Gannon, F.; Reynolds, C.; Zimmerman, R.; Keane, M.G.; Kaplan, F.S. Bone Formation and Inflammation in Cardiac Valves. *Circulation* **2001**, *103*, 1522–1528. [CrossRef] [PubMed]
17. Ooyama, T.; Sakamato, H. Elastase in the Prevention of Arterial Ageing and the Treatment of Atherosclerosis. *Novartis Found. Symposia* **2007**, *192*, 307–320. [CrossRef]
18. Schlotter, F.; Halu, A.; Pham, T.; Rogers, M.A.; Sharma, A.; Seidman, C.E.; Loscalzo, J.; Seidman, J.G.; Aikawa, M.; Singh, S.A.; et al. Spatiotemporal Multi-Omics Mapping Generates a Molecular Atlas of the Aortic Valve and Reveals Networks Driving Disease. *Circulation* **2018**, *138*, 377–393. [CrossRef] [PubMed]
19. Bäck, M.; Aranyi, T.; Cancela, M.L.; Carracedo, M.; Conceição, N.; Leftheriotis, G.; Macrae, V.; Martin, L.; Nitschke, Y.; Pasch, A.; et al. Endogenous Calcification Inhibitors in the Prevention of Vascular Calcification: A Consensus Statement From the COST Action EuroSoftCalcNet. *Front. Cardiovasc. Med.* **2019**, *5*, 196. [CrossRef]
20. Small, A.; Kiss, D.; Giri, J.; Anwaruddin, S.; Siddiqi, H.; Guerraty, M.; Chirinos, J.A.; Ferrari, G.; Rader, D.J. Biomarkers of Calcific Aortic Valve Disease. *Arter. Thromb. Vasc. Biol.* **2017**, *37*, 623–632. [CrossRef]
21. Liu, A.C.; Joag, V.R.; Gotlieb, A.I. The Emerging Role of Valve Interstitial Cell Phenotypes in Regulating Heart Valve Pathobiology. *Am. J. Pathol.* **2007**, *171*, 1407–1418. [CrossRef] [PubMed]
22. Normand, J.; Loire, R.; Zambartas, C. The anatomical aspects of adult aortic stenosis. *Eur. Heart J.* **1988**, *9*, 31–36. [CrossRef] [PubMed]

23. Lu, K.-C.; Wu, C.-C.; Yen, J.-F.; Liu, W.-C. Vascular Calcification and Renal Bone Disorders. *Sci. World J.* **2014**, *2014*, 1–20. [CrossRef]
24. Tinica, G.; Chistol, R.O.; Enache, M.; Constantin, M.M.L.; Ciocoiu, M.; Furnica, C. Long-term graft patency after coronary artery bypass grafting: Effects of morphological and pathophysiological factors. *Anatol. J. Cardiol.* **2018**, *20*, 275–282. [CrossRef] [PubMed]
25. Badran, A.A.; Vohra, H.A.; Livesey, S.A. Unoperated severe aortic stenosis: Decision making in an adult UK-based population. *Ann. R. Coll. Surg. Engl.* **2012**, *94*, 416–421. [CrossRef] [PubMed]
26. Toker, M.E.; Eren, E.; Guler, M.; Kirali, K.; Yanartas, M.; Balkanay, M.; Yakut, C. Second and third cardiac valve reoperations: Factors influencing death and long-term survival. *Tex. Heart Inst. J.* **2009**, *36*, 557–562.
27. Ranganath, N.K.; Koeckert, M.S.; Smith, D.E.; Hisamoto, K.; Loulmet, D.F.; Galloway, A.C.; Grossi, E.A. Aggressive tissue aortic valve replacement in younger patients and the risk of re-replacement: Implications from microsimulation analysis. *J. Thorac. Cardiovasc. Surg.* **2019**, *158*, 39–45.e1. [CrossRef]
28. Chakravarty, T.; Patel, A.; Kapadia, S.; Raschpichler, M.; Smalling, R.W.; Szeto, W.Y.; Abramowitz, Y.; Cheng, W.; Douglas, P.S.; Hahn, R.T.; et al. Anticoagulation After Surgical or Transcatheter Bioprosthetic Aortic Valve Replacement. *J. Am. Coll. Cardiol.* **2019**, *74*, 1190–1200. [CrossRef]
29. Chen, Y.; Zhao, X.; Wu, H. Arterial Stiffness. *Arter. Thromb. Vasc. Biol.* **2020**, *40*, 1078–1093. [CrossRef]
30. Tyson, K.L.; Reynolds, J.L.; McNair, R.; Zhang, Q.; Weissberg, P.L.; Shanahan, C.M. Osteo/Chondrocytic Transcription Factors and Their Target Genes Exhibit Distinct Patterns of Expression in Human Arterial Calcification. *Arter. Thromb. Vasc. Biol.* **2003**, *23*, 489–494. [CrossRef]
31. Zhu, D.; MacKenzie, N.C.W.; Millán, J.L.; Farquharson, C.; Macrae, V.E. The Appearance and Modulation of Osteocyte Marker Expression during Calcification of Vascular Smooth Muscle Cells. *PLoS ONE* **2011**, *6*, e19595. [CrossRef] [PubMed]
32. Speer, M.Y.; Yang, H.-Y.; Brabb, T.; Leaf, E.; Look, A.; Lin, W.-L.; Frutkin, A.; Dichek, D.; Giachelli, C.M. Smooth Muscle Cells Give Rise to Osteochondrogenic Precursors and Chondrocytes in Calcifying Arteries. *Circ. Res.* **2009**, *104*, 733–741. [CrossRef]
33. Li, X.; Yang, H.-Y.; Giachelli, C.M. Role of the Sodium-Dependent Phosphate Cotransporter, Pit-1, in Vascular Smooth Muscle Cell Calcification. *Circ. Res.* **2006**, *98*, 905–912. [CrossRef] [PubMed]
34. Dalfino, G.; Simone, S.; Porreca, S.; Cosola, C.; Balestra, C.; Manno, C.; Schena, F.P.; Grandaliano, G.; Pertosa, G. Bone morphogenetic protein-2 may represent the molecular link between oxidative stress and vascular stiffness in chronic kidney disease. *Atherosclerosis* **2010**, *211*, 418–423. [CrossRef] [PubMed]
35. Zhu, D.; MacKenzie, N.C.W.; Shanahan, C.M.; Shroff, R.C.; Farquharson, C.; Macrae, V.E. BMP-9 regulates the osteoblastic differentiation and calcification of vascular smooth muscle cells through an ALK1 mediated pathway. *J. Cell. Mol. Med.* **2015**, *19*, 165–174. [CrossRef]
36. Li, X.; Yang, H.-Y.; Giachelli, C.M. BMP-2 promotes phosphate uptake, phenotypic modulation, and calcification of human vascular smooth muscle cells. *Atherosclerosis* **2008**, *199*, 271–277. [CrossRef]
37. Villa-Bellosta, R.; Sorribas, V. Phosphonoformic Acid Prevents Vascular Smooth Muscle Cell Calcification by Inhibiting Calcium-Phosphate Deposition. *Arter. Thromb. Vasc. Biol.* **2009**, *29*, 761–766. [CrossRef] [PubMed]
38. He, F.; Wang, H.; Ren, W.-Y.; Ma, Y.; Liao, Y.-P.; Zhu, J.-H.; Cui, J.; Deng, Z.-L.; Su, Y.-X.; Gan, H.; et al. BMP9/COX-2 axial mediates high phosphate-induced calcification in vascular smooth muscle cells via Wnt/β-catenin pathway. *J. Cell. Biochem.* **2018**, *119*, 2851–2863. [CrossRef]
39. Derwall, M.S.; Malhotra, R.; Lai, C.S.; Beppu, Y.; Aikawa, E.; Seehra, J.S.; Zapol, W.M.; Bloch, K.D.; Yu, P.B. Inhibition of Bone Morphogenetic Protein Signaling Reduces Vascular Calcification and Atherosclerosis. *Arter. Thromb. Vasc. Biol.* **2012**, *32*, 613–622. [CrossRef]
40. Davies, M.R.; Lund, R.J.; Hruska, K.A. BMP-7 Is an Efficacious Treatment of Vascular Calcification in a Murine Model of Atherosclerosis and Chronic Renal Failure. *J. Am. Soc. Nephrol.* **2003**, *14*, 1559–1567. [CrossRef]
41. Mori, K.; Shioi, A.; Jono, S.; Nishizawa, Y.; Morii, H. Expression of matrix Gla protein (MGP) in an in vitro model of vascular calcification. *FEBS Lett.* **1998**, *433*, 19–22. [CrossRef]
42. Luo, G.; Ducy, P.; McKee, M.D.; Pinero, G.J.; Loyer, E.; Behringer, R.R.; Karsenty, G. Spontaneous calcification of arteries and cartilage in mice lacking matrix GLA protein. *Nat. Cell Biol.* **1997**, *386*, 78–81. [CrossRef] [PubMed]
43. Munroe, P.P.; Olgunturk, R.R.; Fryns, J.-P.J.-P.; Van Maldergem, L.; Ziereisen, F.; Yuksel, B.B.; Gardiner, M.R.; Chung, E.E. Mutations in the gene encoding the human matrix Gla protein cause Keutel syndrome. *Nat. Genet.* **1999**, *21*, 142–144. [CrossRef] [PubMed]
44. Yao, Y.; Zebboudj, A.F.; Shao, E.; Perez, M.; Boström, K. Regulation of Bone Morphogenetic Protein-4 by Matrix GLA Protein in Vascular Endothelial Cells Involves Activin-like Kinase Receptor 1. *J. Biol. Chem.* **2006**, *281*, 33921–33930. [CrossRef] [PubMed]
45. Zebboudj, A.F.; Imura, M.; Boström, K. Matrix GLA Protein, a Regulatory Protein for Bone Morphogenetic Protein-2. *J. Biol. Chem.* **2002**, *277*, 4388–4394. [CrossRef] [PubMed]
46. Malhotra, R.; Burke, M.F.; Hoeft, K.; Mayeur, C.; Jiramongkolchai, P.; Kumar, R.; Buys, E.S.; Yu, P.B.; Bloch, K.D.; Bloch, D.B.; et al. Inhibition of Bone Morphogenetic Protein Signal Transduction Prevents the Medial Vascular Calcification Associated with Matrix Gla Protein Deficiency. *PLoS ONE* **2015**, *10*, e0117098. [CrossRef] [PubMed]

47. Cranenburg, E.C.M.; Van Spaendonck-Zwarts, K.Y.; Bonafé, L.; Crettol, L.M.; Rödiger, L.A.; Dikkers, F.G.; Van Essen, A.J.; Superti-Furga, A.; Alexandrakis, E.; Vermeer, C.; et al. Circulating matrix γ-carboxyglutamate protein (MGP) species are refractory to vitamin K treatment in a new case of Keutel syndrome. *J. Thromb. Haemost.* **2011**, *9*, 1225–1235. [CrossRef] [PubMed]
48. Schurgers, L.J.; Spronk, H.M.H.; Soute, B.A.M.; Schiffers, P.M.; Demey, J.G.R.; Vermeer, C. Regression of warfarin-induced medial elastocalcinosis by high intake of vitamin K in rats. *Blood* **2006**, *109*, 2823–2831. [CrossRef]
49. Goding, J.W.; Terkeltaub, R.; Maurice, M.; Deterre, P.; Sali, A.; Belli, S.I. Ecto-phosphodiesterase/pyrophosphatase of lymphocytes and non-lymphoid cells: Structure and function of the PC-1 family. *Immunol. Rev.* **1998**, *161*, 11–26. [CrossRef] [PubMed]
50. Nitschke, Y.; Yan, Y.; Buers, I.; Kintziger, K.; Askew, K.; Rutsch, F. ENPP1-Fc prevents neointima formation in generalized arterial calcification of infancy through the generation of AMP. *Exp. Mol. Med.* **2018**, *50*, 1–12. [CrossRef]
51. Okawa, A.; Nakamura, I.; Goto, S.; Moriya, H.; Nakamura, Y.; Ikegawa, S. Mutation in Npps in a mouse model of ossification of the posterior longitudinal ligament of the spine. *Nat. Genet.* **1998**, *19*, 271–273. [CrossRef] [PubMed]
52. MacKenzie, N.C.W.; Zhu, D.; Milne, E.M.; Hof, R.V.T.; Martin, A.; Quarles, D.L.; Millán, J.L.; Farquharson, C.; Macrae, V.E. Altered Bone Development and an Increase in FGF-23 Expression in Enpp1$^{-/-}$ Mice. *PLoS ONE* **2012**, *7*, e32177. [CrossRef]
53. Rutsch, F.; Böyer, P.; Nitschke, Y.; Ruf, N.; Lorenz-Depierieux, B.; Wittkampf, T.; Weissen-Plenz, G.; Fischer, R.-J.; Mughal, Z.; Gregory, J.W.; et al. Hypophosphatemia, Hyperphosphaturia, and Bisphosphonate Treatment Are Associated With Survival Beyond Infancy in Generalized Arterial Calcification of Infancy. *Circ. Cardiovasc. Genet.* **2008**, *1*, 133–140. [CrossRef] [PubMed]
54. Ruf, N.; Uhlenberg, B.; Terkeltaub, R.; Nürnberg, P.; Rutsch, F. The mutational spectrum ofENPP1as arising after the analysis of 23 unrelated patients with generalized arterial calcification of infancy (GACI). *Hum. Mutat.* **2004**, *25*, 98. [CrossRef]
55. Stella, J.; Buers, I.; Van De Wetering, K.; Höhne, W.; Rutsch, F.; Nitschke, Y. Effects of Different Variants in theENPP1Gene on the Functional Properties of Ectonucleotide Pyrophosphatase/Phosphodiesterase Family Member 1. *Hum. Mutat.* **2016**, *37*, 1190–1201. [CrossRef] [PubMed]
56. Roberts, F.; Zhu, D.; Farquharson, C.; Macrae, V.E. ENPP1 in the Regulation of Mineralization and Beyond. *Trends Biochem. Sci.* **2019**, *44*, 616–628. [CrossRef]
57. Huesa, C.; Zhu, D.; Glover, J.D.; Ferron, M.; Karsenty, G.; Milne, E.M.; Millan, J.L.; Ahmed, S.F.; Farquharson, C.; Morton, N.M.; et al. Deficiency of the bone mineralization inhibitor NPP1 protects mice against obesity and diabetes. *Dis. Model. Mech.* **2014**, *7*, 1341–1350. [CrossRef]
58. Roberts, F.L.; Rashdan, N.A.; Phadwal, K.; Markby, G.R.; Dillon, S.; Zoll, J.; Berger, J.; Milne, E.; Orriss, I.R.; Karsenty, G.; et al. Osteoblast-specific deficiency of ectonucleotide pyrophosphatase or phosphodiesterase-1 engenders insulin resistance in high-fat diet fed mice. *J. Cell. Physiol.* **2021**, *236*, 4614–4624. [CrossRef]
59. Golub, E.E. Role of matrix vesicles in biomineralization. *Biochim. Biophys. Acta Gen. Subj.* **2009**, *1790*, 1592–1598. [CrossRef]
60. Cui, L.; Rashdan, N.A.; Zhu, N.; Milne, E.M.; Ajuh, P.; Milne, G.; Helfrich, M.H.; Lim, K.; Prasad, S.; Lerman, D.A.; et al. End stage renal disease-induced hypercalcemia may promote aortic valve calcification via Annexin VI enrichment of valve interstitial cell derived-matrix vesicles. *J. Cell. Physiol.* **2017**, *232*, 2985–2995. [CrossRef]
61. Hutcheson, J.D.; Goettsch, C.; Bertazzo, S.S.; Maldonado, N.; Ruiz, J.L.; Goh, W.; Yabusaki, K.; Faits, T.; Bouten, C.C.; Franck, G.; et al. Genesis and growth of extracellular-vesicle-derived microcalcification in atherosclerotic plaques. *Nat. Mater.* **2016**, *15*, 335–343. [CrossRef] [PubMed]
62. Chen, N.X.; O'Neill, K.D.; Chen, X.; Moe, S.M. Annexin-Mediated Matrix Vesicle Calcification in Vascular Smooth Muscle Cells. *J. Bone Miner. Res.* **2008**, *23*, 1798–1805. [CrossRef]
63. New, S.E.P.; Goettsch, C.; Aikawa, M.; Marchini, J.F.; Shibasaki, M.; Yabusaki, K.; Libby, P.; Shanahan, C.M.; Croce, K.; Aikawa, E. Macrophage-Derived Matrix Vesicles. *Circ. Res.* **2013**, *113*, 72–77. [CrossRef]
64. Kapustin, A.N.; Chatrou, M.L.L.; Drozdov, I.; Zheng, Y.; Davidson, S.M.; Soong, D.; Furmanik, M.; Sanchis, P.; De Rosales, R.T.M.; Alvarez-Hernandez, D.; et al. Vascular Smooth Muscle Cell Calcification Is Mediated by Regulated Exosome Secretion. *Circ. Res.* **2015**, *116*, 1312–1323. [CrossRef] [PubMed]
65. Goettsch, C.; Hutcheson, J.D.; Aikawa, E. MicroRNA in Cardiovascular Calcification. *Circ. Res.* **2013**, *112*, 1073–1084. [CrossRef] [PubMed]
66. Chaturvedi, P.; Chen, N.X.; O'Neill, K.; McClintick, J.N.; Moe, S.M.; Janga, S.C. Differential miRNA Expression in Cells and Matrix Vesicles in Vascular Smooth Muscle Cells from Rats with Kidney Disease. *PLoS ONE* **2015**, *10*, e0131589. [CrossRef]
67. Chen, N.X.; O'Neill, K.D.; Moe, S.M. Matrix vesicles induce calcification of recipient vascular smooth muscle cells through multiple signaling pathways. *Kidney Int.* **2018**, *93*, 343–354. [CrossRef]
68. Tsuchiya, K.; Nakajima, S.; Hosojima, S.; Nguyen, D.T.; Hattori, T.; Le, T.M.; Hori, O.; Mahib, M.R.; Yamaguchi, Y.; Miura, M.; et al. Caspase-1 initiates apoptosis in the absence of gasdermin D. *Nat. Commun.* **2019**, *10*, 1–19. [CrossRef]
69. Proudfoot, D.; Skepper, J.N.; Hegyi, L.; Bennett, M.R.; Shanahan, C.M.; Weissberg, P.L. Apoptosis Regulates Human Vascular Calcification In Vitro. *Circ. Res.* **2000**, *87*, 1055–1062. [CrossRef] [PubMed]
70. Chen, Z.; Gordillo-Martinez, F.; Jiang, L.; He, P.; Hong, W.; Wei, X.; Staines, K.A.; Macrae, V.E.; Zhang, C.; Yu, D.; et al. Zinc ameliorates human aortic valve calcification through GPR39 mediated ERK1/2 signalling pathway. *Cardiovasc. Res.* **2021**, *117*, 820–835. [CrossRef]
71. Kim, H.; Kim, H.-J.; Lee, K.; Kim, J.-M.; Kim, H.S.; Kim, J.-R.; Ha, C.-M.; Choi, Y.-K.; Lee, S.J.; Kim, J.-Y.; et al. α-Lipoic acid attenuates vascular calcification via reversal of mitochondrial function and restoration of Gas6/Axl/Akt survival pathway. *J. Cell. Mol. Med.* **2011**, *16*, 273–286. [CrossRef] [PubMed]

72. El Husseini, D.; Boulanger, M.-C.; Fournier, D.; Mahmut, A.; Bossé, Y.; Pibarot, P.; Mathieu, P. High Expression of the Pi-Transporter SLC20A1/Pit1 in Calcific Aortic Valve Disease Promotes Mineralization through Regulation of Akt-1. *PLoS ONE* **2013**, *8*, e53393. [CrossRef]
73. Chavkin, N.W.; Chia, J.J.; Crouthamel, M.H.; Giachelli, C.M. Phosphate uptake-independent signaling functions of the type III sodium-dependent phosphate transporter, PiT-1, in vascular smooth muscle cells. *Exp. Cell Res.* **2015**, *333*, 39–48. [CrossRef]
74. Carracedo, M.; Artiach, G.; Arnardottir, H.; Bäck, M. The resolution of inflammation through omega-3 fatty acids in atherosclerosis, intimal hyperplasia, and vascular calcification. *Semin. Immunopathol.* **2019**, *41*, 757–766. [CrossRef]
75. Gomel, M.A.; Lee, R.; Grande-Allen, K.J. Comparing the Role of Mechanical Forces in Vascular and Valvular Calcification Progression. *Front. Cardiovasc. Med.* **2019**, *5*, 197. [CrossRef]
76. Simard, L.; Côté, N.; Dagenais, F.; Mathieu, P.; Couture, C.; Trahan, S.; Bossé, Y.; Mohammadi, S.; Pagé, S.; Joubert, P.; et al. Sex-Related Discordance Between Aortic Valve Calcification and Hemodynamic Severity of Aortic Stenosis. *Circ. Res.* **2017**, *120*, 681–691. [CrossRef]
77. Nitsche, C.; Koschutnik, M.; Kammerlander, A.; Hengstenberg, C.; Mascherbauer, J. Gender-specific differences in valvular heart disease. *Wien. Klin. Wochenschr.* **2020**, *132*, 61–68. [CrossRef] [PubMed]
78. Stout, R.W. Atherosclerosis in males and females. *Horm. Atheroscler.* **1982**, 97–111. [CrossRef]
79. Pérez-López, F.R.; Larrad-Mur, L.; Kallen, A.; Chedraui, P.; Taylor, H.S. Review: Gender Differences in Cardiovascular Disease: Hormonal and Biochemical Influences. *Reprod. Sci.* **2010**, *17*, 511–531. [CrossRef] [PubMed]
80. Lai, J.; Ge, Y.; Shao, Y.; Xuan, T.; Xia, S.; Li, M. Low serum testosterone level was associated with extensive coronary artery calcification in elderly male patients with stable coronary artery disease. *Coron. Artery Dis.* **2015**, *26*, 437–441. [CrossRef]
81. Calderon-Margalit, R.; Siscovick, D.; Merkin, S.S.; Wang, E.; Daviglus, M.L.; Schreiner, P.J.; Sternfeld, B.; Williams, O.D.; Lewis, C.E.; Azziz, R.; et al. Prospective Association of Polycystic Ovary Syndrome With Coronary Artery Calcification and Carotid-Intima-Media Thickness. *Arter. Thromb. Vasc. Biol.* **2014**, *34*, 2688–2694. [CrossRef]
82. Zhu, D.; Li, X.; Macrae, V.E.; Simoncini, T.; Fu, X. Extragonadal Effects of Follicle-Stimulating Hormone on Osteoporosis and Cardiovascular Disease in Women during Menopausal Transition. *Trends Endocrinol. Metab.* **2018**, *29*, 571–580. [CrossRef]
83. Dalal, P.K.; Agarwal, M. Postmenopausal syndrome. *Indian J. Psychiatry* **2015**, *57*, 222–232. [CrossRef] [PubMed]
84. Nakao, J.; Orimo, H.; Ooyama, T.; Shiraki, M. Low serum estradiol levels in subjects with arterial calcification. *Atherosclerosis* **1979**, *34*, 469–474. [CrossRef]
85. Lopez-Pier, M.A.; Lipovka, Y.; Koppinger, M.P.; Harris, P.R.; Konhilas, J.P. The clinical impact of estrogen loss on cardio-vascular disease in menopausal females. *Med. Res. Arch.* **2018**, *6*, 1663. [PubMed]
86. Hodis, H.N.; Mack, W.J.; Shoupe, D.; Azen, S.P.; Stanczyk, F.Z.; Hwang-Levine, J.; Budoff, M.J.; Henderson, V.W. Methods and baseline cardiovascular data from the Early versus Late Intervention Trial with Estradiol testing the menopausal hormone timing hypothesis. *Menopause* **2015**, *22*, 391–401. [CrossRef]
87. Manson, J.E.; Allison, M.A.; Rossouw, J.E.; Carr, J.J.; Langer, R.D.; Hsia, J.; Kuller, L.H.; Cochrane, B.B.; Hunt, J.R.; Ludlam, S.E.; et al. Estrogen Therapy and Coronary-Artery Calcification. *N. Engl. J. Med.* **2007**, *356*, 2591–2602. [CrossRef]
88. Osako, M.K.; Nakagami, H.; Koibuchi, N.; Shimizu, H.; Nakagami, F.; Koriyama, H.; Shimamura, M.; Miyake, T.; Rakugi, H.; Morishita, R. Estrogen Inhibits Vascular Calcification via Vascular RANKL System. *Circ. Res.* **2010**, *107*, 466–475. [CrossRef]
89. Wu, X.; Zhao, Q.; Chen, Z.; Geng, Y.-J.; Zhang, W.; Zhou, Q.; Yang, W.; Liu, Q.; Liu, H. Estrogen inhibits vascular calcification in rats via hypoxia-induced factor-1 α signaling. *Vascular* **2020**, *28*, 465–474. [CrossRef]
90. Peng, Y.-Q.; Xiong, D.; Lin, X.; Cui, R.-R.; Xu, F.; Zhong, J.-Y.; Zhu, T.; Wu, F.; Mao, M.-Z.; Liao, X.-B.; et al. Oestrogen Inhibits Arterial Calcification by Promoting Autophagy. *Sci. Rep.* **2017**, *7*, 1–14. [CrossRef] [PubMed]
91. Nanao-Hamai, M.; Son, B.-K.; Hashizume, T.; Ogawa, S.; Akishita, M. Protective effects of estrogen against vascular calcification via estrogen receptor α-dependent growth arrest-specific gene 6 transactivation. *Biochem. Biophys. Res. Commun.* **2016**, *480*, 429–435. [CrossRef]
92. Balica, M.; Bostrom, K.I.; Shin, V.; Tillisch, K.; Demer, L.L. Calcifying Subpopulation of Bovine Aortic Smooth Muscle Cells Is Responsive to 17 & beta-Estradiol. *Circulation* **1997**, *95*, 1954–1960. [CrossRef]
93. McRobb, L.S.; McGrath, K.C.; Tsatralis, T.; Liong, E.C.; Tan, J.T.; Hughes, G.; Handelsman, D.J.; Heather, A.K. Estrogen Receptor Control of Atherosclerotic Calcification and Smooth Muscle Cell Osteogenic Differentiation. *Arter. Thromb. Vasc. Biol.* **2017**, *37*, 1127–1137. [CrossRef]
94. Harada, N.; Sasano, H.; Murakami, H.; Ohkuma, T.; Nagura, H.; Takagi, Y. Localized expression of aromatase in human vascular tissues. *Circ. Res.* **1999**, *84*, 1285–1291. [CrossRef]
95. Park, B.-J.; Shim, J.-Y.; Lee, Y.-J.; Lee, J.-H.; Lee, H.-R. Inverse relationship between bioavailable testosterone and subclinical coronary artery calcification in non-obese Korean men. *Asian J. Androl.* **2012**, *14*, 612–615. [CrossRef]
96. Travison, T.G.; O'Donnell, C.J.; Bhasin, S.; Massaro, J.M.; Hoffmann, U.; Vasan, R.S.; D'Agostino, R.B.; Basaria, S. Circulating Sex Steroids and Vascular Calcification in Community-Dwelling Men: The Framingham Heart Study. *J. Clin. Endocrinol. Metab.* **2016**, *101*, 2160–2167. [CrossRef]
97. Subramanya, V.; Zhao, D.; Ouyang, P.; Ying, W.; Vaidya, D.; Ndumele, C.E.; Heckbert, S.R.; Budoff, M.J.; Post, W.S.; Michos, E.D. Association of endogenous sex hormone levels with coronary artery calcium progression among post-menopausal women in the Multi-Ethnic Study of Atherosclerosis (MESA). *J. Cardiovasc. Comput. Tomogr.* **2019**, *13*, 41–47. [CrossRef] [PubMed]

98. McRobb, L.; Handelsman, D.J.; Heather, A.K. Androgen-Induced Progression of Arterial Calcification in Apolipoprotein E-Null Mice Is Uncoupled from Plaque Growth and Lipid Levels. *Endocrinology* **2009**, *150*, 841–848. [CrossRef] [PubMed]
99. Zhu, D.; Hadoke, P.W.F.; Wu, J.; Vesey, A.T.; Lerman, D.A.; Dweck, M.R.; Newby, D.E.; Smith, L.B.; Macrae, V.E. Ablation of the androgen receptor from vascular smooth muscle cells demonstrates a role for testosterone in vascular calcification. *Sci. Rep.* **2016**, *6*, 24807. [CrossRef] [PubMed]
100. Son, B.-K.; Akishita, M.; Iijima, K.; Ogawa, S.; Maemura, K.; Yu, J.; Takeyama, K.; Kato, S.; Eto, M.; Ouchi, Y. Androgen Receptor-dependent Transactivation of Growth Arrest-specific Gene 6 Mediates Inhibitory Effects of Testosterone on Vascular Calcification. *J. Biol. Chem.* **2010**, *285*, 7537–7544. [CrossRef] [PubMed]
101. Akishita, M.; Hashimoto, M.; Ohike, Y.; Ogawa, S.; Iijima, K.; Eto, M.; Ouchi, Y. Low testosterone level as a predictor of cardiovascular events in Japanese men with coronary risk factors. *Atherosclerosis* **2010**, *210*, 232–236. [CrossRef]
102. Achar, S.; Rostamian, A.; Narayan, S.M. Cardiac and Metabolic Effects of Anabolic-Androgenic Steroid Abuse on Lipids, Blood Pressure, Left Ventricular Dimensions, and Rhythm. *Am. J. Cardiol.* **2010**, *106*, 893–901. [CrossRef]
103. Moisan, M.-P.; Castanon, N. Emerging Role of Corticosteroid-Binding Globulin in Glucocorticoid-Driven Metabolic Disorders. *Front. Endocrinol.* **2016**, *7*, 160. [CrossRef]
104. Kuiper, G.G.; Enmark, E.; Pelto-Huikko, M.; Nilsson, S.; Gustafsson, J.A. Cloning of a novel receptor expressed in rat prostate and ovary. *Proc. Natl. Acad. Sci. USA* **1996**, *93*, 5925–5930. [CrossRef]
105. Filardo, E.J.; Quinn, J.A.; Frackelton, A.R.; Bland, K.I. Estrogen Action Via the G Protein-Coupled Receptor, GPR30: Stimulation of Adenylyl Cyclase and cAMP-Mediated Attenuation of the Epidermal Growth Factor Receptor-to-MAPK Signaling Axis. *Mol. Endocrinol.* **2002**, *16*, 70–84. [CrossRef]
106. Murphy, E. Estrogen Signaling and Cardiovascular Disease. *Circ. Res.* **2011**, *109*, 687–696. [CrossRef]
107. Jakacka, M.; Ito, M.; Weiss, J.; Chien, P.-Y.; Gehm, B.D.; Jameson, J.L. Estrogen Receptor Binding to DNA Is Not Required for Its Activity through the Nonclassical AP1 Pathway. *J. Biol. Chem.* **2001**, *276*, 13615–13621. [CrossRef]
108. Burns, K.A.; Li, Y.; Arao, Y.; Petrovich, R.M.; Korach, K.S. Selective Mutations in Estrogen Receptor α D-domain Alters Nuclear Translocation and Non-estrogen Response Element Gene Regulatory Mechanisms. *J. Biol. Chem.* **2011**, *286*, 12640–12649. [CrossRef]
109. Curtis, S.W.; Washburn, T.F.; Sewall, C.; DiAugustine, R.P.; Lindzey, J.; Couse, J.F.; Korach, K.S. Physiological coupling of growth factor and steroid receptor signaling pathways: Estrogen receptor knockout mice lack estrogen-like response to epidermal growth factor. *Proc. Natl. Acad. Sci. USA* **1996**, *93*, 12626–12630. [CrossRef]
110. Simoncini, T.; Hafezi-Moghadam, A.; Brazil, D.P.; Ley, K.; Chin, W.W.; Liao, J.K. Interaction of oestrogen receptor with the regulatory subunit of phosphatidylinositol-3-OH kinase. *Nat. Cell Biol.* **2000**, *407*, 538–541. [CrossRef]
111. Mendelsohn, M.E.; Karas, R.H. The Protective Effects of Estrogen on the Cardiovascular System. *N. Engl. J. Med.* **1999**, *340*, 1801–1811. [CrossRef]
112. Ueda, K.; Adachi, Y.; Liu, P.; Fukuma, N.; Takimoto, E. Regulatory Actions of Estrogen Receptor Signaling in the Cardiovascular System. *Front. Endocrinol.* **2020**, *10*, 909. [CrossRef]
113. Teoh, J.-P.; Li, X.; Simoncini, T.; Zhu, D.; Fu, X. Estrogen-Mediated Gaseous Signaling Molecules in Cardiovascular Disease. *Trends Endocrinol. Metab.* **2020**, *31*, 773–784. [CrossRef]
114. Kloner, R.A.; Carson, C.; Dobs, A.; Kopecky, S.; Mohler, E.R. Testosterone and Cardiovascular Disease. *J. Am. Coll. Cardiol.* **2016**, *67*, 545–557. [CrossRef]
115. Tostes, R.C.; Carneiro, F.S.; Carvalho, M.H.C.; Reckelhoff, J.F. Reactive oxygen species: Players in the cardiovascular effects of testosterone. *Am. J. Physiol. Integr. Comp. Physiol.* **2016**, *310*, R1–R14. [CrossRef]
116. Thomas, P. Membrane Androgen Receptors Unrelated to Nuclear Steroid Receptors. *Endocrinology* **2019**, *160*, 772–781. [CrossRef] [PubMed]
117. Gonzales, R.J.; Ansar, S.; Duckles, S.P.; Krause, D.N. Androgenic/Estrogenic Balance in the Male Rat Cerebral Circulation: Metabolic Enzymes and Sex Steroid Receptors. *Br. J. Pharmacol.* **2007**, *27*, 1841–1852. [CrossRef] [PubMed]
118. Brinkmann, A.O. Molecular Mechanisms of Androgen Action—A Historical Perspective. *Adv. Struct. Saf. Stud.* **2011**, *776*, 3–24. [CrossRef]
119. Fujimoto, R.; Morimoto, I.; Morita, E.; Sugimoto, H.; Ito, Y.; Eto, S. Androgen receptors, 5 alpha-reductase activity and androgen-dependent proliferation of vascular smooth muscle cells. *J. Steroid Biochem. Mol. Biol.* **1994**, *50*, 169–174. [CrossRef]
120. Mukherjee, T.K.; Dinh, H.; Chaudhuri, G.; Nathan, L. Testosterone attenuates expression of vascular cell adhesion molecule-1 by conversion to estradiol by aromatase in endothelial cells: Implications in atherosclerosis. *Proc. Natl. Acad. Sci. USA* **2002**, *99*, 4055–4060. [CrossRef] [PubMed]
121. Beery, A.K.; Zucker, I. Sex bias in neuroscience and biomedical research. *Neurosci. Biobehav. Rev.* **2011**, *35*, 565–572. [CrossRef] [PubMed]
122. Beery, A.K. Inclusion of females does not increase variability in rodent research studies. *Curr. Opin. Behav. Sci.* **2018**, *23*, 143–149. [CrossRef] [PubMed]
123. Becher, O.J.; Holland, E.C. Genetically Engineered Models Have Advantages over Xenografts for Preclinical Studies. *Cancer Res.* **2006**, *66*, 3355–3359. [CrossRef] [PubMed]
124. Sider, K.L.; Blaser, M.C.; Simmons, C.A. Animal Models of Calcific Aortic Valve Disease. *Int. J. Inflamm.* **2011**, *2011*, 1–18. [CrossRef] [PubMed]

125. Rattazzi, M.; Bennett, B.J.; Bea, F.; Kirk, E.A.; Ricks, J.L.; Speer, M.; Schwartz, S.M.; Giachelli, C.M.; Rosenfeld, M.E. Calcification of Advanced Atherosclerotic Lesions in the Innominate Arteries of ApoE-Deficient Mice. *Arter. Thromb. Vasc. Biol.* **2005**, *25*, 1420–1425. [CrossRef]
126. Awan, Z.; Denis, M.; Bailey, D.; Giaid, A.; Prat, A.; Goltzman, D.; Seidah, N.G.; Genest, J. The LDLR deficient mouse as a model for aortic calcification and quantification by micro-computed tomography. *Atherosclerosis* **2011**, *219*, 455–462. [CrossRef]
127. Watanabe, R.; Fujita, N.; Sato, Y.; Kobayashi, T.; Morita, M.; Oike, T.; Miyamoto, K.; Kuro-O, M.; Michigami, T.; Fukumoto, S.; et al. Enpp1 is an anti-aging factor that regulates Klotho under phosphate overload conditions. *Sci. Rep.* **2017**, *7*, 1–12. [CrossRef]
128. Kauffenstein, G.; Pizard, A.; Le Corre, Y.; Vessières, E.; Grimaud, L.; Toutain, B.; Labat, C.; Mauras, Y.; Gorgels, T.G.; Bergen, A.A.; et al. Disseminated arterial calcification and enhanced myogenic response are associated with abcc6 deficiency in a mouse model of pseudoxanthoma elasticum. *Arter. Thromb. Vasc. Biol.* **2014**, *34*, 1045–1056. [CrossRef] [PubMed]
129. Herrmann, J.; Babic, M.; Tölle, M.; Van Der Giet, M.; Schuchardt, M. Research Models for Studying Vascular Calcification. *Int. J. Mol. Sci.* **2020**, *21*, 2204. [CrossRef]
130. Scatena, M.; Jackson, M.F.; Speer, M.Y.; Leaf, E.M.; Wallingford, M.C.; Giachelli, C.M. Increased Calcific Aortic Valve Disease in response to a diabetogenic, procalcific diet in the LDLr $^{-/-}$ ApoB 100/100 mouse model. *Cardiovasc. Pathol.* **2018**, *34*, 28–37. [CrossRef]
131. Liao, R.; Wang, L.; Li, J.; Sun, S.; Xiong, Y.; Li, Y.; Han, M.; Jiang, H.; Anil, M.; Su, B. Vascular calcification is associated with Wnt-signaling pathway and blood pressure variability in chronic kidney disease rats. *Nephrology* **2019**, *25*, 264–272. [CrossRef]
132. Price, P.A.; Faus, S.A.; Williamson, M.K. Warfarin Causes Rapid Calcification of the Elastic Lamellae in Rat Arteries and Heart Valves. *Arter. Thromb. Vasc. Biol.* **1998**, *18*, 1400–1407. [CrossRef]
133. Shobeiri, N.; Adams, M.; Holden, R. Vascular Calcification in Animal Models of CKD: A Review. *Am. J. Nephrol.* **2010**, *31*, 471–481. [CrossRef] [PubMed]
134. Karas, R.H.; Schulten, H.; Pare, G.; Aronovitz, M.J.; Ohlsson, C.; Gustafsson, J.-A.; Mendelsohn, M.E. Effects of Estrogen on the Vascular Injury Response in Estrogen Receptor α,β (Double) Knockout Mice. *Circ. Res.* **2001**, *89*, 534–539. [CrossRef] [PubMed]
135. Li, Z.; Kuhn, G.; Schirmer, M.; Müller, R.; Ruffoni, D. Impaired bone formation in ovariectomized mice reduces implant integration as indicated by longitudinal in vivo micro-computed tomography. *PLoS ONE* **2017**, *12*, e0184835. [CrossRef] [PubMed]
136. Marek, I.; Canu, M.; Cordasic, N.; Rauh, M.; Volkert, G.; Fahlbusch, F.B.; Rascher, W.; Hilgers, K.F.; Hartner, A.; Menendez-Castro, C. Sex differences in the development of vascular and renal lesions in mice with a simultaneous deficiency of Apoe and the integrin chain Itga8. *Biol. Sex Differ.* **2017**, *8*, 1–13. [CrossRef]
137. Ferencik, M. Insights Into Coronary Plaque Microstructure Differences Between Women and Men. *Circ. Cardiovasc. Imaging* **2016**, *9*, 005343. [CrossRef]
138. Tang, Y.; Shah, T.A.; Yurkow, E.J.; Rogers, M.B. Post-transcriptional regulation of aortic calcification in KLOTHO deficient mice: Impact of miR-145 and miR-378. *Biorivex.* **2020**. pre-print. [CrossRef]
139. Shah, T.A.; Tang, Y.; Yurkow, E.J.; Rogers, M. B Post-Transcriptional Bone Morphogenetic Protein 2 (BMP2) Gene Regulation in Aorta. *Biorivex.* **2019**. pre-print. [CrossRef]
140. Pereira, T.M.; Nogueira, B.V.; Lima, L.C.; Porto, M.L.; Arruda, J.A.; Vasquez, E.C.; Meyrelles, S.S. Cardiac and vascular changes in elderly atherosclerotic mice: The influence of gender. *Lipids Health Dis.* **2010**, *9*, 87. [CrossRef] [PubMed]
141. Qiao, J.H.; Xie, P.Z.; Fishbein, M.C.; Kreuzer, J.; Drake, T.A.; Demer, L.L.; Lusis, A.J. Pathology of atheromatous lesions in inbred and genetically engineered mice. Genetic determination of arterial calcification. *Arterioscler Thromb.* **1994**, *14*, 1480–1497. [CrossRef] [PubMed]
142. Wang, S.S.; Martin, L.J.; Schadt, E.E.; Meng, H.; Wang, X.; Zhao, W.; Ingram-Drake, L.; Nebohacova, M.; Mehrabian, M.; Drake, T.A.; et al. Disruption of the aortic elastic lamina and medial calcification share genetic determinants in mice. *Circ Cardiovasc Genet.* **2009**, *2*, 573–582. [CrossRef] [PubMed]
143. Nakamura, T.; Akishita, M.; Kozaki, K.; Toba, K.; Orimo, H.; Ouchi, Y. Influence of sex and estrogen on vitamin D-induced arterial calcification in rats. *Geriatr Gerontol Int.* **2002**, *3*, 145–149. [CrossRef]
144. Kohn, M.H.; Price, R.E.; Pelz, H.J. A cardiovascular phenotype in warfarin-resistant Vkorc1 mutant rats. *Artery Res.* **2008**, *2*, 138–147. [CrossRef]
145. Ng, K.; Hildreth, C.M.; Avolio, A.P.; Phillips, J.K. Angiotensin-converting enzyme inhibitor limits pulse-wave velocity and aortic calcification in a rat model of cystic renal disease. *Am J Physiol Renal Physiol.* **2011**, *301*, F959–F966. [CrossRef]
146. Dixon, J.A.; Spinale, F.G. Large Animal Models of Heart Failure. *Circ. Heart Fail.* **2009**, *2*, 262–271. [CrossRef]
147. Warren, H.S.; Fitting, C.; Hoff, E.; Adib-Conquy, M.; Beasley-Topliffe, L.; Tesini, B.; Liang, X.; Valentine, C.; Hellman, J.; Hayden, D.; et al. Resilience to Bacterial Infection: Difference between Species Could Be Due to Proteins in Serum. *J. Infect. Dis.* **2010**, *201*, 223–232. [CrossRef]
148. Cimini, M.; Boughner, D.R.; Ronald, J.A.; Aldington, L.; Rogers, K.A. Development of aortic valve sclerosis in a rabbit model of atherosclerosis: An immunohistochemical and histological study. *J. Heart Valve Dis.* **2005**, *14*, 365–375.
149. Rajamannan, N.M.; Subramaniam, M.; Caira, F.; Stock, S.R.; Spelsberg, T.C. Atorvastatin inhibits hypercholesterolemia-induced calcification in the aortic valves via the Lrp5 receptor pathway. *Circulation* **2005**, *112*, I229–I234.
150. Marechaux, S.; Corseaux, D.; Vincentelli, A.; Richardson, M.; Ung, A.; Susen, S.; Zawadzki, C.; Beregi, J.-P.; Ezekowitz, M.D.; Jude, B.; et al. Identification of tissue factor in experimental aortic valve sclerosis. *Cardiovasc. Pathol.* **2009**, *18*, 67–76. [CrossRef] [PubMed]

151. Choi, B.; Lee, S.; Song, J.-K.; Kim, S.-M.; Lee, E.-J.; Lee, S.R.; Kim, D.-H.; Jang, J.Y.; Kang, S.-W.; Lee, K.-U.; et al. Dipeptidyl Peptidase-4 Induces Aortic Valve Calcification by Inhibiting Insulin-Like Growth Factor-1 Signaling in Valvular Interstitial Cells. *Circulation* **2017**, *135*, 1935–1950. [CrossRef] [PubMed]
152. Xu, J.; Nie, M.; Li, J.; Xu, Z.; Zhang, M.; Yan, Y.; Feng, T.; Zhao, X.; Zhao, Q. Effect of pioglitazone on inflammation and calcification in atherosclerotic rabbits. *Herz* **2017**, *43*, 733–740. [CrossRef] [PubMed]
153. Chen, Y.; Waqar, A.B.; Nishijima, K.; Ning, B.; Kitajima, S.; Matsuhisa, F.; Chen, L.; Liu, E.; Koike, T.; Yu, Y.; et al. Macrophage-derived MMP-9 enhances the progression of atherosclerotic lesions and vascular calcification in transgenic rabbits. *J. Cell. Mol. Med.* **2020**, *24*, 4261–4274. [CrossRef] [PubMed]
154. Beute, T.J.; Goehler, M.; Parker, J.; Boeve, T.; Heiser, J.; Murphy, E.; Timek, T.; Willekes, C.L. Long-Term Outcomes of Mosaic Versus Perimount Mitral Replacements: 17-Year Follow-Up of 940 Implants. *Ann. Thorac. Surg.* **2020**, *110*, 508–515. [CrossRef] [PubMed]
155. Badin, J.K.; Progar, V.; Pareddy, A.; Cagle, J.; Alloosh, M.; Sturek, M. Effect of Age on Diabetogenicity of Alloxan in Ossabaw Miniature Swine. *Comp. Med.* **2019**, *69*, 114–122. [CrossRef] [PubMed]
156. Van Ditzhuijzen, N.S.; Heuvel, M.V.D.; Nieman, K.; Mulder, M.T.; Zijlstra, F.; Duncker, D.J.; Van Beusekom, H.M.; Regar, E.; Sorop, O.; Rossi, A.; et al. Serial Coronary Imaging of Early Atherosclerosis Development in Fast-Food-Fed Diabetic and Nondiabetic Swine. *JACC Basic Transl. Sci.* **2016**, *1*, 449–460. [CrossRef] [PubMed]
157. Sider, K.L.; Zhu, C.; Kwong, A.V.; Mirzaei, Z.; De Langé, C.F.; Simmons, C.A. Evaluation of a porcine model of early aortic valve sclerosis. *Cardiovasc. Pathol.* **2014**, *23*, 289–297. [CrossRef]
158. Simmons, C.A.; Grant, G.R.; Manduchi, E.; Davies, P.F. Spatial Heterogeneity of Endothelial Phenotypes Correlates With Side-Specific Vulnerability to Calcification in Normal Porcine Aortic Valves. *Circ. Res.* **2005**, *96*, 792–799. [CrossRef]
159. McCoy, C.M.; Nicholas, D.Q.; Masters, K.S. Sex-Related Differences in Gene Expression by Porcine Aortic Valvular Interstitial Cells. *PLoS ONE* **2012**, *7*, e39980. [CrossRef]
160. Masjedi, S.; Lei, Y.; Patel, J.; Ferdous, Z. Sex-related differences in matrix remodeling and early osteogenic markers in aortic valvular interstitial cells. *Heart Vessel.* **2016**, *32*, 217–228. [CrossRef]